Clinical advances in cardiovascular magnetic resonace imaging and angiography

Bosch, H.C.M. van den

Clinical Advances in Cardiovascular Magnetic Resonance Imaging and Angiography

Cover: Harrie van den Bosch
Layout: Tiny Wouters
Production: GVO drukkers & vormgevers B.V.

ISBN: 978-94-6332-339-0

Publication of this thesis was financially supported by Catharina Ziekenhuis Eindhoven and Bracco Imaging.

Clinical Advances in Cardiovascular Magnetic Resonance Imaging and Angiography

PROEFSCHRIFT

ter verkrijging van
de graad van Doctor aan de Universiteit Leiden,
op gezag van Rector Magnificus prof. mr. C.J.J.M. Stolker,
volgens besluit van het College van Promoties
te verdedigen op donderdag 17 mei 2018
klokke 16.15 uur

door

Hendricus Cornelis Marinus van den Bosch

geboren te Eindhoven
in 1965

Promotor:

Prof. dr. A. de Roos

Copromotor:

Dr. ir. J.J.M. Westenberg

Promotiecommissie:

Prof. dr. H.J. Lamb
Prof. dr. T. Leiner, Universitair Medisch Centrum Utrecht
Prof. dr. B.K. Velthuis, Universitair Medisch Centrum Utrecht
Prof. dr. M.V. Huisman
Dr. A.V. Tielbeek, Catharina Ziekenhuis Eindhoven

Contents

Chapter 1

General introduction and outline

Background

Over the last decades, Cardiovascular Magnetic Resonance (CMR) imaging has evolved into an accurate and reliable imaging modality for the radiologist to be used in clinical practice and research. CMR imaging is a noninvasive imaging technique providing invaluable information to evaluate the cardiovascular system without the need of ionizing radiation.[1]

In the early days of magnetic resonance imaging (MRI), imaging was performed on magnets with low field strength (for example 0.35 and 0.5 Tesla (T)). Nowadays in clinical routine, CMR is performed on 1.5T systems and high-field strength 3T whole-body MRI scanners have been introduced in clinical practice over the past few years.

The potential benefit of 3T MRI is providing images with increased signal-to-noise ratio (SNR) when compared to 1.5T.[2] High-field MRI systems enable acquisition with higher spatial resolution within a similar imaging time. Advances in MRI hardware and software technology have improved image quality enormously.

Whereas CMR was firstly used as an added imaging evaluation possibility for some patients in selected centers, additional to conventional techniques such as echocardiography, X-ray, or digital subtraction angiography, it has developed into an established first-in-line imaging modality in diagnosis, patient work-up and treatment planning for various cardiac and vascular diseases.

For cardiac imaging, CMR imaging has become a gold standard for evaluating ventricular volumes and function[3] and for imaging of myocardial infarction and viability.[4] It's noninvasiveness and radiation-free nature are important benefits for patients, especially in young patients or when serial follow-up is requested.

Image acquisition can be acquired with two-dimensional (2D), three-dimensional (3D) or four-dimensional (4D), when a 3D volume dataset is obtained in time-resolved manner. Thereby providing the opportunity for unlimited access of arbitrary imaging planes for accurate evaluation and quantitation. These are important advantages of CMR imaging over for example echocardiography as imaging is not hampered by the availability of acoustic windows.

The use of contrast agents plays an important role in CMR imaging. Especially, the value of delayed-enhancement imaging of myocardial scarring and viability in ischemic heart disease is well recognized and has gained widespread acceptance in daily practice.[5,6] Delayed-enhancement CMR imaging provides the opportunity to evaluate the transmural extent of infarcted myocardium with superior spatial resolution when compared to nuclear medicine techniques and improved diagnosis is to be expected.[7,8] Delayed-enhancement imaging requires multiple long breath holds from patients, which especially for patients with heart disease could be an important limitation. Free-breathing alternatives were very much desired and in this thesis, the application of one such approach is explored.

Contrast agents play also an important role in MR angiography (MRA). The paramagnetic behavior of a contrast medium injected in the blood pool and imaged with a whole body MRI system will result in a high contrast in signal intensity between the blood vessel and its surrounding tissue. In clinical routine, contrast-enhanced MRA (CE-MRA) is widely used for diagnosis and treatment planning in patients with peripheral arterial occlusive disease. The field strength of the MRI scanner is crucial in creating this contrast in signal. In this thesis, the performance of a high field strength system (3T) is being compared to 1.5T MRI with conventional digital subtraction angiography (DSA) serving as standard of reference.
Administration of MRI contrast agents can - although uncommon - cause allergic reactions and the association with adverse events, especially serious incidents with nephrogenic systemic fibrosis in patients with renal failure, have been reported in recent years.[9,10] Therefore, alternative imaging biomarkers in patients with peripheral arterial occlusive disease that can be obtained without the use of contrast agents need to be considered. Arterial wall thickness and stiffness are relatively new imaging biomarkers that can be obtained from non-contrast CMR, which may have prognostic value when evaluating the severity and progress of atherosclerosis. In this thesis, the value of these biomarkers will be assessed with non-contrast CMR for risk assessment and prediction of outcome in patients with peripheral arterial occlusive disease.

Outline of the thesis

Chapter 2 provides an introduction to cardiac MRI with special focus on the assessment of normal cardiac anatomy. The planning of the specific cardiac MR imaging planes is described along with an illustrative description of the normal cardiac anatomical structures that are visualized on CMR images. Additionally, some aspects of cardiac imaging on (ultra-) high-field MRI are addressed.
In **chapter 3**, the assessment of myocardial scarring with delayed-enhancement imaging is compared in a free-breathing protocol versus a sequence which uses breath-holding.
Chapter 4 describes various techniques that are currently available and applied for MRA. Furthermore, several anatomical regions that are imaged by MRA are addressed and the state-of-the-art is discussed, with special focus on the carotid arteries, thoracic and abdominal aorta, renal arteries, mesenteric artery, and the peripheral arteries.
Chapter 5 and **6** evaluate the diagnostic accuracy of single-injection, three-station, moving-table CE-MRA with high spatial resolution in patients with peripheral arterial occlusive disease (PAOD) at 1.5T and 3T, respectively. In **chapter 5**, the use of sensitivity encoding and random central–k-space segmentation in a centric filling order is evaluated with conventional DSA serving as the standard of reference. In **chapter 6,** single-injection, three-station, moving-table CE-MRA at 3T is compared to 1.5T CE-MRA. Also in this study, DSA is used as the standard of reference
Chapters 7 and 8 evaluate new imaging biomarkers for the severity of atherosclerosis which can be obtained without the use of contrast agents. In **chapter 7,** the associations between aortic wall stiffness, expressed by the pulse wave velocity (PWV) and sampled in various areas of the aorta, the arterial wall thickness, sampled in the common carotid artery, and the severity of PAOD, are evaluated.
Chapter 8 explores the prognostic value of outcome of these CMR imaging biomarkers in the patient populations with symptomatic PAOD in comparison with traditional risk factors (age, gender, BMI, hypertension, diabetes mellitus, levels of triglyceride and HDL in blood plasma samples, ABI and Fontaine class) over a follow-up period of six years.
Finally, in **chapter 9**, the conclusions are summarized.

References

1. Geva T. Magnetic resonance imaging: historical perspective. J Cardiovasc magn Reson 2006;8: 573-580.
2. Hinton DP, Wald LL, Pitts J, et al. Comparison of cardiac MRI on 1.5 and 3.0 Tesla clinical whole body systems. Invest Radiol. 2003;38:436-422.
3. Moon JC, Lorenz CH, Francis JM, Smith GC, Pennell DJ. Breath-hold FLASH and FISP cardiovascular MR imaging: left ventricular volume differences and reproducibility. Radiology. 2002;223:789-797.
4. Dweck MR, Williams MC, Moss AJ, Newby DE, Fayad ZA.Computed Tomography and Cardiac Magnetic Resonance in Ischemic Heart Disease. J Am Coll Cardiol. 2016;68:2201-2216.
5. Kim RJ, Fieno DS, Parrish TB, Harris K, Chen EL, Simonetti O, Bundy J, Finn JP, Klocke FJ, Judd RM. Relationship of MRI delayed contrast enhancement to irreversible injury, infarct age, and contractile function. Circulation. 1999;100:1992-2002.
6. Kim RJ, Wu E, Rafael A, Chen EL, Parker MA, Simonetti O, Klocke FJ, Bonow RO, Judd RM. The use of contrast-enhanced magnetic resonance imaging to identify reversible myocardial dysfunction. N Engl J Med. 2000 Nov 16;343:1445-53.
7. Klein C, Nekolla SG, Bengel F, Momose M, Sammer A, Haas F, Schnackenburg B, Delius W, Mudra H, Wolfram D, Schwaiger M. Assessment of myocardial viability with contrast-enhanced magnetic resonance imaging: comparison with positron emission tomography. Circulation 2002;105:162–167.
8. Wagner A, Mahrholdt H, Holly TA, Elliott MD, Regenfus M, Parker M, Klocke FJ, Bonow RO, Kim RJ, Judd RM. Contrast-enhanced MRI and routine single photon emission computed tomography (SPECT) perfusion imaging for detection of subendocardial myocardial infarcts: an imaging study. Lancet 2003; 361:374–379.
9. Prince M, Zhang H, Roditi G, Leiner T, Kucharczyk W. Risk factors for NSF: a literature review. J Magn Reson Imaging. 2009;30(6):1298-1308.
10. Thomson H, Morcos S, Almen T, Bellin M, Bertolotto M, Bongartz G, Clement O, Leander P, Heinz-Peer G, Reimer P, Stacul F, van der Molen A, Webb J. Nephrogenic systemic fibrosis and gadolinium-based contrast media: updated ESUR contrast medium safety committee guidelines. Eur Radiol. 2013;23(2):307-318.

Chapter 2

CMR: Imaging Planes and Anatomy

Harrie CM van den Bosch
Jos JM Westenberg
Albert de Roos

based on
Chapter 7 CMR: Imaging Planes and Anatomy
in MRI and CT of the Cardiovascular System, 3rd Edition, 2013
Charles B Higgins and Albert de Roos
Lippincott Williams & Wilkens

Cardiac magnetic resonance (CMR) imaging has the ability to provide arbitrary views of the cardiac structures which can be chosen freely since this modality is not hampered by the availability of acoustic windows, as in echocardiography. Even though echocardiography, x-ray LV angiography, and cardiac computed tomography (CT) are nowadays commonly used techniques for evaluating cardiac disease in clinical practice, CMR has evolved to become the preferential technique for anatomic and functional cardiac imaging.

Two-dimensional (2D), single-plane, multiple-2D, or three-dimensional (3D) imaging is possible with CMR. Furthermore, temporal information of the dynamics of the heart can be provided as imaging is synchronized to the cardiac frequency, using either prospective triggering or retrospective gating.[1] With prospective triggering, the operator will set the expected heart rate before the acquisition and triggering will be performed according to this chosen heart rate. With retrospective gating, imaging is performed continuously and additionally the ECG signal will be stored. In retrospect, k-space filling is synchronized to the stored ECG. This synchronization enables time-resolved imaging and multiple phases of the cardiac cycle can be obtained. The acquired views in multiple phase of the heart can be presented in cine mode, providing functional information on the temporal behavior of the cardiac structures.

Imaging planes in CMR are usually obtained in the orientation to the axes of the heart, or oriented to the major axes of the body. Therefore, the standard CMR planes of the heart are comparable to the standard cardiac views known and established in other noninvasive imaging modalities such as echocardiography, cardiac CT, x-ray LV angiography, and nuclear techniques (e.g., single-photon emission computed tomography [SPECT] and positron emission tomography [PET]). Compared to cardiac CT, x-ray angiography, and nuclear techniques, CMR allows noninvasive, high-resolution imaging without using ionizing radiation. Furthermore, the morphology of the right ventricle (RV) is excellent delineated by CMR, whereas in echocardiography the assessment of RV geometry and function is challenging because of the particular crescentic shape of the RV wrapping around the left ventricle (LV).[2]

The choice for a specific scan protocol is mainly determined by the diagnostic question which has to be answered. In CMR imaging, both static and dynamic images of the heart can be acquired. Therefore, it is important to be adequately informed by the referring clinician prior to the CMR examination. Standardized nomenclature for cross-sectional anatomy has been described,[3] facilitating comparison between different techniques and proper communication in clinical practice. The 17-segment model of the LV, proposed by the American Heart Association (AHA), is nowadays widely used and accepted in clinical CMR imaging, as in other cross-sectional imaging modalities (e.g., cardiac CT and nuclear techniques). The recommended model comprehends six basal segments, six mid-ventricular segments, four apical (distal) segments, and one true apex (Figure 2.1). These 17 segments are routinely evaluated when regional LV performance is questioned.

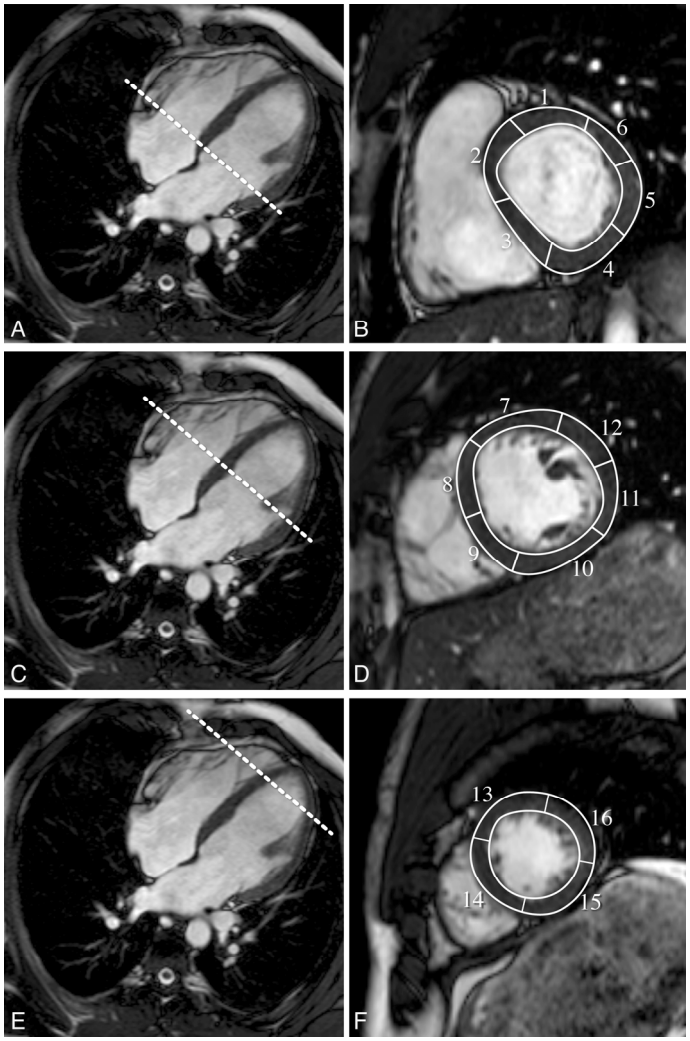

Figure 2.1 The standardized 17 segments of LV as proposed by the American Heart Association. At basal **(B)** and mid-ventricular **(D)** level, the myocardium is divided into six segments each, and at apical **(F)** level, the myocardium is divided into four segments. Nomenclature: Segment 1, basal anterior; 2, basal anteroseptal; 3, basal inferoseptal; 4, basal inferior; 5, basal inferolateral; 6, basal anterolateral; 7, midanterior; 8, mid-anteroseptal; 9, mid-inferoseptal; 10, mid-inferior; 11, mid-inferolateral; 12, mid-anterolateral; 13, apical anterior; 14, apical septal; 15, apical inferior; 16, apical lateral. Segment 17 (not presented) is the true apex, which can be evaluated on a long-axis view. Dashed lines on the four-chamber view **(A**,**C**, and **E)** indicate the planning of the acquisition level.

Another important issue in clinical CMR imaging is the ability of the patient to cooperate during the examination and to perform breath-holding. If a patient is capable to perform breath-holding, successive scan planes are obtained with accelerated imaging, with the patient usually performing breath-holding in expiration. Preferably, image planes in CMR imaging are acquired in mid- or end-expiration, as the anatomic level may be obtained more reproducible compared to planes which are scanned in inspiration.[4]

For planning purposes, new generation clinical MR scanners provide the possibility to plan the various scan planes interactively with real-time imaging. During free-breathing CMR, planning can be performed accurately. After all scan planes are defined and obtained interactively, the acquisition of the cine long-axis (LA) and short-axis (SA) views may be performed during breath-holding. This interactive approach for planning is fast, reliable, and patient friendly, and essential in patients who are not capable to hold their breath consecutively, for example, patients with respiratory disease or with heart failure. Fully automated CMR planning methods have also been described and can provide accurate and reproducible measurements of LV dimensions.[5]

With CMR, the choice of scanning technique is aimed at the choice between bright-blood and black-blood imaging, which essentially determines the contrast between myocardium and the intra-cardiac blood pool. For the assessment of left and right ventricular function, fast gradient-echo sequences are usually performed in combination with steadystate free precession (SSFP) technique (balanced-TFE, True-FISP, Fiesta) for optimal contrast. On these images, the blood pool is presented with bright signal whereas the myocardium is represented dark with low signal. This results in an excellent definition of the LV endocardial and epicardial borders, which is required for accurate image segmentation during cardiac volume and function quantification Typically, SSFP images should be acquired with slice thickness of 6 to 8 mm and temporal resolution better than 45 milliseconds to obtain optimal accuracy in ventricular function assessment.[6,7]

In addition, cardiac morphology can be evaluated by double-inversion, black-blood, spin-echo sequences with fat suppression, providing static images of the heart with high spatial resolution (optimally, in-plane acquired resolution of better than 2x2 mm and slice thickness of 5 to 8 mm) in the orientation of the heart or the patient's body axes. These images are, for example, obtained in the work-up of congenital heart disease or cardiac tumors (Figure 2.2).

In the remainder of this chapter, the planning of the specific imaging planes will be discussed, as well as the normal cardiac structures that are visualized. Furthermore, the aspects of cardiac imaging on (ultra-) high-field MRI will be addressed.

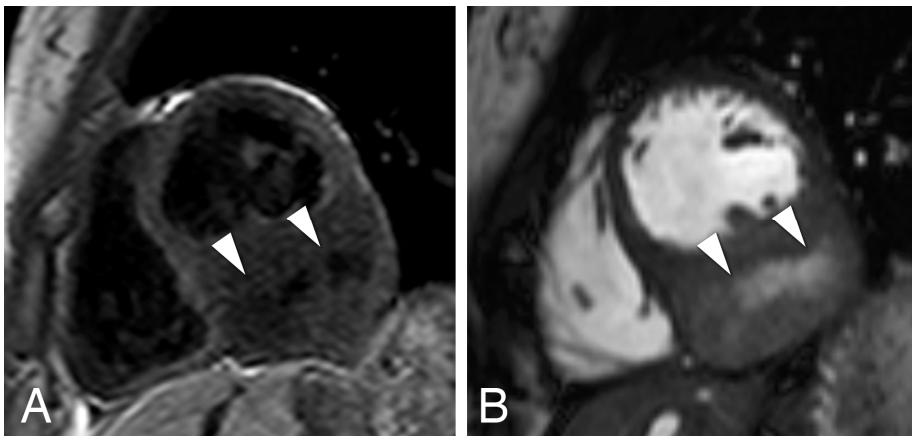

Figure 2.2 Black-blood **(A)** and bright-blood **(B)** short-axis acquisition illustrating a cardiac sarcoma (*arrow heads*) in the inferior wall, acquired in a 19-year-old female.

Cardiac Axis Imaging Planes

To acquire imaging planes in the direction of the cardiac axes, multi-stack, single-shot SSFP scout views are used for planning. If available, free-breathing real-time scanning can be used instead that is advantageous for patient's comfort. Perpendicular to an anatomical transverse image, displaying the heart's four chambers, an acquisition plane is chosen through the middle of the atrioventricular junction at the level of the mitral valve and running through the apex (Figure 2.3). This plane is the so-called vertical long-axis (VLA) plane. On this VLA view, a plane is defined intersecting the apex and the middle of the mitral valve, resulting in the horizontal long-axis (HLA) view. The HLA view is almost comparable to the four-chamber view; however, in this HLA view often a part of the LV outflow tract (LVOT) is visualized. On the acquired HLA plane, the SA views covering the entire LV are planned parallel to the ring of the mitral valve and perpendicular to the line intersecting the apex.
For reasons of reproducibility and comparison, the true two- and four-chamber view can still be obtained. The twochamber view is planned perpendicular to the anterior and inferior wall of the LV through the center of the LV cavity on a mid-ventricular SA image intersecting the apex. On the two-chamber view, the apex, anterior and inferior wall of the LV, the mitral valve, and left atrium can be analyzed (Figure 2.4A). The four-chamber view is planned also on a mid-ventricular SA image by a plane through the center of the LV cavity and the acute margin of the RV, also intersecting the apex. The four-chamber view depicts the inferior interventricular septum, the anterior

lateral wall of the LV, the free wall of the RV, left and right atrium as the interatrial septum, and both the mitral and tricuspid valves (Figure 2.4B).

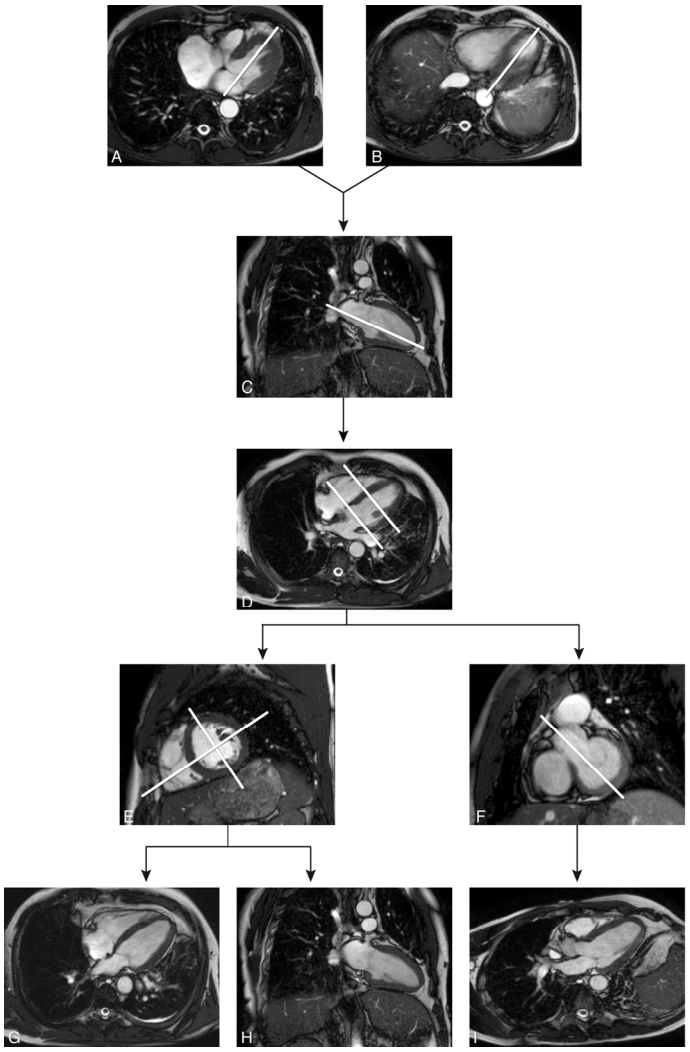

Figure 2.3 Planning acquisition of standard cardiac views. On two transverse slices **(A)** and **(B),** the left ventricular vertical long-axis (VLA) **(C)** is planned by a plane transecting the mitral valve and the apex. The horizontal long-axis (HLA) **(D)** is obtained by acquiring a plane transecting the VLA through the mitral valve and apex. A short-axis image can be obtained perpendicular to HLA, at mid-ventricular **(E)** and basal level **(F).** The four-chamber **(G)** of the LV is obtained as indicated from a plane transecting both LV and RV. The two-chamber **(H)** of the LV is acquired perpendicular to the fourchamber. The three-chamber LV **(I)** is obtained from a plane transecting the LV through the LVOT.

Routinely, the three-chamber or the so-called LVOT view is planned perpendicular to a basal SA plane. This view also intersects the apex. The LVOT view (Figure 2.4C) depicts the apex, the anterior interventricular wall, the LVOT, the inferior lateral wall, as the aortic and mitral valve, respectively. The standard SSFP cine CMR protocol for assessing LV function should include the two-, four-, and three-chamber views in combination with SA images covering the entire LV, resulting in scans covering all described 17 LV segments in two directions.

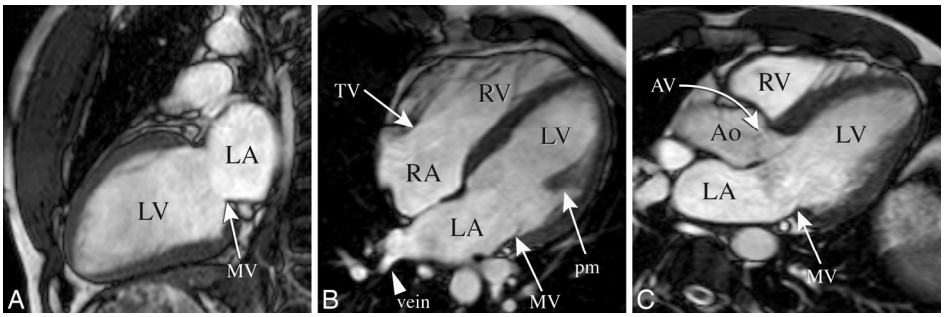

Figure 2.4 Normal cardiac anatomy on two-**(A)**, four**(B)**-, and three-chamber **(C)** views. LA, left atrium; LV, left ventricle; MV, mitral valve; TV, tricuspid valve; RV, right ventricle; RA, right atrium; pm, papillary muscle; AV, aortic valve; Ao, aorta.

In addition, the RV outflow tract can be obtained. This view can be planned on a coronal image, depicting the outflow tract of the RV. Alternatively, an optimized view of the RV outflow tract view can be obtained from a plane outlining the tricuspid valve plane and the outflow tract. On this plane, the outflow tract, pulmonary valve, tricuspid valve, and the basal (diaphragmatic) part of the RV wall are all visualized (Figure 2.5).

Body Axes Imaging Planes

For the evaluation of cardiac morphology, the pericardium, the great thoracic vessels, and (para-)cardiac masses imaging planes can be used oriented to the main body axes. Also, the transverse (or axial), coronal (frontal), and sagittal planes are well known to surgeons and other clinicians, as these anatomic orientations are similar to clinical (cardiac) CT. Black- and bright-blood sequence approaches (Fig. 7.6) can be used in optimally adjusted planes to answer specific clinical questions. These imaging sequences provide static images in single phase, not suitable for quantification of LV

or RV dimensions, as end-diastolic diameters or wall thickness. For this analysis, SSFP multiphase images with appropriate temporal resolution are more suitable.

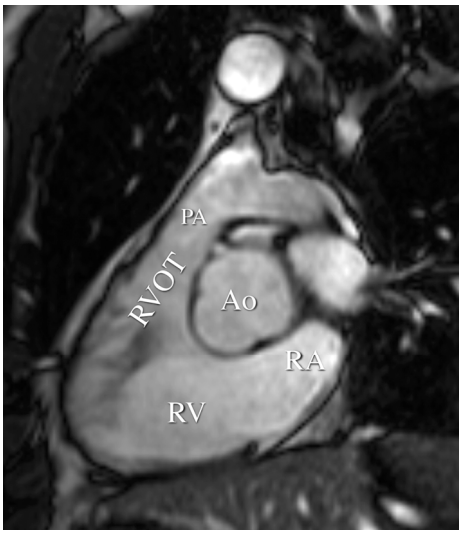

Figure 2.5 Bright-blood acquisition of the right ventricle, illustrating the right ventricular outflow tract (RVOT). PA, pulmonary artery; RVOT, right ventricular outflow tract; Ao, aorta; RA, right atrium; RV, right ventricle.

Transversely oriented planes (Figure 2.7) are especially useful for the evaluation of thoracic vascular structures as the ascending and descending thoracic aorta, the superior and inferior vena cava, the pulmonary trunk, and right and left pulmonary artery. The right and left pulmonary veins (PVs) entering the left atrium are also well depicted. Images in transverse orientation through the heart allow studying morphology of the ventricles and atria, as their internal relationship. Also the RV free wall, the RV outflow tract (infundibulum), the pericardium, and mediastinum are well depicted. It has been described that RV volume and function quantification by planimetry can be performed more accurately on transversely oriented images instead of SA images.[8]

Coronal or frontal anatomic views can be very instructive to analyze the connection between the heart and the great vessels. In the heart, the LVOT and the left atrium with its branches are clearly imaged. An advantage of the frontal view is the similarity to the chest x-ray, well known to the clinicians. On sagittal images, the RV outflow tract in relation to the pulmonary valve is well outlined and the connection of the right atrium with the superior and inferior vena cava can be studied.

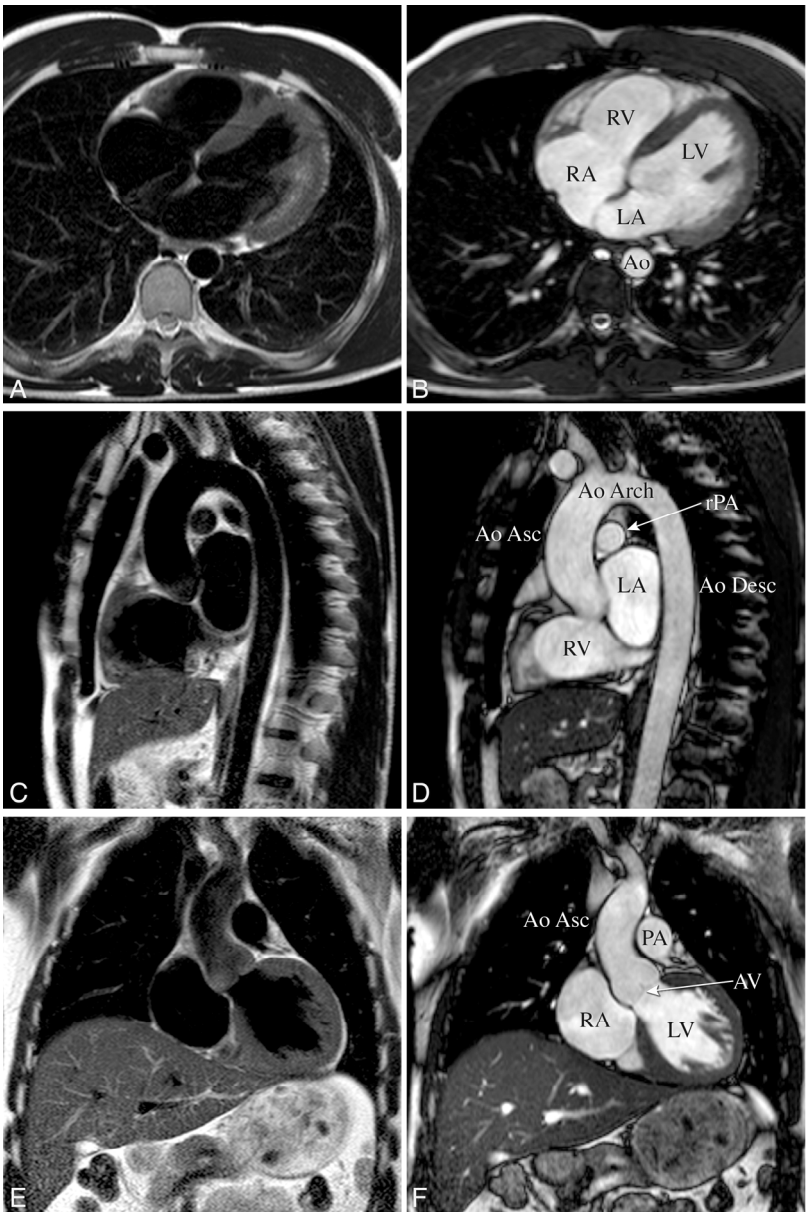

Figure 2.6 Normal cardiac anatomy on black-blood and brightblood acquisitions, in transverse **(A** and **B)**, sagittal **(C** and **D)**, and coronal **(E** and **F)** views. RV, right ventricle; LV, left ventricle; RA, right atrium; LA, left atrium; Ao, aorta; rPA, right pulmonary artery; Ao Asc, ascending aorta; LA, left atrium; RV, right ventricle; Ao Desc, descending aorta; PA, pulmonary artery; AV, aortic valve.

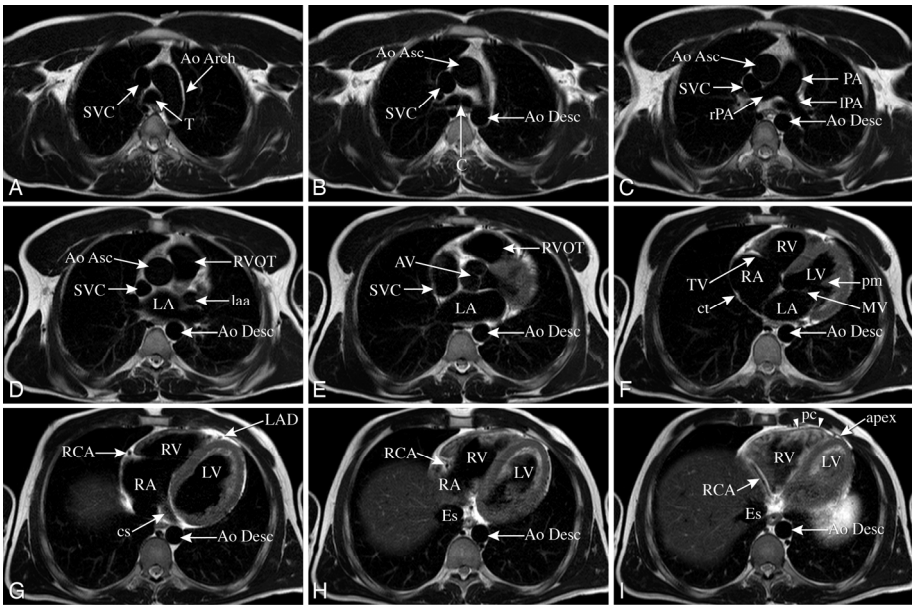

Figure 2.7 Normal cardiac anatomy on transverse black-blood acquisitions. SVC, superior vena cava; T, trachea; Ao Asc, ascending aorta; Ao Desc, descending aorta; C, carina; rPA, right pulmonary artery; PA, pulmonary artery; lPA, left pulmonary artery; LA, left atrium; RVOT, right ventricular outflow tract; LA, left atrium; laa, left atrial appendage; AV, aortic valve; RV, right ventricle; RA, right atrium; TV, tricuspid valve; LV, left ventricle; pm, papillary muscle; MV, mitral valve; LAD, left arterial descending coronary artery; RCA, right coronary artery; cs, coronary sinus; ct, crista terminalis; Es, esophagus; pc, pericard.

Anatomy

CMR images present distinct anatomic features of both atria and ventricles. New generation MRI scanners provide morphologic characteristics in great detail and CMR images are used to evaluate cardiac anatomy in patients with complex cardiac anomalies. For evaluation, either transverse (Figure 2.7) or longitudinal planes, SA (Figure 2.8) or LA cardiac views can be chosen.

The pericardial sac encloses the heart and the roots of the great vessels. The pericardium consists of two layers. The outer fibrous pericardium is attached anteriorly to the sternum, posteriorly to the thoracic spine, and inferiorly to the diaphragm. The inner, serous pericardium can be divided into a parietal and a visceral layer. The parietal layer of the inner pericardium is closely attached to the outer fibrous pericardium. The visceral layer forms the epicardium, covering the epicardial surface of the heart and the epicardial fat and coronary arteries. The pericardial cavity

is outlined by the parietal and visceral layer of the inner pericardium. Normal pericardium presents a low-signal intensity on MRI, and can be well visualized by surrounding epicardial and pericardial fat. Normally, the pericardium measures less than 4 mm on CMR images. Posteriorly to the ascending aorta reaches the superior pericardial recess. Effusion in this recess has to be differentiated from mediastinal pathology, for example, lymphadenopathy.

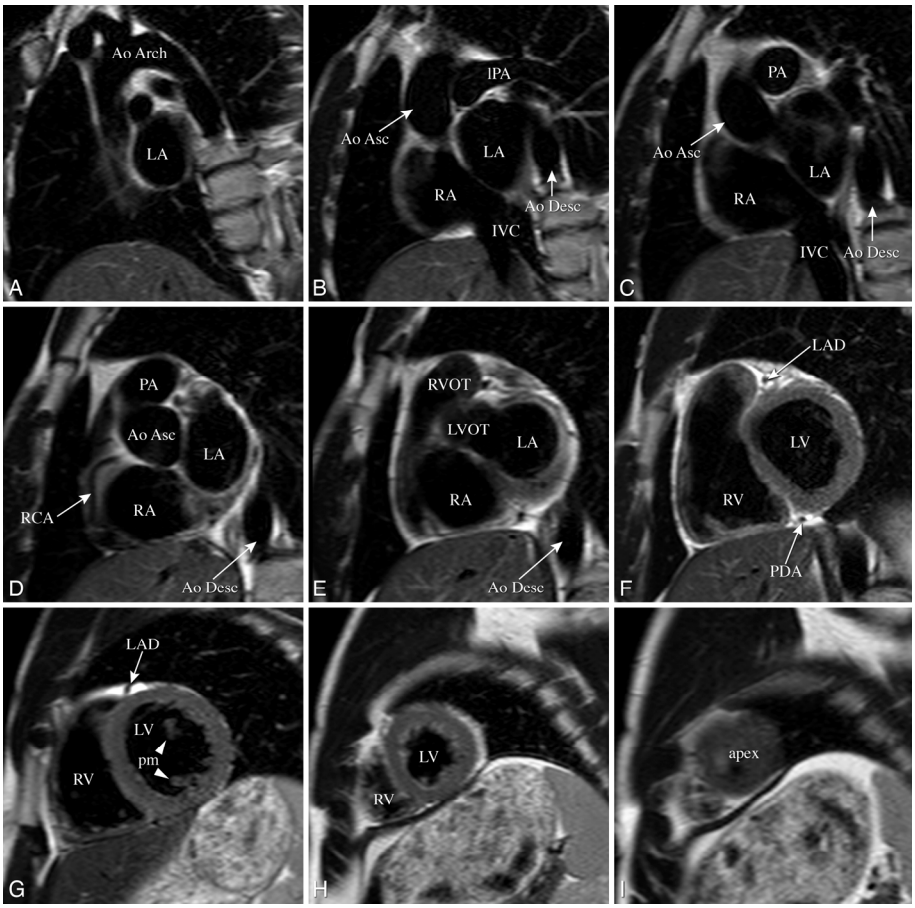

Figure 2.8 Normal cardiac anatomy on shortaxis, black-blood acquisitions. LA, left atrium; lPA, left pulmonary artery; Ao Asc, ascending aorta; RA, right atrium; Ao Desc, descending aorta; IVC, inferior vena cava; PA, pulmonary artery; RCA, right coronary artery; RVOT, right ventricular outflow tract; LVOT, left ventricular outflow tract; LAD, left arterial descending coronary artery; LV, left ventricle; RV, right ventricle; PDA, posterior arterial descending coronary artery; pm, papillary muscle.

In normal cardiac anatomy the right atrium can be recognized by a broad-based triangular appendage. At the base, the tricuspid valve, positioned between the right atrium and the RV, is located closer to the apex when compared to the mitral valve on the left side. The right atrium receives venous blood from the superior and inferior vena cava, and the coronary sinus. The coronary sinus enters the right atrium in the posterior atrioventricular groove. In the right atrium, the Eustachian valve (Ev) (Figure 2.9) can be recognized at the orifice of the inferior vena cava. The crista terminalis separates the anterior and posterior part, two embryologic distinctive parts of the right atrium. The crista terminalis can present diverse, as prominent, broad-based or thin, valve-like (Figure 2.10). Chiari's network is another normal anatomic variant that can be identified. Chiari's network is a congenital remnant of the right valve of the sinus venosus, in literature a prevalence of 1.5% to 2% has been described.[9]

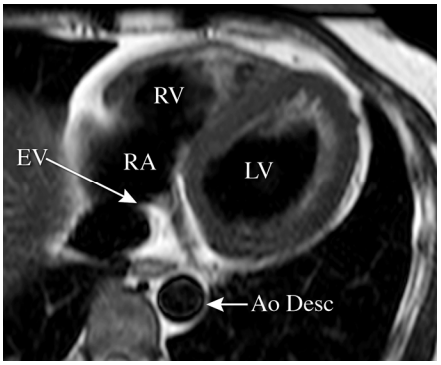

Figure 2.9 Transverse black-blood acquisition illustrating the Eustachian valve. RV, right ventricle; Ev, Eustachian valve; RA, right atrium; LV, left ventricle; Ao Desc, descending aorta.

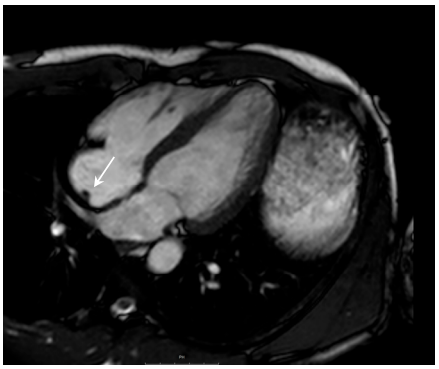

Figure 2.10 Four-chamber bright-blood acquisition illustrating a prominent crista terminalis (arrow head) in the right atrium.

The appendage of the left atrium has a narrow attachment to the atrium and is more tubular shaped. Characteristically, the left atrium receives in total four PVs, two on both sides, although several variations of this occur. Nowadays, imaging the venous anatomy of the heart is becoming more relevant. Moreover, in the preablation work-up the referring clinician needs to be informed about the exact anatomy of the left atrium and spatial orientation of the PV ostia. In patients with atrial fibrillation, MR or CT images of the left atrium and PVs are used to guide the interventional procedure, and provide indispensable information regarding PV anatomy, ostial dimensions, and shape.[10,11] Three-dimensional MR or CT reconstructions of the left atrium can be superimposed on fluoroscopy images during the interventional procedure, thereby facilitating optimal catheter positioning and improving procedural results.[12]
The interatrial septum separates the two atria and can be appreciated as a thin line. As part of the interatrial septum, the fossa ovalis is very thin and can hardly be depicted on CMR images due to the limited spatial acquisition resolution. In some patients, the septum may be infiltrated by lipomatous tissue and thereby thickened (Figure 2.11) or show localized bulging (aneurysm).

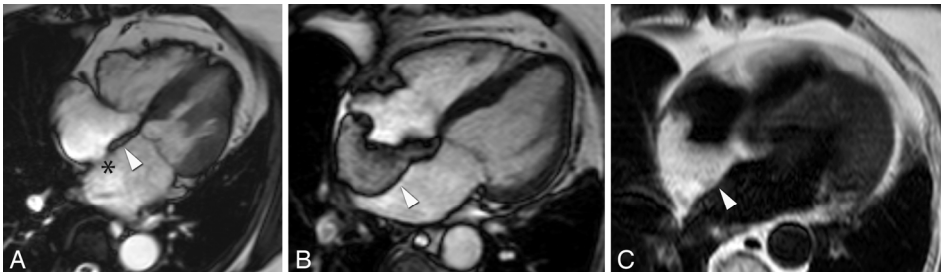

Figure 2.11 Four-chamber, bright-blood **(A** and **B)** and black-blood **(C)** acquisitions, illustrating lipomatous hypertrophy of the intra-atrial septum (arrow heads). The fossa ovalis is indicated by star.

The RV is normally triangular in shape and anteriorly orientated to the right. Morphologically, the RV has typical features that can be depicted on CMR images. The RV shows a muscular moderator band (Figure 2.12), carrying branches of the conducting system. Also, the RV contains a muscular outflow tract (infundibulum or conus arteriosus) and typically, the RV wall is more trabeculated as compared to the LV. In normal anatomy, the LV is positioned posteriorly and LVOT lacks a muscular wall. The interventricular septum consists of a muscular and membranous part. Especially, the membranous part is very thin and sometimes not depicted on CMR images.

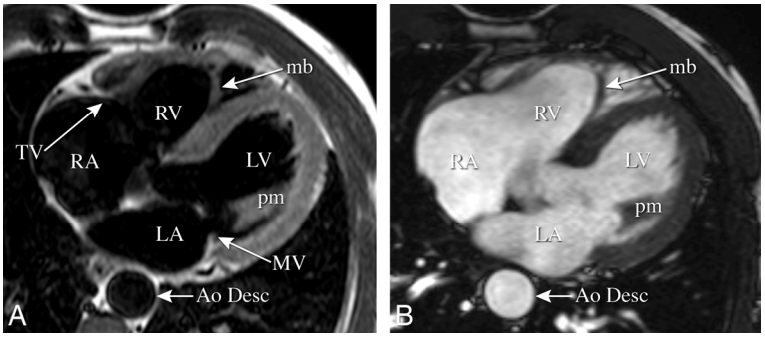

Figure 2.12 Transverse black-blood **(A)** and bright-blood **(B)** acquisitions illustrating the moderator band (mb) in the right ventricle. mb, moderator band; RV, right ventricle; TV, tricuspid valve; RA, right atrium; LV, left ventricle; pm, papillary muscle; LA, left atrium; MV, mitral valve; Ao Desc, descending aorta.

At the outlet of each of the four chambers of the heart, one-way valves are positioned that ensure blood flow in the proper direction. The blood flow through the atria into the ventricles is regulated by the atrioventricular valves: The tricuspid valve on the right side and the mitral valve on the left side, respectively. The pulmonary valve guards the outflow tract of the RV toward the pulmonary trunk, and the aortic valve connects the LVOT to the thoracic aorta. The tricuspid valve comprises three cusps, whereas the mitral valve exists of two cusps. Both the pulmonary and the aortic valve (Figure 2.13) consist of three cusps.

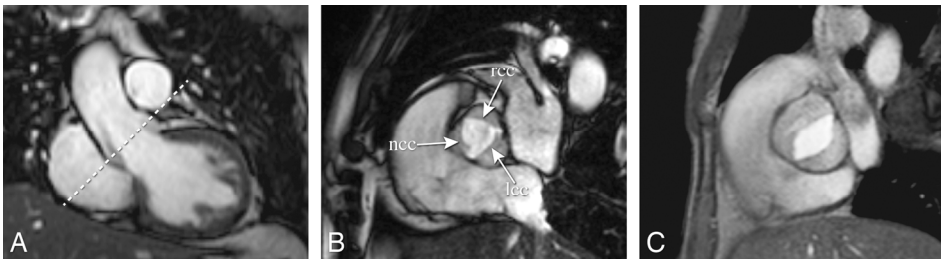

Figure 2.13 A segmented gradient-echo acquisition illustrating the aortic valve area at peak systole. In **(A)**, the planning of the acquisition plane is presented (*dotted line*). In **(B)**, a normal valve with three cusps is presented (lcc, left coronary cusp; rcc, right coronary cusp; ncc, noncoronary cusp), while in **(C)**, a bicuspid aortic valve is presented, with a fused noncoronary and left coronary cusp.

Opening of the atrioventricular valves is predominantly determined by pressure differences between the atria and ventricles. These differences are the result of the isovolumic relaxation of the ventricles. Furthermore, the motion of the valves is regulated by papillary muscles, which originate from the inferior myocardial wall and are connected to the valve leaflets by chordae tendineae. During contraction of the ventricle the papillary muscles contract as well, pulling on the chordae tendineae, closing the valves and preventing blood flow from the ventricles into the atria (i.e., regurgitation). Normally, in the RV three papillary muscles can be depicted: The anterior, the posterior, and the septal papillary muscle, respectively. The LV reveals two larger papillary muscles, the anterior and posterior papillary muscle.
Cine SSFP LA and SA images, as well as transverse images are all well suited for depicting morphology and function of the valvular apparatus. The valve leaflets can be depicted if spatial resolution is adequate. Dedicated acquisitions of specific valvular planes are used to image the valve area, which is especially useful when studying aortic valve competence. Both SSFP as well as fast gradient-echo sequences are used. Papillary muscles are well visualized on both cine brightblood as well as black-blood sequences. Chordae tendineae, on the other hand, are usually not sufficiently visualized by MRI due to the limited spatial resolution.

(Ultra -) High-Field Imaging

A decade ago, high-field 3-T whole-body MRI scanners have been introduced in clinical practice. Past studies reported 20% to 150% improvement in signal-to-noise ratio (SNR) for SSFP acquisitions at 3-T MRI when compared to 1.5 T,[13] but with the increase in field strength an increasing effect of imaging artifacts also occurred. For CMR imaging, SSFP techniques have been implemented at 3 T and optimized,[14] but especially SSFP sequences are more prone to field inhomogeneities, resulting in artifacts that may hamper image evaluation. The major source of artifact is off-resonance effects that become more pronounced at higher field strength.[15] Effective shimming of the B_0 magnetic field is paramount, but the heart is a difficult organ to shim owing to the complex field patterns in that region of the body (e.g., due to the lungs and liver).[16] Dedicated shim systems providing higher-order, cardiacphase–specific shimming have reported improved field homogeneity across the heart,[17] but currently, SSFP at high field remains not 100% reliable for use in CMR imaging. Alternative to SSFP sequences, multiple-phase fast gradient-echo sequences without SSFP may be used at high-field 3-T MRI or beyond.
Feasibility of CMR imaging at ultra-high–field 7-T MRI was first demonstrated by Snyder et al..[18] Besides the above-mentioned susceptibility artifacts, that are even more pronounced at 7 T, radio-frequency (RF) heating effects will limit the application

of SSFP at ultra-high–field even further. The specific absorption rate (SAR) level increases by the square of the field strength, and therefore, the use of SSFP has not yet been demonstrated at 7 T. Brandts et al. showed the feasibility of assessing LV volumes, function, and atrial–ventricular flow at 7-T MRI using standard multislice, multiphase cine gradient-echo and phase-contrast techniques, and they demonstrated similar quantitative results as compared to the gold standard of 1.5-T CMR.[19] Still, without the availability of dedicated hardware such as dedicated transmit/receive coils, and optimized imaging techniques, CMR at 7 T will remain an area of research.

References

1. Lenz GW, Haacke EM, White RD. Retrospective cardiac gating: A review of technical aspects and future directions. *Magn Reson Imaging.* 1989;7(5):445–455.
2. Ho SY, Nihoyannopoulos P. Anatomy, echocardiography, and normal right ventricular dimensions. *Heart.* 2006;92:I2–I13.
3. Cerqueira MD, Weismann NJ, Dilsizian V, et al. Standardized myocardial segmentation and nomenclature for tomographic imaging of the heart: A statement for healthcare professionals from the Cardiac Imaging Committee of the Council on Clinical Cardiology of the American Heart Association. *Circulation.* 2002;105:539–542.
4. Uribe S, Muthurangu V, Boubertakh R, et al. Whole-heart cine MRI using real-time respiratory self-gating. *MRM.* 2007;57:606–613.
5. Danilouchkine M, Westenberg J, Reiber J, et al. Accuracy of short-axis cardiac MRI automatically derived from scout acquisitions in free-breathing and breath-holding modes. *MAGMA.* 2005;18:7–18.
6. Miller S, Simonetti OP, Carr J, et al. MR imaging of the heart with cine true fast imaging with steady-state precession: Influence of spatial and temporal resolutions on left ventricular functional parameters. *Radiology.* 2002;223:263–269.
7. Kramer CM, Barkhausen J, Flamm SD, et al. Standardized cardiovascular magnetic resonance imaging (CMR) protocols, society for cardiovascular magnetic resonance: Board of trustees task force on standardized protocols. *J Cardiovasc Magn Reson.* 2008;10:10–35.
8. Alfakih K, Plein S, Bloomer T, et al. Comparison of right ventricular volume measurements between axial and short axis orientation using steady-state free precession magnetic resonance imaging. *J Magn Reson Imaging.* 2003;18:25–32.
9. Schneider B, Hofmaan T, Justen MH, et al. Chiari's network: Normal variant or risk factor for arterial embolic events. *J Am Coll Cardiol.* 1995;26:203–210.
10. Mansour M, Holmvang G, Sosnovik D, et al. Assessment of pulmonary vein anatomic variability by magnetic resonance imaging: Implications for catheter ablation techniques for atrial fibrillation. *J Cardiovasc Electrophysiol.* 2004;15(4):387–393.
11. Van der Voort PH, van den Bosch HCM, Post JC, et al. Determination of the spatial orientation and shape of pulmonary vein ostia by contrast-enhanced magnetic resonance angiogrpahy. *Europace.* 2006;8(1):1–6.
12. Stevenhagen J, van der Voort PH, Dekker LRC, et al. Three-dimensional CT overlay in comparison to Cartomerge for pulmonary vein antrum isolation. *J Cardiovasc Electrophysiol.* 2010;21:634–639.
13. Hinton DP, Wald LL, Pitts J, et al. Comparison of cardiac MRI on 1.5 and 3.0 Tesla clinical whole body systems. *Invest Radiol.* 2003;38:436–442.
14. Schär M, Kozerke S, Fischer S, et al. Cardiac SSFP imaging at 3 Tesla. *MRM.* 2004;51:799–806.
15. Tyler DJ, Hudsmith LE, Petersen SE, et al. Cardiac cine MR-imaging at 3 T: FLASH vs. SSFP. *J Cardiovasc Magn Reson.* 2006;8(5):709–715.
16. Atalay MK, Poncelet BP, Kantor HL, et al. Cardiac susceptibility artifacts arising from the heart–lung interface. *Magn Reson Med.* 2001;45:341–345.
17. Kubach MR, Bornstedt A, Hombach V, et al. Cardiac phase-specific shimming (CPSS) for SSFP MR cine imaging at 3 T. *Phys Med Biol.* 2009;54(20):N467–N478.
18. Snyder CJ, DelaBarre L, Metzger GJ,et al. Initial results of cardiac imaging at 7 Tesla. *Magn Reson Med.* 2009;61:517–524.
19. Brandts A, Westenberg JJ, Versluis MJ, et al. Quantitative assessment of left ventricular function in humans at 7 T. *Magn Reson Med.* 2010;64(5):1471–1477.

Chapter 3

Free-Breathing MRI for the Assessment of Myocardial Infarction: Clinical Validation

Harrie CM van den Bosch
Jos JM Westenberg
Johannes C Post
Glenn Yo
Jan Verwoerd
Lucia JM Kroft
Albert de Roos

AJR Am J Roentgenol. 2009; 192(6):277-281

Abstract

Objective

The objective of our study was to validate free-breathing 2D inversion recovery delayed-enhancement MRI for the assessment of myocardial infarction compared with a breath-hold 3D technique.

Subjects and Methods

Institutional review board approval and written informed consent were obtained. Thirty-two patients (25 men, seven women; mean age, 68 years; age range, 39–84 years) underwent breath-hold gradient-echo 3D inversion-recovery delayed-enhancement MRI and free-breathing respiratory-triggered 2D inversion-recovery delayed-enhancement MRI of the heart (scanning time, 50–80 seconds). Infarct size was quantitatively analyzed as a percentage of the left ventricle. The location and transmural extent of myocardial infarction were assessed by visual scoring. Intraclass correlation and Bland-Altman analysis were used to evaluate the agreement between the techniques for infarct quantification. Kappa statistics were used to analyze the visual score.

Results

Excellent agreement between the two techniques was observed for infarct quantification (intraclass correlation = 0.99 [p<0.01]; mean difference ± SD = 0.32% ± 2.4%). The agreement in assessing transmural extent of infarction was good to excellent between the free-breathing technique and the 3D breath-hold technique (kappa varied between 0.70 and 0.96 for all segments). No regions of infarction were missed using the free-breathing approach.

Conclusion

The free-breathing 2D delayed-enhancement MRI sequence is a fast and reliable tool for detecting myocardial infarction.

Introduction

In recent years MRI has gained widespread acceptance for assessing ischemic heart disease. In particular, the assessment of myocardial infarction using delayed-enhancement MRI is now routinely used for predicting recovery of left ventricle function after revascularization therapy.[1,2] Delayed-enhancement MRI provides the opportunity to evaluate the transmural extent of infarcted myocardium with superior spatial resolution compared with nuclear medicine techniques.[3–5]

Validated techniques for delayed-enhancement MRI include breath-hold approaches using a segmented 2D fast low-angle shot inversion-recovery sequence and a rapid 3D inversion-recovery acquisition.[6] Previous studies have shown good correlation between the two techniques for showing myocardial infarction and viability.[7,8]

A potential drawback of the segmented 2D fast low-angle shot inversion-recovery approach is the relatively long acquisition time. Images are acquired during 10–16 breath-holds of at least 10 heartbeats to cover the entire left ventricle in the short-axis orientation. Inability to perform adequate breath-holding and image misregistration may result in suboptimal results using this 2D approach.

The advantage of the 3D technique is that the acquisition of images encompasses the entire heart in a single breath-hold.[8] However, depending on the patient's heart rate, the 3D approach requires a breath-hold time of more than 20 seconds. Not all patients are able to perform such long breath-holds during acquisition, for example, patients with heart failure or respiratory discomfort. Therefore, it would be clinically desirable to have a delayed-enhancement MRI technique available that is not dependent on the ability of patients to hold their breath repetitively or for relatively long periods of time.

Recently, several new free-breathing delayed-enhancement MRI sequences in combination with navigator technology have been reported.[9,10] However, the use of navigator echo-gated techniques requires scanning times of several minutes, causing possible respiratory artifacts because of diaphragmatic drift and gross patient movement. Another limitation of the navigator approach is that the entire acquisition should be completed in less than 2 minutes to minimize changes in contrast concentration over time.[9] In addition, averaged, motion-corrected free-breathing delayed-enhancement MRI may suffer from artifacts because of through-plane motion, especially for acquisitions in the long-axis orientation.[11]

Most recently, the use of a 2D single-shot inversion-recovery steady-state free procession (SSFP) delayed-enhancement MRI sequence acquired during a single breath-hold has been reported for viability imaging.[12] This fast, 2D single-shot delayed-enhancement MRI sequence in conjunction with respiratory triggering using a respiratory belt allows the acquisition of delayed-enhancement MR images during free breathing.

To our knowledge, no previous study has been performed to validate this free-breathing 2D single-shot inversion-recovery SSFP delayed-enhancement MRI sequence approach for assessing myocardial infarction. Accordingly, the purpose of our study is to validate the free-breathing respiratory-triggered 2D single-shot inversion-recovery SSFP delayed-enhancement MRI sequence for the assessment of myocardial viability compared with the accepted 3D technique with breath-holding.

Subjects and Methods

Patients

In this study, 33 consecutive patients with clinically suspected chronic myocardial infarction were included. All patients were referred for MRI for evaluation of possible ischemic cardiomyopathy. The study was approved by the medical ethics committee and written informed consent was obtained from each patient. In one patient, the MR examination was terminated because of claustrophobia. Therefore, in 32 patients (25 men and seven women; mean age, 68 years; age range, 39–84 years) the MRI protocol was successfully completed.
Imaging was performed with the patient in the supine position on a 1.5-T MR system (Achieva, release 10.3; Philips Healthcare) with master gradients (maximum amplitude, 30 mT/m) using a dedicated 5-element phased-array cardiac coil and vector cardiographic triggering.

Delayed-Enhancement MRI Protocols

All patients were imaged using a free-breathing respiratory-triggered 2D single-shot inversion inversion-recovery SSFP delayed-enhancement MRI sequence and a breath-hold 3D fast-field echo (FFE, gradient-echo) inversion-recovery delayed-enhancement MRI sequence. The order in which the two different delayed-enhancement techniques were performed alternated in successive patients. Both delayed-enhancement MRI sequences were acquired in the short-axis orientation covering the entire left ventricle from base to apex. Delayed-enhancement MR images were acquired 10-15 minutes after IV contrast injection of gadoteridol (ProHance, Bracco) at 0.2 mmol per kilogram of body weight. Nulling of normal myocardium was accomplished by defining the optimum inversion time on scout images, which were performed before delayed-enhancement MRI examinations. ECG gating was used and acquisition was performed after every R wave trigger.
The free-breathing 2D approach consisted of a single-shot inversion-recovery SSFP delayed-enhancement MRI technique. Respiratory motion was triggered using a respiratory belt. Typical imaging parameters were as follows: TR/TE, 3.0/1.49; flip

angle, 45°; sensitivity encoding (SENSE)[13] factor, 1.5; acquired voxel size, 1.68 × 1.68 × 10.0 mm. The scanning time was between 50 and 80 seconds depending on the frequency of respiration. Images were acquired at end-diastole during an acquisition window of 292 milliseconds.
The breath-hold 3D technique consisted of a gradient-echo (FFE) inversion-recovery delayed-enhancement MRI sequence. The entire left ventricle was imaged during end-expiratory breath-hold. Typically, the breath-hold time was 24 seconds for a heart rate of 70 beats per minute. The imaging parameters were 3.7/1.15; flip angle, 15°; SENSE factor, 2.0; acquired voxel size, 1.71 × 1.71 × 10.0 mm. By radiofrequency excitation, one echo was acquired during an acquisition window of 217 milliseconds at end-diastole.

Qualitative and Quantitative Data Analysis

Delayed-enhancement MR images were presented in the same random order as acquired (the order in which the two different delayed-enhancement techniques were performed alternated in successive patients), and observers were blinded to the type of MRI sequence and patient information.

Image quality analysis

Image quality of the free-breathing 2D and the breath-hold 3D techniques was assessed by visual grading in consensus by two experienced cardiac MR radiologists, one with 10 years of experience and the other with more than 20 years of experience in cardiac MRI. Overall image quality was rated per scan per patient according to the following 4-point scale: 1, nondiagnostic; 2, diagnostic but with suboptimal image quality or motion artifacts; 3, good image quality but with some blurring or motion artifacts; and 4, excellent image quality with little or no motion artifacts.

Quantitative analysis of contrast-to-noise ratio (CNR)

The CNR between infarcted, enhanced myocardium and unenhanced myocardium in the same anatomic region for both MRI techniques was calculated by one reader. Regions of interests (ROI) to determine signal intensity (SI) were defined for the infarcted, enhanced myocardium and for the unenhanced myocardium in the same acquired image for both techniques. An additional ROI (± 10 cm^2) was placed in the field of view but outside the patient's body to determine the SD of noise.
The following equation was used:

$$CNR = [(SI_{infarct} - SI_{unenhanced}) / SD_{noise}].$$

Quantitative analysis of infarct size

For assessing the presence and extent of delayed enhancement representing infarcted myocardial tissue, delayed-enhancement MR images in the short-axis orientation of the left ventricle were divided into 16 segments, as recommended previously.[14] Endocardial and epicardial contours of the left ventricle and areas of hyper-enhancement within these contours were outlined manually on short-axis images. Infarct size was expressed as a percentage of left ventricular mass (% LV) by using the formula: [Σ (areas with delayed enhancement / left ventricular areas between endocardial and epicardial contours)] ×100.

Quantitative analysis of delayed-enhancement location and transmurality

Maximum transmural extent of hyper-enhancement in relation to the thickness of the myocardium was determined. The 16 segments in the short-axis orientation were graded on a 5-point scale in which the score of 0 indicated no hyper-enhancement; a score of 1, hyper-enhancement of 1–25% of wall thickness in each segment; a score of 2, hyper-enhancement of 26–50%; a score of 3, hyper-enhancement of 51–75%; and a score of 4, hyper-enhancement of 76–100% of the myocardial wall thickness.[1] Infarct location was assigned to the segmental level.

Statistical Analysis

Continuous variables are expressed as mean ± SD and range when appropriate. Agreement between both acquisition techniques (2D technique with free breathing and 3D technique with breath-holding) regarding image quality, infarct location, and transmurality was evaluated by weighted kappa statistics. Agreement in infarct size was evaluated by the two-way mixed intraclass correlation for absolute agreement. The approach described by Bland and Altman[15] was followed to study systematic differences. Mean differences and CIs were determined and statistical significance was tested using paired-samples Student's *t* tests. A *p* value of 0.05 was considered statistically significant.

Results

The free-breathing respiratory-triggered 2D single-shot inversion-recovery SSFP delayed-enhancement MRI sequence was completed successfully in all patients (100% success rate), whereas the breath-hold 3D gradient-echo inversion-recovery delayed-enhancement MRI sequence failed in two patients because of inability to perform adequate breath-holding and irregular heart rate (success rate, 94%). These two patients were excluded from the analysis.

Twenty-two of 30 patients who were evaluated with both methods showed regions of myocardial hyper-enhancement at both imaging techniques, confirming the presence of ischemic cardiomyopathy (Figure 3.1). In the remaining eight patients, no infarcted regions were identified with either technique.

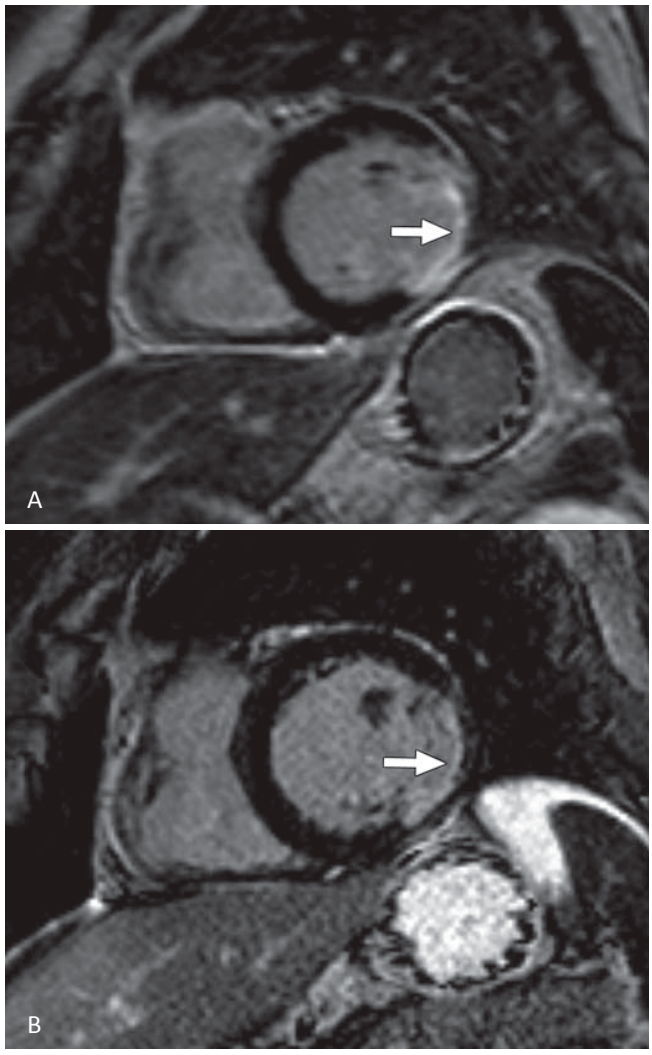

Figure 3.1 58-year-old man with myocardial infarction in inferolateral segment after occlusion of left circumflex artery. **(A)** Breath-hold 3D gradient-echo inversion-recovery delayed-enhancement MR image shows myocardial infarction (*arrow*) with hyperintense signal intensity. Extent of infarction is subendocardial. **(B)** Free-breathing 2D single-shot inversion-recovery SSFP delayed-enhancement MR image shows myocardial infarction (*arrow*) with hyperintense signal intensity. Extent of infarction is subendocardial. For both sequences area of infarction is identical.

Image Quality

Image quality was scored visually and graded on a 4-point scale. For the 2D free-breathing technique, 20 cases were scored as good and 12 cases as excellent (mean score, 3.3). For the 3D technique, two patients were not included because the data could not be obtained. In two cases, the image quality score was 2 (diagnostic but suboptimal). In 19 cases, image quality was good, and in the remaining nine cases, image quality was excellent (mean score, 3.2).

Quantitative Analysis of CNR

The CNR between infarcted, enhanced myocardium and unenhanced myocardium was significantly higher in the free-breathing 2D MRI approach compared with the breath-hold 3D MRI approach (545 ± 201 vs 327 ± 156, p<0.001).

Quantitative Analysis of Infarct Size

Quantitative analysis revealed excellent agreement between the two delayed-enhancement MRI techniques for the estimation of infarct size expressed as percentage of left ventricular mass. Intraclass correlation was 0.99 (p<0.01). Mean infarct size was 11% ± 12% with a range of 0%–65% for free-breathing 2D MRI versus 11% ± 12% with a range of 0%–61% for breath-hold 3D MRI. Differences, presented in a Bland-Altman plot (Figure 3.2), were small (0.32% ± 2.4%), not statistically significant (p=0.46), and nonsystematic. The 95% CI was small (−4.4% to 5.0%).

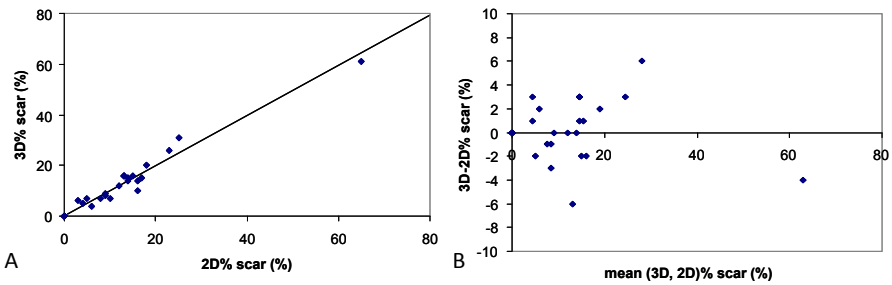

Figure 3.2 Comparison of techniques: free-breathing 2D single-shot inversion-recovery steady-state free precession delayed-enhancement MRI (2D) and breath-hold 3D gradient-echo inversion-recovery delayed-enhancement MRI (3D). **(A)** Graphic shows relation between infarct size expressed as percentage of left ventricular mass for 2D imaging versus infarct size assessed with 3D imaging. **(B)** Bland-Altman plot shows differences between 2D and 3D imaging are small (0.32% ± 2.4%), not statistically significant (p = 0.46), and nonsystematic; 95% CI is small (−4.4% to 5.0%).

Data distribution revealed a single outlier that could affect the statistical results. Removing this outlier—in this patient, the 2D technique with free-breathing revealed a scar of 65%, whereas the 3D technique with breath-holding showed 61%—shows comparable results: intraclass correlation, 0.98 (p<0.01); mean infarct size, 9% ± 7% (range, 0%–25%) for free-breathing 2D MRI versus 9% ± 8% (range, 0%–31%) for breath-hold 3D MRI with small (0.5% ± 2.3%), not statistically significant (p=0.28), and nonsystematic differences and a small 95% CI (−4.0% to 5.0%).

Location and Transmurality

In the 30 patients with diagnostic images for both scanning methods, 16-segment analysis showed good agreement in presence and transmurality of delayed enhancement. No regions of infarction were missed on the free-breathing 2D images compared with the breath-hold 3D technique.

In 468 of 480 segments, the classification of the transmural extent with the free-breathing 2D scanning showed good concordance with the breath-hold 3D technique (Figure 3.3). For all segments, the weighted kappa varied between 0.70 and 0.96. In the remaining 12 segments, the difference between the two methods was a maximum of one grade.

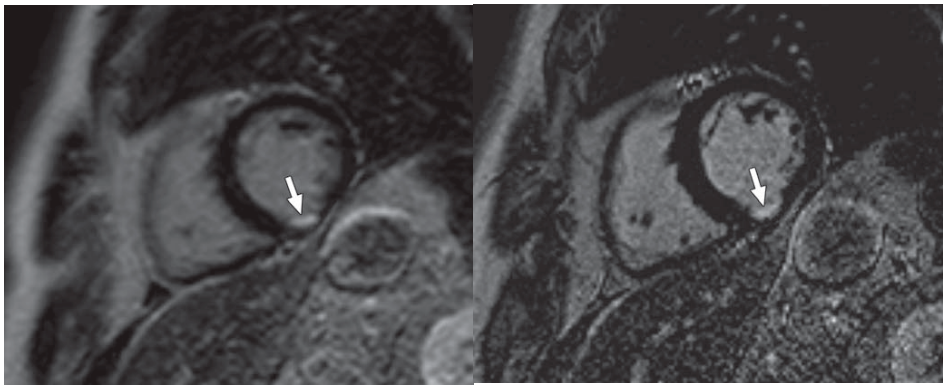

Figure 6.3 61-year-old man with myocardial infarction in inferior segment after occlusion of right coronary artery. **(A)** Breath-hold 3D gradient-echo inversion-recovery delayed-enhancement MR image shows myocardial infarction (*arrow*) with hyperintense signal intensity. **(B)** Free-breathing 2D single-shot inversion-recovery steady-state free precession delayed-enhancement MR image shows myocardial infarction (*arrow*) with hyperintense signal intensity. Both techniques show excellent agreement of maximum transmural extent of hyper-enhancement in relation to thickness of myocardium.

Discussion

The main findings of our study are the following: First, free-breathing, respiratory-triggered 2D single-shot inversion-recovery SSFP delayed-enhancement MRI is comparable to breath-hold 3D segmented gradient-echo inversion-recovery delayed-enhancement MRI when used for quantification of left ventricular scar. Second, the 2D technique with free breathing is well-tolerated and provides an alternative when patients are not capable of performing breath-holding. Third, CNR is higher for the 2D technique with free breathing compared with the 3D breath-hold technique. The free-breathing technique was successfully completed in all patients, whereas two patients failed to complete the 3D delayed-enhancement breath-hold examination because of inability to perform adequate breath-holding, underscoring the potential use of the 2D approach in patients who have difficulties with breath-holding during image acquisition.

The reference standard for assessing viability by delayed hyperenhancement is 2D inversion-recovery fast low-angle shot imaging.[6,16] The long acquisition time and use of multiple breath-holds to cover the entire left ventricle are considered major drawbacks. Single breath-hold imaging in conjunction with a 3D MRI sequence has been validated against the 2D reference standard as an alternative acquisition to overcome the limitations of the 2D technique.[7,8] The necessary breath-hold time for the 3D sequence is significantly shorter compared with the 2D approach, whereas the two techniques agree very closely for assessing the transmural extent of infarction. A high technical success rate for the 3D acquisition has been reported.[7,8,17]

In the current study, we compared a free-breathing 2D technique that was triggered to respiratory motion with the use of a respiratory belt to a standard breath-hold 3D technique. The acquisition time varies between 50 and 80 seconds for the free-breathing technique compared with approximately 25 seconds of breath-hold for the 3D technique, depending on respiratory frequency and the heart rate, respectively. The data for the 3D technique are acquired over several heartbeats, making this technique more sensitive to motion artifacts because of heart rate variability and arrhythmia. The free-breathing respiratory triggered 2D single-shot sequence overcomes this limitation by acquiring one slice during one R-R interval and may therefore be less sensitive to arrhythmia.

The spatial resolution was similar for both techniques. The CNR was significantly higher in the free-breathing 2D MRI approach compared with the breath-hold 3D MRI approach (545 ± 201 vs. 327 ± 156, $p<0.001$). In recent literature, it has been shown that a 2D single-shot inversion-recovery SSFP delayed-enhancement MRI sequence has a lower CNR compared with a segmented 2D fast low-angle shot inversion-recovery sequence. In concordance with our results, Huber et al.[12,18] have shown that assessment of the volume of infarcted myocardium is possible with excellent correlation.

The results of this study show that the visual scores of infarct location and transmural extent are very similar between both techniques, indicating the potential clinical use of the free-breathing approach. In a limited number of segments, a difference between the two techniques was found, but the difference was not more than one grade when using the 5-point scale for transmurality of infarction. No areas of infarction went undetected using the free-breathing technique compared with the reference standard. Furthermore, when comparing the quantitative analysis of infarct size, the two techniques revealed close agreement, underscoring the reliability of the free- breathing approach for infarct imaging.

The performance of inversion-recovery delayed-enhancement techniques is sensitive to the selection of the appropriate inversion time. In our study, the optimal inversion time was selected for both the breath-hold 3D approach and the free-breathing 2D approach separately. Therefore, we believe that we have minimized the possible effect of changes of infarct size over time after the administration of the contrast agent. No systematic differences regarding infarct size were observed between the two techniques.

We acknowledge some possible limitations of the current study. The use of the respiratory belt requires a relatively stable and reproducible respiration pattern that can be registered through the belt. The acquisition time of the images may therefore vary between 50 and 80 seconds depending on the breathing pattern. Furthermore, the 2D free-breathing technique was compared with the 3D breath-hold technique, whereas 2D inversion-recovery fast low-angle shot imaging with breath-holding is more commonly used as a standard of reference.[6,16]

The excellent diagnostic value and clinical success rate of the 2D free-breathing technique support its clinical application as a possible first-line or second-line technique for assessing myocardial viability, depending on patient compliance and ability to follow breathing instructions.

In conclusion, the free-breathing, respiratory-triggered single-shot inversion-recovery approach appears to be a fast and reliable technique to assess myocardial infarct size and transmurality after administration of a gadolinium-based contrast agent.

References

1. Kim RJ, Wu E, Rafael A, et al. The use of contrast-enhanced magnetic resonance imaging to identify reversible myocardial dysfunction. *N Engl J Med* 2000; 343:1445–1453.
2. Edelman RR. Contrast-enhanced MR imaging of the heart: overview of the literature. *Radiology* 2004; 232:653–668.
3. Klein C, Nekolla SG, Bengel F, et al. Assessment of myocardial viability with contrast-enhanced magnetic resonance imaging: comparison with positron emission tomography. *Circulation* 2002;105:162–167.
4. Wagner A, Mahrholdt H, Holly TA, et al. Contrast-enhanced MRI and routine single photon emission computed tomography (SPECT) perfusion imaging for detection of subendocardial myocardial infarcts: an imaging study. *Lancet* 2003; 361:374–379.
5. Kitagawa K, Sakuma H, Hirano T, et al. Acute myocardial infarction: myocardial viability assessment in patients early thereafter—comparison of contrast-enhanced MR imaging with resting ^{201}TI SPECT. *Radiology* 2003; 226:138–144.
6. Simonetti OP, Kim RJ, Fieno DS, et al. An improved MR imaging technique for the visualization of myocardial infarction. *Radiology* 2001;218:215–223.
7. Kühl HP, Papavasiliu TS, Beek AM, Hofman MB, Heusen NS, van Rossum AC. Myocardial viability: rapid assessment with delayed contrast-enhanced MR imaging with three-dimensional inversion-recovery prepared pulse sequence. *Radiology* 2004; 230:576–582.
8. Dewey M, Laule M, Taupitz M, et al. Myocardial viability: assessment with three-dimensional MR imaging in pigs and patients. *Radiology* 2006;239:703–709.
9. Saranathan M, Rochitte CE, Foo TK. Fast, threedimensional free-breathing MR imaging of myocardial infarction: a feasibility study. *Magn Reson Med* 2004; 51:1055–1060.
10. Spuentrup E, Buecker A, Karassimos E, Günther RW, Stuber M. Navigator-gated and real-time motion corrected free-breathing MR imaging of myocardial late enhancement. *Rofo* 2002; 174:562–567.
11. Kellman P, Larson A, Hsu L, et al. Motion-corrected free-breathing delayed enhancement imaging of myocardial infarction. *Magn Reson Med* 2005; 53:194–200.
12. Huber A, Schoenberg SO, Spannagl B, et al. Single-shot inversion recovery trueFISP for assessment of myocardial infarction. *AJR* 2006; 186:627–633.
13. Pruessmann KP, Wieger M, Scheidegger MB, Boesiger P. SENSE: sensitivity encoding for fast MRI. *Magn Reson Med* 1999; 42:952–962.
14. Cerqueira MD, Weissman NJ, Dilsizian V, et al. Standardized myocardial segmentation and nomenclature for tomographic imaging of the heart. *Circulation* 2002; 105:539–542.
15. Bland JM, Altman DG. Statistical methods for assessing agreement between two methods of clinical measurement. *Lancet* 1986; 1:307–310.
16. Kim RJ, Fieno DS, Parrish TB, et al. Relationship of MRI delayed contrast enhancement to irreversible injury, infarct age and contractile function. *Circulation* 1999; 100:1992–2002.
17. Peukert D, Laule M, Taupitz M, et al. 3D and 2D delayed-enhancement magnetic resonance imaging for detection of myocardial infarction: preclinical and clinical results. *Acad Radiol* 2007;14:788–794.
18. Huber A, Schönberg SO, Spannagl B, Rieber J, Klauss V, Reiser MF. Determining myocardial viability in myocardial infarct: comparison of single and multislice MRI techniques with turboFlash and trueFISP sequences [in German]. *Radiologe* 2004; 44:146–151.

Chapter 4

Cardiovascular Magnetic Resonance Angiography: Carotids, Aorta, and Peripheral Vessels

Harrie CM van den Bosch
Jos JM Westenberg
Albert de Roos

based on
Chapter 45 Cardiovascular Magnetic Resonance Angiography: Carotids, Aorta, and Peripheral Vessels
in Cardiovascular Magnetic Resonance, 3rd Edition, 2018
Warren J Manning and Dudley J Pennell
Elsevier

Magnetic resonance angiography (MRA) is an important imaging modality for the diagnosis, clinical work-up and treatment planning in patients suspected for a wide range of vascular pathology. The aim of MRA is to visualize the arterial and/or venous system by creating high contrast between blood flow and its surrounding stationary tissue. To fulfill this aim, several techniques may be used in clinical practice. Depending on its demands and the conditions required to optimally visualize specific vessels of interest, imaging techniques are chosen. In the first part of this Chapter, techniques will be addressed that are currently available and applied for MRA. Contrast-enhanced MRA (CE-MRA) is probably the most widely used MRA technique. CE-MRA is applied either by fast imaging of the first-pass of an intravenously injected bolus of a gadolinium chelate agent, or by a prolonged imaging approach with a blood-pool contrast agent. The latter approach is applied when imaging requires a time window that surpasses the first arterial pass. Because of the reported adverse events (i.e., nephrogenic systemic fibrosis, accumulation of gadolinium in the brain, kidneys and bone tissue) associated with gadolinium (Gd)-based contrast agents, an increasing interest in non-CE-MRA techniques is currently observed. Black-blood and bright-blood non-CE-MRA techniques will be discussed. Finally, flow imaging by time-resolved three-dimensional phase contrast (i.e. 4D flow MRI), with the aid of newly developed visualization tools, is a relatively new technique that may be used to visualize complex flow structures and add quantitative hemodynamic information as well.
In the second part of this Chapter, we will address the anatomical regions that are imaged by MRA and discuss the state-of-the-art. Special focus will be on the carotid arteries, thoracic and abdominal aorta, renal arteries, mesenteric artery, and the peripheral arteries.

Contrast Enhanced MR Angiography: technical approach

In CE-MRA, vessels in the field-of view of interest are imaged during the arterial first-pass of intravenously injected paramagnetic contrast material.[1] These contrast agents have a short T1 relaxation time and will produce high signal on T1-weighted images. In clinical practice, Gd-bound chelates, for example DTPA (diethylenetriamine pentaacetic acid), are used as paramagnetic contrast agents. The gadolinium ion is a rare-earth element, and toxic to humans when unbound. Therefore, in MRI, gadolinium contrast is based on chelates and thereby, controlling the distribution of gadolinium within the body and to overcome toxicity however maintaining their contrast enhancement capacity. A very important property of these chelates is their chemical stability, which depends on the chemical structure and ionicity of the complex.[2] A stable chelate has less tendency to release free gadolinium ions in the

human body. Gadolinium chelates can be distinguished in two structural categories: macrocyclic and linear gadolinium chelates. In macrocyclic structures, the gadolinium chelate is more stable and, therefore, the chance of free gadolinium ions in the body is reduced. Breaking of the bond between gadolinium and the chelate (transmetallation) is more likely to occur with linear agents than with macrocyclic agents. However, even the fact that macrocyclic agents are more resistant to transmetallation, development of NSF is described in patients with severe renal failure after several gadolinium contrast administrations.[3] Most reported cases of nephrogenic systemic fibrosis are linked with linear Gd-chelates. Awareness of this association has given rise to effective screening of patient with possible renal failure, use of more stable Gd-chelates, and international recommendations for the use of Gd-based contrast agents in daily practice.[4,5,6]

Gd-chelates create intravascular signal by shortening the T1 relaxation time of blood in proportion to the concentration of contrast material. At 1.5T, T1 of blood is 1200 ms. The T1 relaxation time is shortened by gadolinium according to equation 1[7]:

$1/T1 = 1/1200\ ms + R_1[Gd]$ *{Equation 1}*

R_1 = T1 relaxivity of gadolinium, [Gd] = gadolinium concentration in blood.

Gadolinium-enhanced MRA is insensitive to blood flow, in contrast to non-CE-MRA techniques as time-of-flight (TOF) and phase-contrast (PCA) MRA. Consequently, in CE-MRA, image quality is not degraded by flow disturbances.

Gadolinium contrast agents can be classified depending on their distribution in tissue after intravenous administration, e.g. extracellular or intravascular. Most of the gadolinium chelates used in clinical routine are extracellular agents. After intravascular administration they diffuse rapidly through the capillary walls into the extravascular space. In CE-MRA, arteries are preferably imaged during the initial passage of contrast. Timing of starting the image acquisition is essential to reduce signal from gadolinium diffused to the extracellular space and to overcome venous enhancement, which can lead to artifacts and image degradation.

The application of CE-MRA was improved by the introduction of Gd-chelates that have the capability to bind to larger molecules in the blood such as albumin. These contrast agents (e.g. gadobenate dimeglumine) provide a prolonged imaging time window due to a decreased decay time of contrast in blood. The use of such agents enables imaging beyond the initial passage of contrast bolus, which may be a benefit when acquisition needs to be gated to cardiac or respiratory motion, or when high resolution is required in small vessels such as the coronaries.[8] When compared to an extravascular Gd-chelate, blood pool agents show an improved conspicuity of small vessels (9). Further development of macromolecular blood pool agents in the near future may play an important role in CE-MRA.

3D Contrast-enhanced MRA Pulse sequences

The MRI sequence that is used in CE-MRA needs to fulfill the following needs: T1-weighting is required as well as obtaining a large 3D volume with sufficient spatial resolution, preferably fast within the first-pass of contrast and within a breath hold to suppress respiratory motion. Therefore, fast T1-weighted 3D spoiled gradient-echo (GRE) sequences are used for image acquisition. In clinical routine, 3D CE-MRA preferentially is performed on a 1.5T or 3T system with strong gradient systems to reduce scan time as such that 3D datasets can be acquired during breath-holding. Typically, short repetition times (TR) and echo times (TE) are used, 3-8 ms and 1-3 ms, respectively. Flip angle is 20^{o}-40^{o} to achieve optimized T1-weighting.
Furthermore, subsampling imaging techniques such as parallel imaging are implemented to reduce total scan time.[10] Advanced k-space sampling techniques (spiral, keyhole, echo planar imaging) may be used as well to speed up acquisition.
At postprocessing, the 3D nature of the dataset allows viewing of the data from any desired angle, i.e. by creating multi-planar reformats (MPR) or rotational maximum-intensity-projection (MIP). This results in multiple images in various anatomic orientations. Thin (i.e., <3 mm thick) slices are required in order to provide a useful evaluation of these images. In some situations, it may be useful to use thicker slices (e.g., 10 mm) to reduce the number of slices and allow faster scanning. Although the ability to rotate the MIP is lost with such thick slices, scan times can be as short as 1 second.

Bolus timing

Precise bolus timing is essential for first-pass CE-MRA. Arterial imaging is performed in the time window between arterial and venous enhancement and this time window depends on the rate of contrast agent injection, and will be patient specific.[11] The transit time of contrast from the injection site (usually in the veins in the arm) to the field-of-view with the vessels of interest depends on several factors, e.g. injection rate, injection site, heart rate, and stroke volume.
The gadolinium contrast concentration in the arterial blood is proportional to the injection rate and inversely proportional to the cardiac output:

$[Gd]_{arterial}$ = injection rate (mol/sec) / cardiac output (L/sec) *{Equation 2}*

T1 for blood is related to the injection rate and cardiac output by combining equation 1 and 2.[12]
Maximum arterial signal intensity is achieved when the start of the acquisition and the contrast infusion are synchronized such that peak arterial gadolinium concentration coincides with the acquisition of the central portion of k-space.[13] The center of k-space contributes most to overall image contrast, whereas the periphery of k-space

provides image information of details and contributes to spatial resolution. Therefore, for improved arterial/venous differentiation central k-lines have to be sampled before venous return. In CE-MRA, different types of k-space filling can be used in the available 3D pulse sequences. It is important to adjust bolus timing to the order of k-space filling used.
In linear ordering, lines of k-space can be acquired in any order (high k-space lines first, low k-space lines first, or at random). Linear ordering can be used in a CE-MRA protocol when precise timing of the contrast bolus is difficult or arrival time may be prolonged.
For most CE-MRA examinations, elliptical-centric ordering is the preferred k-space sampling method used. Typically, the center of k-space is acquired first and the periphery later (e.g. elliptic-centric, CENTRA ("Contrast-ENhanced Timing Robust Angiography"),[14] DRKS ("Differential Rate K-space Sampling"), or PEAKS ("PEak Arterial K-Space filling")).
To determine the delay between the start of the venous contrast injection and the start of the acquisition, either a small test bolus or fluoroscopic real-time imaging can be used. The timing method by using a test bolus (1 to 2 mL) is robust and easy to perform. However, it will lengthen the procedure with a few minutes and requires an additional administration of contrast. In fluoroscopic real-time imaging, the inflow of contrast is imaged in the field-of-view with the vessels of interest. At the moment of contrast arrival, the acquisition is started automatically, however, a disadvantage can be the short delay of a few seconds, which is needed to switch from the fluoroscopic real-time imaging to the actual start of CE-MRA acquisition.

Contrast-enhanced versus non-contrast-enhanced MRA

In recent years the association between CE-MRA and nephrogenic systemic fibrosis (NSF) has been reported.[15,16] The occurrence of NSF has been described exclusively in patients with severe renal failure and developed most frequently after administration of linear Gd-chelates.[4]
Moreover, gadolinium accumulation in tissue in patients without renal impairment has been reported in several studies. Kanda et al. reported residual gadolinium concentrations in the brain, particularly in the dentate nucleus and globus pallidus, of patients without severe renal dysfunction[17] and foci of hyperintensity on unenhanced T1-weighted MR images associated with previous administration of linear Gd-chelates and may be associated to the total number of previous gadolinium-based contrast material administrations.[18] Deposition of gadolinium has also been demonstrated in bone, skin, and, liver.[19,20]

Currently, previous administration of macrocyclic Gd-chelates showed no association with gadolinium accumulation in tissue yet,[21,22] however, these macrocyclic contrast chelates have been in use in clinical practice for a shorter time than the linear chelates.
Nevertheless, the application of CE-MRA and the amount of administered contrast is of clinical importance, especially in patients with impaired renal function. Awareness of NSF-related incidents associated with CE-MRA and reports on accumulation of gadolinium in various tissues have also led to a renewed interest in non-CE-MRA. Improvements in MR hardware and software, including the widespread availability of parallel imaging have helped to reduce acquisition times and have made some non-CE-MRA methods clinically practical.
Non-CE-MRA methods may be classified into three categories, black-blood, bright-blood and 4D flow visualization.

Black-blood imaging

Black-blood imaging of blood vessels uses double-inversion recovery to null the signal of flowing blood.[23] This technique is flow-sensitive. Two 180º inversion recovery prepulses are applied to null the signal of flowing blood: the first prepulse is non-slice selective and inverts the longitudinal magnetization vector in the entire body, while the second prepulse is slice selective and inverts the magnetization in the imaging slice back to its original orientation. Signal of blood entering the imaging slice after the second prepulse has undergone reinversion and will appear dark in the images. ECG-gated partial Fourier Fast Spin-Echo (FSE) is the sequence of choice,[24,25] using a slice thickness of 6 to 8 mm stacked in the transverse plane of the chest or in a double-oblique sagittal view of the aorta (i.e., the candy cane view). Single-shot FSE (SSFSE) sequences are much faster than basic FSE sequences and allow for acquisition of the entire imaging stack in a single breath-hold. Fat saturation is recommended to increase the conspicuity of aortic wall hematoma.[26] Despite being an established technique, black-blood imaging is prone to artifacts, as inadequate nulling of blood signal may occur by slow flow, or when in-plane blood flow is present.

Bright-blood imaging: Time-Of-Flight (TOF)

TOF methods depend on the inflow enhancement of flowing blood and the relative saturation of longitudinal magnetization of stationary tissue to produce high contrast. The longitudinal magnetization from the background tissue is suppressed by multiple RF excitations, such that the magnetic spins associated with background tissue do not have sufficient time to fully regain their longitudinal magnetization. Saturation of background signal will reach a steady-state determined by the flip angle, repetition

time and the T1 of the background tissue. This saturation will make stationary tissue appear dark in TOF images. The bright signal intensity of flowing blood is the consequence of the continuous inflow of fresh, unsaturated blood into the imaging slice, which produces more signal than the surrounding stationary tissue, as the latter was repeatedly exposed to RF pulses.[27] This effect is known as flow-related enhancement[28] and can be maximized by using sequences with a short repetition time (TR). Ideally, the imaging slice should be thin and oriented perpendicular to the direction of flow. Electrocardiographic (ECG) gating can be used to optimize synchronization of acquisition to the blood flow to the cardiac cycle and consequently to the signal present in the artery of interest.
2D and 3D TOF techniques are in use. 2D TOF with consecutive slices stacked together can produce excellent contrast in the vessels when the imaging slices are planned perpendicular to the vessels of interest. When in-plane flow occurs, the longitudinal magnetization of blood will become saturated and signal is progressively lost. Additionally, venous signal may be suppressed with presaturation slabs, positioned parallel and next to the imaging slices, in order to saturate longitudinal magnetization of blood flowing into the imaging slice from the opposite side of arterial blood flow. Resolution of 2D TOF is often limited by the used slice thickness. However, thin slice acquisitions are possible, but acquisition time will increase with the amount of slices required to cover the vasculature and signal-to-noise ratio will decrease with decreasing slice thickness.
3D TOF may be performed with isotropic voxel sizes of 1 mm^3. High resolution is essential to visualize small branch vessels, stenosis or to provide a clear delineation of tortuous vessels. 3D TOF has to deal with saturation effects of arterial blood flow, especially slow flow. On the other hand, SNR will be increased by using 3D imaging. Decreasing the flip angle may reduce excessive saturation effects.

Bright-blood imaging: Phase Contrast Angiography (PCA)

In PCA, the contrast between flowing blood and the surrounding stationary tissue is generated by the flow-induced phase shift in the transverse magnetization of the moving blood. As the magnetic field strength and the precession frequency of spins are linearly related, the precession frequency will increase when spins move along a positive gradient in the magnetic field. Compared to spins that remain fixed in position (i.e., in stationary tissue), moving spins (i.e., in flowing blood) will accumulate phase in the transverse magnetization. This phase shift is proportional to its velocity and the gradient strength.[29] In addition to such a velocity-sensitive acquisition, a velocity-compensation acquisition is defined. Such acquisition uses a bipolar gradient with equal positive and negative effect to achieve no difference in net phase shift between spins moving with uniform velocity. PCA uses the subtraction of both velocity-sensitive and velocity-compensation acquisitions to visualize moving spins.

The velocity can be directly quantified from the resultant phase images. A priori to the acquisition the velocity sensitivity needs to be determined by choosing the Venc, i.e., the outer limit of the velocity range that is encoded by the phase shift of +180° and -180°.

TOF and PCA, two conventional bright-blood non-CE-MRA techniques, were highly time consuming and moreover, suffered from artifacts caused by turbulence and in-plane saturation. In a meta-analysis,[30] the sensitivity and specificity for the detection of significant stenosis (>50% luminal reduction) for 2D TOF ranged from 64% to 100% and 68% to 96%, compared to 92% to 100% and 91% to 99%, respectively for CE-MRA. Such limitations resulted in declining interest for TOF and PCA in favor of CE-MRA. However, in association with the reported adverse events from gadolinium usage, an increase in interest in new bright-blood non-CE-MRA techniques is occurring.

Bright-blood imaging: Steady-State Free-Precession (SSFP)

SSFP produces high signal intensity for blood, due to the inherently T2/T1-weighted image contrast which is high for all fluids, independent from inflow effects. ECG-gated cine acquisitions with SSFP are used to visualize the anatomy of thoracic aorta with breath-hold sequences. Aneurysms, coarctation and stenosis or dissection flaps can be visualized using this approach. The aortic root is best evaluated in multiple planes, including long-axis planes of the left ventricular outflow tract (LVOT). The remainder of the thoracic aorta is best evaluated with images in the transverse plane of the chest and in the double-oblique sagittal candy-cane view. SSFP sequences are susceptible to magnetic field inhomogeneity, which are particularly present at high field strength. Off-resonance artifacts may result in non-diagnostic images. Dedicated shimming algorithms may aid in minimizing these off-resonance artifacts.

Bright-blood imaging: Dixon

Another relatively new bright-blood approach relies on an old technique based on the chemical shift between both water and fat. Dixon's water-fat separation[31] uses the phase shift from the water-fat resonance frequency and by using carefully chosen multiple echo times, excellent separation between water and fat is achieved in four distinct images: separate water and fat images as well as images with signal from both tissues in- and out-of-phase. The Dixon technique may be applied for MRA purposes, its application may be promising for imaging of the coronaries as well as the thoracic aorta.[32]

Blood flow visualization with 4D flow MRI

Phase-contrast imaging enables quantitation of blood flow velocity in the direction of a magnetic field gradient. In addition to conventional through-plane one-directional velocity-encoding, advanced 3D time-resolved imaging is possible with velocity-encoding in all three directions, providing the temporal distribution of a velocity vector field, representing the flow of blood inside a 3D volume (i.e., so-called 4D flow data).[33] Visualization tools such as streamline and pathline visualization have been developed to display this data and to segment blood vessels of interest from their surrounding tissue. The usability of this technique has been shown in the aorta and pulmonary arteries, the carotid artery, the abdominal circulation as well as the circulation in the brain. While this technique is still a research application, a lot of effort has been made in recent years to translate this technique towards the clinic.[34] The additional hemodynamic information (e.g. wall shear stress, stenotic pressure drop, pulse wave velocity, viscous energy dissipation) which becomes available with 4D flow MRI in combination with the excellent 3D visualization possibilities of complex vascular structures and pathologies, may eventually push this modality towards a clinical viable application.

Artifacts in CE-MRA

In CE-MRA, images with maximum arterial signal intensity are obtained when the acquisition of the central portion of k-space coincides with peak arterial gadolinium concentration. Timing of bolus arrival and imaging within the time window of arterial enhancement is critical to minimize artifacts. Starting the acquisition too early, when the contrast bolus is still arriving in the vessels of interest, can cause ringing or so-called Maki artifacts.[13] Starting the acquisition too late will lead to imaging outside the time window of arterial enhancement, causing venous enhancement hampering the evaluation of arterial vasculature. Such artifacts may result in degradation of image quality and misclassified diagnosis.

Artifacts are most evident when the center of k-space is acquired before the peak of intravascular gadolinium arrival.[13] The Maki artifact for example, results in a central dark line in the vessel, from which a so-called pseudo-dissection can appear, when the contrast bolus arrives in the vessel of interest after sampling of the central k-lines. Overestimation of the length of a stenosis can occur due to signal loss because of turbulence and in-plane saturation. Generally, this latter artifact is not present in CE-MRA, however, signal loss can occur in the stenosis caused by high velocity rates, especially in combination with low contrast material concentration.[35]

Erroneously, an occlusion can be apparent in tortuous arteries when the vessel of interest is not completely covered inside the field-of-view. Parallel to vessels with very high signal intensity ghosts (i.e. phase artifact) can be seen.[36]
Movement of the patient between the acquisition of the mask and the CE-MRA may lead to subtraction artifacts, leading to image degradation. Signal loss caused by susceptibility can be seen when clips, metallic stents or prostheses are present.

In non-CE-MRA, artefacts may also results in image degradation or even lead to misdiagnosis. Post-stenotic signal loss due to turbulence or in-plane saturation in phase contrast imaging may lead to an overestimation of a stenosis. When the a priori set velocity sensitivity (Venc) is too low, aliasing will occur in the velocity images and when uncorrected will result in a decrease in signal in the phase contrast magnitude images.
On the other hand, slow flow in TOF imaging may lead to similar misdiagnosis when vascular signal decreases. In black-blood imaging, in-plane flow may lead to vascular enhancement and inadequate signal suppression when the imaging slice is too thick.
SSFP is very susceptible to off-resonance artifacts, especially at higher field strength and non-optimal shimming, which may degrade image quality to the point of non-evaluable for clinical diagnosis.

Magnetic resonance angiography of the extracranial carotid arteries

Atherosclerosis of the extracranial carotid arteries is an important cause of stroke.[37] Worldwide stroke is a major health concern, for example approximately 795,000 patients with a stroke are reported in the United States every year.[38] Around 610,000 patients are new attacks and 185,000 patients experience a recurrent episode of stroke. Stroke can lead to significant disability in nonfatal cases and accounts for approximately 1 of every 20 deaths in the United States.
Carotid atherosclerosis is a significant factor for risk stratification and is associated with more than a doubling in the risk of stroke after a transient ischemic attack.[39]
Therefore, accurate evaluation of the extracranial carotid artery is essential.
For evaluating the severity of carotid stenosis, digital subtraction angiography (DSA) remains the standard of reference. This imaging approach has certain limitations, including invasiveness and the use of ionizing radiation. Moreover, DSA involves a small risk of stroke on the order of around 0.5-4%.[40]
Therefore, nowadays non-invasive imaging techniques play an important role in the routine assessment of patients with suspected carotid artery. Non-invasive techniques

as duplex ultrasound (DUS), CE-MRA and computed tomography angiography (CTA) are widely available and have replaced invasive arteriography in daily clinical routine.
When compared to DSA, non-invasive imaging techniques generally are less accurate for low degree carotid artery stenoses. Meta-analysis showed sensitivity and specificity for DUS of 36% and 91% respectively for 50% to 69% stenosis degree of the internal carotid artery, 77% and 97% respectively for CE-MRA, and 67% and 79% respectively for CTA.[41] Non-invasive techniques revealed higher sensitivity and specificity for high grade stenosis (70%-99%), DUS 89% and 84%, CE-MRA 94% and 93%, and CTA 77% and 95%, respectively.
Duplex ultrasound is widely available, easy accessible, cost-effective and often used as a first line investigation in standardized protocols assessing carotid vascular disease.[42] In experienced hands it is an accurate test, however it has higher interobserver variability and lower sensitivity and specificity when compared to CE-MRA and CTA. Guidelines of the American Heart Association (AHA) and the American College of Cardiology Foundation recommend evaluation of the carotid artery by MRA or CTA, when DUS provides equivocal or non-diagnostic results.[43] When DUS detects a significant stenosis (>70%) it is useful to evaluate stenosis severity by performing MRA or CTA. For assessing carotid artery stenosis, CE-MRA show a comparable accuracy.
However, CTA has some limitations. CTA requires the use of ionizing radiation and administration of larger intravenous contrast volumes, application iodinated contrast with possible toxicity and adverse reaction, and, moreover, calcification in plaque may hamper stenosis gradation. Therefore, it is becoming common practice to combine DUS, as first line screening modality followed by CE-MRA for gradation of carotid stenosis.
CE-MRA is the MRA technique of choice to evaluate carotid vascular disease (Figure 4.1). Typically, 3D CE-MRA data are acquired in a coronal plane. In CE-MRA of the carotid arteries bolus timing is essential, since venous return in the neck veins occurs fast. Spatial resolution of 0.71 mm^3 at 1.5T and 0.54 mm^3 at 3T are recommended.[44] Generally, single dose of gadolinium-based contrast agent (0.1 mmol/kg) is sufficient to achieve excellent image quality and resolution at 1.5T. Several studies showed that dose reduction to half dose (0.05 mmol/kg) is feasible at 3T without compromising SNR and spatial resolution.[45,46]
In several studies TOF MRA showed good sensitivity and specificity in detecting stenosis of the carotid bifurcation.[47,48] However, CE-MRA offers high resolution imaging of larger field-of-view in shorter acquisition times[49,50] and therefore, has replaced TOF MRA in clinical practice.
Development of new non-CE-MRA sequences show promising results and could have the potential to become an alternative imaging approach in evaluating carotid vascular disease. Zhoa et al.[51] showed that 3D black-blood MR imaging provided high agreement for stenosis measurements as compared to DSA. 3D black-blood MR imaging depicted longer lesion length than DSA, because it is able to define vessel wall

morphology and distribution of plaque. When compared to CE-MRA, 3D black-blood MRA show accurate measurement of carotid stenosis[52] and sensitivity and specificity comparable with CTA.[51]

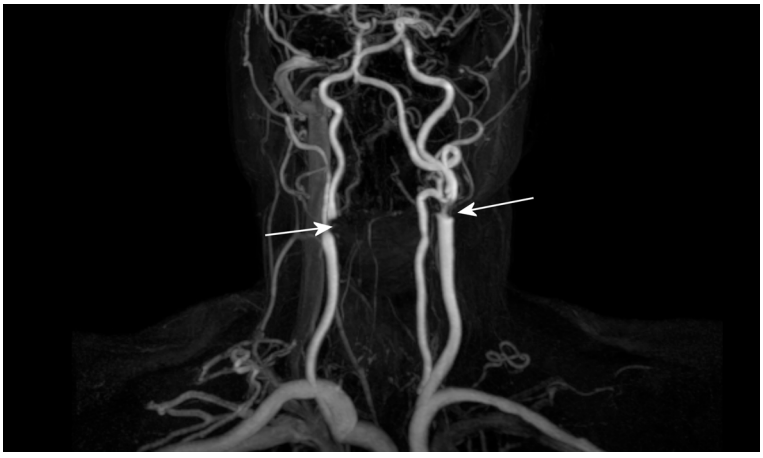

Figure 4.1 CE-MRA shows a significant stenosis of the proximal internal carotid artery on both sides (arrows).

Other vascular disease of the carotid artery can also be diagnosed by CE-MRA. Fibromuscular dysplasia (FMD) is a non-atherosclerotic, non-inflammatory arteriopathy with segmental involvement of small- and medium sized arteries. The etiology is unknown and the extracranial carotid, vertebral, and renal arteries are most frequently affected. The so-called string-of-beads sign of the involved arteries is a classic pattern seen in FMD, but also other imaging findings are described, as aneurysm, fusiform arterial ectasia, and vascular loops. FMD can accurately be diagnosed using CE-MRA, however, a negative result on CE-MRA does not rule out the diagnosis of FMD. Therefore, DSA is still mandatory in patients with high clinical suspicion of FMD.[53]

Carotid artery dissection is one of the most common causes of stroke in young patients. Dissection can occur after trauma, but may arise spontaneously. In patients suspected for carotid artery dissection, CE- MRA is the imaging modality of choice.[54,55] Mural hematoma can be visualized by performing additional axial T1W images with fat suppression. Although DSA is the reference standard for evaluation of the lumen of the carotid artery, it does not provide details of the arterial wall. In suspected cases it is important to reformat acquired high-resolution isovolumetric voxels in axial thin slices to eventually depict an intimal flap.

Magnetic resonance angiography of the aorta

Diseases of the thoracic and abdominal aorta can be examined by several imaging modalities. Over the last decade non-invasive imaging techniques have improved significantly and therefore, the need for DSA as imaging tool in clinical practice has decreased. With non-invasive techniques the risks of arterial catheterization and the use of iodinated contrast medium can be avoided.

A wide spectrum of vascular diseases affecting the thoracic and abdominal aorta can be evaluated by angiographic imaging, including aortic aneurysm, suspected aortic dissection, penetrating atherosclerotic ulcer, arterial occlusive disease in atherosclerosis, genetic diseases (e.g. Marfan syndrome), and congenital abnormalities such as coarctation of the aorta. For imaging the thoracic aortic lumen, current established non-invasive techniques such as transthoracic echocardiography (TTE), transesophageal echocardiography (TEE), MRA and CTA are able to provide additional information of the aortic wall and the relationship of vascular disease to surrounding tissue. Echocardiography is most commonly used as a first line imaging modality, but also MRA and CTA are widely used. The abdominal aorta is most typically imaged by ultrasound, MRA, and CTA,[56] whereas echocardiography is the most frequently used imaging modality for evaluating the aortic root and proximal ascending aorta.

In a standardized echocardiographic examination the thoracic aorta is routinely assessed.[57] Despite the fact that TTE is limited for assessing the complete thoracic aorta, it still permits adequate assessment of several aortic segments, especially adequate when monitoring aortic root diameters.[58] Moreover, TTE can be used as a screening tool for proximal ascending aorta dilatation.

Due to the proximity of the esophagus to the thoracic aorta, TEE is often used in thoracic aorta assessment to overcome the limitations of TTE. TEE reveals high resolution images and unlike TTE allows gradual assessment of the thoracic aorta from the aortic root to the descending aorta.[59,60] However, if echocardiography reveals inconclusive information or when abnormalities are present, another imaging modality is required for further work-up.

CTA is an important imaging technique in vascular diseases of the thoracic and abdominal aorta. Especially in acute aortic syndrome (i.e. aorta dissection, intramural hematoma, penetrating atherosclerotic ulcer, and contained aortic rupture) CTA plays a key role and is the preferred primary imaging technique. Multi-slice CT scanners are widely available and can provide images with high spatial resolution. Therefore, CTA has essentially replaced invasive DSA. Diagnostic accuracy of CTA for the detection of dissection and traumatic injury are excellent. Sensitivity and specificity for the detection of dissection are 100%.[61] Steenburg et al.[62] reported a sensitivity of 96.0%, a specificity of 99.8%, and accuracy of 99.8% for multislice CTA as compared with DSA in patients with acute thoracic aortic injury.

The role of MRA in the evaluation of acute aortic syndrome is limited. Monitoring acute, unstable patients in the MRI scanner is more complicated and acquisition times are longer. However, MRA has several advantages over CTA such as the above mentioned radiation-free nature of the imaging modality in which the need for iodinated contrast medium is avoided. Therefore, MRA is highly suitable for evaluation of aortic disease in young patients and for follow-up studies.[63]
CE-MRA has emerged as the preferred MRA technique for evaluation of thoracic and abdominal vascular pathology independent of blood flow. High-resolution 3D image acquisition permits multi-planar and MIP reconstructions in any desired plane for detailed image evaluation (Figure 4.2). 3D CE-MRA acquisition does not require ECG triggering and can be performed during a single breath hold of approximately 15 to 20 seconds.

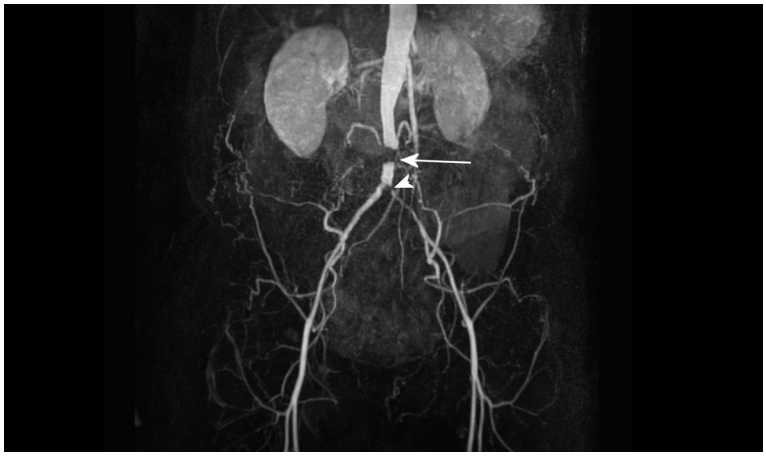

Figure 4.2 CE-MRA shows a short distal aortic occlusion (arrow) and a significant stenosis of the proximal left common iliac artery (arrowhead).

For optimizing SNR surface phased-array coils are used for imaging the thoracic and abdominal aorta, however, sufficient image quality can also be achieved by applying the body coil. Positioning of the surface phased array coil in thoracic aorta imaging is important as the volume stack should include the proximal brachiocephalic arteries. When imaging the abdominal aorta, positioning of the 3D volume is essential such that the acquired volume contains the proximal course of major arterial braches as the cephalic trunk, superior mesenteric artery, renal arteries and iliac arteries.
For both the thoracic and abdominal aortic CE-MRA, patients are routinely imaged in supine position.

The imaging protocol of the thoracic aorta consists of a survey or localizer sequence, SSFP cine imaging, contrast bolus timing sequence (test bolus or fluoroscopic real-time imaging), 3D CE-MRA sequence pre- and post-contrast and, depending on vascular disease, T1-weighted post-contrast sequence to rule out for example aortitis. Single-shot fast spin echo or SSFP acquired during breath holding can serve as a localizer sequence in three directions. For optimal planning and positioning of the 3D CE-MRA imaging volume, it is essential that the survey scan is performed in the same breath holding position as utilized for the 3D CE-MRA acquisition. Preferably, this breath holding is end-expiration since end-expiration is more reproducible when compared to end-inspiration.[64] SSFP images are acquired with ECG triggering and during breath holding. Preferably, two directions (axial and parasagittal planes) are acquired. SSFP images provide additional information about the vessel wall and surrounding tissue.

The pre-contrast 3D scan is acquired to verify proper positioning of the 3D volume and to rule out possible aliasing artifacts. For 3D CE-MRA, 0.1–0.2 mmol/kg body weight contrast medium is administered. The 3D dataset can be obtained in coronal, sagittal, or parasagittal plane. Covering the thoracic aorta in a coronal plane requires a larger volume and consequently, longer breath holding maintaining high spatial resolution. Therefore, in clinical practice, sagittal or parasagittal plane is favored. Typically, the field-of-view ranges from 30 to 40 cm.

Usually, the abdominal aorta is imaged in the coronal plane and the field-of-view varies between 35 and 40 cm. For both thoracic and abdominal CE-MRA, spatial resolution of at least 1–1.5 mm should be used.[65]

In CE-MRA of the thoracic and abdominal aorta, optimally two post-contrast datasets are obtained. Large aneurysms or false lumen in aortic dissection may have slow flow and therefore, require a longer time interval between contrast injection and 3D image acquisition to become fully enhanced. As a consequence, they may be only fully established during the second 3D volume acquisition. Moreover, distinction between slow flow and therefore potential non-filling with contrast of the lumen can be distinguished better from thrombus.

Additionally, ECG-triggered T1-weighted images with fat suppression can be acquired to analyze the aortic wall. Phase contrast sequences can be performed to quantify flow.

Non-CE-MRA of the thoracic aorta can also provide additional information of the aortic wall and surrounding tissue, and therefore, this acquisition is an important sequence within the standard MRA imaging protocol. Non-CE-MRA by SSFP may serve as a useful alternative for evaluation and follow-up of aortic disease when compared to CE-MRA in patients with contraindications to gadolinium use or with poor intravenous access. SSFP showed high diagnostic accuracy for aortic dimensions and vascular pathology, and similar reader confidence, when compared to CE-MRA.[66,67]

For the detection of aortic disease, free breathing 3D SSFP MRA with navigator gating

showed a 100% diagnostic accuracy with CE-MRA serving as reference standard.[68] Furthermore, SSFP showed significantly higher image quality of the aortic root, whereas non-ECG-gated CE-MRA images may suffer motion artifacts in this region hindering diagnostic image evaluation.

In CE-MRA, post-processing of the acquired 3D dataset is essential. On MPR and MIP reconstructions aortic vascular pathology can be assessed in relation to the origin of branching vessels. For serial follow-up examinations in patients with aortic dilatation, consistency and accuracy of aortic diameter measurements is critical, since increase in diameter may have important impact on risk stratification and on planning of surgical intervention.[69,70] The maximal diameter should be measured perpendicular to the axis of flow, double oblique or so-called centerline reconstruction.[71] Double oblique measurements of aortic diameter provided better agreement with the reference standard of planimetry than axial measurements and therefore, may have potentially important impact on surgical decision-making.[72]

Aneurysm of the thoracic aorta is often an incidental finding during TTE for cardiac screening or on chest X-ray in asymptomatic patients. Aortic aneurysm may lead to aortic rupture or aortic dissection. These acute events may be rapidly fatal in a large proportion of patients,[73] therefore, serial follow-up examinations in this patient population is vital. CE-MRA is a robust and accurate imaging modality for evaluation of the entire aorta and is favorable for long-term follow-up examinations without the need of ionizing radiation or iodinated contrast (Figure 4.3).

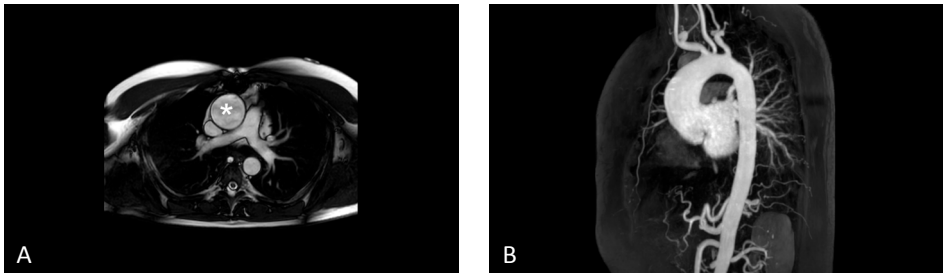

Figure 4.3 **(A)** Bright-blood steady-state free-precession axial image shows an aneurysm of the ascending aorta (asterix). **(B)** 3D CE-MRA (sagittal maximum-intensity-projection) of the same patient.

Reports showed a high accuracy for the detection of thoracic and abdominal aneurysms with a sensitivity of 100% and specificity of 100%, respectively, when compared to surgery or DSA.[74,75]

Atherosclerosis more often causes aneurysm formation in the descending and abdominal aorta, whereas dilatation of the ascending aorta more frequently occurs in aortic valvular disease as in aortic valvular regurgitation and in patients with bicuspid

valves. Other causes of aortic aneurysm are connective tissue disease (i.e. Marfan syndrome, Ehlers-Danlos, and Loeys-Dietz syndrome), Turner syndrome, inflammatory disease, trauma, chronic dissection or aortic surgery. Hypertension, smoking, hypercholesterolemia, and low high-density lipoprotein cholesterol are also significantly associated with aortic dilatation.[76,77]

Aneurysms can be classified in true and false aneurysms. A true aneurysm involves all three layers of the aortic wall, i.e. the intima, media, and adventitia. In a so-called false aneurysm, a disruption in the arterial wall causes blood leakage and an aneurysm contained by only the adventitia or surrounding tissue. The disruption may be caused by trauma, iatrogenic origin (e.g. percutaneous or surgical procedures), or inflammation. Risk of aneurysm rupture is higher in a false aneurysm when compared to true aneurysms.[78]

Morphologically, two types of aneurysms can be recognized: fusiform and saccular aneurysms. A fusiform aneurysm is concentric and involves dilatation of the full circumference of the aortic wall. A saccular aneurysm is eccentric and consists of a asymmetric outpouching of a part of the artic wall.

Bacterial infections of the aortic wall can cause the formation of mycotic aneurysms. The most common infecting organisms are Staphylococcus aureus and Salmonella. Mycotic aneurysms are usually saccular and are more prone to rupture. For optimal treatment early diagnosis is essential. Normally, patients present with signs of infection, including fever or sometimes sepsis. Often bacteremia is present, however negative blood cultures do not rule out the presence of mycotic aneurysm.[79] Therefore, imaging is very important for diagnosis. Besides the saccular aneurysm, CE-MRA can demonstrate additional perivascular inflammatory changes as soft tissue inflammation, edema, gas, and irregularity of the aortic wall leading to the diagnosis of mycotic aneurysm.

In aortic dissection, intraluminal blood penetrates into the media layer of the aortic wall through a tear in the intima, thereby dissecting the aortic wall. The proximal ascending aorta and the descending aorta distal to the origin of the left subclavian artery are the two most common sites where the aortic dissection is initiated and the intimal tear occurs. The bleeding between the dissected layers of the aortic wall forms the false lumen. Distention of the false lumen may narrow and compress the true lumen. Bleeding within the medial layer of the aortic wall can also cause the formation of a localized intramural hematoma (IMH) and facilitate the development of an intimal tear.

Currently, two classification systems - DeBakey and Stanford classification - are most frequently used for aortic dissection.[80] The DeBakey classification subdivides aortic dissection in type I, II, and III. In DeBakey type I aortic dissection the ascending and descending aorta are involved, in type II only the ascending aorta and aortic arch, and in type III the ascending aorta and arch are spared. The Stanford classification differentiates type A and type B aortic dissection. Type A involves the ascending aorta,

and eventually extending distally. Type B aortic dissections start out in the descending aorta and spare the ascending aorta and arch. If not operated, patients with acute type A aortic dissection have a high mortality of 50% within the first 48 hours,[81] therefore, surgery is the treatment of choice. Patients with type B dissection are often treated medically with close surveillance to identify possible progression of the dissection. Herewith, sequential imaging of the thoracic and, if necessary, abdominal aorta is essential. CTA is the imaging technique of choice in patients suspected for aortic dissection in acute setting. CE-MRA is an excellent technique for multiple follow-up examinations, without ionizing radiation or the use of iodinated contrast. For MRI, high sensitivity and specificity of both 98% in the diagnosis of aortic dissection were reported.[82,83]

T1-weighted imaging can determine blood in the aortic wall and additional T2-weighted imaging can further help to analyze the blood compounds characteristics and age of IMH. CE-MRA clearly reveals the extent of aortic dissection and the possible extension into arterial side braches. Moreover, branching arteries originating from the true or false lumen can be evaluated. Both SSFP images and CE-MRA can clearly visualize the intimal flap. However, MIP images may obscure the intimal flap and therefore, dissection may be missed. Therefore, it remains important to review both source images of the CE-MRA sequence, together with SSFP images and MPR in patients with suspicion of or known aortic dissection. It is not advisable to make a diagnosis based solely on the projection images.

Magnetic resonance angiography of the renal arteries

Renal artery stenosis is regarded one of the most common manifestations of systemic atherosclerosis. It is a progressive disease and is more seen in elderly. Increased prevalence in patients with coronary artery disease and peripheral artery disease are reported.[84,85] Typically, stenosis of the renal artery either involves the origin of the renal artery or the proximal third part or it is caused by an aortal atherosclerotic plaque impinging on the ostium of the renal artery. Patients with renal artery stenosis often have bilateral renal artery stenoses.[86] Luminal diameter narrowing of more than 50 to70% is considered hemodynamically significant.

In young patients, renal arterial stenosis can be caused by fibromuscular dysplasia (FMD). FMD is a idiopathic, non-atherosclerotic, segmental disease of the arterial wall leading to stenosis, aneurysm, dissection and/or occlusion of small to medium-sized arteries, especially renal and carotid arteries and predominantly occurs in young and female patients. When the renal arteries are involved, it may cause secondary hypertension.[87]

The standard of reference to determine the diagnosis of renal artery stenosis anatomically is catheter renal angiography, i.e. DSA. Direct measurement of hemodynamic characteristics is possible by involving transstenotic pressure measurements and if necessary, revascularization can be performed immediately. However, DSA has known limitations as the use of ionizing radiation and iodinated contrast. Moreover, DSA is an invasive imaging tool with possible risk of complications.

Nowadays, non-invasive imaging modalities have replaced DSA in the diagnosis and work-up in patients with suspected renal artery stenosis in clinical practice. Doppler ultrasonography is a frequently used imaging modality to evaluate renal vasculature. DUS is a widely available, non-invasive and radiation-free technique that allows anatomic assessment of renal artery stenosis and measurement of renal artery flow patterns. To characterize significant renal artery stenosis, several DUS measures have been proposed, e.g. renal-to-aortic peak systolic ratio,[88,89] and renal peak systolic velocity.[90,91] Zeisbrich et al.[92] showed that real-time contrast-enhanced ultrasonography was superior to conventional Doppler ultrasonography in microvascular perfusion changes in allografts. Contrast-enhanced ultrasonography can play a role as a complementary imaging tool to assess renal artery stenosis and detailed qualitative and quantitative information on renal microvascular perfusion. Doppler ultrasonography is, however, time consuming, highly operator dependent, and can be technical challenging in obese patients.

Modern multi-slice CT scanners permit rapid high resolution imaging with accurate first-pass contrast timing in patients with renal arterial disease. High accuracy of CTA for diagnosing significant atherosclerotic renal stenosis has been reported, with a sensitivity and specificity of 94% and 93%, respectively.[93] Also high sensitivity and specificity of 100% and 99%, respectively was described for detecting in-stent recurrent stenosis in patients following percutaneous revascularization.[94] Limitations of CTA are the use of ionizing radiation and iodinated contrast. Another disadvantage of CTA is its inability to perform physiologic assessment of renal arterial stenosis and, moreover, severe renal artery calcification may obscure arterial lumen narrowing and limiting evaluation of stenosis.

CE-MRA is a reliable and fast non-invasive imaging technique providing accurate visualization of the renal arteries and accessory renal arteries.[95] Meta-analysis showed a sensitivity and specificity of 88% to 100%, respectively.[96] 3D CE-MRA provides anatomic evaluation of renal arteries. Additionally PCA images can be acquired, adding functional information about renal arterial flow (Figure 4.4). In clinical practice, this can help for example in the analysis of the hemodynamic significance of an intermediate-grade renal artery stenosis (40%–70%), which cannot be reliably derived from vessel diameter measurements alone. In these cases, PCA can be used as an adjunct to CE-MRA for assessing and grading the hemodynamic relevance of intermediate-grade renal stenosis for decision on proper treatment strategies.[97,98]

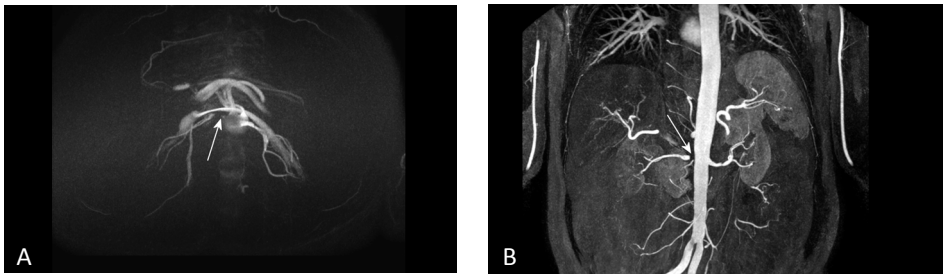

Figure 4.4 **(A)** 3D CE-MRA (maximum-intensity-projection) shows a short stenosis of the right proximal renal artery (arrow). **(B)** 3D phase contrast MRA shows a signal void at the site of the hemodynamic significant stenosis (arrow).

Typically, an MR imaging protocol for renal artery evaluation consists of a survey or localizer sequence, a contrast bolus timing sequence (test bolus or fluoroscopic real-time imaging), a 3D CE-MRA sequence pre- and post-contrast, and a PCA sequence. For optimizing signal and image quality a body phased-array coil should be applied. A fast 2D balanced-gradient-echo sequence or Fast Spin Echo (FSE) sequence can be used as survey sequence. The survey scan is performed in the same breath holding position as utilized for the 3D CE-MRA acquisition. Preferably, this breath holding is end-expiration.[64] A pre-contrast 3D scan is acquired to control proper positioning of the 3D volume and rule out aliasing artifacts. After intravenous administration of Gd contrast (0.1–0.2 mmol/kg body weight), the 3D CE-MRA sequence is performed. Typically, the 3D CE-MRA images have an acquired in-plane resolution of approximately 1 mm × 1 mm and a slice thickness of 2-2.5 mm. The 3D volume is positioned in coronal plane and acquired during breath holding (less than 20 seconds). Following the 3D CE-MRA the PCA sequence is acquired with a standardized typical velocity of 35 cm/s in the right-left direction, 35 cm/s in the anterior-posterior, and 100 cm/s in the feet-head direction, respectively. Post-processing of the acquired 3D CE-MRA and PCA data, using multi-planar reconstruction and maximum intensity projection is essential for renal artery evaluation and permits detailed analysis in all desired planes. In all patients, but especially in those with suspected renal artery stenosis, referred for CE-MRA, the eGFR should be assessed prior to the MRI examination, to rule out possible NFS-related complications.

Significant renal artery stenosis may activate the renin-angiotensin-aldosteron system and is associated with arterial hypertension, ischemic nephropathy, and chronic kidney disease. The main options for treatment of renal arterial stenosis include percutaneous or surgical by-pass revascularization, or medical therapy. Large, randomized trials showed no significant difference in systolic blood pressure[99] or only revealed a reduction of 2 mmHg in systolic blood pressure in patients with

revascularization in combination with medical therapy when compared to medical therapy alone.[100] Moreover, renal artery revascularization did not show significant clinical benefit concerning prevention of clinical events.[99,100]
However, meta-analysis also showed that patients with atherosclerotic renal artery stenosis proofed better control of diastolic blood pressure and a reduction in the mean number of antihypertensive drugs after endovascular treatment.[101,102]
Selected subgroups of patients, e.g. patients with accelerated or malignant hypertension, difficult to control blood pressure, young patients with FMD, or at risk of progressive nephropathy and end-organ failure may benefit from renal arterial revascularization.[103,104]

Magnetic resonance angiography of the mesenteric arteries

Atherosclerotic vascular disease of the mesenteric arteries is the leading cause of chronic mesenteric ischemia (CMI). In asymptomatic elderly patients, significant mesenteric arterial disease, i.e. a stenosis of more than 70% or an occlusion, has been reported in 18% in a population-based prevalence study.[105] However, significant mesenteric arterial stenosis does not necessarily indicate the presence of mesenteric ischemia clinically.[106] The mean reason for this is that the mesenteric arterial circulation contains multiple collateral pathways between the celiac artery, superior mesenteric artery and inferior mesenteric artery. Therefore, involvement of atherosclerosis in the mesenteric arteries in patients with generalized atherosclerosis infrequently leads to symptoms of chronic mesenteric ischemia. The collateral pathways of the mesenteric arterial circulation include the pancreatico-duodenal arcade, arc of Riolan, arc of Buhler, arc of Barkow and the marginal artery of Drummond. In general in patients with symptoms of CMI, two of the three mesenteric arteries show significant stenosis or occlusion.[107,108] Mostly, patients with stenosis of one of the three mesenteric arteries do not present symptoms of CMI,[109] however, CMI has been reported in isolated mesenteric arterial stenosis.[110]
In patients with CMI, mesenteric arterial stenosis or occlusion compromise the blood flow to the intestine leading to postprandial abdominal pain, so-called angine abdominale. Typically, this pain starts within 30 minutes of eating and can last for several hours. This may lead to avoidance of food and significant weight loss. Patients may also present with atypical symptoms as nausea, vomiting, diarrhea, constipation, or colitis. In the majority of patients, diagnosis of CMI is established in an advanced stage of the disease.
The incidence of CMI increases with age, is more prevalent in women and in patients with risk factors for atherosclerotic vascular disease such as history of smoking, hypertension, and hyperlipidemia.[111] Less commonly CMI occurs in young patients

with fibromuscular dysplasia, Takayasu's vasculitis, polyarteritis nodosa, arterial dissection, abdominal aortic anaurysm or post-radiation therapy.

Clinical diagnosis of CMI is established on clinical symptoms and consistent imaging characteristics. Identification of stenotic arterial mesenteric disease without associated clinical symptoms is not diagnostic of CMI.

For diagnosing CMI, conventional DSA remains the reference standard. Advantageously, an endovascular therapeutic procedure can be performed at the time of diagnosis of mesenteric arterial stenosis. However, DSA is an invasive procedure with the already mentioned disadvantages such as the exposure to radiation, nephrotoxic iodinated contrast, and the invasive procedure is associated with complications.[112] In common clinical practice, MRA and CTA have replaced DSA as imaging tool in the work-up of patients suspected for CMI.

In patients suspected of CMI, Doppler ultrasound is useful for screening and is the preferred initial imaging modality. Visualization of high-grade stenoses in the celiac artery or superior mesenteric artery associated with CMI may be technically challenging, especially due to overlying bowel gas or patient's habitus. When compared to angiography, the celiac and superior mesenteric artery are accurately visualized in more than 80% and 90%, respectively.[113] The inferior mesenteric artery can hardly be evaluated by Doppler ultrasound due to its anatomical location.[114] Peak systolic velocity (PSV) has been widely used for evaluating celiac and superior mesenteric arterial disease with a sensitivity and specificity for diagnosing hemodynamically significant stenosis of 92% and 96%, and 87% and 80%, respectively.[115]

Van Petersen et al.[116] showed that stenosis in the celiac or superior mesenteric artery results in an increase of flow velocities in the other mesenteric arteries. The increase in flow was correlated with the presence of collateral vessels. This may lead to overgrading or mimicking stenosis in the other mesenteric artery. Therefore, Doppler ultrasound should be used only as an initial screening imaging tool and in case of demonstrated arterial stenosis further evaluation by performing MRA or CTA is required.

CTA is considered the first-line alternative to diagnostic DSA for evaluation of CMI.[114] Especially in the emergency situation of the suspicion of an acute mesenteric ischemia, CTA is the most appropriate imaging modality. It is a fast non-invasive imaging technique and widely available. Acquired 3D data sets can be post-processed in varying planes and other causes for abdominal pain can be evaluated. For stenosis grading of mesenteric arteries high sensitivity and specificity of 100% and 95%, respectively with DSA as the reference standard were reported.[117] However, diagnostic value of CTA may be limited with the presence of extensive calcifications. Other known drawbacks include the use of radiation and iodinated contrast, therefore, CE-MRA is a an accurate and reliable alternative non-invasive imaging tool for diagnosing CMI. 3D CE-MRA has a high sensitivity and specificity ranging from

92-100% and 95-100%, respectively.[117,118,119] CE-MRA has, however, a limited role in the evaluation of distal mesenteric arteries and depicting stenosis in the inferior mesenteric artery.[120,121]

Routinely, 3D CE-MRA is acquired with the patient in supine position utilizing a surface phased-array coil for optimizing SNR. As with other previously described 3D CE-MRA protocols, the mesenteric arteries are evaluated with a protocol which comprises a survey or localizer sequence, a contrast bolus timing sequence (test bolus or fluoroscopic real-time imaging), and a 3D CE-MRA sequence pre- and post-contrast. Spatial resolution and slice thickness should be tailored for the individual patient that the 3D volume can be imaged in one single breath-hold. The same breath holding position is utilized for the survey scan and the 3D CE-MRA acquisition. The pre-contrast 3D scan can be used to check correct positioning of the 3D volume and rule out aliasing artifacts, as was discussed previously. 3D CE-MRA sequence is performed after intravenous administration of Gd contrast (0.1–0.2 mmol/kg body weight). The 3D volume slab is positioned in sagittal plane, if the primary clinical indication is to determine arterial disease of the mesenteric arteries, which occurs mostly proximal in the course of the mesenteric arteries. Also the coronal plane can be used to include the aorta and portal vein. In addition to the arterial phase, the sequence can be repeated to obtain the portal and systemic venous phase. Typically, images are required with an in-plane resolution of approximately 1–2 mm and a slice thickness of 1–2 mm, resulting in a breath-hold of 10–20 seconds.[122]

CE-MRA should be performed in both inspiration and expiration when median arcuate ligament syndrome is suspected (Figure 4.5). In median arcuate ligament syndrome, the celiac artery is compressed by the central tendon of the diaphragm crura. The classical finding is a smooth narrowing of the proximal celiac artery in expiration, diminishing or disappearing in inspiration. With inspiration, the celiac artery moves inferiorly and more vertically alleviating the compression of the ligamentous band. By performing 3D CE-MRA in both inspiration and expiration the diagnosis can be obtained and differentiated from atherosclerotic arterial disease.

Non-CE- MRA such as TOF and PCA are flow-dependent MR techniques and may suffer from decreased sensitivity and specificity due to slow flow and artefacts from turbulence overestimating stenosis. SSFP techniques demonstrated a superior visualization of the inferior mesenteric artery when compared to CE-MRA[123] and may play a role in patients with contra-indications for intravenous administration of Gd-based or iodinated contrast media.

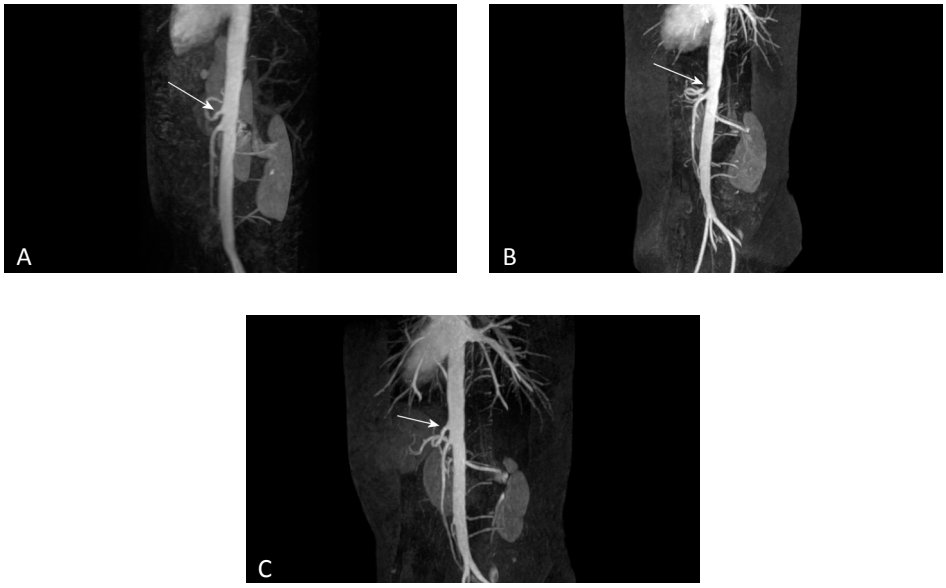

Figure 4.5 A patient diagnosed with the arcuate ligament syndrome shows significant narrowing of the celiac artery (arrow) on CE-MRA (maximum-intensity-projection) during expiration **(A)** disappearing in inspiration **(B)** (arrow). **(C)** shows CE-MRA during inspiration after surgical release of the median arcuate ligament (arrow).

Magnetic resonance angiography of the peripheral arteries

Peripheral arterial disease (PAD) is a common clinical manifestation of atherosclerosis and is – together with coronary artery disease and stroke – one of the leading causes of atherosclerotic cardiovascular morbidity.[124] It has been estimated that around 8.5 million people in the United States of America are effected by PAD over the age of 40 years.[125] Due to raised life expectancy, the prevalence of PAD increased over the last decades by more than 20% and has become a global problem affecting more than 200 million people worldwide,[124] causing a global increase in morbidity and mortality associated with PAD.[126] Prevalence rates increase with age, and the prevalence in men and women is similar.[127] However, in the last decades women experienced a more dramatic increase in morbidity and mortality from PAD when compared with men.[126] Risk factors significantly associated with the incidence of PAD are smoking, diabetes mellitus, hypertension, hypercholesterolemia, and chronic kidney disease.[128] Markers of inflammation and thrombosis are also associated with PAD.[129] Intermittent claudication is the classic symptom in PAD, however described in only about 10% of patients with PAD,[130] whereby men are more likely to have classic symptoms of

claudication. The large majority of patients show a wide range of leg symptoms or are even asymptomatic.

PAD is associated with increased risk for cardiac and cerebral events[131,132] and moreover, several reports showed an up to six times higher risk for mortality from cardiovascular causes and a 2.5 times higher overall mortality rate in patients with symptomatic PAD.[127,133] Therefore, assessment of risk factors for risk stratification in patients with PAD is very relevant.[134]

Assessment of risk factors such as hypertension, diabetes mellitus, body mass index, levels of triglyceride and high-density lipoprotein in blood plasma samples, and ankle-brachial index is essential when risk factor reduction is pursued. Moreover, the usefulness of non-invasive imaging for risk assessment in cardiovascular disease is recognized,[135] e.g. the assessment of MR imaging biomarkers such as mean MRA stenosis and pulse wave velocity showed prognostic value for all-cause mortality and cardiac events in patients with symptomatic PAD.[136]

Clinically, symptoms in patients with PAD can be staged according the Fontaine or Rutherford classification. The Fontaine classification[137,138] is divided in four different stages, stage I: asymptomatic, stage IIa: intermittent claudication after more than 200 meters of pain free walking, stage IIb: intermittent claudication after less than 200 meters of walking, stage III: rest pain or nocturnal pain, and stage IV: ischemic ulcers or gangrene.

The Rutherford classification[137,138] is divided in three grades. Grade I compromises category 0: asymptomatic, category 1: mild claudication, category 2: moderate claudication, and category 3: severe claudication. Grade II compromises category 4: ischemic rest pain, and category 5: minor tissue loss, nonhealing ulcer or focal gangrene. Grade III compromises category 6: major, severe ischemic ulcers or gangrene. Both the Fontaine and the Rutherford classifications may be used routinely in clinical practice or in research settings.

For the evaluation of patients with symptomatic PAD, several non-invasive tests such as segmental blood pressure, pulse volume recording, Doppler ultrasonography and ankle-brachial index (ABI) are widely available. These inexpensive techniques are easily repeatable and commonly used for the initial screening to analyze the presence and location of atherosclerotic arterial disease of the run-off arteries.[139,140] However, Doppler ultrasonography is highly operator dependent[141] and has several other drawbacks, such as hampered evaluation of peripheral arteries in obese patients and it is difficult to obtain consistent high image quality in the run-off vessels distal to the popliteal artery. ABI is commonly used as a first-line diagnostic imaging tool in clinical practice. Normal ABI range of 1.00 to 1.40, and an abnormal value is defined as ≤0.90.[142] ABI values of 0.91 to 0.99 are regarded “borderline” and values >1.40 are an indication for non-compressible arteries. Moreover, several studies reported ABI to predict all-cause mortality and cardiovascular events in cardiovascular disease.[143,144,145] A low ABI is a strong indicator of the presence of PAD, however, due

to false-negative rates a normal ABI does not rule out the risk of PAD[146] and ABI may underestimate the prevalence of atherosclerotic arterial disease of the lower extremities when compared to CE-MRA.[147]

DSA is still considered as a standard reference for the evaluation of stenosis in PAD. However, due to the invasive character and the risk of possible complications DSA is generally not used as a diagnostic imaging tool. Moreover, because of technical developments of non-invasive imaging techniques such as CTA and MRA, DSA is consequently indicated only in patients with symptomatic PAD for whom percutaneous revascularization is planned or in patients with contra-indications for performing a CTA or MRA examination.

For further work-up and planning of revascularization in patients with symptomatic PAD, CTA and MRA are widely available and used in clinical practice. CTA is an accurate technique for evaluating stenosis severity in patients with PAD. Modern multi-slice CT scanners allow rapid acquisition of high-resolution, thin CT images. Accurate timing of the data acquisition during maximal arterial contrast enhancement provides detailed imaging of the run-off arteries. Meta-analysis estimated a sensitivity and specificity for CTA of 96% and 95%, respectively. However, CTA requires radiation and the use of iodinated contrast material as stated before. Moreover, arterial wall calcification may compromise diagnostic image quality and hamper stenosis evaluation especially in patients with diabetes mellitus and renal failure.[148]

For the detection of peripheral arterial disease, CE-MRA is superior to the conventional non-CE-MRA techniques, such as 2D TOF or PCA. These conventional and older non-CE-MRA techniques were highly time consuming and moreover, suffered from artifacts caused by turbulence and in-plane saturation. In a meta-analysis,[149] the sensitivity and specificity for the detection of significant stenosis (>50% luminal reduction) for 2D TOF ranged from 64% to 100% and 68% to 96%, and for CE-MRA 92% to 100% and 91% to 99%, respectively.

In CE-MRA the run-off vessels are imaged during the arterial first pass of gadolinium-based contrast material after intravenous injection (Figure 4.6). Precise bolus timing is essential for CE-MRA. Starting the acquisition too early, when the contrast bolus is still arriving in the vessels of interest, can cause ringing or Maki artefacts.[13] Starting the acquisition too late can cause venous enhancement hampering image quality, especially in de lower legs. Arterial imaging is thus performed in the time window between arterial and venous enhancement. This time window depends on the rate of contrast agent injection, and will be patient specific.[11] Arterial enhancement must coincide with data read-out of the central k-lines, and for improved arterial/venous differentiation, the central k-lines have to be sampled before venous return.

To cover the whole region of the distal abdominal aorta and the run-off vessels, two methods are clinically used: the single-injection 3-station moving-table (bolus-chase) technique and the multi-station/multi-injection method. In both methods, imaging is performed in a coronal orientation with usually three stations with overlapping field-

of-views , covering the complete anatomic region. Typically, the first station covers the distal abdominal aorta and pelvic region, the second station the upper legs and the third station lower legs. The quadrature body coil (QBC) or phased-array surface coils are used for signal transmission and reception. In both techniques, 3D volumes are planned on acquired 2D TOF survey images. Thereafter, pre-contrast mask images are acquired in all stations. Subtraction of the pre-contrast mask images from the contrast-enhanced images will suppress surrounding tissue.[150]

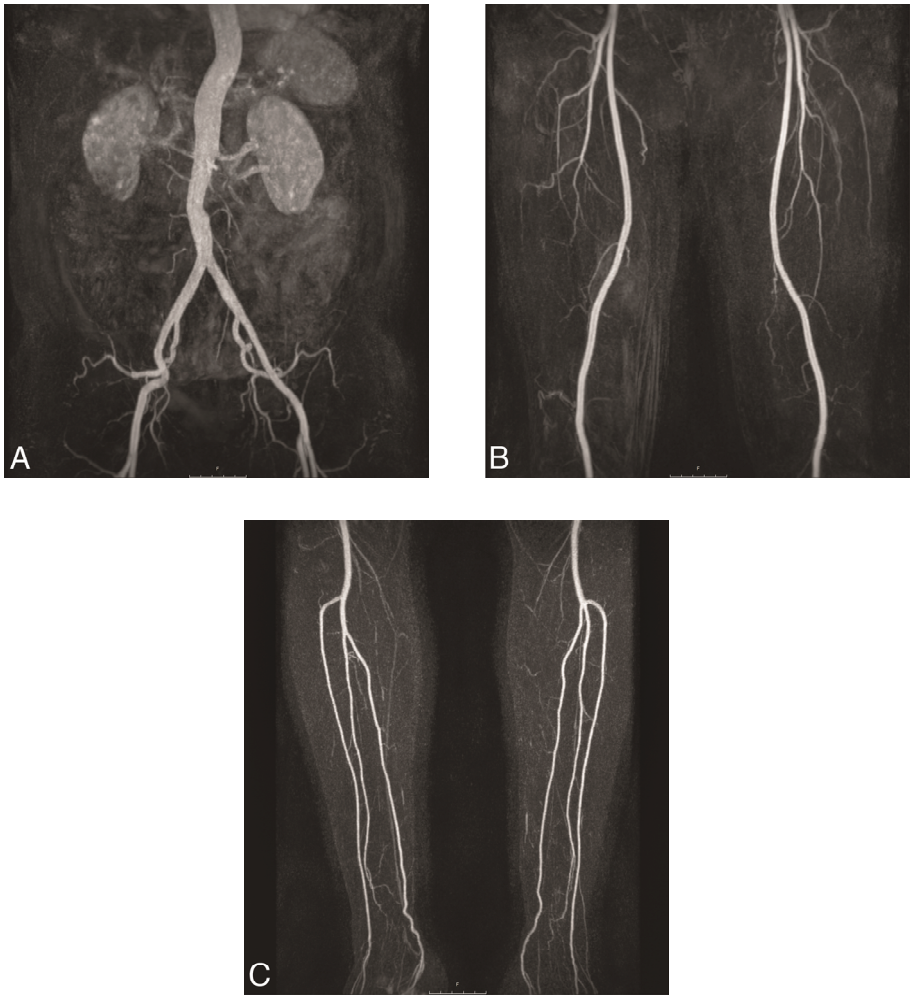

Figure 4.6 CE-MRA showing normal anatomy of the peripheral arteries.

In the bolus-chase technique, a biphasic contrast material injection protocol is typically used. The first half of the contrast bolus is administered at a flow rate of 1.0-1.2 mL/s and the remaining half at 0.5-0.6 mL/s. Contrast injection is followed by a saline flush at 0.5-0.6 mL/s. Modern commercially available 1.5T and 3T MR scanners allow acquisition of CE-MRA of the run-off vessels with a bolus-chase technique with excellent diagnostic performance.[151]

In the multi-station/multi-injection approach, the three regions of the legs stations are acquired sequentially with two or three separate bolus injections of contrast medium.[152] Contrast is injected at a rate of 1 to 1.5 mL/s, resulting in high signal intensity in the arteries. However, a disadvantage of this approach is that it is more time consuming, when compared to the bolus-chase technique. However, in patients with multiple risk factors, adequate arterial enhancement with minimal venous enhancement can be obtained with this technique.[153] The first station covering the distal abdominal aorta and pelvic region is acquired during breath-holding and the acquired resolution is of the first two stations is 1.3 mm × 1.3mm with a slice thickness of 3 mm, typically. The third station covering the lower leg scan be acquired with a submillimeter voxel size, allowing accurate diagnostic evaluation.[154]

Acquired high-resolution image data can be post-processed using multi-planar reconstructions or maximum intensity projections, however for obtaining an adequate diagnosis, evaluation of 2D source images is essential. Furthermore, the role of CE-MRA in the evaluation of possible restenosis in (metallic) stents is limited due to dephasing of MRI signal, causing signal void. New developments in MR imaging technology provide large homogeneous field-of-view at 3T revealing robust CE-MRA of the complete vascular tree of the run-off vessels allowing accurate clinical evaluation of patient on high field 3T scanners.[151] Moreover, two-point Dixon fat suppression allows subtractionless CE- MRA, avoiding possible misregistration artifacts between pre-contrast mask dataset and contrast-enhanced images.[155] Furthermore, new techniques, such as three-station bolus-chase MR angiography with real-time fluoroscopic tracking and precise triggering of table motion can provide high- resolution imaging of the run-off vessels. These new developments potentially can reduce contrast material dose and examination time.[156]

References

1. Prince M, Yucel E, Kaufman J, Harrison D, Geller S. Dynamic gadolinium-enhanced three-dimensional abdominal MR arteriography. J Magn Reson Imaging. 1993;3(6):677-881.
2. Port M, Idée J, Medina C, Robic C, Sabatou M., Corot, C. Efficiency, thermodynamic and kinetic stability of marketed gadolinium chelates and their possible clinical consequences: a critical review. Biometals. 2008;21(4):469-490.
3. Reilly R. Risk for nephrogenic systemic fibrosis with Gadoteridol (ProHance) in patients who are on long-term hemodialysis. Clin J Am Soc Nephrol. 2008;3(3):747-751.
4. Thomson H, Morcos S, Almen T, Bellin M, Bertolotto M, Bongartz G, Clement O, Leander P, Heinz-Peer G, Reimer P, Stacul F, van der Molen A, Webb J. Nephrogenic systemic fibrosis and gadolinium-based contrast media: updated ESUR contrast medium safety committee guidelines. Eur Radiol. 2013;23(2): 307-318.
5. Huckle J, Altun E, Jay M, Semelka R. Gadolinium deposition in humans: when did we learn that gadolinium was deposited in vivo? Invest Radiol. 2016;51(4):236–240.
6. Edwards B, Laumann A, Nardone B, Miller F, Restaino J, Raisch D, McKoy J, Hammel J, Bhatt K, Bauer K, Samaras A, Fisher M, Bull C, Saddleton E, Belknap S, Thomsen H, Kanal E, Cowper S, Abu Alfa A, West D. Advancing pharmacovigilance through academic-legal collaboration: the case of gadolinium-based contrast agents and nephrogenic systemic fibrosis—a Research on Adverse Drug Events and Reports (RADAR) report. Br J Radiol. 2014;87(1042):20140307.
7. Prince M. Gadolinium-enhanced MR aortography. Radiology. 1994;191(1):155-164.
8. Prompona M, Cyran C, Nikolaou K, Bauner K, Reiser M, Huber A. Contrast-enhanced whole-heart MR coronary angiography at 3.0 T using the intravascular contrast agent gadofosveset. Invest Radiol. 2009;44(7):369-374.
9. Jaspers K, Versluis B, Leiner T, Dijkstra P, Oostendorp M, Van Golde J, Post M, Backes W. MR angiography of collateral arteries in a hind limb ischemia model: comparison between blood pool agent Gadomer and small contrast agent Gd-DTPA. PloS One. 2011;6(1):e16159.
10. Wilson G, Hoogeveen R, Willinek W, Muthupillai R, Maki J. Parallel imaging in MR angiography. Top Magn Reson Imaging. 2004;15(3):169-185.
11. Prince M, Chabra S, Watts R, Chen C, Winchester P, Khilnani N, Trost D, Bush H, Kent K, Wang Y. Contrast material travel times in patients undergoing peripheral MR angiography. Radiology. 2002;224(1):55-61.
12. Maki J, Prince M, Chenevert T. Optimizing three-dimensional gadolinium-enhanced magnetic resonance angiography. Invest Radiol. 1998;33(9):528-537.
13. Maki J, Prince M, Londy F, Chenevert T. The effects of time-varying intravascular signal intensity and k-space acquisition order on three-dimensional MR angiography image quality. J Magn Reson Imaging. 1996;6(4): 642-651.
14. Willinek W, Gieseke J, Conrad R, Strunk H, Hoogeveen R, von Falkenhausen M, Keller E, Urbach H, Kuhl C, Schild H. Randomly segmented central k-space ordering in high-spatial-resolution contrast-enhanced MR angiography of the supra-aortic arteries: initial experience. Radiology. 2002; 225(2): 583-588.
15. Grobner T. Gadolinium, a specific trigger for the development of nephrogenic fibrosing dermopathy and nephrogenic systemic fibrosis? Nephrol Dial Transplant. 2006;21(4): 1104-1108.
16. Prince M, Zhang H, Roditi G, Leiner T, Kucharczyk W. Risk factors for NSF: a literature review. J Magn Reson Imaging. 2009;30(6): 1298-1308.
17. Kanda T, Fukusato T, Matsuda M, Toyoda K, Oba H, Kotoku J, Haruyama T, Kitajima K, Furui S. Gadolinium-based contrast agent accumulates in the brain even in subjects without severe renal dysfunction: evaluation of autopsy brain specimens with inductively coupled plasma mass spectroscopy. Radiology. 2015;276(1): 228-232.
18. Kanda T, Ishii K, Kawaguchi H, Kitajima K, Takenaka D. High signal intensity in the dentate nucleus and globus pallidus on unenhanced T1-weighted MR images: relationship with increasing cumulative dose of a gadolinium-based contrast material. Radiology. 2014;270(3): 834-841.

19. Murata N, Gonzalez-Cuyar L, Murata K, Fligner C, Dills R, Hippe D, Maravilla K. Macrocyclic and other non-group 1 gadolinium contrast agents deposit low levels of gadolinium in brain and bone tissue: preliminary results from 9 patients with normal renal function. Invest Radiol. 2016;51(7): 447-453.
20. Wang Y-X, Schroeder J, Siegmund H, Idée J-M, Fretellier N, Jestin-Mayer G, Factor C, Deng M, Kang W, Morcos S. Total gadolinium tissue deposition and skin structural findings following the administration of structurally different gadolinium chelates in healthy and ovariectomized female rats. Quant Imaging Med Surg. 2015;5(4): 534-545.
21. Kanda T, Osawa M, Oba H, Toyoda K, Kotoku J, Haruyama T,Takeshita K, Furui S. High signal intensity in dentate nucleus on unenhanced T1-weighted MR images: association with linear versus macrocyclic gadolinium chelate administration. Radiology. 2015;275(3): 803–809.
22. Radbruch A, Weberling L, Kieslich P, Eidel O, Burth S, Kickingereder P, Heiland S, Wick W, Schlemmer H-P, Bendszus M. Gadolinium retention in the dentate nucleus and globus pallidus is dependent on the class of contrast agent . Radiology. 2015;275(3): 783-791.
23. Simonetti O, Finn J, White R, Laub G, Henry D. “Black blood” T2-weighted inversion-recovery MR imaging of the heart. Radiology. 1996;199(1): 49-57.
24. Miyazaki M, Akahane M. Non-contrast enhanced MR angiography: established techniques. J Magn Reson Imaging. 2012;35(1): 1-19.
25. Miyazaki M, Lee V. Nonenhanced MRangiography. Radiology. 2008;248(1): 20-43.
26. Holloway B, Rosewarne D, Jones R. Imaging of thoracic aortic disease. Br J Radiol. 2011;84(Spec Iss 3): S338-354.
27. Axel L. Blood flow effects in magnetic resonance imaging. Am J Roentgenol. 1984;143(6): 1157-1166.
28. Bradley W, Waluch V. Blood flow: magnetic resonance imaging. Radiology. 1985;154(2): 443-450.
29. Lotz J, Meier C, Leppert A, Galanski M. Cardiovascular flow measurement with phase-contrast MR imaging: basic facts and implementation. Radiographics. 2002;22(3): 651-671.
30. Nelemans P, Leiner T, de Vet H, van Engelshoven J. Peripheral arterial disease: meta-analysis of the diagnostic performance of MR angiography. Radiology. 2000; 217(1): 105-114.
31. Dixon W. Simple proton spectroscopic imaging. Radiology. 1984;153(1): 189-194.
32. Nezafat M, Henningsson M, Ripley D, Dedieu N, Greil G, Greenwood J, Börnert P, Plein S, Botnar R. Coronary MR angiography at 3T: fat suppression versus water-fat separation. J Cardiovasc Magn Reson. 2014;16(Suppl 1): 175.
33. Calkoen E, Roest A, van der Geest R, de Roos A, Westenberg J. Cardiovascular function and flow by 4-dimensional magnetic resonance imaging techniques: new applications. J Thorac Imaging. 2014;29(3): 185-196.
34. Dyverfeldt P, Bissell M, Barker A, Bolger A, Carlhäll C, Ebbers T, Francios C, Frydrychowicz A, Geiger J, Giese D, Hope M, Kilner P, Kozerke S, Myerson S, Neubauer S, Wieben O, Markl M. 4D flow cardiovascular magnetic resonance consensus statement. J Cardiovasc Magn Reson. 2015;17(1): 72.
35. Mitsuzaki K, Yamashita Y, Onomichi M, et al. Delineation of simulated vascular stenosis with Gd-DTPA-enhanced 3D gradient echo MR angiography: An experimental study. J Comput Assist Tomogr. 2000;24(1): 77-82.
36. Korosec F, Mistretta C. MR angiography: basic principles and theory. Magn Reson Imaging Clin N Am. 1998;6(2): 223-256.
37. Inzitari D, Eliasziw M, Gates P, Sharpe B, Chan R, Meldrum H, Barnett H. The causes and risk of stroke in patients with asymptomatic internal-carotid-artery stenosis. N Engl J Med. 2000;342(23): 1693-1701.
38. Mozaffarian D, Benjamin E, Go AS, Arnett D, Blaha M, Cushman M, Das S, de Ferranti S, Després J-P, Fullerton H, Howard V, Huffman M, Isasi C, Jiménez M, Judd S, Kissela B, Lichtman J, Lisabeth L, Liu S, Mackey R, Magid D, McGuire D, Mohler III E, Moy C, Muntner P, Mussolino M, Nasir K, Neumar R, Nichol G, Palaniappan L, Pandey D, Reeves M, Rodriguez C, Rosamond W, Sorlie P, Stein J, Towfighi A, Turan T, Virani S, Woo D, Yeh R, Turner M, on behalf of the American Heart Association Statistics Committee and Stroke Statistics Subcommittee. Heart disease and stroke statistics-2016 update. A report from the American Heart Association. Circulation. 2016; 133(4): 38-361.

39. Amarenco P, Lavallée P, Labreuche J, Albers G, Bornstein N, Canhão P, Caplan L, Donnan G, Ferro J, Hennerici M, Molina C, Rothwell P, Sissani L, Školoudík D, Steg P, Touboul P-J, Uchiyama S, Vicaut E, Wong L. One-year risk of stroke after transient ischemic attack or minor stroke. N Engl J Med. 2016;374(16): 1533-1542.
40. Hankey G, Warlow C, Sellar R. Cerebral angiographic risk in mild cerebrovascular disease. Stroke. 1990;21(2): 209-222.
41. Wardlaw J, Chapel F, Best J, Wartolowska K, Berry E. Noninvasive imaging compared with intra-arterial angiography in the diagnosis of symptomatic carotid stenosis: a meta-analysis. Lancet. 2006;367(9521): 1503-1512.
42. Arous E, Simons J, Flahive J, Beck A, Stone D, Hoel A, Messina L, Schanzer A. National variation in preoperative imaging, carotid duplex ultrasound criteria, and threshold for surgery for asymptomatic carotid artery stenosis. J Vasc Surg. 2015;62(4): 937-944.
43. Brot T, Halperin J, Abbara S, Bacharach J, Barr J, Bush R, Cates C, Creager M, Fowler S, Friday G, Hertzberg V, McIff E, Moore W, Panagos P, Riles Th, Rosenwasser R, Taylor A. 2011 guideline on management of patients with extracranial carotid and vertebral artery disease: executive summary. J Am Coll Cardiol. 2011;57(8): 1002-1044.
44. DeMarco J, Willinek W, Finn J, Huston III J. Current state-of-the-art 1.5T and 3T extracranial carotid contrast-enhanced magnetic resonance angiography. Neuroimag Clin N Am. 2012;22(2): 235-257.
45. Dehkharghani S, Qiu D, Albin L, Saindane A. Dose reduction in contrast-enhanced cervical MR angiography: Field strength dependency of vascular signal intensity, contrast administration, and arteriographic quality. Am J Roentgenol. 2015; 204(6): W701-W706.
46. Tomasian A, Salamon N, Lohan DG, Jalili M, Villablanca J, Finn J. Supraaortic arteries: Contrast material dose reduction at 3.0-T high-spatial-resolution MR angiography-feasibility study. Radiology. 2008;249: 980-990.
47. Townsend T, Saloner D, Pan X, Rapp J. Contrast material-enhanced MRA overestimates severity of carotid stenosis, compared with 3D time-of-flight MRA. J Vasc Surg. 2003;38(1): 36-40.
48. Patel M, Kuntz K, Klufas R, Kim D, Kramer J, Polak J, Skillman J, Whittemore A, Edelman R, Kent K. Preoperative assessment of the carotid bifurcation. Can magnetic resonance angiography and duplex ultrasonography replace contrast arteriography? Stroke. 1995;26(10): 1753-1758.
49. DeMarco J, Schonfeld S, Keller I, Bernstein M. Contrast-enhanced carotid MR angiography with commercially available triggering mechanisms and elliptic centric phase encoding. Am J Roentgenol. 2001;12(3): 175-181.
50. Wright V, Olan W, Dick B, Yu H, Alberts-Grill N, Latour L, Baird A. Assessment of CE-MRA for the rapid detection of supra-aortic vascular disease. Neurology. 2005;65(1): 27-32.
51. Zhao H, Wang J, Liu X, Zhao X, Hippe D, Cao Y, Wan J, Yuan C, Xu J. Assessment of carotid artery atherosclerotic disease by using three-dimensional fast black-blood MR imaging: comparison with DSA. Radiology. 2005;274(2): 508-516.
52. Mihai G, Winner M, Raman S, Rajagopalan S, Simonetti O, Chung Y. Assessment of carotid stenosis using three-dimensional T2-weighted dark blood imaging: initial experience. J Magn Reson Imaging. 2012 Feb;35(2): 449-55.
53. Varennes L, Tahon F, Kastler A, Grand S, Thony F, Baguet J, Detante O, Touzé E, Krainik A. Fibromuscular dysplasia: what the radiologist should know: a pictorial review. Insights Imaging. 2015;6(3): 295-307.
54. Debette S, Leys D. Cervical-artery dissections: predisposing factors, diagnosis, and outcome. Lancet Neurol. 2009; 8(7): 668-678.
55. Ben Hassena W,. Machet A, Edjlali-Goujon M, Legranda L, Ladouxa A, Mellerioa C, Bodiguela E, Gobin-Metteila M-P,Trystrama D, Rodriguez-Regenta C, Masa J-L, Plat M, Oppenheima C, Medera J-F,Naggaraa O. Imaging of cervical artery dissection.Diagn Interv Imaging. 2014; 95(12): 1151-1161.
56. Desjardins B, Dill KE, Flamm SD, Francois CJ, Gerhard-Herman MD, Kalva SP, Mansour MA, Mohler ER 3rd, Oliva IB, Schenker MP, Weiss C, Rybicki FJ; American College of Radiology. ACR Appropriateness Criteria® pulsatile abdominal mass, suspected abdominal aortic aneurysm. Int J Cardiovasc Imaging. 2013;29(1): 177-183.

57. Douglas P, Garcia M, Haines D, Lai W, Manning W, Patel AR, Picard M, Polk D, Ragosta M, Ward R, Weiner R. Appropriate use of echocardiography. J Am Soc Echocardiogr. 2011;24(3): 229-267.
58. Evangelista A, Flachskampf F, Erbel R, Antonini-Canterin F, Vlachopoulos C, Rocchi G, Sicari R, Nihoyannopoulos P, Zamorano J. Echocardiography in aortic diseases: EAE recommendations for clinical practice. Eur J Echocardiogr. 2010;11(3): 645-658.
59. Flachskampf F, Decoodt P, Fraser A, Daniel W, Roelandt J. Recommendations for performing transesophageal echocardiography. Eur J Echocardiogr. 2001;2(1): 8–21.
60. Flachskampf F, Badano L, Daniel W, Feneck R, Fox K, Fraser A, Pasquet A, Pepi M, Perez de Isla L, Zamorano J, Roelandt J, Piérard L. Recommendations for transoesophageal echocardiography-update 2010. Euro Heart J Cardiovasc Imaging. 2010;11(7): 557-576.
61. Sommer T, Fehske W, Holzknecht N, Smekal A, Keller E, Lutterbey G, Kreft B, Kuhl C, Gieseke J, Abu-Ramadan D, Schild H. Aortic dissection: a comparative study of diagnosis with spiral CT, multiplanar transesophageal echocardiography, and MR imaging. Radiology. 1996;199(2): 347-352.
62. Steenburg S, Ravenel J. Acute traumatic thoracic aortic injuries: experience with 64-MDCT. Am J Roentgenol. 2008;191(5): 1564-1569.
63. Erbel R, Aboyans V, Boileau C, Bossone E, Di Bartolomeo R, Eggebrecht H, Evangelista A, Falk V, Frank H, Gaemperli O, Grabenwöger M, Haverich A, Iung B, Manolis A, Meijboom F, Nienaber CA, Roffi M, Rousseau H, Sechtem U, Sirnes P, Allmen R, Vrints C; ESC committee for practice guidelines. 2014 ESC guidelines on the diagnosis and treatment of aortic diseases. Eur Heart J. 2014;35(41): 2873-2926.
64. Plathow C, Ley S, Zaporozhan J, Schöbinger M, Gruenig E, Puderbach M, Eichinger M, Meinzer H, Zuna I, Kauczor H. Assessment of reproducibility and stability of different breath-hold maneuvers by dynamic MRI: comparison between healthy adults and patients with pulmonary hypertension. Eur Radiol. 2006;16(1):173-179.
65. Kramer C, Barkhausen J, Flamm S, Kim R, Nagel E. Standardized cardiovascular magnetic resonance imaging (CMR) protocols, society for cardiovascular magnetic resonance: board of trustees task force on standardized protocols. J Cardiovasc Magn Reson. 2008;10:35.
66. Lim R, Winchester P, Bruno M, Xu J, Storey P, McGorty K, Sodickson D, Srichai M. Highly accelerated single breath-hold noncontrast thoracic MRA: evaluation in a clinical population. Invest Radiol. 2013;48(3): 145-151.
67. Mayil S. Krishnam, Tomasian A, Malik S, Desphande V, Laub G, Ruehm S. Image quality and diagnostic accuracy of unenhanced SSFP MR angiography compared with conventional contrast-enhanced MR angiography for the assessment of thoracic aortic diseases. Eur Radiol. 2010;20(6): 1311–1320.
68. Srichai M, Kim S, Axel L, Babb J, Hecht E. Non-gadolinium-enhanced 3-dimensional magnetic resonance angiography for the evaluation of thoracic aortic disease: a preliminary experience. Tex Heart Inst J. 2010;37(1): 58-65.
69. Hiratzka L, Bakris G, Beckman J, Bersin R, Carr V, Casey D Jr, Eagle K, Hermann L, Isselbacher E, Kazerooni E, Kouchoukos N, Lytle B, Milewicz D, Reich D, Sen S, Shinn J, Svensson L, Williams D; American College of Cardiology Foundation/American Heart Association Task Force on Practice Guidelines; American Association for Thoracic Surgery; American College of Radiology; American Stroke Association; Society of Cardiovascular Anesthesiologists; Society for Cardiovascular Angiography and Interventions; Society of Interventional Radiology; Society of Thoracic Surgeons; Society for Vascular Medicine. 2010 ACCF/AHA/AATS/ACR/ASA/SCA/SCAI/SIR/STS/SVM Guidelines for the diagnosis and management of patients with thoracic aortic disease. A Report of the American College of Cardiology Foundation/American Heart Association Task Force on Practice Guidelines, American Association for Thoracic Surgery, American College of Radiology,American Stroke Association, Society of Cardiovascular Anesthesiologists, Society for Cardiovascular Angiography and Interventions, Society of Interventional Radiology, Society of Thoracic Surgeons,and Society for Vascular Medicine. J Am Coll Cardiol. 2010;55(14): e27-e129.
70. Cozijnsen L, Braam R, Waalewijn R, Schepens M, Loeys B, van Oosterhout M, Barge-Schaapveld D, Mulder B. What is new in dilatation of the ascending aorta? Review of current literature and practical advice for the cardiologist. Circulation. 2011;123(8): 924-928.

71. Svensson L, Adams D, Bonow R, Kouchoukos N, Miller D, O'Gara P, Shahian D, Schaff H, Akins C, Bavaria J, Blackstone E, David T, Desai N, Dewey T, D'Agostino R, Gleason T, Harrington K, Kodali S, Kapadia S, Leon M, Lima B, Lytle B, Mack M, Reardon M, Reece T, Reiss G, Roselli E, Smith C, Thourani V, Tuzcu E, Webb J, Williams M. Aortic valve and ascending aorta guidelines for management and quality measures. Ann Thorac Surg. 2013;95(6 Suppl): S1-66.
72. Mendoza D, Kochar M, Devereux R, Basson C, Min J, Holmes K, Dietz H, Milewicz D, LeMaire S, Pyeritz R, Bavaria J, Maslen C, Song H, Kroner B, Eagle K, Weinsaft J; GenTAC (National registry of genetically triggered thoracic aortic aneurysms and cardiovascular conditions) study investigators. Impact of image analysis methodology on diagnostic and surgical classification of patients with thoracic aortic aneurysms. Ann Thorac Surg. 2011;92(3): 904-912.
73. Landenhed M, Engstrom G, Gottsater A, Caulfield M, Hedblad B, Newton-Cheh C, Melander O, Gustav Smith G. Risk profiles for aortic dissection and ruptured or surgically treated aneurysms: a prospective cohort study. J Am Heart Assoc. 2015 Jan 21;4(1): e001513.
74. Prince M. Gadolinium-enhanced MR aortography. Radiology. 1994;191(1): 155–164.
75. Arlart I, Gerlach A, Kolb M, Erpenbach S, Würstlin S. MR-Angiographie mit Gd-DTPA zum Staging des abdominellen Aortenaneurysmas: Korrelation mit DSA und CT Gadopentate dimeglumine enhanced MR angiography (MRA) for staging AAA: a correlation with DSA and CT. Fortschr Röntgenstr. 1997;167(9): 257-263.
76. Singh K, Bønaa K, Jacobsen B, Bjørk L, Solberg S. Prevalence of and risk factors for abdominal aortic aneurysms in a population-based study: The Tromsø Study. Am J Epidemiol. 2001;154(3): 236-244.
77. Forsdahl S, Singh K, Solberg S, Jacobsen B. Risk factors for abdominal aortic aneurysms: a 7-year prospective study: the Tromsø Study, 1994-2001. Circulation. 2009;119(16): 2202-2208.
78. Tessier D, Stone W, Fow R, Abbas M, Andrews J, Bower T, Gloviczki P. Clinical features and management of splenic artery pseudoaneurysm: case series and cumulative review of literature. J Vasc Surg. 2003;38(5): 969-974.
79. Deipolyi A, Rho J, Khademhosseini A, Oklu R. Diagnosis and management of mycotic aneurysms. Clin Imag. 2016;40(2): 256-262.
80. Christoph A. Nienaber. The role of imaging in acute aortic syndromes. Eur Heart J Cardiovasc Imaging. 2013;14(1): 15-23.
81. Chiappini B, Schepens M, Tan E, Dell' Amore A, Morshuis W, Dossche K, Bergonzini M, Camurri N, Reggiani L, Marinelli G, Di Bartolomeo R. Early and late outcomes of acute type A aortic dissection: analysis of risk factors in 487 consecutive patients. Eur Heart J. 2005;26(2): 180–186.
82. Nienaber C, von Kodolitsch Y, Nicolas V, Siglow V, Piepho A, Brockhoff C, Koschyk D, Spielmann R. The diagnosis of thoracic aortic dissection by noninvasive imaging procedures. N Engl J Med. 1993;328(1): 1–9.
83. Shiga T, Wajima Z, Apfel C, Inoue T, Ohe Y. Diagnostic accuracy of transesophageal echocardiography, helical computed tomography, and magnetic resonance imaging for suspected thoracic aortic dissection systematic review and meta-analysis. Arch Intern Med. 2006;166(13): 1350-1356.
84. Harding M, Smith L, Himmelstein S, Harrison K, Phillips H, Schwab S, Hermiller J, Davidson C, Bashore T. Renal artery stenosis: prevalence and associated risk factors in patients undergoing routine cardiac catheterization. J Am Soc Nephrol. 1992;2(11): 1608-1616.
85. Olin J, Melia M, Young J, Graor R, Risius B. Prevalence of atherosclerotic renal artery stenosis in patients with atherosclerosis elsewhere. Am J Med. 1990;88(1N): 46N-51N.
86. Rimmer J, Gennari F. Atherosclerotic renovascular disease and progressive renal failure. Ann Intern Med. 1993;118(9): 712-719.
87. Sanidas E, Seferou M, Papadopoulos D, Makris A, Viniou N, Chantziara V, Cennimata V, Papademetriou V. Renal fibromuscular dysplasia: a not so common entity of secondary hypertension. J Clin Hypertens. 2016;18(3): 240-246.
88. Kohler T, Zierler R, Martin R, Nicholls S, Bergelin R, Kazmers A, Beach K, Strandness D. Noninvasive diagnosis of renal artery stenosis by ultrasonic duplex scanning. J Vasc Surg. 1986;4(5): 450-456.
89. Taylor D, Kettler M, Moneta G, Kohler T, Kazmers A, Beach K, Strandness D. Duplex ultrasound scanning in the diagnosis of renal artery stenosis: a prospective evaluation. J Vasc Surg. 1988;7(2): 363-369.

90. Olin J, Piedmonte M, Young J, De Anna S, Grubb M, Childs M. The utility of duplex ultrasound scanning of the renal arteries for diagnosing significant renal artery stenosis. Ann Intern Med. 1995;122(1): 833-838.
91. Hoffmann U, Edwards JM, Carter S, Goldman M, Harley J, Zaccardi M, Strandness D. Role of duplex scanning for the detection of atherosclerotic renal artery disease. Kidney Int. 1991;39(6): 1232-1239.
92. Zeisbrich M, Kihm L, Drüschler F, Zeier M, Schwenger V. When is contrast-enhanced sonography preferable over conventional ultrasound combined with Doppler imaging in renal transplantation? Clin Kidney J. 2015;8(5): 606-614.
93. Rountas C, Vlychou M, Vassiou K, Liakopoulos V, Kapsalaki E, Koukoulis G, Fezoulidis I, Stefanidis I. Imaging modalities for renal artery stenosis in suspected renovascular hypertension: prospective intraindividual comparison of color Doppler US, CT angiography, GD-enhanced MR angiography, and digital subtraction angiography. Ren Fail. 2007;29(13): 295-302.
94. Steinwender C, Schutzenberger W, Fellner F, Hönig S, Schmitt B, Focke C, Hofmann R, Leisch F. 64-Detector CT angiography in renal artery stent evaluation: prospective comparison with selective catheter angiography. Radiology. 2009;252(1): 299-305.
95. Bakker J, Beek F, Beutler J, Hene R, de Kort G, de Lange E, Moons K, Mali W. Renal artery stenosis and accessory renal arteries: accuracy of detection and visualization with gadolinium-enhanced breath-hold MR angiography. Radiology. 1998;207(2): 497-504.
96. Vasbinder G, Nelemans P, Kessels A, Kroon A, de Leeuw P, van Engelshoven J. Diagnostic tests for renal artery stenosis in patients suspected of having renovascular hypertension: a meta-analysis. Ann Intern Med. 2001;135(6): 401-411.
97. Prince M, Schoenberg S, Ward J, Londy F, Wakefield T, Stanley J. Hemodynamically significant atherosclerotic renal artery stenosis: MR angiographic features. Radiology. 1997;205(1): 128-136.
98. Leiner T, Nelemans P, de Haan M, de Leeuw P, van Engelshoven J, Vasbinder G. Addition of phase-contrast data to anatomical evaluation substantially improves the diagnostic accuracy of dynamic contrast-enhanced renal MR angiography for the detection of renal artery stenosis. In: RSNA Annual Meeting Abstract Book. 2006:540.
99. ASTRAL Investigators, Wheatley K, Ives N, Gray R, Kalra P, Moss J, Baigent C, Carr S, Chalmers N, Eadington D, Hamilton G, Lipkin G, Nicholson A, Scoble J. Revascularization versus medical therapy for renal-artery stenosis. N Engl J Med. 2009;361(20): 1953-1962.
100. Cooper C, Murphy T, Cutlip D, Jamerson K, Henrich W, Reid D, Cohen D, Matsumoto A, Steffes M, Jaff M, Prince M, Lewis E, Tuttle K, Shapiro J, Rundback J, Massaro J, D'Agostino R, Dworkin L; CORAL Investigators. Stenting and medical therapy for atherosclerotic renal-artery stenosis. N Engl J Med. 2014;370(1): 13-22.
101. Caielli P, Frigo A, Pengo M, Rossito G, Maiolino G, Seccia, T, Calo L, Miotto D, Rossi G. Treatment of atherosclerotic renovascular hypertension: review of observational studies and a meta-analysis of randomized clinical trials. Nephrol Dial Transplant. 2015;30(4): 541-553.
102. Kumbhani D, Bavry A, Harvey J, de Souza R, Scarpioni R, Bhatt D, Kapadia S. Clinical outcomes after percutaneous revascularization versus medical management in patients with significant renal artery stenosis: a meta-analysis of randomized controlled trials. Am Heart J. 2011;161(3): 622-630.
103. Bavishi C, de Leeuw P, Messerli F. Atherosclerotic renal artery stenosis and hypertension: pragmatism, pitfalls, and perspectives Am J Med. 2016;129(6): 635.e5-635.e14.
104. Mohan I, Bourke V. The management of renal artery stenosis: an alternative interpretation of ASTRAL and CORAL. Eur J Vasc Endovasc Surg. 2015;49(4): 465-473.
105. Hansen K, Wilson D, Craven T, Pearce J, English W, Edwards M, Ayerdi J, Burke G. Mesenteric artery disease in the elderly. J Vasc Surg. 2004;40(1): 45-52.
106. Roobottom C, Dubbins P. Significant disease of the celiac and superior mesenteric arteries in asymptomatic patients: predictive value of Doppler sonography. Am J Roentgenol. 1993;161(5): 985–988.
107. Parameshwarappa S, Savlania A, Viswanathan S, Gadhinglajkar S, Raman K, Unnikrishnan M. Chronic mesenteric ischemia and therapeutic paradigm of mesenteric revascularization. Indian J Gastroenterol. 2014;33(2): 169-174.

108. Matsumoto A, Tegtmeyer C, Fitzcharles E, Selby J, Tribble C, Angle J, Kron I. Percutaneous transluminal angioplasty of visceral arterial stenoses: results and long-term clinical follow-up. J Vasc Interv Radiol. 1995;6(2): 165-174.
109. Brandt L, Boley S. AGA technical review on intestinal ischemia. Gastroenterology. 2000;118(5): 954-968.
110. Carrick R, Borge M, Labropolous N, Rodriguez H. Chronic mesenteric ischemia resulting from isolated lesions of the superior mesenteric artery a case report. Angiology. 2005;56(6): 785-788.
111. Cangemi J, Picco M. Intestinal ischemia in the elderly. Gastroenterol Clin North Am. 2009;38(3): 527-540.
112. Balduf L, Langsfeld M, Marek J, Tullis M, Kasirajan K, Matteson B. Complication rates of diagnostic angiography performed by vascular surgeons. Vasc Endovascular Surg. 2002;36(6): 439-445.
113. Moneta G, Lee R, Yeager R, Taylor L, Porter J. Mesenteric duplex scanning: a blinded prospective study. J Vasc Surg. 1993;17(1): 79-84.
114. Oliva I, Davarpanah A, Rybicki F, Desjardins B, Flamm S, Francois C, Gerhard-Herman M, Kalva S, Ashraf Mansour M, Mohler E, Schenker M, Weiss C, Dill K. ACR appropriateness criteria: imaging of mesenteric ischemia. Abdom Imaging. 2013;38(4): 714-719.
115. Moneta GL. Screening for mesenteric vascular insufficiency and follow-up of mesenteric artery bypass procedures. Semin Vasc Surg. 2001;14(3): 186-192.
116. Van Petersen A, Kolkman J, Meerwaldt R, Huisman A, van der Palen J, Zeebregts C, Geelkerken R. Mesenteric stenosis, collaterals, and compensatory blood flow. J Vasc Surg. 2014;60(1): 111–119.
117. Schaefer P, Pfarr J, Trentmann J, Wulff A, Langer C, Siggelkow M, Groß J, Knabe H, Schaefer F. Comparison of noninvasive imaging modalities for stenosis grading in mesenteric arteries. Rofo. 2013;185(7): 628-634.
117. Meaney J, Prince M, Nostrant T, Stanley J. Gadolinium-enhanced MR angiography of visceral arteries in patients with suspected chronic mesenteric ischemia. J Magn Reson Imaging. 1997;7(1): 171–176.
119. Holland G, Dougherty L, Carpenter J, Golden M, Gilfeather M, Slossman F, Schnall M, Axel L. Breath-hold ultrafast three-dimensional gadolinium-enhanced MR angiography of the aorta and the renal and other visceral abdominal arteries. Am J Roentgenol.1996;166(4): 971–81.
120. Jaster A, Choudhery S, Ahn R, Sutphin P, Kalva S, Anderson M, Pillai A. Anatomic and radiologic review of chronic mesenteric ischemia and its treatment. Clin Imaging. 2016;40(5): 961–969.
121. Laissy J, Trillaud H, Douek P. MR angiography: noninvasive vascular imaging of the abdomen. Abdom Imaging. 2002;27(5): 488-506.
122. Hagspiel K, Flors L, Hanley M, Norton P. Computed tomography angiography and magnetic resonance angiography imaging of the mesenteric vasculature. Tech Vasc Interv Radiol. 2015;18(1): 2-13.
123. Iozzelli A, D'Orta G, Aliprandi A, Secchi F, Di Leo G, Sardanelli F. The value of true-FISP sequence added to conventional gadolinium-enhanced MRA of abdominal aorta and its major branches. Eur J Radiol. 2009;72(3): 489-493.
124. Fowkes FG, Rudan D, Rudan I, Aboyans V, Denenberg JO, McDermott MM, Norman PE, Sampson UK, Williams LJ, Mensah GA, Criqui MH. Comparison of global estimates of prevalence and risk factors for peripheral artery disease in 2000 and 2010: a systematic review and analysis. Lancet. 2013;382(9901): 1329–1340.
125. Allison MA, Ho E, Denenberg JO, Langer RD, Newman AB, Fabsitz RR, Criqui MH. Ethnic-specific prevalence of peripheral arterial disease in the United States. Am J Prev Med. 2007;32(4): 328–333.
126. Sampson UK, Fowkes FG, McDermott MM, Criqui MH, Aboyans V, Norman PE, Forouzanfar MH, Naghavi M, Song Y, Harrell FE Jr, Denenberg JO, Mensah GA, Ezzati M, Murray C. Global and regional burden of death and disability from peripheral artery disease: 21 world regions, 1990 to 2010. Glob Heart. 2014;9(1): 145-158.
127. Norgren L, Hiatt WR, Dormandy JA, Nehler MR, Harris KA, Fowkes FG; TASC II Working Group. Inter-society consensus for the management of peripheral arterial disease (TASC II). J Vasc Surg. 2007;45(suppl S): S5-S67.
128. Eraso LH, Fukaya E, Mohler ER 3rd, Xie D, Sha D, Berger JS. Peripheral arterial disease, prevalence and cumulative risk factor profile analysis. Eur J Prev Cardiol. 2014;21(6): 704-711.
129. Khawaja FJ, Kullo IJ. Novel markers of peripheral arterial disease. Vasc Med. 2009; 4(4): 381-392.

130. Hirsch AT, Criqui MH, Treat-Jacobson D, Regensteiner JG, Creager MA, Olin JW, Krook SH, Hunninghake DB, Comerota AJ, Walsh ME, McDermott MM, Hiatt WR. Peripheral arterial disease detection, awareness, and treatment in primary care. JAMA. 2001;286(11): 1317–1324.
131. Criqui MH, Ninomiya JK, Wingard DL, Ji M, Fronek A. Progression of peripheral arterial disease predicts cardiovascular disease morbidity and mortality. J Am Coll Cardiol. 2008; 52(21): 1736-1742.
132. Araki Y, Kumakura H, Kanai H, Kasama S, Sumino H, Ichikawa A, Ito T, Iwasaki T, Takayama Y, Ichikawa S, Fujita K, Nakashima K, Minami K, Kurabayashi M. Prevalence and risk factors for cerebral infarction and carotid artery stenosis in peripheral arterial disease. Atherosclerosis 2012;223(2): 473-477.
133. Sigvant B, Lundin F, Wahlberg E. The risk of disease progression in peripheral arterial disease is higher than expected: a meta-analysis of mortality and disease progression in peripheral arterial disease. Eur J Vasc Endovasc Surg. 2016;51(3): 395-403.
134. Goff DC Jr, Lloyd-Jones DM, Bennett G, Coady S, D'Agostino RB Sr, Gibbons R, Greenland P, Lackland DT, Levy D, O'Donnell CJ, Robinson JG, Schwartz JS, Shero ST, Smith SC Jr, Sorlie P, Stone NJ, Wilson PW; American College of Cardiology/American Heart Association Task Force on Practice Guidelines 2013 ACC/AHA guideline on the assessment of cardiovascular risk: a report of the American College of Cardiology/American Heart Association Task Force on Practice Guidelines. J Am Coll Cardiol. 2014;63(25): 2935-2959.
135. Greenland P, Alpert JS, Beller GA, Benjamin EJ, Budoff MJ, Fayad ZA, Foster E, Hlatky MA, Hodgson JM, Kushner FG, Lauer MS, Shaw LJ, Smith SC Jr, Taylor AJ, Weintraub WS, Wenger NK, Jacobs AK, Smith SC Jr, Anderson JL, Albert N, Buller CE, Creager MA, Ettinger SM, Guyton RA, Halperin JL, Hochman JS, Kushner FG, Nishimura R, Ohman EM, Page RL, Stevenson WG, Tarkington LG, Yancy CW; American College of Cardiology Foundation; American Heart Association. ACCF/AHA guideline for assessment of cardiovascular risk in asymptomatic adults: a report of the American College of Cardiology Foundation/American Heart Association Task Force on Practice Guidelines. J Am Coll Cardiol. 2010;56(25): e50-e103.
136. Van den Bosch H, Westenberg J, Setz-Pels W, Kersten E, Tielbeek A, Duijm L, Post J, Teijink J, de Roos A. Prognostic value of cardiovascular MR imaging biomarkers on outcome in peripheral arterial disease: a 6-year follow-up pilot study. Int J Cardiovasc Imaging. (Epub ahead of print).
137. Dormandy JA, Rutherford RB. Management of peripheral arterial disease (PAD). TASC Working Group. TransAtlantic Inter-Society Consensus (TASC) J Vasc Surg. 2000 Jan;31(1): S1–S296.
138. Norgren L, Hiatt WR, Dormandy JA, Nehler MR, Harris KA, Fowkes FG; TASC II Working Group. Inter-Society Consensus for the Management of Peripheral Arterial Disease (TASC II). J Vasc Surg. 2007 Jan;45(Suppl S): S5-67.
139. Hirsch AT, Haskal ZJ, Hertzer NR, Bakal CW, Creager MA, Halperin JL, Hiratzka LF, Murphy WR, Olin JW, Puschett JB, Rosenfield KA, Sacks D, Stanley JC, Taylor LM Jr, White CJ, White J, White RA, Antman EM, Smith SC Jr, Adams CD, Anderson JL, Faxon DP, Fuster V, Gibbons RJ, Hunt SA, Jacobs AK, Nishimura R, Ornato JP, Page RL, Riegel B; American Association for Vascular Surgery; Society for Vascular Surgery; Society for Cardiovascular Angiography and Interventions; Society for Vascular Medicine and Biology; Society of Interventional Radiology; ACC/AHA Task Force on Practice Guidelines Writing Committee to Develop Guidelines for the Management of Patients With Peripheral Arterial Disease; American Association of Cardiovascular and Pulmonary Rehabilitation; National Heart, Lung, and Blood Institute; Society for Vascular Nursing; TransAtlantic Inter-Society Consensus; Vascular Disease Foundation. ACC/AHA 2005 Practice guidelines for the management of patients with peripheral arterial disease (lower extremity, renal, mesenteric, and abdominal aortic): a collaborative report from the American Association for Vascular Surgery/Society for Vascular Surgery, Society for Cardiovascular Angiography and Interventions, Society for Vascular Medicine and Biology, Society of Interventional Radiology, and the ACC/AHA Task Force on Practice Guidelines (Writing Committee to Develop Guidelines for the Management of Patients With Peripheral Arterial Disease): endorsed by the American Association of Cardiovascular and Pulmonary Rehabilitation; National Heart, Lung, and Blood Institute; Society for Vascular Nursing; TransAtlantic Inter-Society Consensus; and Vascular Disease Foundation. Circulation. 2006;113(11): e463-654.

140. Rooke TW, Hirsch AT, Misra S, Sidawy AN, Beckman JA, Findeiss LK, Golzarian J, Gornik HL, Halperin JL, Jaff MR, Moneta GL, Olin JW, Stanley JC, White CJ, White JV, Zierler RE; Society for Cardiovascular Angiography and Interventions; Society of Interventional Radiology; Society for Vascular Medicine; Society for Vascular Surgery. 2011 ACCF/AHA focused update of the guideline for the management of patients with peripheral artery disease (updating the 2005 guideline): a report of the American College of Cardiology Foundation/ American Heart Association Task Force on Practice Guidelines. J Am Coll Cardiol. 2011;58(19): 2020-2045.
141. O'Keeffe ST, Persson AV. Use of noninvasive vascular laboratory in diagnosis of venous and arterial disease. Cardiol Clin. 1991;9(3):429–442.
142. Ankle Brachial Index Collaboration, Fowkes FG, Murray GD, Butcher I, Heald CL, Lee RJ, Chambless LE, Folsom AR, Hirsch AT, Dramaix M, deBacker G, Wautrecht JC, Kornitzer M, Newman AB, Cushman M, Sutton-Tyrrell K, Fowkes FG, Lee AJ, Price JF, d'Agostino RB, Murabito JM, Norman PE, Jamrozik K, Curb JD, Masaki KH, Rodríguez BL, Dekker JM, Bouter LM, Heine RJ, Nijpels G, Stehouwer CD, Ferrucci L, McDermott MM, Stoffers HE, Hooi JD, Knottnerus JA, Ogren M, Hedblad B, Witteman JC, Breteler MM, Hunink MG, Hofman A, Criqui MH, Langer RD, Fronek A, Hiatt WR, Hamman R, Resnick HE, Guralnik J, McDermott MM. Ankle brachial index combined with Framingham Risk Score to predict cardiovascular events and mortality: a meta-analysis. JAMA. 2008;300(2): 197-208.
143. Newman AB, Shemanski L, Manolio TA, Cushman M, Mittelmark M, Polak JF, Powe NR, Siscovick D. Ankle-arm index as a predictor of cardiovascular disease and mortality in the Cardiovascular Health Study: the Cardiovascular Health Study Group. Arterioscler Thromb Vasc Biol.1999;19(3): 538-545.
144. McDermott MM, Feinglass J, Slavensky R, Pearce WH. The ankle-brachial index as a predictor of survival in patients with peripheral vascular disease. J Gen Intern Med. 1994;9(8): 445-449.
145. McKenna M, Wolfson S, Kuller L. The ratio of ankle and arm arterial pressure as an independent predictor of mortality. Atherosclerosis. 1991;87(2-3): 119-128.
146. Doobay AV, Anand SS. Sensitivity and specificity of the ankle-brachial index to predict future cardiovascular outcomes: a systematic review. Arterioscler Thromb Vasc Biol. 2005;25(7): 1463–1469.
147. Wikström J, Hansen T, Johansson L, Lind L, Ahlström H. Ankle brachial index <0.9 underestimates the prevalence of peripheral artery occlusive disease assessed with whole-body magnetic resonance angiography in the elderly. Acta Radiol. 2008;49(2):143-149.
148. Meyer BC, Werncke T, Foert E, Kruschewski M, Hopfenmüller W, Ribbe C, Wolf KJ, Albrecht T. Do the cardiovascular risk profile and the degree of arterial wall calcification influence the performance of MDCT angiography of lower extremity arteries? Eur Radiol. 2010;20(2):497-505.
149. Nelemans PJ, Leiner T, de Vet HC, van Engelshoven JM. Peripheral arterial disease: meta-analysis of the diagnostic performance of MR angiography. Radiology. 2000;217(1): 105-114.
150. Ho KY, de Haan MW, Kessels AG, Kitslaar PJ, van Engelshoven JM. Peripheral vascular tree stenosis: detection with subtracted and nonsubtracted MR angiography. Radiology. 1998;206(3): 673-681.
151. van den Bosch HC, Westenberg JJ, Caris R, Duijm LE, Tielbeek AV, Cuypers PW, de Roos A. Peripheral arterial occlusive disease: 3.0-T versus 1.5-T MR angiography compared with digital subtraction angiography. Radiology. 2013;266(1): 337-346.
152. Watanabe Y, Dohke M, Okumura A, Amoh Y, Ishimori T, Oda K, Hayashi T, Hiyama A, Dodo Y. Dynamic subtraction contrast-enhanced MR angiography: Technique, clinical applications, and pitfalls. Radiographics. 2000;20(1): 135-152.
153. Dinter DJ, Neff KW, Visciani G, Lachmann R, Weiss C, Schoenberg SO, Michaely HJ. Peripheral bolus-chase MR angiography: analysis of risk factors for nondiagnostic image quality of the calf vessels- a combined retrospective and prospective study. Am J Roentgenol. 2009;193(1): 234-240.
154. Bezooijen R, van den Bosch HC, Tielbeek AV, Thelissen GR, Visser K, Hunink MG, Duijm LE, Wondergem J, Buth J, Cuypers PW. Peripheral arterial disease: sensitivity-encoded multiposition MR angiography compared with intraarterial angiography and conventional multiposition MR angiography. Radiology. 2004;231(1): 263-271.
155. Leiner T, Habets J, Versluis B, Geerts L, Alberts E, Blanken N, Hendrikse J, Vonken EJ, Eggers H. Subtractionless first-pass single contrast medium dose peripheral MR angiography using two-point Dixon fat suppression. Eur Radiol. 2013;23(8): 2228-2235.

156. Johnson CP, Weavers PT, Borisch EA, Grimm RC, Hulshizer TC, LaPlante CC, Rossman PJ, Glockner JF, Young PM, Riederer SJ. Three-station three-dimensional bolus-chase MR angiography with real-time fluoroscopic tracking. Radiology. 2014;272(1): 241-251.

Chapter 5

Peripheral Arterial Disease: Sensitivity-encoded Multiposition MR Angiography Compared with Intraarterial Angiography and Conventional Multiposition MR Angiography

Roland Bezooijen
Harrie CM van den Bosch
Alexander V Tielbeek
Guilaume RP Thelissen
Karen Visser
Myriam Hunink
Lucien EM Duijm
John HM Wondergem
Jaap Buth
Philip WM Cuypers

Radiology 2004;231(1):263-271

Abstract

A sensitivity-encoded magnetic resonance (MR) angiography protocol was developed in which imaging times in the pelvic and upper-leg positions were reduced and isotropic submillimeter voxel volumes were acquired in the lower-leg position. To achieve this, sensitivity encoding and random central-k-space segmentation in a centric filling order were applied. Results with this technique were compared with those with midstream aortic digital subtraction angiography (DSA) (as the reference standard) and conventional MR angiography in 15 patients with peripheral vascular disease. The results show that sensitivity-encoded MR angiography demonstrates increased diagnostic accuracy in comparison to that with conventional MR angiography and depicts more open infragenual arterial segments compared with both midstream aortic DSA.

Introduction

Contrast material–enhanced magnetic resonance (MR) angiography has evolved in only a few years to be a safe, fast, reproducible, and reliable imaging technique.[1–9] With the increasing availability of high-field-strength (1.5-T) MR imaging systems, MR angiography is now widely used for the detection of stenosis in patients with peripheral arterial disease. In MR angiography, the length of the imaged volume in one acquisition is limited to approximately 40–50 cm. Thus, more than one acquisition is required to image the entire vascular tree from the abdominal aorta down to the infragenual arteries.

In general, two MR angiography protocols are used: single-injection multiposition[4–6,10] or multi-injection multiposition.[7–9,11] Compared with the single-injection protocol, the multi-injection protocol has the following advantages: It has almost no limitation of imaging duration for each volume, which allows higher spatial resolution, and it can be performed with any system without the need for special hardware. However, the contrast material volume for each position is limited. More important, by the time the lower-leg arteries are imaged, contrast material from previous acquisitions will cause both venous and tissue enhancement. Although subtraction techniques are used in the multi-injection protocol, venous and tissue enhancement might lead to a lower contrast (or vessel)-to-noise ratio.

In a single-injection multi-position protocol, all three positions (pelvis, upper leg, and lower leg) should be acquired while contrast material is confined to the lower-limb arteries. In MR angiography, the contrast material bolus travels down the arterial tree at an average of 6 seconds per position, and venous enhancement at the ankle occurs approximately 68 seconds after the start of contrast material injection into a decubital vein.[12] The infragenual arteries of a healthy person would be completely filled with contrast material at approximately 18 seconds after the start of the acquisition of the first (pelvic) position. This clearly indicates the limited length of the arterial window despite the large range in venous arrival times and the fact that contrast material travels more slowly in men and the elderly and in patients with aortic aneurysm, arterial occlusive disease, and cardiac disease.[12] Therefore, contrast material may arrive in the venous system while images are being acquired at the most distal position. This venous enhancement can cause non-diagnostic MR images of infragenual arteries. Hence, imaging of the abdomen and upper-leg arteries must become faster to prevent venous enhancement. To better detect and evaluate infragenual arteries, spatial resolution should be increased. An increase in spatial resolution is possible, however, only at the cost of prolonged acquisition times. Current single-injection multi-position contrast-enhanced MR angiography protocols are designed to acquire images as quickly as possible with an acceptable spatial resolution.

New MR imaging techniques have become available. Sensitivity encoding (SENSE; Philips Medical Systems, Best, the Netherlands)[13–15] increases imaging speed without the loss of spatial resolution or reduction of spatial coverage. Random central–k-space segmentation in a centric filling order, a variant of centric k-space filling (CENTRA [contrast-enhanced timing robust angiography]; Philips Medical Systems), allows longer acquisition times without venous enhancement.

The purpose of this prospective study was to compare a single-injection multiposition contrast-enhanced MR angiography protocol with sensitivity encoding and random central–k-space segmentation in a centric filling order (hereafter, sensitivity-encoded MR angiography) with a conventional single-injection multiposition contrast-enhanced MR angiography protocol (hereafter, conventional MR angiography) in patients with peripheral arterial disease. Midstream aortic intra-arterial digital subtraction angiography (DSA) was used as the standard of reference.

Materials and Methods

From March 15 to April 30, 2001, 19 consecutive patients referred to undergo DSA to evaluate symptoms of peripheral arterial disease were asked to participate. One patient was excluded because of a pacemaker, and two patients refused participation. One patient refused to undergo conventional MR angiography and was excluded from the analysis. Therefore, 15 patients were included in the study (13 men and two women; mean age, 66 years; age range, 52-77 years). Patients participated on a voluntary basis, and written informed consent was obtained. Approval was obtained from the institutional review board of the hospital. DSA, conventional MR angiography, and sensitivity-encoded MR angiography were performed within a 1-week interval (mean, 3.5 days). There were no statistically significant differences between the age distributions by sex (p=.171, nonparametric Mann-Whitney U test). Twelve of the 15 patients had mild to severe claudication, two patients had rest pain, and one patient was referred for evaluation of ulcerations in a diabetic foot. No adverse reactions or complications were encountered during or after any of the imaging examinations.

Conventional MR Angiography

Conventional MR angiography (Mobi-Trak; Philips Medical Systems) was performed with a 1.5-T MR system (Gyroscan NT Intera, release 7.1.1; Philips Medical Systems). Patients were positioned feetfirst. For immobilization and alignment of the arteries from the abdominal aorta to the lower-leg arteries, the patients' legs were strapped and fixed in a leg support. A quadrature body coil was used for signal transmission and reception. A survey image was obtained with a two-dimensional multisection turbo

field-echo sequence (image matrix, 256x128; 30 transverse sections; section thickness, 3.3 mm; section gap, 11 mm) in three positions. Automatically generated coronal and sagittal maximum intensity projection images were used for volume planning at conventional MR angiography. The time delay between the start of contrast material injection and the start of the acquisition was determined by means of bolus timing in a thick section with automatic complex subtraction (BolusTrak; Philips Medical Systems). The conventional MR angiography protocol included automated table movement, image reconstruction, and generation of subtraction and maximum intensity projection images. The imaging parameters are presented in Table 5.1.

A biphasic contrast material injection protocol was used: 39 mL of gadoteridol (Prohance; Bracco-Byk Gulden, Konstanz, Germany) was injected by using an MR imaging–compatible injector (Spectris MR injector; Medrad, Indianola, Pa): injection of volume 1, 20 mL at a flow rate of 0.6 mL/sec; injection of volume 2, 19 mL at 0.3 mL/sec with a subsequent saline flush. Total injection duration was 96.6 seconds. Total examination time (patient in and out of the MR unit) ranged from 20 to 30 minutes. After automatic postprocessing at the console of the MR system, the subtracted data were sent to a remote work position (Easy Vision; Philips Medical Systems) for reconstruction and interpretation of the images. No subtraction artifacts were encountered.

Sensitivity-encoded MR Angiography

Sensitivity-encoded MR angiography was performed with the same 1.5-T MR system by using a prerelease version of 8.1 software. For more accurate planning, some parameters in the survey protocol were adjusted (image matrix, 184x256; reconstruction matrix, 256x512; 60 transverse sections; section thickness, 3 mm; section gap, 4 mm). Acquisition of a reference MR image to determine the sensitivity of each element in a four-element synergy (phased-array) body coil is mandatory for application of sensitivity encoding. The abdominal reference MR image was obtained in continuity with the survey acquisition, and after an automated table movement, the lower-leg reference image was obtained. For optimal correlation, both the reference image and the dynamic MR image of the abdomen (aorto-iliac position) were obtained at end expiration. The bolus timing protocol was identical to that in conventional MR angiography.

Table 5.1 Comparison of Imaging Parameters for Standard and Sensitivity-encoded MR Angiography.

		Station		
Parameter	All Volumes	Abdomen	Upper legs	Lower legs
Repetitiom time msec/ echo time msec	6.1 / 1.55	4.8 / 1.36	4.2 / 1.27	4.3 / 1.4
Flip abgle (degrees)	35	20	20	20
No. of sections	35	40	30	60
Tickness (mm)	3.0	2.2	2.0	1.0
Zero interpolation	To 7.0 1.5-mm-thick sections	To 80 1.1-mm-tick sections	To 60 1.0-mm-thick sections	To 120 0.5-mm-tick sections
Volume tickness (cm)	10.5	8.8	6.0	6.0
Field of view (mm)	430	430	430	430
Matrix				
Size (pixel)	512 x 180	384 x 192	416 x 208	432 x 432
Imaging percentage	NA	50 (384 x 384)	50 (416 x 416)	100
Voxel volume (mm^3)				
Acquired	6.0	5.3	4.3	0.98 isotropic
Interpolated	1.06	0.76	0.71	0.35
Coll	Quadrature body	Four-element synergy	Quadrature body	Four-element synergy
Application in sensitivity-encoded MR angiography	NA	Sensitivity encoding (SENSE factor 2)	NA	Constant level appearance
k.Space filling	Abdomen, linear, upper leg, low to high; lower leg, low to high	Linear	Random segmentation of k space	Random segmentation of k space
Imaging time (sec)	31	18	19	79
Table movement	Automatic	Manual during imaging of contrast material	Manual during imaging of contrast material	Manual during imaging of contrast material

NA = not applicable.

MR imaging protocols were used for the abdominal arteries (repetition time msec/echo time msec, 4.8/1.36; section thickness, 2.2 mm; field of view, 430 mm; image matrix, 384x192; acquired voxel volume, 5.3 mm^3), upper-leg arteries (4.2/1.27; section thickness, 2.0 mm; field of view, 430 mm; image matrix, 416x208; acquired voxel volume, 4.3 mm^3), and lower-leg arteries (4.3/1.4; section thickness, 1.0 mm; field of view, 430 mm; image matrix, 432x432; acquired voxel volume, 0.98 mm^3). These sequences were repeated in reverse order after administration of contrast material (Table 5.1). Some further adjustments were made. In the upper- and lower-leg positions, random central–k space segmentation in a centric filling order was applied. The center of k space was written 4 seconds after volume acquisition started, and the central region of k space was filled during the first 4 seconds of volume acquisition in random order (as opposed to centric or elliptic centric orders). Thus, central k space, which provides image contrast, was filled during the arterial imaging window. If venous enhancement occurred, it would be during peripheral k space filling, which provides image resolution. The writing of the exact center of k space 4 seconds after the start of volume acquisition makes this technique less sensitive for early timing errors (Figure 5.1). In the abdomen and lower-leg positions, constant level appearance (CLEAR; Philips Medical Systems) was applied, and a reference MR image was obtained to measure B_1 inhomogeneity and thus non-uniform coil sensitivity. CLEAR is a software tool that compensates for non-uniform coil sensitivity and provides a more homogeneous image comparable to that acquired with a quadrature body coil.

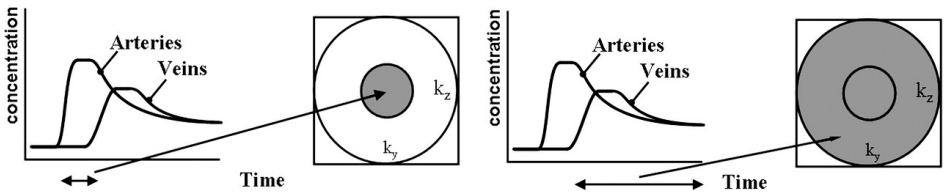

Figure 5.1 Left: During the arterial window, the three-dimensional center of k space is written, which provides image contrast. Right: By the time contrast material arrives in the veins, the periphery of k space is written, which provides image detail.

In the abdomen position, sensitivity encoding was applied in the phase-encoding (left-to-right) direction. Two coil elements were positioned beside each other (two in front and two in back), which led to reduced signal at the borders of the field of view in the feet-to-head direction in comparison to that with a quadrature body coil. Constant level appearance was applied to compensate for the reduced signal. Furthermore, the overlap between the abdomen and upper-leg volume was increased to 8 cm, which reduced total image coverage from 128 to 123 cm. To improve the contrast-to-noise

ratio, the flow rate of contrast material was increased. A biphasic injection was applied to ensure that central k space of the lower-leg position was acquired during passage of the arterial bolus: injection of volume 1, 15 mL at a flow rate of 0.8 mL/sec; injection of volume 2, 25 mL at 0.4 mL/sec. Owing to the changed parameters, central k space of the lower-leg position was filled 49 seconds after the start of the acquisition of the abdomen position. Reduced imaging time, by means of sensitivity encoding, and increased spatial resolution would lead to a reduction of the signal-to-noise ratio. To compensate for this reduction, we used a phased-array coil instead of the quadrature body coil and we increased the contrast material injection rate to improve the signal-to-noise ratio. Furthermore, we reduced the flip angle to 20° because, according to the hardware automated estimation of the signal-to-noise ratio, this was the optimal flip angle for the given MR imaging parameters. This value is also near the theoretic optimum of 25° to 55° [16]. Total examination time ranged from 45 to 55 minutes. No subtraction artifacts were encountered.

DSA Imaging

DSA was performed with a dedicated angiography system (Multistar T.O.P.; Siemens Medical Engineering, Forchheim, Germany) with non-ionic contrast material (iomeprol, Iomeron 350; Bracco-Byk Gulden, Konstanz, Germany). Contrast material was injected at variable flow rates and volumes depending on the catheter tip location and segment imaged. DSA was performed by means of puncture of the common femoral artery. The tip of a 4-F pigtail or straight catheter was positioned in the infrarenal abdominal aorta. The conventional imaging protocol included acquisition of overlapping images from the distal abdominal aorta down to the dorsal pedal artery of both legs. Magnification images and views of suspected stenoses were obtained in two orthogonal directions. When the original images of the infragenual arteries did not have good quality, an intra-arterial vasodilator was administered (slow manual injection of 25 mg of Papaverin [Pharma Chemie, Haarlem, the Netherlands]) to optimize contrast material delivery. An experienced vascular radiologist (A.V.T. or L.E.M.D.) supervised all procedures.

Image Evaluation

The arterial tree in each patient was divided into 29 segments, including the infrarenal aorta, common iliac arteries, external iliac arteries, common femoral arteries, superficial femoral arteries above the abductor canal, superficial femoral arteries below the abductor canal, supragenual popliteal arteries, and infragenual popliteal arteries, as well as the tibiofibular trunk, proximal and distal halves of the anterior tibial arteries, proximal and distal halves of the posterior tibial arteries, and proximal and distal halves of the peroneal arteries.

The most severe stenosis in each arterial segment was chosen for classification. Stenoses were graded by using the following equation: percentage stenosis = (1 - [*D*/*N*]) x 100, where *D* is the measured diameter of the residual lumen at the point of maximal narrowing in a segment, and *N* is the measured diameter at a normal point in that arterial segment. Stenoses were graded on enlarged maximum intensity projection and source MR angiographic images or DSA images by using the digital ruler on a workstation. For segments from the aorta to the popliteal arteries, categories of percentage stenosis were 0%-24%, 25%-49%, 50%-74%, 75%-99%, and 100% (occlusion). Since the diameter of infragenual arteries is 2-3 mm and section thickness in conventional MR angiography is 3 mm, we chose the following categories for stenoses in the infragenual arteries: 0%-49% stenosis, 50%-99% stenosis of one segment, 50%-99% diffuse stenosis in one segment, and 100% stenosis (occlusion). In case a segment could not be scored reliably as a result of poor contrast material delivery at DSA, poor contrast resolution at MR angiography, or an artifact, no grade was assigned. The occurrence of venous enhancement in a segment and the degree of evaluation impairment were scored as grade 0, no venous enhancement; grade 1, venous enhancement present, grading not difficult; grade 2, venous enhancement present, grading suboptimal; or grade 3, venous enhancement present, grading not possible.

MR angiographic images were read by two MR angiography radiologists (H.C.M.v.d.B., J.W., both with 4 years of experience in MR angiography) independently and unaware of the results of other and prior investigations. At least 6 weeks separated the readings of conventional and sensitivity-encoded MR angiographic images. DSA images was read by two vascular radiologists (A.V.T., L.E.M.D.) independently and unaware of the results of other and prior investigations. Final MR angiography and DSA classifications was reached by consensus. If the two readers could not reach consensus, the opinion of an independent radiologist was conclusive.

Statistical Analysis

For the statistical analysis, we considered only segments that were graded on the basis of all three modalities. With DSA as the standard of reference, sensitivity and specificity were calculated with the following categories for disease severity: 50% or more stenosis, 50% or more diffuse stenosis (only infragenual segments), 75% or more stenosis (only non-infragenual segments), and occlusion (100% stenosis). The 95% CIs were constructed for both sensitivity and specificity.[17] A McNemar test was used to determine the statistical significance of differences in sensitivity and specificity between conventional and sensitivity-encoded MR angiography. Furthermore, the number of open infragenual segments was determined at DSA, conventional MR angiography, and sensitivity-encoded MR angiography. Open was defined as not occluded and visible on images of sufficient diagnostic image quality

(ie, sufficient contrast, evaluation not compromised by venous enhancement). A McNemar test was used to compare the number of open infragenual segments between DSA, conventional MR angiography, and sensitivity-encoded MR angiography. A *p* value less than .05 was considered to indicate a statistically significant difference. In the statistical analysis, interdependence between the diagnostic interpretation of arterial segments was not taken into account. The disease severity of arterial segments is correlated within a patient, but this does not necessarily mean that the diagnostic interpretation is also correlated. Therefore, we did not consider the possible correlation between diagnostic interpretation of arterial segments in our analysis.

Results

Owing to a technical error, constant level appearance could not be applied in one patient. In another patient, movement caused artifacts in both conventional and sensitivity-encoded MR angiographic images, but the three images had sufficient image quality for evaluation, and none of these segments were excluded from the analysis. At conventional MR angiography in five patients, venous enhancement occurred in 70 segments of the infragenual arteries, and 15 of the segments could not be evaluated (grade 3 venous enhancement). In three of these five patients at sensitivity-encoded MR angiography, venous enhancement occurred but it did not result in any segments that could not be graded (p<.01) (Table 5.2).

Table 5.2 Occurrence of Venous Enhancement in Infragenual Arterial Segments at Conventional Compared with Sensitivity-encoded MR Angiography.

Grade with Sensitivity-encoded MR Angiography	Grade with Conventional MR Angiography				
	0	1	2	3	Total
0	126	25	20	10	181*
1	0	0	10	5	15†
2	0	0	0	0	0*
3	0	0	0	0	0‡
Total	126	25	30	15	

Data are the number of segments. Grade 0, no venous enhancement; grade 1, venous enhancement present, grading not difficult; grade 2, venous enhancement present, grading suboptimal; grade 3, venous enhancement present, grading not possible. * p<.001; † p <.16; ‡ P<.01.

In all, 381 arterial segments were evaluated with the three imaging techniques; 207 segments were imaged from the aorta to the popliteal artery, and 174 were imaged in the infragenual arteries (Tables 5.3-5.6).

Table 5.3 Stenosis at Standard MR Angiography and DSA.

Stenosis at Conventional MR Angiography	Stenosis at DSA				
	<25%	25%-49%	50%-74%	75%-99%	Occlusion (100%)
<25%	152	4	3	0	0
25%-49%	10	7	3	0	0
50%-74%	1	5	8	1	0
75%-99%	0	0	0	0	1
Occlusion (100%)	0	0	0	0	12

Data are the number of segments. Imaging was performed from the aorto-iliac arteries to the femorpopliteal arteries.

Table 5.4 Stenosis at Sensitivity-encoded MR Angiography and DSA.

Stenosis at Sensitivity-encoded MR Angiography	Stenosis at DSA				
	<25%	25%-49%	50%-74%	75%-99%	Occlusion (100%)
<25%	159	2	1	0	0
25%-49%	3	14	2	0	0
50%-74%	1	1	10	0	0
75%-99%	0	0	1	1	1
Occlusion (100%)	0	0	0	0	13

Data are the number of segments. Imaging was performed from the aorto-iliac arteries to the femoropopliteal arteries.

Table 5.5 Stenosis at Conventional MR Angiography and DSA.

Stenosis at Conventional MR Angiography	Stenosis at DSA			
	<50%	One Stenosis 50%-99%	Diffuse Stenosis 50%-74%	Occlusion (100%)
<50%	94	4	1	30
One stenosis, 50%-99%	5	2	1	0
Diffuse stenosis, 50%-99%	6	3	6	9
Occlusion (100%)	7	1	1	31

Data are the number of segments. Imaging was performed in the infragenual arteries.

Table 5.6 Stenosis at Sensitivity-encoded MR Angiography and DSA.

Stenosis Sensitivity-encoded MR Angiography	Stenosis at DSA			
	<50%	One Stenosis 50%-99%	Diffuse Stenosis 50%-74%	Occlusion (100%)
<50%	105	4	1	3
One stenosis, 50%-99%	7	6	0	0
Diffuse stenosis, 50%-99%	0	0	7	7
Occlusion (100%)	0	0	1	33

Data are the number of segments of the infragenual arteries.

In the aortic to popliteal arteries, the sensitivity of sensitivity-encoded MR angiography for detection of stenosis of 50% or more (89%, 25 of 28 segments; 95% CI: 73%, 96%) was higher than that of conventional MR angiography (79%, 22 of 28 segments; 95% CI: 60%, 90%) (Figure 5.2).

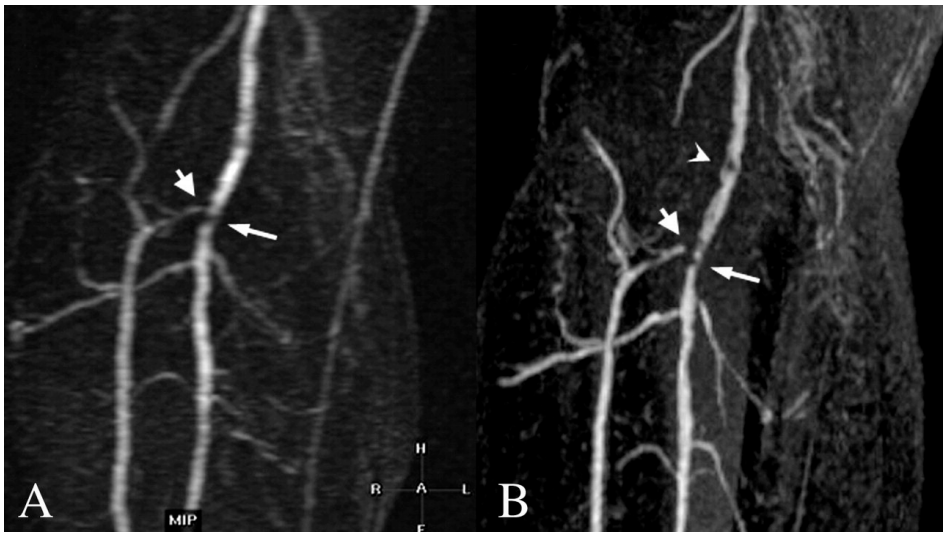

Figure 5.2 Coronal MR angiographic images in the proximal left lower leg of a 65-year-old man with moderate to severe claudication. **(A)** Conventional maximum intensity projection image (6.1/1.55; section thickness, 3 mm; field of view, 430 mm; image matrix, 512x180; acquired voxel volume, 6.0 mm_3) shows a subtotal stenosis at the origin of the anterior tibial artery (short arrow) and a significant stenosis in the tibiofibular trunk (long arrow). **(B)** Sensitivity-encoded maximum intensity projection image (4.3/1.4; section thickness, 1 mm; field of view, 430 mm; image matrix, 432x432; acquired voxel, 0.98 mm_3) of the proximal left lower leg. There is good correlation with the findings in **A**. As a result of the sixfold increase in spatial resolution in **B**, much better detail is seen. Diffuse arterial wall irregularity and a large plaque that causes a significant stenosis in the popliteal artery (arrowhead) are visible in **B** but not in **A**.

The specificity of sensitivity-encoded MR angiography (99%, 177 of 179 segments; 95% CI: 96%, 100%) was similar to that of conventional MR angiography (97%, 173 of 179 segments; 95% CI: 93%, 98%) (Figure 5.3). The sensitivity of sensitivity-encoded MR angiography for detection of occlusions and stenoses of 75% or more was also higher than that for conventional MR angiography. Specificities were equal (Table 5.7).

In the infragenual arteries, the sensitivity for the detection of one significant stenosis was 87% (54 of 62 segments; 95% CI: 77%, 93%) with both conventional and sensitivity-encoded MR angiography. The specificity showed a statistically significant increase from 84% (94 of 112 segments; 95% CI: 76%, 90%) with conventional MR angiography to 93% (104 of 112 segments; 95% CI: 88%, 97%; *p*=.013) with sensitivity-encoded MR angiography. For the detection of diffuse stenosis in arterial segments, the specificity was significantly higher with sensitivity-encoded MR angiography than

that with conventional MR angiography. However, sensitivities were similar for sensitivity-encoded MR angiography and conventional-MR-angiography (Table 5.8).

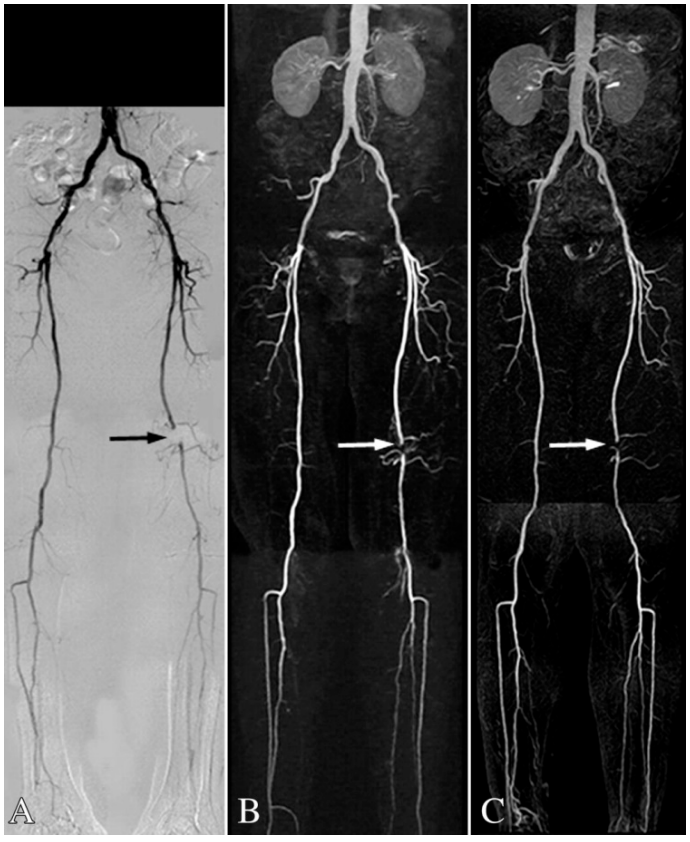

Figure 5.3 Coronal MR images in a 54-year-old woman show excellent agreement for a short arterial occlusion in the distal two-thirds of the superficial femoral artery on the left (arrow). **(A)** Anteroposterior DSA image. **(B)** Conventional maximum intensity projection image. **C**, Sensitivity-encoded maximum intensity projection image. Images in **A** and **B** were obtained with the same parameters in all three positions (6.1/1.55; section thickness, 3 mm; field of view, 430 mm; image matrix, 512x180; acquired voxel volume, 6.0 mm^3). Image in **C** was obtained with the following imaging parameters in the abdomen (4.8/1.36; section thickness, 2.2 mm; field of view, 430 mm; image matrix, 384x192; acquired voxel volume, 5.3 mm_3), upper legs (4.2/1.27; section thickness, 2.0 mm; field of view, 430 mm; image matrix, 416x208; acquired voxel volume, 4.3 mm^3), and lower legs (4.3/1.4; section thickness, 1.0 mm; field of view, 430 mm; image matrix, 432x432; acquired voxel volume, 0.98 mm^3).

Table 5.7 Sensitivity and Specificity of Standard and Sensitivity-encoded MR Angiography for Stenosis from Aorta to Popliteal Arteries.

Measurement	Standard MR Angiography			Sensitivity-encoded MR Angiography		
	≥50% Stenosis	≥75% Stenosis	Occlusion (100%)	≥50% Stenosis	≥75% Stenosis	Occlusion (100%)
Sensitivity	79 (60,90)	93 (69, 99)	92 (67,99)	89 (73, 96)	100 (78,100)	100 (77, 100)
Specificity	97 (93, 98)	100 (98, 100)	100 (98, 100)	99 (96, 100)	100 (97, 100)	100 (98, 100)

Data are percentages. Numbers in parentheses are the 95% CI.

Table 5.8 Sensitivity and Specificity of Standard and Sensitivity-encoded MR Angiography for Stenosis in Infragenual Arteries.

Measurement	Standard MR Angiography			Sensitivity-encoded MR Angiography		
	One Stenosis 50%-99%	Diffuse Stenosis 50%-99%	Occlusion (100%)	One Stenosis 50%-99%	Diffuse Stenosis 50%-99%	Occlusion (100%)
Sensitivity	87 (77, 93)	90 (79, 96)	72 (57,83)	87 (77, 93)	92 (82,97)	78 (61, 85)
Specificity	84 (76, 90)	86 (79, 91)	93 (87, 96)	94 (88, 97)*	100 (97, 100)†	99 (96, 100)

Data are percentages. Numbers in parentheses are the 95% CI.

* Compared with standard MR angiography, p=.013; † Compared with standard MR angiography, p<.01.

Sensitivity-encoded MR angiography depicted significantly more open infragenual arterial segments (n=162) than were depicted at midstream aortic DSA (n=145, p<.001) and conventional MR angiography (n=143, p<.001) (Figures 5.4, 5.5).

Discussion

In this study, we compared an optimized single-injection multi-position contrast-enhanced MR angiography protocol (sensitivity-encoded MR angiography) with DSA and a conventional single-injection multi-position contrast-enhanced MR angiography protocol (conventional MR angiography) in patients with peripheral arterial disease. We found that the application of sensitivity encoding and random central–k-space segmentation in a centric filling order and the acquisition of submillimeter isotropic voxels in the lower legs in a single-injection multi-position contrast-enhanced MR angiography protocol improve diagnostic performance and increase the number of open infragenual arterial segments that are detected.

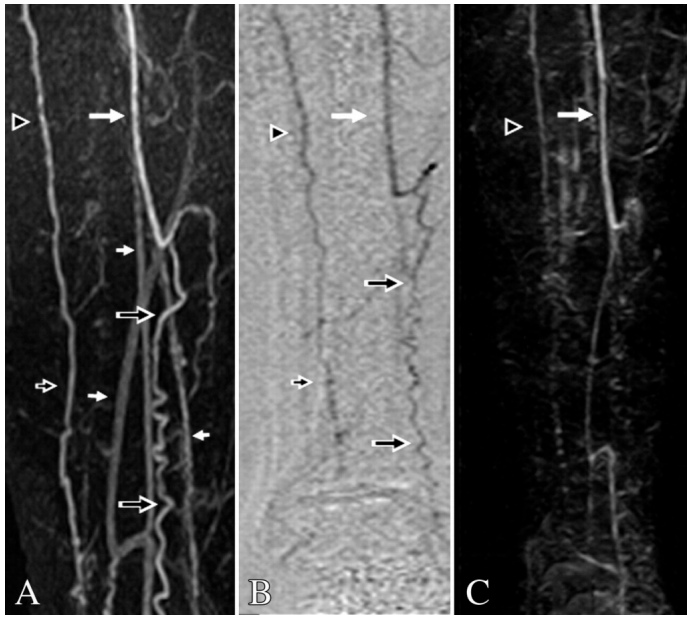

Figure 5.4 Coronal images in the right lower leg in a 66-year-old man with extensive small vessel disease. **(A)** Sensitivity-encoded maximum intensity projection image was obtained with the following parameters: 4.3/1.4; section thickness, 1 mm; field of view, 430 mm; image matrix, 432x432; acquired voxel volume, 0.98 mm_3. Posterior tibial artery and distal half of the peroneal artery are occluded. Venous enhancement is visible (short solid arrows) but, because of the increased spatial resolution, does not cause diagnostic difficulty. Tortuous collateral vessel (large open arrows) from peroneal artery (large solid arrow) is clearly seen, as is a collateral vessel (short open arrow) from anterior tibial artery (arrowhead). **(B)** DSA image shows excellent agreement with **A**. **(C)** Conventional maximum intensity projection image (6.1/1.55; section thickness, 3 mm; field of view, 430 mm; image matrix, 512x180; acquired voxel volume, 6.0 mm_3) in right lower leg. Collateral vessels from peroneal (solid arrow) and anterior tibial (open arrowhead) arteries are not visible because of limited spatial resolution.

A common drawback of single-injection multi-position contrast-enhanced MR angiography protocols is the difficult evaluation of infragenual arteries because of small vessel diameter and venous enhancement. With sensitivity-encoded MR angiography, the sixfold increase in spatial resolution and isotropic voxels and prevention of venous enhancement enabled more accurate measurement of stenoses, better distinction between occlusion and stenosis, and better delineation between arteries and veins. Thus, we achieved statistically significant increases in specificity for the detection of significant stenoses and the number of open infragenual segments in a comparison between sensitivity-encoded MR angiography and conventional MR angiography.

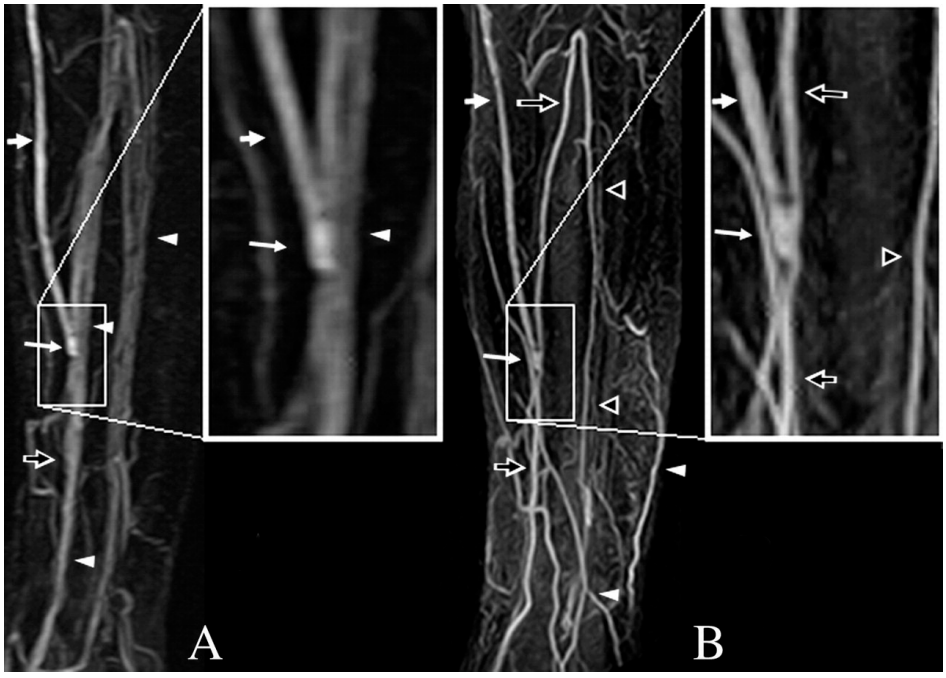

Figure 5.5 Coronal MR images in the left lower leg of a 76-year-old man. **(A)** Conventional maximum intensity projection image (6.1/1.55; section thickness, 3 mm; field of view, 430 mm; image matrix, 512x180; acquired voxel volume, 6.0 mm_3) and detail image show bypass graft (short solid arrows) from common femoral artery to distal posterior tibial artery (open arrow). Owing to venous enhancement (arrowheads) and relatively large voxels, distal anastomosis (long solid arrow) and outflow arteries cannot be evaluated. **(B)** Sensitivity-encoded maximum intensity projection image (4.3/1.4; section thickness, 1 mm; field of view, 430 mm; image matrix, 432x432; acquired voxel volume, 0.98mm_3) and detail image show clearly the bypass graft (short solid arrows), distal anastomosis (long solid arrow) and outflow arteries, posterior tibial artery (short open arrow), backflow through posterior tibial artery (long open arrows) to peroneal artery (open arrowheads). There is some venous enhancement in the superficial venous system (solid arrowheads) that does not hamper image evaluation.

Review of the literature showed a wide range of sensitivity and specificity values for three-dimensional contrast-enhanced MR angiography. Sensitivity varied from 81% to 100% and specificity from 83% to 99%.[18–20] For segments from the aorta to popliteal segments, these values ranged from 92% to 100% for sensitivity and 91% to 99% for specificity. In the current study, we compared sensitivity-encoded MR angiography directly with conventional MR angiography and found better diagnostic performance with the former. In a comparison of our results to those in the literature for conventional MR angiography protocols, sensitivity and specificity for both conventional and sensitivity-encoded MR angiography were in the same range,

although sensitivity of conventional MR angiography in segments from the aorta to popliteal arteries was slightly lower. Still, it is difficult to compare the results of different studies because of differences in study population, study design, and MR angiography protocols.

Time-of-flight MR angiography has higher sensitivity than that for midstream aortic DSA[21] and conventional angiography[22,23] for detection of open infragenual arteries in the diagnostic work-up for bypass surgery. Findings in our study showed equivalent results: Sensitivity-encoded MR angiography depicted significantly more open infragenual segments than were depicted with midstream aortic DSA. This explains the relatively low sensitivity of sensitivity-encoded MR angiography for the detection of occlusions in the infragenual arteries. A drawback in our study design is that highly selective DSA was not performed in the infragenual arteries. Selective DSA is considered the investigation of choice in patients with severe peripheral vascular disease.[24] Although an intra-arterial vasodilator was administered to optimize contrast material delivery at midstream aortic DSA, it was not injected selectively; therefore, the effect is less. Use of midstream aortic DSA as the standard of reference can produce a bias in favor of sensitivity-encoded MR angiography. No power analysis for sample size was calculated in the current study; therefore, further study to compare sensitivity-encoded MR angiography with highly selective DSA in a larger population is needed.

Compared with conventional single-injection multi-position MR angiography, sensitivity-encoded MR angiography depicts more diagnostic vessel segments and less venous enhancement. Comparable results were achieved with multi-injection time-resolved MR angiography.[25] Compared with multi-injection time-resolved MR angiography, sensitivity-encoded MR angiography provides higher spatial resolution and isotropic voxel volumes. Furthermore, in sensitivity-encoded MR angiography, conventional phased-array surface coils are used instead of a dedicated coil for the lower-leg position. This makes sensitivity-encoded MR angiography feasible in any clinical setting.

Application of sensitivity encoding (SENSE factor 2) in the pelvic position reduced acquisition time by a factor of 2. Shorter repetition time (reduced flip angle) and decreased volume thickness reduced acquisition time even more. Instead of merely reducing acquisition time, we accepted a time loss to improve spatial resolution. Compared with that in conventional MR angiography, total acquisition time of the pelvic and upper-leg position was reduced by 25 seconds in sensitivity encoded MR angiography. In contrast to that with conventional MR angiography, venous enhancement occurred only occasionally in sensitivity-encoded MR angiography. Further reduction in imaging time may lead to (central) k-space filling before the arterial contrast material bolus has arrived, which would result in artifacts and/or nondiagnostic findings.

Recently, a study was performed to apply sensitivity encoding in peripheral MR angiography.[26] The authors demonstrate that the technique is robust, and high-spatial-resolution images are acquired in the below-knee vessels. In sensitivity-encoded MR angiography, imaging times in the abdomen and upper-leg positions were 18 and 19 seconds compared with 11 and 12 seconds, respectively, with the WakiTrak protocol. The slightly longer imaging times in sensitivity-encoded MR angiography decrease the risk of acquisitions that are faster than the travel time of the contrast material bolus. Patients often have one or more of the characteristics for decreased speed of an arterial contrast material bolus. The acquired volumes were larger with sensitivity-encoded MR angiography (abdomen, 8.8 cm; upper leg, 6.0 cm; lower leg, 6.0 cm) than those with the Wakitrak protocol (abdomen, 8.1 cm; upper leg, 5.1 cm; lower leg, 3.8 cm), which makes planning easier and allows inclusion of elongated arteries. In sensitivity-encoded MR angiography, patients' legs were fixed in the conventional leg support to provide a venous pool in the calf to reduce contrast enhancement in the deep venous system and prevent movement. These features seem to make sensitivity-encoded MR angiography more robust. Furthermore, results with the Wakitrak protocol have not been compared with those with conventional MR angiography or DSA.

In the future, use of a higher SENSE factor and the development of a dedicated lower-extremity coil with the possibility of application of the sensitivity-encoded technique in all the positions might lead to faster acquisition, increasing spatial resolution, or the possibility of adding an extra position to the MR angiography protocol. A 3.0-T MR system is now commercially available. The higher signal obtained at the higher field strength will allow even faster acquisition or higher spatial resolution, while the signal-to-noise ratio and the contrast-to-noise ratio at the levels in a 1.5-T MR system are maintained. In addition, the development of new contrast agents with a shorter T1 will allow increased speed and spatial resolution.

For adequate therapy planning in patients with peripheral arterial disease, accurate images of the arteries are essential. In patients with extensive small-vessel disease and in those who have undergone bypass graft surgery, venous enhancement at MR angiography occurs more often. The clinical implication of findings in the current study is that sensitivity-encoded MR angiography can provide more accurate and detailed three-dimensional images of the infragenual arteries without venous enhancement, because random central– k-space segmentation in a centric filling order is applied and isotropic submillimeter voxel volumes are acquired. Sensitivity-encoded MR angiography depicts more open infragenual segments than are depicted with either midstream aortic DSA or conventional MR angiography, which provides the surgeon with more arteries for possible distal graft anastomosis. Conventional MR angiography shows good diagnostic performance in the aorta and iliac, femoral, and popliteal arteries and has some advantages over sensitivity-encoded MR angiography. These advantages are that no coils have to be set up and that it is easy to plan, is fully

automated, can be performed by one technician, and takes less time. Because the number of MR examinations that can be performed is limited and, in clinical practice, the number of referrals for MR angiography of the peripheral arteries is increasing, we now perform sensitivity-encoded MR angiography in patients referred for evaluation of small-vessel disease, infragenual arterial disease, or necrosis of the foot or for imaging before or after bypass graft surgery. The importance of high-spatial-resolution MR angiography images without venous enhancement, as provided with sensitivity-encoded MR angiography, is greatest in these selected patients.

In conclusion, application of sensitivity encoding and random central–k-space segmentation in a centric filling order and acquisition of submillimeter isotropic voxel volumes in the lower leg increase the diagnostic accuracy of single-injection multi-position contrast-enhanced MR angiography.

References

1. Wasser MN. Magnetic resonance angiography of peripheral vascular disease. J Comput Assist Tomogr 1999; 23(suppl 1):S129–S133.
2. Grist TM. MRA of the abdominal aorta and lower extremities. J Magn Reson Imaging 2000; 11:32–43.
3. Rofsky NM, Adelman MA. MR angiography in the evaluation of atherosclerotic peripheral vascular disease. Radiology 2000; 214:325–338.
4. Ho KY, Leiner T, de Haan MW, Kessels AG, Kitslaar PJ, van Engelshoven JM. Peripheral vascular tree stenoses: evaluation with moving-bed infusion-tracking MR angiography. Radiology 1998;206: 683-692.
5. Leiner T, Ho KY, Nelemans PJ, de Haan MW, van Engelshoven JM. Three-dimensional contrast-enhanced moving-bed infusion-tracking (MoBI-track) peripheral MR angiography with flexible choice of imaging parameters for each field of view. J Magn Reson Imaging 2000; 11:368–377.
6. Ruehm SG, Hany TF, Pfammatter T, Schneider E, Ladd M, Debatin JF. Pelvic and lower extremity arterial imaging: diagnostic performance of three-dimensional contrastenhanced MR angiography. AJR Am J Roentgenol 2000; 174:1127–1135.
7. Winterer JT, Laubenberger J, Scheffler K, et al. Contrast-enhanced subtraction MR angiography in occlusive disease of the pelvic and lower limb arteries: results of a prospective intraindividual comparative study with digital subtraction angiography in 76 patients. J Comput Assist Tomogr 1999; 23:583–589.
8. Meaney JF, Ridgway JP, Chakraverty S, et al. Stepping-table gadolinium-enhanced digital subtraction MR angiography of the aorta and lower extremity arteries: preliminary experience. Radiology 1999;211:59–67.
9. Korosec FR, Frayne R, Grist TM, Mistretta CA. Time-resolved contrast-enhanced 3D MR angiography. Magn Reson Med 1996;36:345–351.
10. Ho VB, Choyke PL, Foo TK, et al. Automated bolus chase peripheral MR angiography: initial practical experiences and future directions of this work-in-progress. J Magn Reson Imaging 1999; 10:376–388.
11. Mistretta CA, Grist TM, Korosec FR, et al. 3D time-resolved contrast-enhanced MR DSA: advantages and tradeoffs. Magn Reson Med 1998; 40:571–581.
12. Prince MR, Chabra SG, Watts R, et al. Contrast material travel times in patients undergoing peripheral MR angiography. Radiology 2002; 224:55–61.
13. Pruessmann KP, Weiger M, Scheidegger MB, Boesiger P. SENSE: sensitivity encoding for fast MRI. Magn Reson Med 1999;42:952–962.
14. Weiger M, Pruessmann KP, Kassner A, et al. Contrast-enhanced 3D MRA using SENSE. J Magn Reson Imaging 2000; 12:671–677.
15. Weiger M, Pruessmann KP, Boesiger P. Cardiac real-time imaging using SENSE: SENSitivity Encoding scheme. Magn Reson Med 2000; 43:177–184.
16. Westenberg JJ, Wasser MN, van der Geest RJ, et al. Gadolinium contrast-enhanced three-dimensional MRA of peripheral arteries with multiple bolus injections: scan optimization in vitro and in vivo. Int J Card Imaging 1999; 15:161–173.
17. Berry CC. A tutorial on confidence intervals for proportions in diagnostic radiology. AJR Am J Roentgenol 1990; 154:477–480.
18. Visser K, Hunink MG. Peripheral arterial disease: gadolinium-enhanced MR angiography versus color-guided duplex US—a meta-analysis. Radiology 2000; 216:67–77.
19. Nelemans PJ, Leiner T, de Vet HC, van Engelshoven JM. Peripheral arterial disease: meta-analysis of the diagnostic performance of MR angiography. Radiology 2000; 217:105–114.
20. Koelemay MJ, Lijmer JG, Stoker J, Legemate DA, Bossuyt PM. Magnetic resonance angiography for the evaluation of lower extremity arterial disease: a metaanalysis. JAMA 2001; 285:1338–1345.
21. Baum RA, Rutter CM, Sunshine JH, et al. Multicenter trial to evaluate vascular magnetic resonance angiography of the lower extremity. American College of Radiology Rapid Technology Assessment Group. JAMA 1995; 274:875–880.

22. Levy MM, Baum RA, Carpenter JP. Endovascular surgery based solely on noninvasive preprocedural imaging. J Vasc Surg 1998; 28:995–1005.
23. Owen RS, Carpenter JP, Baum RA, Perloff LJ, Cope C. Magnetic resonance imaging of angiographically occult runoff vessels in peripheral arterial occlusive disease. N Engl J Med 1992; 326:1577–1581.
24. Gates J, Hartnell GG. Optimized diagnostic angiography in high-risk patients with severe peripheral vascular disease. Radio-Graphics 2000; 20:121–133.
25. Hany TF, Carroll TJ, Omary RA, et al. Aorta and runoff vessels: single-injection MR angiography with automated table movement compared with multi-injection time resolved MR angiography—initial results. Radiology 2001; 221:266–272.
26. Maki JH, Wilson GJ, Eubank WB, Hoogeveen RM. Utilizing SENSE to achieve lower position submillimeter isotropic resolution and minimal venous enhancement in peripheral MR angiography. J Magn Reson Imaging 2002; 15:484–491.

Chapter 6

Peripheral Arterial Occlusive Disease: 3.0-T versus 1.5-T MR Angiography Compared with Digital Subtraction Angiography

Harrie CM van den Bosch
Jos JM Westenberg
Ralph Caris
Lucien EM Duijm
Alexander V Tielbeek
Philip WM Cuypers
Albert de Roos

Radiology 2013; 266:337-346

Abstract

Purpose
To prospectively evaluate the diagnostic accuracy of 3-T versus 1.5-T contrast material–enhanced (CE) magnetic resonance (MR) angiography with high spatial resolution in patients who have peripheral arterial occlusive disease, with conventional digital subtraction angiography (DSA) serving as the reference standard.

Materials and Methods
Institutional review board approval and written informed consent were obtained. DSA and standardized single-injection, three-station, moving-table CE MR angiography, with similar acquisition protocols and contrast agent doses at 3 T and 1.5 T, were consecutively performed in 19 patients (13 men and six women; mean age ± standard deviation, 67 years ± 9). Stenosis was scored visually in 500 arterial segments (97.5% of all available) in consensus by two radiologists in a blinded manner (the radiologists were unaware of the field strength and prior DSA and MR angiographic results and used randomized analysis order). Contrast-to-noise ratio was determined in the vascular tree of both legs. Statistical significance in stenosis scoring was evaluated by using generalized estimating equations. Contrast-to-noise differences were evaluated with paired *t* tests. Agreement between MR angiography and DSA was evaluated by using Fleiss-Cohen κ statistics.

Results
Both 3-T and 1.5-T CE MR angiography showed similar excellent agreement with DSA regarding stenosis classification (κ =0.96 and 0.93, respectively). All sensitivity and specificity values exceeded 90%. Mean contrastto-noise ratio was 3.0–4.2 times higher at 3 T than at 1.5 T.

Conclusion
Standardized single-injection, three-station, moving-table 3-T CE MR angiography is reliable for classification of stenosis in patients suspected of having peripheral arterial occlusive disease, and diagnostic performance was similar to that seen with 1.5-T MR angiography. There was a significantly increased contrast-to-noise ratio for identical contrast agent dose at 3-T MR angiography.

Introduction

Contrast material–enhanced (CE) magnetic resonance (MR) angiography has evolved in recent years into a reliable imaging technique in patients with peripheral arterial occlusive disease (PAOD). Previous studies have shown good correlation between CE MR angiography and conventional digital subtraction angiography (DSA) for stenosis detection.[1–4]

In clinical routine, CE MR angiography with 1.0-T and 1.5-T MR imagers is now widely used for diagnosis and treatment planning. In daily practice, a single-injection, three-station, multiposition CE MR angiographic protocol covering the peripheral arterial tree from the aorta to the lower legs is a clinically accepted routine.[5,6] Other examination approaches have also been reported, such as moving-table hybrid CE MR angiography[7–9] and step-bystep CE MR angiography.[10]

In the past few years, high-fieldstrength 3-T whole-body MR imaging units have been introduced in clinical practice. The potential benefit of 3-T MR imaging is an increased signal-tonoise ratio (SNR), which enables acquisition with higher spatial resolution within a similar imaging time and with similar contrast agent dose.[11,12]

Until recently, a drawback of 3-T whole-body MR imaging units was a restricted field of view (FOV) compared with 1.5-T MR imaging due to the limited homogeneity of the magnetic field; this limited FOV hampered imaging of large anatomic regions.[13] Advances in MR imaging technology, such as improved integrated quadrature whole-body coils, have led to the availability of a large homogeneous magnetic field. Thus, the FOV at 3 T is similar to that with 1.5 T, which allows visualization of the complete runoff vascular tree with a single-injection, three-station, moving-table protocol.

Several studies have shown that 3-T CE MR angiography is feasible in large vascular territories, such as the abdominal arteries[14] and other regions.[15,16] Recent reports showed promising results in patients who have PAOD with use of a time-resolved CE MR angiographic approach,[17] high-acceleration parallel imaging,[18,19] and blood pool agents.[20] However, to our knowledge, no previously published study has evaluated the diagnostic accuracy of peripheral CE MR angiography with a single-injection, three-station, moving-table protocol at 3 T versus 1.5 T.

The hypothesis of our study was that because of these recent advances in 3-T MR imaging technology—which offers FOV similar to that available with 1.5-T MR imaging—single-injection, three-station, moving-table 3-T CE MR angiography will offer diagnostic performance at least similar to that of 1.5-T CE MR angiography in patients with PAOD. Therefore, the purposes of our study were to prospectively evaluate the diagnostic accuracy of 3-T CE MR angiography with high spatial resolution in patients with PAOD and to compare it with that of 1.5-T CE MR angiography involving a similar acquisition protocol, with conventional DSA serving as the reference standard.

Materials and Methods

Patients

In our study, 20 consecutive patients clinically suspected of having PAOD were included from July 2008 to February 2009. Patients were referred to our department for further work-up. This sample size potentially results in 540 evaluable arterial segments, a number similar to or higher than that reported in previously published studies that compared CE MR angiography with DSA.[3,6,9,10,19,20]

Seventeen patients (85%) presented with intermittent claudication (Fontaine classification, 2): 10 patients (50%) with pain-free claudication while walking more than 200 m and seven patients (35%) with pain-free claudication while walking less than 200 m. One patient (5%) presented with pain at rest (Fontaine classification, 3) and two patients (10%) had necrosis (Fontaine classification, 4).

The institutional review board approved the study, and written informed consent was obtained from all patients. One patient (Fontaine classification, 2) was excluded because of claustrophobia. Therefore, 19 patients (13 men and six women; mean age ± standard deviation [SD], 67 years ± 9; range, 53–82 years) underwent peripheral CE MR angiography at both 3-T and 1.5-T MR imaging (order was defined per available examination time slot). Both CE MR angiographic examinations were performed within a 1-week period in which no intervention occurred. DSA was performed within a mean of 23 days (range, 6–33 days) after the latest CE MR angiographic examination (with no vascular intervention taking place between CE MR angiography and DSA). DSA was used as the reference standard.

CE MR angiography was performed with 3-T MR imaging (Achieva X-series, release 2.1; Philips Healthcare, Best, the Netherlands) and 1.5-T MR imaging (Achieva, release 2.5; Philips Healthcare). In all patients, the glomerular filtration rate was greater than 60 mL/min per 1.73 m^2. No adverse reactions or complications occurred during or after MR angiography or DSA.

MR Angiographic Protocols

A three-station, single-injection protocol was used for both 3-T and 1.5-T CE MR angiography. A biphasic contrast agent protocol was used. Gadoterate meglumine (Guerbet, Paris, France), 0.2 mmol per kilogram of body weight, was injected by using an MR imaging–compatible injector (Spectris MR injector; Medrad, Indianola, Pa).The first half of the contrast agent bolus was administered at 1.2 mL/sec and the remaining half at 0.6 mL/sec. Contrast agent injection was followed by 15-mL saline flush at 0.6 mL/sec. To determine timing of arrival of contrast agent, a 2-mL test bolus was administered at 1.2 mL/sec, followed by 15-mL saline flush at 1.2 mL/sec.

For 1.5-T CE MR angiography, a quadrature body coil was used for signal transmission

and reception in the pelvic and thigh stations and a four-element phased-array coil was used for the calf station. For 3-T CE MR angiography, a quadrature body coil was used in all three stations. In this study, imaging parameters at 3-T CE MR angiography were intentionally kept similar to those used for 1.5-T CE MR angiography. Imaging parameters of the three-dimensional fast gradient-echo sequences at 3-T and 1.5-T CE MR angiography are presented in Table 6.1. At 1.5-T CE MR angiography, the first station was acquired with linear k-space filling; at 3-T CE MR angiography, reversed linear k-space filling was used. At both MR angiographic protocols, the second and third stations were acquired with centric k-space filling. Table speed was set at 180 mm/sec between all imaged stations.

Table 6.1 Acquisition parameters for 1.5T and 3T contrast-enhanced MRA.

	1.5T CE-MRA				
station	**TR/TE**	**flip angle (°)**	**FOV (mm)**	**acquisition resolution (mm^3)**	**acquisition time (s)**
Pelvic	2.5/1.00	25	430	1.28×1.68×3.00	13.3
Thigh	2.5/1.00	25	430	1.28×1.68×3.00	13.3
Calf	4.7/1.45	25	430	0.96×1.07×1.40	43.2
	3T CE-MRA				
Pelvic	3.6/1.25	20	410	1.25×1.84×3.70	14.6
Thigh	3.6/1.26	20	410	1.30×1.75×3.00	14.6
Calf	5.5/1.80	30	410	0.80×0.90×1.40	74.7

CE: contrast-enhanced; TR: repetition time msec; TE: echo time msec; FOV: Field-of-View.

DSA Imaging

DSA was performed with a dedicated angiographic system (Multistar T.O.P.; Siemens Medical Engineering, Forchheim, Germany) by using nonionic contrast agent (iomeprol, Iomeron 350; Bracco s.p.a., Milan, Italy). The tip of a 4-F pigtail or straight catheter was positioned in the infrarenal abdominal aorta after retrograde puncturing of the common femoral artery and insertion of a 5- or 6-F introducer sheath (Cordis, Rhoden, the Netherlands). DSA images of the infrarenal aorta and iliac arteries were obtained in anteroposterior, leftoblique, and right-oblique projections. For each series, a 15-mL contrast bolus was administered with a power injector (Medrad, Warrendale, Pa) at a flow rate of 18 mL/sec. Typically, 117–124 mL of contrast agent was administrated. A 5-F celiac catheter (Cordis) was used for selective catheterization of the contralateral extremity, and, unless there was an iliac occlusion, the catheter tip was placed in the external iliac artery. The imaging protocol for the contralateral extremity included acquisition of overlapping images from the common femoral artery down to the dorsal pedal artery by repeated 7-mL manual injections of contrast agent. Magnification views of suspected stenoses were obtained in two orthogonal projections. When image quality in the calf station was not adequate, an intraarterial vasodilator was administered (slow manual injection of 25 mg papaverine [Pharma Chemie, Haarlem, the Netherlands]) to optimize delivery of contrast agent.

The celiac catheter was then removed and DSA of the ipsilateral extremity was performed by manual injection of contrast agent through the femoral sheath. Imaging parameters included a matrix of 1024 x 1024 and FOV of 14–40 cm. All procedures were performed by two interventional radiologists (L.D. and A.T., with >15 and 20 years of experience with DSA, respectively).

Quantitative Data Analysis

MR angiographic images were presented in random order, and observers were blinded to the MR field strength and patient information. The 1.5-T and 3-T images were reviewed intermixed at random and in consensus by two MR radiologists (H.v.d.B. and R.C., with 14 and 5 years of experience with CE MR angiography, respectively); the reviewers were unaware of the results of prior CE MR angiographic or DSA examinations but did know the total number of examinations per patient. DSA images were reviewed in consensus by the same two interventional radiologists (L.D. and A.T.), who were unaware of CE MR angiographic findings.

The arterial tree in each patient was divided into the following 27 segments: the infrarenal aorta, common iliac arteries, external iliac arteries, common femoral arteries, superficial femoral arteries, popliteal arteries in the thigh station, popliteal arteries in the calf station, tibiofibular trunk, and the proximal and distal halves of the anterior and posterior tibial arteries and peroneal arteries. The dorsalis pedis and plantar arteries were not completely included in the FOV. The most severe stenosis in each segment was presented in the classification. Stenosis severity was visually graded according to the following equation: percentage stenosis = [1 - (*D/N)]* x 100%, where *D* is the minimal diameter in the stenosis and *N* is the normal diameter, visually estimated from a reference diameter proximal and distal to the lesion. Categories of percentage stenosis were as follows: 1 (0%), normal vessel; 2 (1%–50%), wall irregularities or mild stenosis; 3 (51%–75%), moderate stenosis; 4 (76%–99%), severe stenosis; and 5 (100%), occlusion. Stenoses were graded on maximum-intensity-projection images and on source images. Both CE MR angiographic and DSA images were analyzed on a remote workstation.

Quantitative analysis of SNR and contrast-to-noise ratio (CNR) for the external iliac artery, superficial femoral artery, and popliteal artery in the right and the left leg of each patient were calculated by one radiologist (H.v.d.B.). Regions of interests to determine signal intensity were manually defined and equivalent in size and location for 3 T and 1.5 T (calculation of signal intensity was not blinded). An additional region of interest (approximately 10 cm^2) was placed in the FOV but was outside the patient's body to determine the SD of noise. SNR was calculated by dividing signal intensity measured in the artery by SD of noise. CNR was defined by signal intensity measured in the artery compared with signal intensity in the surrounding tissue, divided by SD of noise.

Statistical Analysis

Only segments that were evaluated with both 3-T and 1.5-T CE MR angiography and DSA were considered. Sensitivity, specificity, and positive and negative predictive values, with DSA as the reference standard, were calculated for the following categories of stenosis scoring in each segment: stenosis >0% (1%–100%), stenosis >50% (51%–100%), stenosis >75% (76%–100%), and occlusion (100% stenosis). Regression modeling of proportions was performed by using generalized estimating equations with the use of a robust estimator for the covariance matrix and an autoregressive correlation matrix to take data clustering within the same patient into account.[21] In addition, 95% confidence intervals (CIs) were determined for sensitivity, specificity, and positive and negative predictive values; 95% CIs and *p* values were obtained for differences in these proportions in case of no complete agreement. A *p* value of less than .05 was considered to represent a statistically significant difference. Continuous variables are expressed as the mean ± SD (range) when appropriate. CNR values are also presented by median and quartiles in box-plot presentation. Statistical significance of the differences in CNR at 3 T and 1.5 T was evaluated with a paired *t* test. Agreement between both 1.5-T and 3-T CE MR angiography and DSA regarding stenosis classification was evaluated by using the Fleiss-Cohen quadratic weighted κ statistics, and κ was interpreted as follows: κ value of 0 indicates poor agreement; κ value of 0.01–0.20, minor agreement; κ value of 0.21–0.40, fair agreement; κ value of 0.41–0.60, moderate agreement; κ value of 0.61–0.80, good agreement; and κ value of 0.81–1; excellent agreement.[22] Statistical analysis was performed with SPSS software, version 17 (IBM, Somers, NY).

Results

In 19 of 20 patients, 3-T and 1.5-T CE MR angiography and DSA of the peripheral arteries were successfully performed (see an example in Figure 6.1). Mean total contrast agent dose for DSA was 119 mL ± 10. For CE MR angiography, 13 of 513 segments (2.5%) could not be evaluated because of venous enhancement or patient movement. In four patients, venous enhancement occurred in the calf station at 3-T or 1.5-T CE MR angiography. Two of these patients presented with claudication, one patient with rest pain, and one patient with necrosis. In these four patients, venous enhancement occurred in only one of either MR angiographic examination. In these patients, eight segments (1.5%) showed impaired image quality, resulting in nonevaluable images. Because of movement artifacts in two patients, five segments (1%) were also excluded. Maximal number of evaluable segments per patient was 27, and the minimal number of segments was 24 (mean, 26.2). From the remaining total of 500 segments, 105 segments (21%) were appointed with a relevant stenosis (class 2 or higher) at DSA. The 395 segments classified as class 1 (no stenosis) at DSA were also

classified as class 1 at both 1.5-T and 3-T CE MR angiography. Stenosis classification in the remaining 105 segments was compared for 3-T and 1.5-T CE MR angiography, with DSA serving as the reference standard.

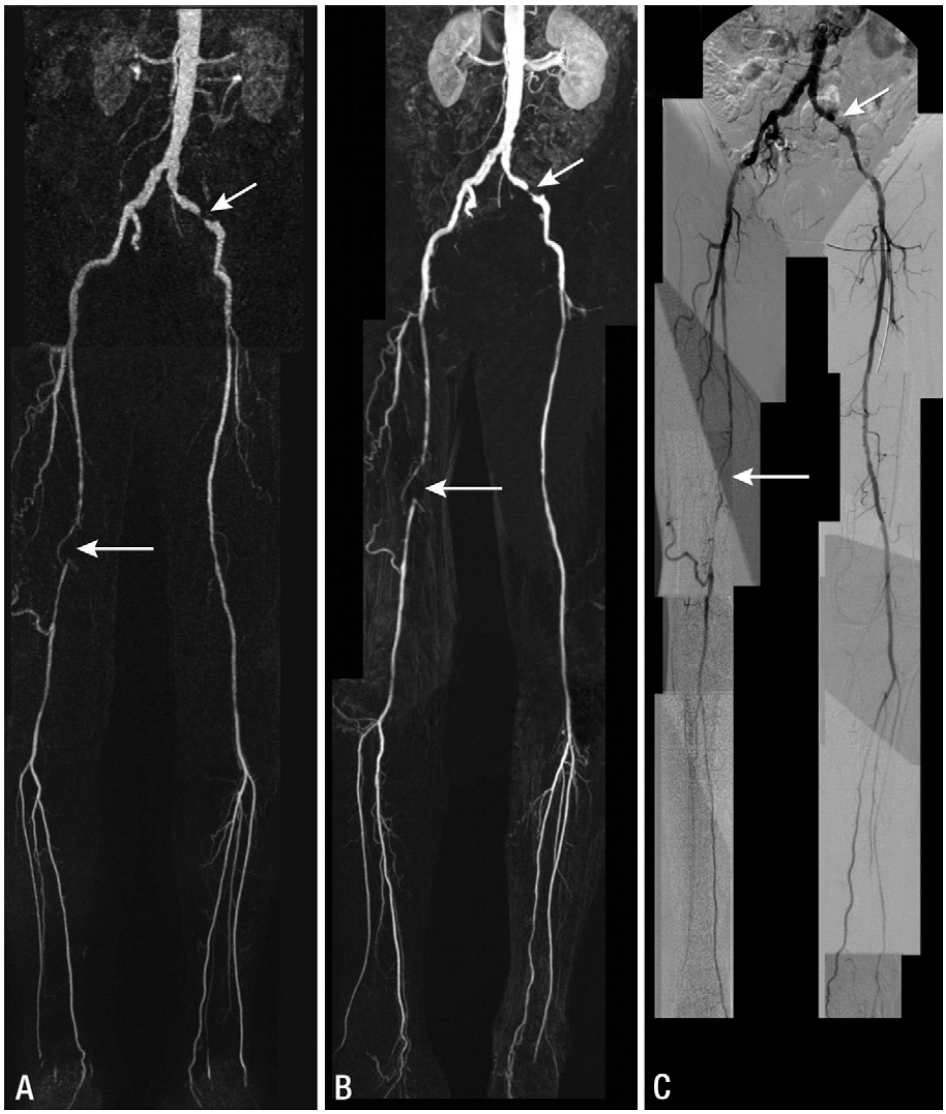

Figure 6.1 Coronal CE MR angiographic maximum-intensity-projection images in 67-year-old man presenting with bilateral claudication. **(A**) 1.5-T and, **(B)** 3-T CE MR angiographic images show a significant stenosis of 80% in the left external iliac artery (short arrow) and an occlusion in the right superficial femoral artery (long arrow). **(C**) There is excellent correlation between MR angiography and DSA, with selective catheterization of both extremities.

Quantitative Analysis of Stenosis Classification

Sensitivity, specificity, and positive and negative predictive values were determined for detection of stenosis greater than 0%, greater than 50%, greater than 75%, and 100% stenosis in each segment with 3-T and 1.5-T CE MR angiography. The results are presented in Table 6.2. For stenosis classification >50%, sensitivity of 3-T CE MR angiography was 99% and sensitivity of 1.5-T CE MR angiography was 92%, with a mean difference of 7 percentage points in favor of 3-T CE MR angiography (p=.052). The lower limit of the CI showed that in 2.5% of the cases, sensitivity of 3-T CE MR angiography still can be 1 percentage point inferior to 1.5-T CE MR angiography. Specificity of 3-T CE MR angiography was 0.1 percentage point inferior to 1.5-T CE MR angiography (p=.30). For stenosis classification >75%, sensitivity of 3-T CE MR angiography was 95% and sensitivity of 1.5-T CE MR angiography was 92%, with a mean difference of 3 percentage points in favor of 3-T CE MR angiography (p=.30). The lower limit of the CI showed that for 2.5% of the cases, sensitivity of 3-T CE MR angiography still can be 3 percentage points inferior to that of 1.5-T CE MR angiography. A maximal value of a 3–percentage point difference in sensitivity may be considered as clinically irrelevant; therefore, the diagnostic performance of 3-T CE MR angiography is considered similar to that of 1.5-T CE MR angiography with use of similar acquisition protocols and contrast agent dose. Specificity was identical for both 3-T and 1.5-T CE MR angiography for stenosis classification >75%. For detection of stenosis >0% and for occlusion detection, sensitivity and specificity of both 3-T and 1.5-T CE MR angiography were identical.

For stenosis classification in each segment, both 3-T and 1.5-T CE MR angiography showed excellent concordance with DSA (κ = 0.96 and 0.93, respectively; cross-tables are presented in Tables 6.3 and 6.4). Agreement between 3-T and 1.5-T CE MR angiography was also very high (κ =0.98; Table 6.5).

Quantitative SNR and CNR Analysis

Mean values ± SDs for SNR and CNR at 1.5-T and 3-T CE MR angiography, measured in the external iliac artery, superficial femoral artery, and popliteal artery, are presented in Table 6.6 for both the left and the right leg. Mean values were for all anatomic regions that were higher at 3-T than at 1.5-T CE MR angiography (all p<.001). Table 6.7 presents the ratios between 1.5-T and 3-T CE MR angiographic SNR and CNR for all anatomic regions. The SNR was on average 2.8–3.9 times higher at 3-T than at 1.5-T CE MR angiography, and the CNR was on average 3.0–4.2 times higher (see an example for the superficial femoral artery in Figure 6.2). Results for CNR for both MR angiographic protocols are also presented in a box plot (Figure 6.3).

Table 6.2 Diagnostic performance for stenosis detection at 3T versus 1.5T contrast-enhanced MRA.

	Stenosis >0%		**Stenosis >50%**		**Stenosis >75%**		**Occlusion**	
	3T	**1.5T**	**3T**	**1.5T**	**3T**	**1.5T**	**3T**	**1.5T**
sensitivity	100% (105/105)	100%	98%	92%	93%	90%	97%	97%
	96%–100%	(105/105)	(63/64)	(59/64)	(56/60)	(54/60)	(35/36)	(35/36)
95%-CI		96%–100%	92%–100%	83%–97%	84%–97%	80%–95%	86%–100%	86%–100%
Difference	not applicable		6%		3%		not applicable	
95%-CI	(complete agreement)		-1%–15%		-3%–11%		(complete agreement)	
p-value McNemar	not applicable		0.13		0.48		not applicable	
	(complete agreement)						(complete agreement)	
specificity	100%	100%	99.5%	99.5%	100%	100%	100%	100%
	(395/395)	(395/395)	(434/436)	(434/436)	(440/440)	(440/440)	(464/464)	(464/464)
95%-CI	99%–100%	99%–100%	98%–100%	98%–100%	99%–100%	99%–100%	99%–100%	99%–100%
p-value McNemar	not applicable		not applicable		not applicable		not applicable	
	(complete agreement)		(complete agreement)		(complete agreement)		(complete agreement)	
positive predictive	100%	100%	97%	97%	100%	100%	100%	100%
value	(105/105)	(105/105)	(63/65)	(59/61)	(56/56)	(54/54)	(35/35)	(35/35)
		96%–100%	89%–99%	89%–99%	94%–100%	93%–100%	90%–100%	90%–100%
95%-CI	96%–100%							
p-value McNemar	not applicable		0.68		0.48		not applicable	
	(complete agreement)						(complete agreement)	
negative predictive	100%	100%	99.8%	99%	99%	99%	99.8%	99.8%
value	(395/395)	(395/395)	(434/435)	(434/439)	(440/444)	(440/446)	(464/465)	(464/465)
95%-CI	96%–100%	99%–100%	99%–100%	97%–100%	98%–100%	97%–100%	99%–100%	99%–100%
p-value McNemar	not applicable		0.37		0.68		not applicable	
	(complete agreement)						(complete agreement)	

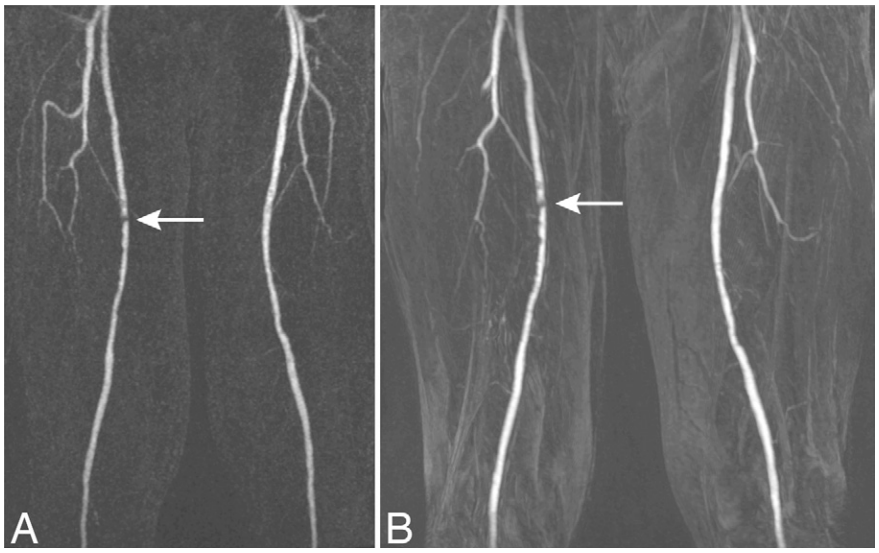

Figure 6.2 Coronal CE MR angiographic maximum-intensity-projection images of the thigh station in a 66-year-old man who presented with right-sided claudication. **(A)** 1.5-T and, **(B)** 3-T CE MR angiographic images show significant stenosis (.75%) in the right superficial femoral artery (arrow). The 3-T CE MR angiographic image presents a 2.0 times higher SNR and 1.9 times higher CNR in the superficial femoral artery with the same contrast dose, as compared with the 1.5-T CE MR angiographic image.

Table 6.3 Agreement between 3T contrast-enhanced MRA and DSA**.**

			DSA		
Stenosis Class per 3-T CE MR Angiography	**1**	**2**	**3**	**4**	**5**
1	395	0	0	0	0
2	0	39	0	0	1
3	0	2	4	3	0
4	0	0	0	21	0
5	0	0	0	0	35

Values are numbers of segments. Class 1, 0% stenosis; class 2, 1%–50%; class 3, 51%–75%; class 4, 76%-99%; class 5: 100%. κ = 0.96.

Table 6.4 Agreement between 1.5T contrast-enhanced MRA and DSA**.**

			DSA		
Stenosis Class per 1.5-T CE MR Angiography	**1**	**2**	**3**	**4**	**5**
1	395	0	0	0	0
2	0	39	2	2	1
3	0	2	2	3	0
4	0	0	0	19	0
5	0	0	0	0	35

Values are numbers of segments. Class 1, 0% stenosis; class 2, 1%–50%; class 3, 51%–75%; class 4, 76%-99%; class 5, 100%. κ = 0.93.

Table 6.5 Agreement between 3T and 1.5T contrast-enhanced MRA.

	DSA				
Stenosis Class per 3-T MR Angiography	**1**	**2**	**3**	**4**	**5**
1	395	0	0	0	0
2	0	41	0	0	0
3	0	2	6	0	0
4	0	1	1	19	0
5	0	0	0	0	35

Values are numbers of segments. Class 1, 0% stenosis; class 2, 1%–50%; class 3, 51%–75%; class 4, 76%–99%; class 5, 100%. κ = 0.98.

Table 6.6 SNR and CNR on 1.5T and 3T CE-MRA

	1.5T CE-MRA				3T CE-MRA			
	SNR	***p***	**CNR**	***p***	**SNR**	***p***	**CNR**	***p***
left external iliac artery	23±5	0.91	21±5	0.88	61±18	0.95	58±17	0.71
right external iliac artery	23±6		21±6		61±20		57±19	
left superficial femoral artery	34±10	0.60	30±10	0.81	108±34	0.22	96±31	0.39
right superficial femoral artery	32±11		29±10		100±47		92±42	
left popliteal artery	26±8	0.48	23±8	0.15	92±46	0.84	84±43	0.86
right popliteal artery	25±9		22±9		92±44		84±39	

SNR: signal-to-noise ratio; CNR: contrast-to-noise ratio.

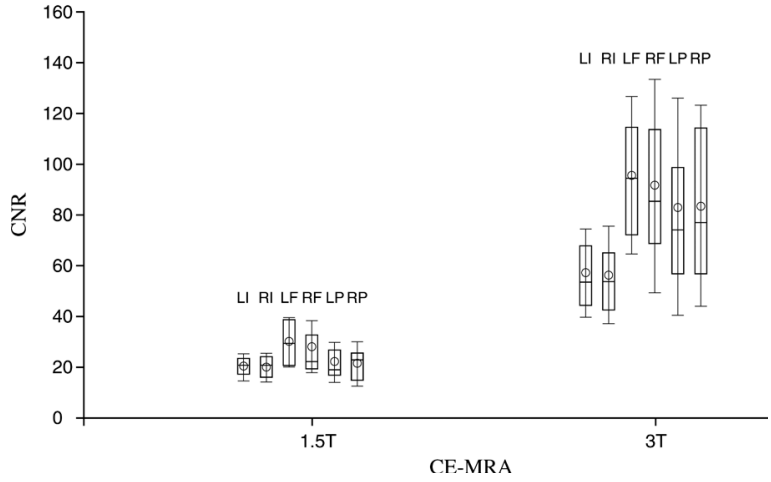

Figure 6.3 Box plot of CNR determined in external iliac artery, superficial femoral artery, and popliteal artery in both left and right leg, imaged with 3-T and 1.5-T CE MR angiography, respectively. Circle in each box represents mean; error bar, standard deviation; box, first and third tertile; and horizonal lines, medians. LF= left femoral; LI = left iliac; LP = left popliteal; RF = right femoral; RI = right iliac; RP = right popliteal.

Table 6.7 Ratios for SNR and CNR between 3T versus 1.5T CE-MRA, measured in the external iliac artery, superficial femoral artery and popliteal artery, in both the left and right leg.

	SNR 3T vs. 1.5T	CNR 3T vs. 1.5T
left external iliac artery	2.8±1.2 (1.5-5.8)	3.0±1.4 (1.6-6.8)
right external iliac artery	2.8±1.2 (1.7-6.2)	3.0±1.4 (1.7-7.0)
left superficial femoral artery	3.4±1.3 (1.4-6.1)	3.4±1.4 (1.4-6.2)
right superficial femoral artery	3.3±1.7 (0.8-7.4)	3.4±1.7 (0.9-7.5)
left popliteal artery	3.8±1.9 (1.2-8.5)	3.9±1.9 (1.3-8.2)
right popliteal artery	3.9±2.3 (1.2-11.1)	4.2±2.4 (1.3-11.5)

SNR: signal-to-noise ratio; CNR: contrast-to-noise ratio

Discussion

In our study, the diagnostic accuracy of single-injection, three-station, moving- table 3-T CE MR angiography was prospectively evaluated in patients with PAOD and compared with that of 1.5-T CE MR angiography, with conventional DSA serving as the reference standard. The main findings of our study are as follows: *(a)* 3-T CE MR angiography showed similar excellent agreement with DSA when compared with 1.5-T CE MR angiography regarding agreement, sensitivity, and specificity for classification of stenosis severity; *(b)* 3-T CE MR angiography achieved, on average, 3.0–4.2 times higher (p<.001) CNR in the external iliac artery, superficial femoral artery, and popliteal artery in both the left and the right leg when compared with 1.5-T CE MR angiography and with use of the same contrast agent dose.

In the imaging work-up of patients with PAOD, noninvasive techniques, such as duplex ultrasonography, computed tomographic (CT) angiography, and CE MR angiography, have become increasingly important. Although DSA is the generally accepted reference standard, noninvasive techniques have proved to be accurate for stenosis assessment.[1,3,5,6,23,24] Moreover, CT angiography and CE MR angiography can provide a detailed roadmap for treatment planning. CE MR angiography has two main advantages over CT angiography: MR angiography provides radiation-free imaging and does not disturb the overlay of calcified plaques (which would hamper stenosis assessment).

To our knowledge, this is the first study to prospectively compare the diagnostic value of 3-T versus 1.5-T CE MR angiography by using a moving-table technique in patients with PAOD, with DSA serving as the reference standard. Since the introduction of 3-T MR imaging in clinical practice, the limited FOV at 3 T hampered the imaging of large anatomic regions.[12,13] Recently, advances in MR imaging technology, such as an improved integrated quadrature body coil, have made possible a large homogeneous magnetic field and, therefore, an FOV at 3-T that is similar to that seen with 1.5-T MR imaging. Our study was performed with 3-T MR imaging with an FOV of 45 cm, as compared with a 48-cm FOV with 1.5-T MR imaging. These large FOVs enable

visualization of the peripheral arterial tree from the aorta to the lower legs with a single-injection, three-station, moving-table technique. We used three overlapping FOVs for both methods: 430 mm each at 1.5-T and 410 mm each at 3-T CE MR angiography. For both 1.5-T and 3-T CE MR angiography, overlap was 30 mm, resulting in total coverages of 1200 mm and 1140 mm for 1.5-T and 3-T CE MR angiography, respectively.

A well-shimmed 3-T MR imaging system may provide B_0 homogeneity similar to that of 1.5-T imaging; however, it is well known that susceptibility effects are larger at 3 T.[15] This may result in undesirable image distortions and signal loss. It has been reported that improved local shimming minimizes these negative effects. Increased B_1 heterogeneity at 3 T can cause locally dependent radiofrequency excitation and consequently may introduce spatial variation of signal across the image. This may result in an obscured visualization across the FOV. However, CNR measurements in various segments showed no significant differences when compared in both legs for 1.5-T and 3-T CE MR angiography. Venous enhancement occurred in the calf station at 3-T and/or 1.5-T CE MR angiography in four patients, resulting in impaired image quality in only eight segments (1.5%). Centric k-space filling was used for the calf station at both 3-T and 1.5-T CE MR angiography to minimize venous contamination.

In our study, both 3-T and 1.5-T CE MR angiography showed excellent agreement with DSA for stenosis detection, with k values of 0.96 and 0.93, respectively; between 3-T and 1.5-T CE MR angiography the k value was 0.98. Furthermore, the sensitivity, specificity, and positive and negative predictive values of 1.5-T CE MR angiography presented in our study are in line with those reported in previous published results.[1,25] Sensitivity and specificity for 3-T CE MR angiography in our study are consistent with recently published results obtained by using a four-station hybrid technique[13] and using a blood pool agent.[19]

SNR and CNR were evaluated at the same anatomic level at 3-T and 1.5-T CE MR angiography in the external iliac artery, superficial femoral artery, and popliteal artery in both legs. In our study, these locations were usually free from overprojection and may be interpreted as representative for peripheral CE MR angiography. The three-fold higher CNR at 3-T CE MR angiography can potentially be traded for higher spatial resolution, which may be beneficial for quantitative stenosis classification, or for more cost-effective lower contrast agent dose.[26] In our study, contrast agent dose and spatial resolution were kept similar for both 3-T and 1.5-T CE MR angiographic protocols to enable interimage comparison. The contrast agent dose for both 3 T and 1.5 T was 0.2 mmol/kg body weight. A recent publication showed the clinical feasibility of low-dose CE MR angiography in combination with continued table movement and time-resolved imaging in patients with PAOD.[17] Another study showed that contrast agent dose for 3-T CE MR angiography can be reduced without compromising image quality by use of multiarray surface coils and a hybrid, dual-phase injection protocol.[27] Further evaluation must be performed to determine the

diagnostic accuracy for these low-dose CE MR angiographic protocols with a single-injection, three-station, moving-table imaging strategy. In the literature, several approaches for contrast agent dose in peripheral CE MR angiography have been reported: 30–40 mL gadolinium fixed dose,[1,3,6] double dose (0.2 mmol/kg body weight),[2] or, more recently, single dose.[28,29] In our hospital, the use of double-dose contrast agent is common. Especially in patients with impaired renal function, the amount of administered contrast agent is of clinical importance.[30] In all patients included in this study, the glomerular filtration rate was determined before MR imaging; for all patients, it was greater than 60 mL/min per 1.73 m^2, indicating no evidence for impaired renal function.

We acknowledge certain limitations of our study. For 3-T CE MR angiography, the build-in quadrature body coil was used for signal transmission and reception. However, for 1.5-T CE MR angiography, a phased-array surface coil was used for imaging the calf station because this is routinely performed in a state-of the-art imaging protocol in daily clinical practice at our institution. The use of a surface coil can potentially benefit SNR in this anatomic region. To date, phased-array surface coils for peripheral CE MR angiography are not offered for 3 T by all MR imaging vendors. However, when dedicated surface coils become commercially available for peripheral 3-T CE MR angiography, this technique may benefit from higher SNR. Additionally, recent developments in coil design, such as built-in analog-to-digital converters, may help improve image quality. In addition, parallel imaging techniques, such as sensitivity encoding, can be implemented to allow reduction in acquisition times.[31] Furthermore, stenosis was not classified quantitatively by diameter and length measurements but rather was assessed visually in consensus. Finally, our sample size was relatively small. From 19 patients, 500 angiographic images were included.

In conclusion, CE MR angiography with a 3-T whole-body imaging system in combination with a standardized single-injection, three-station, moving-table protocol is a reliable tool for stenosis detection and classification in patients suspected of having PAOD. It showed similar excellent agreement with DSA for diagnostic performance when compared with 1.5-T CE MR angiography.

References

1. Ho KY, Leiner T, de Haan MW, Kessels AG, Kitslaar PJ, van Engelshoven JM. Peripheral vascular tree stenoses: evaluation with moving-bed infusion-tracking MR angiography. Radiology 1998;206(3): 683–692.
2. Ersoy H, Rybicki FJ. MR angiography of the lower extremities. AJR Am J Roentgenol 2008;190(6):1675–1684.
3. Bezooijen R, van den Bosch HC, Tielbeek AV, et al. Peripheral arterial disease: sensitivity-encoded multiposition MR angiography compared with intraarterial angiography and conventional multiposition MR angiography. Radiology 2004;231(1):263–271.
4. Goyen M, Debatin JF, Ruehm SG. Peripheral magnetic resonance angiography. Top Magn Reson Imaging 2001;12(5):327–335.
5. Nelemans PJ, Leiner T, de Vet HC, van Engelshoven JM. Peripheral arterial disease: meta-analysis of the diagnostic performance of MR angiography. Radiology 2000;217(1):105–114.
6. Leiner T, Kessels AG, Schurink GW, et al. Comparison of contrast-enhanced magnetic resonance angiography and digital subtraction angiography in patients with chronic critical ischemia and tissue loss. Invest Radiol 2004;39(7):435–444.
7. Tongdee R, Narra VR, McNeal G, et al. Hybrid peripheral 3D contrast-enhanced MR angiography of calf and foot vasculature. AJR Am J Roentgenol 2006;186(6):1746–1753.
8. von Kalle T, Gerlach A, Hatopp A, Klinger S, Prodehl P, Arlart IP. Contrast-enhanced MR angiography (CEMRA) in peripheral arterial occlusive disease (PAOD): conventional moving table technique versus hybrid technique [in German]. Rofo 2004;176(1):62–69.
9. Meissner OA, Rieger J, Weber C, et al. Critical limb ischemia: hybrid MR angiography compared with DSA. Radiology 2005;235(1):308–318.
10. Huber A, Heuck A, Baur A, et al. Dynamic contrast-enhanced MR angiography from the distal aorta to the ankle joint with a step-by-step technique. AJR Am J Roentgenol 2000;175(5):1291–1298.
11. Campeau NG, Huston J 3rd, Bernstein MA, Lin C, Gibbs GF. Magnetic resonance angiography at 3.0 Tesla: initial clinical experience. Top Magn Reson Imaging 2001;12(3):183–204.
12. Leiner T, de Vries M, Hoogeveen R, Vasbinder GB, Lemaire E, van Engelshoven JM. Contrast-enhanced peripheral MR angiography at 3.0 Tesla: initial experience with a whole-body scanner in healthy volunteers. J Magn Reson Imaging 2003;17(5):609–614.
13. Berg F, Bangard C, Bovenschulte H, et al. Feasibility of peripheral contrast-enhanced magnetic resonance angiography at 3.0 Tesla with a hybrid technique: comparison with digital subtraction angiography. Invest Radiol 2008;43(9):642–649.
14. Michaely HJ, Kramer H, Dietrich O, et al. Intraindividual comparison of high-spatial-resolution abdominal MR angiography at 1.5 T and 3.0 T: initial experience. Radiology 2007;244(3):907–913.
15. Lee VS, Hecht EM, Taouli B, Chen Q, Prince K, Oesingmann N. Body and cardiovascular MR imaging at 3.0 T. Radiology 2007;244(3):692–705.
16. Fenchel M, Nael K, Deshpande VS, et al. Renal magnetic resonance angiography at 3.0 Tesla using a 32-element phased-array coil system and parallel imaging in 2 directions. Invest Radiol 2006;41(9):697–703.
17. Attenberger UI, Haneder S, Morelli JN, Diehl SJ, Schoenberg SO, Michaely HJ. Peripheral arterial occlusive disease: evaluation of a high spatial and temporal resolution 3-T MR protocol with a low total dose of gadolinium versus conventional angiography. Radiology 2010;257(3):879–887.
18. Kramer H, Michaely HJ, Matschl V, Schmitt P, Reiser MF, Schoenberg SO. High-resolution magnetic resonance angiography of the lower extremities with a dedicated 36-element matrix coil at 3 Tesla. Invest Radiol 2007;42(6):477–483.
19. Nael K, Krishnam M, Nael A, Ton A, Ruehm SG, Finn JP. Peripheral contrast-enhanced MR angiography at 3.0T, improved spatial resolution and low dose contrast: initial clinical experience. Eur Radiol 2008;18(12):2893–2900.

20. Bonel HM, Saar B, Hoppe H, et al. MR angiography of infrapopliteal arteries in patients with peripheral arterial occlusive disease by using Gadofosveset at 3.0 T: diagnostic accuracy compared with selective DSA. Radiology 2009;253(3):879–890.
21. Pepe MS. The statistical evaluation of medical tests for classification and prediction. Oxford, England: Oxford University Press, 2003; 58–60.
22. Kundel HL, Polansky M. Measurement of observer agreement. Radiology 2003;228(2):303–308.
23. Willmann JK, Baumert B, Schertler Th, et al. Aortoiliac and lower extremity arteries assessed with 16-detector row CT angiography: prospective comparison with digital subtraction angiography. Radiology 2005;236(3):1083–1093.
24. Albrecht Th, Foert E, Holtkamp R, et al. 16-MDCT angiography of aortoiliac and lower extremity arteries: comparison with digital subtraction angiography. AJR Am J Roentgenol 2007;189(3): 702-711.
25. Menke J, Larsen J. Meta-analysis: Accuracy of contrast-enhanced magnetic resonance angiography for assessing steno-occlusions in peripheral arterial disease. Ann Intern Med 2010;153(5):325–334.
26. de Vries M, Ouwendijk R, Flobbe K, et al. Peripheral arterial disease: clinical and cost comparisons between duplex US and contrast-enhanced MR angiography—a multicenter randomized trial. Radiology 2006;240(2):401–410.
27. Habibi R, Krishnam MS, Lohan DG, et al. High-spatial-resolution lower extremity MR angiography at 3.0 T: contrast agent dose comparison study. Radiology 2008;248(2):680–692.
28. Leiner T, Alberts E, Geerts L, et al. Single dose large anatomical coverage contrastenhanced peripheral MRA using a novel broadband digital MR architecture: initial experience [abstr]. In: Proceedings of the Nineteenth Meeting of the International Society for Magnetic Resonance in Medicine. Berkeley, Calif: International Society for Magnetic Resonance in Medicine, 2011; 4767.
29. Wang CC, Liang HL, Hsiao CC, et al. Singledose time-resolved contrast enhanced hybrid MR angiography in diagnosis of peripheral arterial disease: compared with digital subtraction angiography. J Magn Reson Imaging 2010;32(4):935–942.
30. Prince MR, Zhang HL, Roditi GH, Leiner T, Kucharczyk W. Risk factors for NSF: a literature review. J Magn Reson Imaging 2009;30(6):1298–1308.
31. de Vries M, Nijenhuis RJ, Hoogeveen RM, de Haan MW, van Engelshoven JM, Leiner T. Contrast-enhanced peripheral MR angiography using SENSE in multiple stations: feasibility study. J Magn Reson Imaging 2005; 21(1):37–45.

Chapter 7

Site-specific association between distal aortic pulse wave velocity and peripheral arterial stenosis severity: a prospective cardiovascular magnetic resonance study

Harrie CM van den Bosch
Jos JM Westenberg
Wikke Setz-Pels
John HM Wondergem
Ron Wolterbeek
Lucien EM Duijm
Joep AW Teijink
Albert de Roos

J Cardiovasc Magn Reson 2015;17(1):2

Abstract

Background
Vascular disease expression in one location may not be representative for disease severity in other vascular territories, however, strong correlation between disease expression and severity within the same vascular segment may be expected. Therefore, we hypothesized that aortic stiffening is more strongly associated with disease expression in a vascular territory directly linked to that aortic segment rather than in a more remote segment. We prospectively compared the association between aortic wall stiffness, expressed by pulse wave velocity (PWV), sampled in the distal aorta, with the severity of peripheral arterial occlusive disease (PAOD) as compared to atherosclerotic markers sampled in remote vascular territories such as PWV in the proximal aorta and the normalized wall index (NWI), representing the vessel wall thickness, of the left common carotid artery.

Methods
Forty-two patients (23 men; mean age 64±10 years) underwent velocity-encoded cardiovascular magnetic resonance (CMR) in the proximal and distal aorta, whole-body contrast-enhanced MR angiography (CE-MRA) and carotid vessel wall imaging with black-blood CMR in the work-up for PAOD. Strength of associations between aortic stiffness, carotid NWI and peripheral vascular stenosis grade were assessed and evaluated with multiple linear regression.

Results
Stenosis severity correlated well with PWV in the distal aorta (Pearson $rP=0.64$, $p<0.001$, Spearman $rS=0.65$, $p<0.001$) but to a lesser extent with PWV in the proximal aorta ($rP=0.48$, $p=0.002$, $rS=0.22$, $p=0.18$). Carotid NWI was not associated with peripheral stenosis severity ($rP=0.17$, $p=0.28$, $rS=0.14$, $p=0.37$) nor with PWV in the proximal aorta ($rP=0.22$, $p=0.17$) nor in the distal aorta ($rP=0.21$, $p=0.18$). Correlation between stenosis severity and distal aortic PWV remained statistically significant after correction for age and gender.

Conclusions
Distal aortic wall stiffness is more directly related to peripheral arterial stenosis severity than markers from more remote vascular territories such as proximal aortic wall stiffness or carotid arterial wall thickness. Site-specific evaluation of vascular disease may be required for full vascular risk estimation.

Background

It is well known that the expression of vascular disease in one location may not be representative for the severity of disease in other vascular territories. From an observational cardiovascular magnetic resonance (CMR) study in 394 subjects, Barbier et al. reported that unrecognized myocardial infarction was not associated with manifestation of atherosclerosis depicted on whole-body MR angiography, nor with increased intima-media thickness (IMT) sampled in the carotid artery.[1]
However, strong correlation has been reported between vascular disease expression and vascular wall changes within the same vascular segment. Increased wall thickness and wall stiffening in the carotid artery have been associated with the presence of atherosclerotic plaque in patients with hypertension and elderly patients.[2] Additionally, a stronger association between arterial vessel wall thickness and wall stiffness has been demonstrated when these markers were sampled regionally within the same vascular territory of either the aorta or the carotid artery, rather than across vascular territories.[3] Atherosclerosis involves both arterial wall thickening due to fatty degeneration (i.e., atherosis) and arterial wall stiffening due to media degeneration (i.e., sclerosis).[4,5] Atherosclerosis is therefore not limited to luminal narrowing and structural changes in the arterial wall, but is also strongly associated with arterial wall stiffening.[6] The pulse wave velocity (PWV) has been acknowledged as an important indicator for increased aortic stiffness with prognostic value for cardiovascular events.[7,8] With velocity encoded CMR, the PWV can be accurately assessed with high reproducibility, regionally in the aorta.[9]
We hypothesized that aortic stiffening is more strongly associated with the expression of vascular disease in the vascular territory at risk directly linked to that aortic segment rather than in a more remote aortic segment or in other vascular territories. Accordingly, the purpose of this study was to prospectively compare the association between aortic wall stiffness, expressed by pulse wave velocity, sampled in the distal aorta with the severity of peripheral arterial occlusive disease as compared to atherosclerotic markers sampled in remote vascular territories such as PWV in the proximal aorta and normalized wall index[10] describing the vessel wall thickness of the left common carotid artery.

Methods

Patients

In our study, 42 consecutive patients (23 men; mean age 64±10 years) were included who were clinically referred for CE-MRA evaluation and were either suspected for PAOD due to clinical symptoms or already known to be suffering from PAOD and had

to undergo follow-up evaluation. In all patients, a single comprehensive CMR examination was performed consisting of a moving-table CE-MRA of the run-off vessels, carotid vessel wall imaging and assessment of the aortic pulse wave velocity. In all patients, the glomerular filtration rate (GFR) was >60 mL/min/1.73 m^2. No adverse reactions or complications occurred during or after MRA. Institutional Review Board approval and written informed consent was obtained from all patients.
Of note, 16 patients of the present study have been described previously in a study comparing different MRA techniques of the run-off vessels.[11]

CMR protocol

CMR was performed using a 3T CMR system (Achieva X-series, release 2.1; Philips Healthcare, Best, The Netherlands). Whole-body CE-MRA was performed and has been partially described before.[11] In short, first standardized 3-station single-injection CE-MRA was performed, including the abdominal aorta, iliac arteries and run-off vessels. The contrast protocol consisted of a biphasic contrast injection using an CMR-compatible injector (Spectris MR injector; Medrad, Indianola, PA). In total, 0.1 mmol/kg body weight gadoterate meglumine (Gd-DOTA, Guerbet, Paris, France) was administered. The first half of the contrast bolus was administered at 1.2 mL/s and the remaining half at 0.5 mL/s. Contrast injection was followed by 15 mL saline flush at 0.6 mL/s. Timing of the contrast arrival, required to start the acquisition of the CE-MRA, was determined by means of automatic bolus timing (BolusTrak; Philips Healthcare, Best, The Netherlands). For signal transmission and reception a quadrature body coil was used in all three stations. Imaging parameters of the 3D fast gradient-echo (FFE) CE-MRA were as follows: for the pelvic arteries repetition time (TR) 3.6 ms, echo time (TE) 1.25 ms, flip angle 20°, field-of-view (FOV) 410 mm, acquired voxel size 1.25×1.84×3.70 mm^3, reconstructed voxel size 0.73×0.73×1.85 mm^3; for the upper-leg arteries TR/TE 3.6/1.26, flip angle 20°, FOV 410 mm, acquired voxel size 1.30×1.75×3.00 mm^3, reconstructed voxel size 0.73×0.73×1.50 mm^3;for the lower-leg arteries TR/TE 4.7/1.60, flip angle 30°, FOV 410 mm, acquired voxel size 0.80×0.90×1.40 mm^3, reconstructed voxel size 0.71×0.71×0.70 mm^3. The first station was acquired with reversed linear k-space filling, the second and third station were acquired with centric k-space filling. Table speed was set at 180 mm/s between all imaged stations. The fourth station consisting of the thoracic aorta and its supra-aortic braches, including the carotid arteries, was acquired after a second contrast injection (0.1 mmol/kg body weight Gd-DOTA). Timing of contrast arrival was determined by means of automatic bolus timing. For signal transmission and reception a quadrature body coil was used. Imaging parameters were as follows: TR/TE 5.5/1.80, flip angle 30°, FOV 410 mm, acquired voxel size 0.96×0.97×2.00 mm^3, reconstructed voxel size 0.64×0.64×1.00 mm^3. Data were acquired with centric k-space filling.

Preceding to the whole-body CE-MRA procedure, the vessel wall of the left common carotid artery was examined in all patients using multi-slice two-dimensional black blood imaging. On oblique sagittal and oblique coronal survey scans axial slices were planned perpendicular to the course of the common carotid artery (Figure 7.1A). Starting from the carotid flow divider, eight contiguous slices of 2 mm thick were acquired in caudal direction. To maximize contrast between the carotid vessel wall, the lumen blood pool and the surrounding tissue, a 2D dual-inversion-recovery (black-blood) gradient echo technique with spectral selective fat suppression was used. VCG-triggering was used for gated data acquisition at end-diastole. For signal reception, a 2-element Flex-M surface coil was positioned around the neck of the patient. Images were acquired at each RR interval with the following typical parameters: TR/TE 12/3.5, flip angle 45°, FOV 140 mm, two signal averages, acquired voxel size 0.46×0.46×2 mm^3.

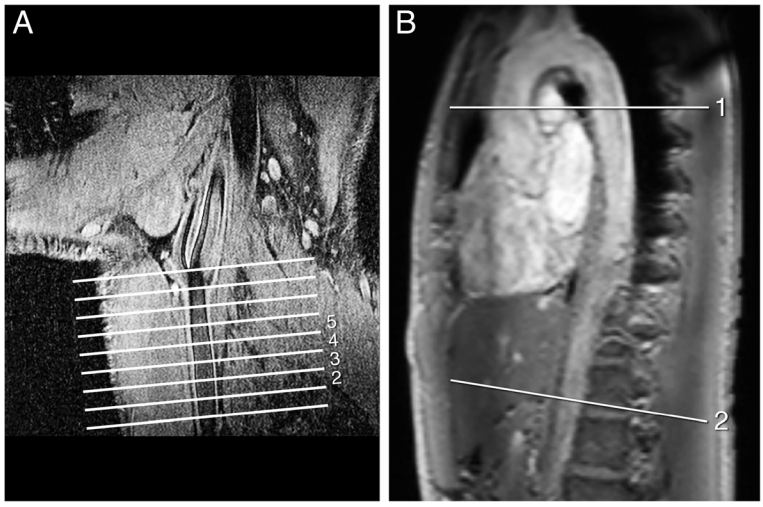

Figure 7.1 Carotid vessel wall thickness and aortic pulse wave velocity. **A**: Multi-slice 2D Black-Blood CMR of the common carotid artery for assessment of vessel wall thickness. Eight cross-sectional slices of the left common carotid artery were acquired, with the last slice adjacent to the bifurcation, however only slice 2 to 5 were included in the analysis. **B**: Proximal and distal aortic Pulse Wave Velocity (PWV) was assessed by two one-directional velocity-encoded CMR acquisitions in through-plane direction, planned perpendicular to the aorta at the level of the pulmonary trunk and at the abdominal aorta, respectively.

The pulse wave velocity, defined as the wave propagation speed, was assessed regionally in the aorta, between the ascending and descending thoracic aorta (i.e., the proximal aorta), and between the thoracic descending and distal abdominal aorta (i.e., the distal aorta) (Figure 7.1B), using a 6-element cardiac coil. Two one-directional

through-plane velocity-encoded CMR acquisitions were performed to assess the flow waveform propagation through the aorta. First, a double-oblique sagittal survey of the aorta was obtained (1C) and used for planning of the velocity-encoded acquisitions. The first velocity-encoded acquisition was planned perpendicular to the ascending aorta at the level of the pulmonary trunk, and transecting both the ascending and thoracic descending aorta. The second acquisition was planned at the most distal aortic location still present in the sagittal survey. Velocity-encoded CMR was performed using a retrospectively VCG-gated gradient-echo sequence with velocity-encoding in through-plane direction: TR/TE 4.9/3.0, flip angle 10°, FOV 320 mm, one signal average, acquired voxel size 2.50×2.50×8.00 mm^3. The maximum number of phases was reconstructed in order to obtain high temporal resolution (the true temporal resolution was 2×TR =9.8 ms). At the proximal level, a velocity sensitivity Venc of 150 cm/s was used and at the distal level, Venc =100 cm/s. Free breathing was allowed during the acquisition.

Image analysis

MR angiographic images were reviewed at random and in consensus by two MR radiologists (HvdB and JW; 15 and 17 years of experience with CE-MRA, respectively). CE-MRA images were analyzed on a remote workstation. The arterial tree from infrarenal aorta down to the peripheral arteries was divided into 27 segments (Figure 7.2): the infrarenal aorta, common iliac arteries, external iliac arteries, common femoral arteries, superficial femoral arteries, popliteal arteries in the thigh station, popliteal arteries in the calf station, tibiofibular trunk, and the proximal and distal halves of the anterior and posterior tibial arteries and peroneal arteries. The severity of each stenosis was visually graded according to a five point scale: class 1 (0%-stenosis), 2 (1-50%), 3 (51-75%), 4 (76-99%) and 5 (100%). The highest stenosis class per segment was determined, and next, the highest stenosis class over all available segments (maximal 27), presenting one value per patient (Max SC), was determined. Also, the mean stenosis class (Mean SC), averaged over all available segments was calculated. While both parameters relate to the severity of PAOD, Max SC relates to the stenosis severity and Mean SC relates to distribution of stenoses in peripheral arterial tree. Stenosis classification per patient was performed blinded from carotid vessel wall and aortic PWV analysis.

Cross-sectional carotid vessel wall area (VWA) and total vessel area were obtained using the previously validated in-house developed software package VesselMass software (Leiden University Medical Center, Leiden, the Netherlands[12]. Inner and outer lumen contours were manually defined. Analysis was performed in four slices out of eight. The mean cross-sectional carotid VWA and total vessel area were averaged over the four included slices, and subsequently the normalized wall index (NWI)[10] was calculated as follows: NWI=VWA/total vessel area.

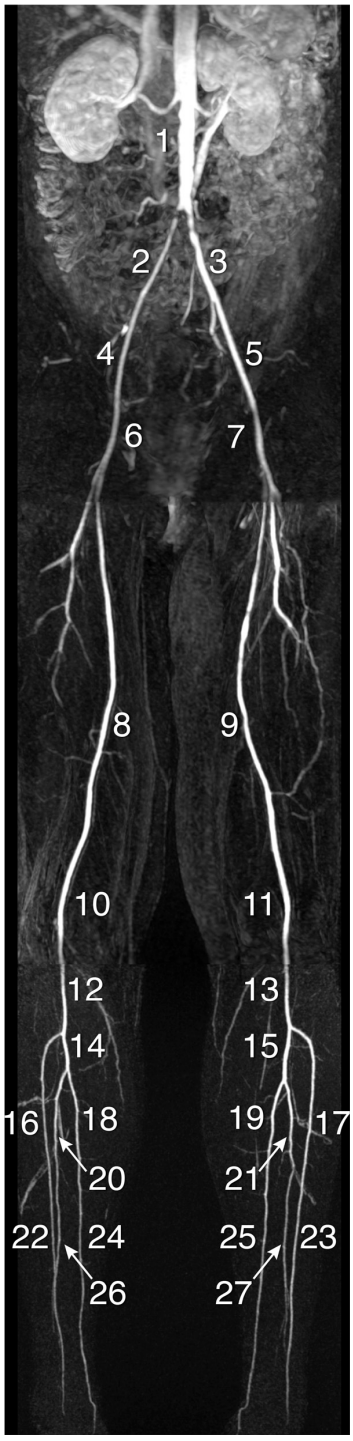

Figure 7.2 Segments of arterial tree from infrarenal aorta to peripheral arteries. Contrast-enhanced MRA of the infra-renal aorta down to the lower leg arteries in a patient with a subtotal stenosis in the right common iliac artery. For each patient, mean and maximal stenosis class were obtained by dividing the arterial tree into 27 segments: the infrarenal aorta (1), common iliac arteries (2,3), external iliac arteries (4 ,5), common femoral arteries (6+7), superficial femoral arteries (8,9), popliteal arteries in the thigh station (10,11), popliteal arteries in the calf station (12,13), tibiofibular trunk (14,15), and the proximal (16-21) and distal (22-27) halves of the anterior and posterior tibial arteries and peroneal arteries.

The aortic PWV was obtained from systolic wave propagation analysis based on the transit-time method which has been validated before.[9] The aortic path length (Δx), describing the distance between sampling sites in the ascending and the thoracic descending aorta for proximal aortic PWV ($PWV_{proximal}$) and between the thoracic and abdominal descending aorta for distal aortic PWV (PWV_{distal}), respectively, was manually determined using MASS software (Leiden University Medical Center, Leiden, The Netherlands), by placing a poly-line along the centerline of the aorta in the sagittal survey images. Each aortic path length measurement was performed twice and averaged. Wave propagation was evaluated from maximal velocity-time curves that were obtained at each sampling site by using FLOW software (Leiden University Medical Center, Leiden, the Netherlands) with automated contour detection for image segmentation. The transit-time defining the wave propagation was assessed from the onset of each wave front, automatically calculated from the intersection of the horizontal line modeling the diastolic flow (averaged over the final 250 ms of the velocity-time curve) and the upslope of the systolic wave which was modeled by a straight line, using linear regression of all values between 20% and 80% of the range of velocity values that are part of the upslope.

Statistical analysis

Kolmogorov-Smirnov tests were performed to test normality of data distribution. Continuous variables are expressed as mean ± standard deviation (SD). Associations between atherosclerotic disease severity (Mean SC and Max SC) and atherosclerotic markers $PWV_{proximal}$, PWV_{distal} and carotid NWI were explored. Furthermore, association between NWI and PWV was examined. Correlation between Mean SC and Max SC and $PWV_{proximal}$, PWV_{distal} and carotid NWI was examined by calculating Pearson (for continuous variables) or Spearman (in case of association with an ordinal variable) correlation coefficients, where appropriate. Multiple linear regression analyses were performed with Mean SC as dependent variable and age, gender and respectively alternating proximal and distal aortic PWV and carotid NWI as predictors. Additionally, interaction between predictors was analyzed. A p-value of <0.05 is considered statistically significant. Statistical analysis was performed using IBM SPSS software version 20 (Armonk, NY, USA).

Results

Patient characteristics are presented in Table 7.1. Thirty-four patients (81%) presented with intermittent claudication (Fontaine classification 2), of which twenty-three patients (55%) with pain-free claudication walking ≥200 m and eleven patients (26%) with pain-free claudication walking <200 m. Five patient (12%) presented with rest pain (Fontaine classification 3) and three patients (7%) with necrosis (Fontaine classification 4). Mean ankle-brachial index (ABI) in rest was 0.75±0.21. CE-MRA was successful in all patients. No imaging artefacts or venous contamination affected the image analysis and image quality was sufficient for stenosis scoring in all segments. Mean SC per patient ranged between 1 (no stenosis) and 3.6, with a mean value ± standard deviation of 1.6 ±0.5. Max SC ranged between 1 and 5, with mean ± SD 4.4 ±1.0 (median 5, interquartile range from 4 to 5). Carotid NWI ranged from 0.20 to 0.59, with mean ± SD of 0.46 ±0.07. PWV ranged from 4.5 m/s to 45.3 m/s in the proximal aorta (mean ± SD 10.1±6.5 m/s) and from 4.4 m/s to 24.4 m/s in the distal aorta (mean ± SD 9.3 ±3.8 m/s). All continuous data were normally distributed according to Kolmogorov-Smirnov tests (all $p>0.05$). In Figure 7.3, scatter plots and box plots are presented to illustrate data distribution and associations between markers. From the distribution of the data in these figures it is obvious that one outlier for Mean SC (Figures 7.3A to 7.3C: data point with Mean SC =3.6) and one outlier for PWV in the proximal aorta (Figures 7.3A,7.3D and 7.3G: data point with PWV =45.3 m/s) might contribute substantially to the correlations. For the patient with Mean SC of 3.6, $PWV_{proximal}$ was 8.8 m/s, PWV_{distal} 9.2 m/s and carotid NWI 0.48. For the patient with $PWV_{proximal}$ 45.3 m/s, the Mean SC was 1.6, PWV_{distal} 13.2 m/s and

carotid NWI 0.57. Analysis was performed on the full dataset as well as on the dataset with these two outliers removed. For the data with outliers removed, mean values ± SD changed for Mean SC 1.5 ±0.4 and for $PWV_{proximal}$ 9.3 ±3.5 m/s.

Table 7.1 Patient characteristics

Gender (male/female)	23 / 19
Age (years)	64 ± 10
Hypertension (yes/no)	28 / 14
Fontaine Class (stages I / IIa / IIb / III / IV)	0 / 23 / 11 / 5 / 3
ABI in rest	0.75 ± 0.21
Mean SC	1.6 ± 0.5
Max SC (median (interquartile range))	5 (4–5)
Carotid NWI	0.46 ± 0.07
$PWV_{proximal}$ (m/s)	10.1 ± 6.5
PWV_{distal} (m/s)	9.3 ± 3.8

ABI: ankle-brachial index; SC: stenosis class; NWI: normalized wall index; PWV: pulse wave velocity

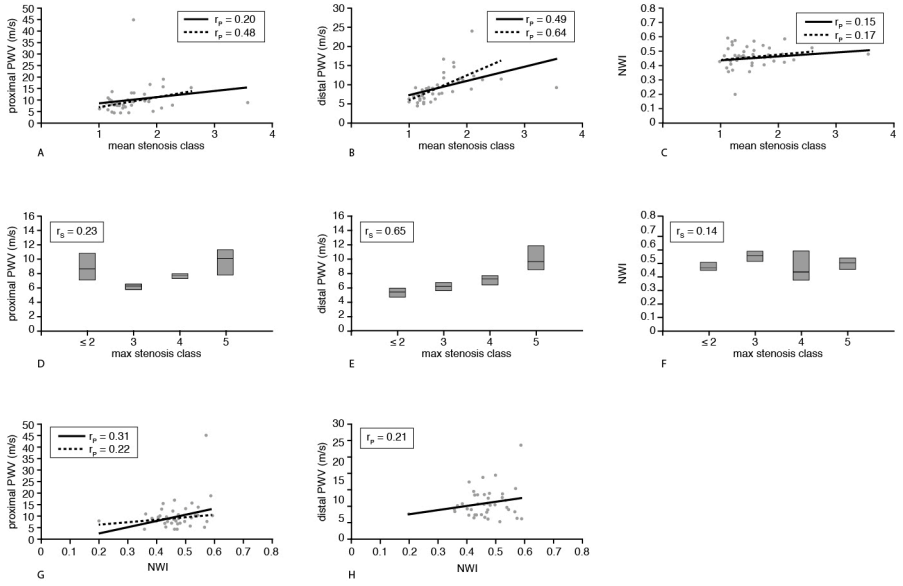

Figure 7.3 Association stenosis severity, PWV, and carotid wall thickness (A-H). Associations between stenosis severity (expressed in mean and max stenosis class), the proximal and distal aortic pulse wave velocity and normalized wall index sampled in the left common carotid artery. Solid line represents correlation between parameters for the full dataset, dashed line represents correlation for dataset with two outliers removed.

In two patients, significant stenoses were found in the carotid arteries: in one patient, a class 3 stenosis was depicted in the right internal carotid artery and in the other

patient, a full occlusion was present in the right internal carotid artery while the left internal carotid artery presented with a class 3 stenosis. All other patients were free from stenoses in the carotid arteries. In 28 patients, no stenosis was present in the distal aorta; 11 patients were graded with a class 2 stenosis in the abdominal aorta, 1 patient with class 3 stenosis, 1 patient with class 4 stenosis and one patient with an occlusion. Spearman correlation coefficients indicated no significant correlations between stenosis severity in the distal aorta and proximal aortic PWV (r_S=−0.09, p=0.59) and distal aortic PWV (r_S=−0.21, p=0.21), respectively. Low correlation was found between stenosis severity in the distal aorta and the carotid NWI (r_S=0.38, p=0.02).
In two patients, no stenoses were depicted on any of the CE-MRA images. Correlations between Mean SC in the complete run-off and proximal and distal aortic PWV and carotid VWA/BSA were evaluated by Pearson correlation coefficients, while correlations between Max SC, proximal and distal aortic PWV and carotid NWI were evaluated by Spearman correlation coefficients, respectively. The results are presented in Table 7.2, both for all data point as well as for the data with two outliers removed.

Table 7.2 Pearson and Spearman correlation coefficients between mean and maximal stenosis severity, proximal and distal aortic PWV and cross-sectional carotid NWI, both for the total dataset as well as for one outlier removed

	All patients included			Two outliers removed		
	Mean SC r_P	Max SC r_S	NWI r_P	Mean SC r_P	Max SC r_S	NWI r_P
$PWV_{proximal}$	0.20 (p=0.22, N=42)	0.23 (p=0.14, N=42)	0.31 (p=0.048, N=42)	0.48 (p=0.002, N=40)	0.22 (p=0.18, N=41)	0.22 (p=0.17, N=41)
PWV_{distal}	0.49 (p=0.001, N=42)	0.65 (p<0.001, N=42)	0.21 (p=0.18, N=42)	0.64 (p<0.001, N=41)	0.65 (p<0.001, N=42)	0.21 (p=0.18, N=42)
NWI	0.15 (p=0.34, N=42)	0.14 (p=0.37, N=42)		0.17 (p=0.28, N=41)	0.14 (p=0.37, N=42)	

PWV: pulse wave velocity, NWI: normalized wall index, SC: stenosis class, r_P: Pearson correlation coefficient, r_S: Spearman correlation coefficient, N: number of samples

None to moderate association between PWV in the proximal aorta and stenosis class (r_P=0.48 for Mean SC and r_s=0.22 for Max SC) was found. Associations between distal aortic PWV and stenosis class are good. However, associations are absent between carotid NWI and stenosis class as well as between carotid NWI and proximal and distal aortic PWV.
In Table 7.3, the results of multiple linear regression between Mean SC and proximal and distal aortic PWV, carotid NWI, age and gender are presented. No significant interaction was found between these predictors (all p>0.05). These tests show that proximal and distal aortic PWV and carotid NWI are all statistically significantly associated with age, but none of these predictors is associated with gender. However,

for these patients, only distal aortic PWV remained significantly associated with Mean SC (with β=0.46, p=0.003), when corrected for age (β=0.30, p=0.04) and gender (β=−0.06, p=0.61).

Table 7.3 Multiple linear regression analysis with mean stenosis class as dependent variable and age, gender and respectively alternating cross-sectional carotid normalized wall index, proximal and distal aortic pulse wave velocity as predictors

	NWI				$PWV_{proximal}$				PWV_{distal}		
	B (SE)	β	p		B (SE)	β	p		B (SE)	β	p
constant	0.13 (0.39)		0.75	constant	0.31 (0.33)		0.36	constant	0.40 (0.29)		0.18
age	0.02 (0.005)	0.50	0.001	age	0.02 (0.01)	0.41	0.01	age	0.01 (0.005)	0.30	0.04
gender	-0.15 (0.11)	-0.21	0.17	gender	-0.11 (0.10)	-0.15	0.28	gender	-0.04 (0.09)	-0.06	0.61
NWI	0.59 (0.76)	0.12	0.44	$PWV_{proximal}$	0.03 (0.02)	0.27	0.08	PWV_{distal}	0.05 (0.01)	0.46	0.003

NWI: normalized wall index, PWV: pulse wave velocity, SE: standard error

Discussion

This study prospectively evaluated the association between aortic wall stiffness, expressed by PWV, sampled in the distal aorta and the severity of PAOD as compared to atherosclerotic markers sampled in remote vascular territories such as the PWV in the proximal aorta and vessel wall thickness of the left common carotid artery. The main findings of our study are: 1) In patients with PAOD, the PWV in the distal aorta is well associated with peripheral arterial stenosis severity. 2) Correlation between peripheral arterial stenosis severity with markers sampled in remote vascular territories such as PWV in the proximal aorta and carotid VWA NWI, are weak to absent, only moderate at best, indicating site-specific association between aortic wall stiffness and peripheral arterial disease severity. 3) Only the correlation between stenosis severity and distal aortic PWV remains statistically significant after correction for age and gender.

PAOD is an important clinical manifestation of atherosclerosis, for which 3T CE-MRA is a reliable diagnostic tool, widely used to detect and grade stenosis severity.[11] However, CE-MRA is not without risks, especially in patients with impaired renal function.[13] The initial test in clinical routine for diagnosing patients with clinical symptoms of PAOD is assessment of the ankle-brachial index (ABI).[14] A low ABI is a strong indicator of the presence of PAOD[15] but a normal ABI, however, does not rule out risk due to the false negative rates.[16] Furthermore, Wikström et al. reported that ABI<0.9 may underestimate the prevalence of PAOD when assessed with CE-MRA.[17] Therefore, the evaluation of other markers associated with the severity of PAOD is warranted. Atherosclerosis is a systemic disease which affects the arterial wall both by

thickening and stiffening. Structural changes in the wall usually occur over a larger part of the arterial tree rather than confined to a localized arterial segment (i.e., diffuse preintrusive wall thickening in contrast to focal intrusive thickening[2]). Maroules et al. recently demonstrated a strong association between wall thickness sampled in the abdominal aorta and the occurrence of cardiovascular events in a large population-based study.[18] Additionally, arterial wall stiffening has been described as an independent predictor of cardiovascular events in patients with hypertension, diabetes and end-stage renal disease[19,20] as well as in the aging population.[21] Moreover, increased carotid arterial wall thickness is associated with carotid wall stiffening and with the presence of atherosclerotic plaque in the carotid artery and the aorta in patients with hypertension and elderly patients.[22]

However, it is well known that the expression of vascular disease in one location may not be representative for the severity of disease in other vascular territories and it is conceivable that disease severity is stronger associated with atherosclerotic markers sampled within the same vascular territory than when sampled in a more remote vascular territory. Barbier et al. demonstrated that unrecognized myocardial infarction is not necessarily associated with atherosclerotic disease severity, depicted from whole-body MR angiography nor with increased intima-media thickness (IMT) sampled in the carotid artery.[1] Furthermore, in a recent publication, Turkbey et al. found no independent association between imaging biomarkers of atherosclerosis such as carotid IMT and distensibility sampled in the ascending aorta.[23] This finding was confirmed by our results, as the association between carotid NWI and the PWV in the proximal aorta was not statistically significant. Furthermore, in a study by Brandts et al. it was shown both in healthy volunteers as well as in patients with hypertension that the aortic PWV correlated more strongly with the aortic VWA than when compared to the carotid VWA.[24] Kröner et al.[3] confirmed these findings in healthy volunteers and added stronger correlations between arterial vessel wall thickness and stiffness when sampled within the same vascular territory of either the aorta or the carotid artery, rather than across vascular territories. These reports underline the suggestion of a strong site-specific coupling between morphologic and functional degenerative changes of the arterial wall and the possible effect on future cardiovascular events.

In our study, 42 consecutive patients referred for CEMRA for the evaluation of severity of PAOD were included. In these patients, the prevalence of significant stenoses in the distal aorta was low (i.e., 7%), and therefore, no association with PWV in this part of the aorta could be demonstrated. However, the stenosis severity detected with CE-MRA in the peripheral arteries correlated well with the PWV sampled in the distal aorta, but to a lesser extent with PWV in the proximal aorta, and no association was found with carotid NWI. Taniwaki et al.[25] showed that in patients with type 2 diabetes mellitus, the presence of PAOD symptoms was more closely associated with increased femoral arterial wall stiffness compared to increased

femoral arterial wall thickness, suggesting that stiffening has a significant impact on clinical symptoms in patients with peripheral vascular disease. In our study, aortic wall stiffness is represented by the PWV, which is defined as the systolic wave front velocity propagating through the aorta. The assessment of PWV by CMR has shown good agreement with invasive pressure measurements, the gold standard for defining PWV.[9,26] Still, data on reproducibility of this assessment is scarce. Grotenhuis et al.[9] evaluated the reproducibility by repeating acquisitions on the same day and reported a coefficient of variation of 9% for PWV assessment in the total aorta by CMR. In a study by Suever et al.,[27] reproducibility of CMR-assessed PWV was compared to applanation tonometry by performing repeated studies on volunteers on the same day. However, no data has been published for repeated acquisitions on separate days, therefore information on the physiological variation of this marker is missing, although CMR-assessed PWV is widely used in clinical research. To our knowledge, this is the first clinical study to evaluate the association between peripheral arterial stenosis severity and regional aortic wall stiffness and carotid vessel wall thickness, all assessed from one comprehensive CMR examination. The results from our study and from literature underline a potentially important role for the site-specific assessment of arterial wall stiffness by PWV regionally in the aorta as this may be required for full estimation of vascular risk in patients with atherosclerosis. The strong site-specific association between distal aortic wall stiffening and the degree of stenosis in the peripheral arteries suggests that sampling within the same vascular territory may be preferred over sampling across vascular territories.

We acknowledge certain limitations of our study. First, it involves a cross-sectional design in a relatively small prospectively included patient population in which the association between atherosclerotic markers and stenosis severity was evaluated. Association, however, does not prove causality. Population-based long-term follow-up studies are required to prove whether distal aortic stiffening indeed is a precursor to PAOD and to elucidate the predictive value of increased wall stiffness in the distal aorta with respect to further development of flow-limiting stenoses in the peripheral arteries. Carotid arterial vessel wall sampling was limited to the left common carotid artery. Prevalence of stenoses in the carotid circulation in this patient population was very low. Adding VWA sampling of the right carotid artery would be possible but this was not performed, however, as it requires additional scan time. Also, no comparison with ultrasound-assessed IMT was performed, additionally to VWA sampling with Black-Blood CMR, but from literature it is known that CMR shows good agreement with ultrasound when sampling IMT.[28] The higher spatial resolution on ultrasound potentially may improve the association between IMT and PAOD stenosis severity, however, CMR has the advantage of providing increased vessel coverage with information on the complete circumference over the length of a vessel, which permits assessment of localized abnormalities without assuming vessel uniformity.

Conclusions

Peripheral arterial stenosis severity is well correlated with aortic PWV sampled in the distal aorta but correlation with markers sampled in remote vascular territories such as PWV in the proximal aorta and carotid arterial wall thickness, is only moderate at best. The association between aortic wall stiffening and stenosis severity in a vascular territory directly linked to this aortic segment suggests that site-specific evaluation of vascular disease may be required for full vascular risk assessment and therefore, regional aortic PWV assessment by CMR may be considered in the clinical workup of PAOD.

References

1. Barbier CE, Nylander R, Themudo R, Ahlström H, Lind L, Larsson EM, Bjerner T, Johansson L. Prevalence of unrecognized myocardial infarction detected with magnetic resonance imaging and its relationship to cerebral ischemic lesions in both sexes. J Am Coll Cardiol. 2011; 58:1372–77.
2. Simon A, Megnien J-L, Gariepy J, Levenson J. Early atherosclerosis in human hypertension. Am J Hypertens. 1998; 11:882–83.
3. Kröner ES, Lamb HJ, Siebelink HM, Putter H, van der Geest RJ, van der Wall EE, de Roos A, Westenberg JJ. Coupling of vessel wall morphology and function in the aorta and the carotid artery: an evaluation with MRI. Int J Cardiovasc Imaging. 2014; 30:91–8.
4. Selvin E, Najjar S, Cornish T, Halushka MK. A comprehensive histopathological evaluation of vascular medial fibrosis: Insights into the pathophysiology of arterial stiffening. Atherosclerosis. 2010; 208: 69-74.
5. Blankenhorn DH, Kramsch DM. Reversal of atherosis and sclerosis. The two components of atherosclerosis. Circulation. 1989; 79:1–7.
6. Van Popele NM, Grobbee DE, Bots ML, Asmar R, Topouchian J, Reneman RS, Hoeks AP, van der Kuip DA, Hofman A, Witteman JC. Association between arterial stiffness and atherosclerosis: the Rotterdam study. Stroke. 2001;32:454–60.
7. Mitchell GF, Hwang SJ, Vasan RS, Larson MG, Pencina MJ, Hamburg NM, Vita JA, Levy D, Benjamin EJ. Arterial stiffness and cardiovascular events: the Framingham Heart Study. Circulation. 2010; 121: 505–11.
8. Karras A, Haymann JP, Bozec E, Metzger M, Jacquot C, Maruani G, Houillier P, Froissart M, Stengel B, Guardiola P, Laurent S, Boutouyrie P, Briet M. Large artery stiffening and remodeling are independently associated with all-cause mortality and cardiovascular events in chronic kidney disease. Hypertension. 2012; 60:1451–57.
9. Grotenhuis HB, Westenberg JJ, Steendijk P, van der Geest RJ, Ottenkamp J, Bax JJ, Jukema JW, de Roos A. Validation and reproducibility of aortic pulse wave velocity as assessed with velocity-encoded MRI. J Magn Reson Imaging. 2009; 20:521–26.
10. Saam T, Yuan C, Chu B, Takaya N, Underhill H, Cai J, Tran N, Polissar NL, Neradilek B, Jarvik GP, Isaac C, Garden GA, Maravilla KR, Hashimoto B, Hatsukami TS. Predictors of carotid atherosclerotic plaque progression as measured by noninvasive magnetic resonance imaging. Atherosclerosis. 2007; 194: 34–42.
11. Van den Bosch HCM, Westenberg JJM, Caris R, Duijm LE, Tielbeek AV, Cuypers PW, de Roos A. Peripheral arterial occlusive disease: 3.0-T versus 1.5-T MR angiography compared with digital subtraction angiography. Radiology. 2013; 266:337–46.
12. Alizadeh DR, Doornbos J, Tamsma JT, Stuber M, Putter H, van der Geest RJ, Lamb HJ, de Roos A. Assessment of the carotid artery by MRI at 3T: a study on reproducibility. J Magn Reson Imaging. 2007; 25:1035–43.
13. Prince MR, Zhang HL, Roditi GH, Leiner T, Kucharczyk W. Risk factors for NSF: a literature review. J Magn Reson Imaging. 2009; 30:1298–308.
14. Langham MC, Englund EK, Mohler ER III, Li C, Rodgers ZB, Floyd TF, Wehrli FW. Quantitative CMR markers of impaired vascular reactivity associated with age and peripheral artery disease. J Cardiovasc Magn Reson Imaging. 2013;15:17.
15. Ouriel K, McDonnell AE, Metz CE, Zarins CK. Critical evaluation of stress testing in the diagnosis of peripheral vascular disease. Surgery. 1982; 91:686–93.
16. Doobay AV, Anand SS. Sensitivity and specificity of the ankle-brachial index to predict future cardiovascular outcomes: a systematic review. Arterioscler Thromb Vasc Biol. 2005; 25:1463–69.
17. Wikström J, Hansen T, Johansson L, Lind L, Ahlström H. Ankle brachial index <0.9 underestimates the prevalence of peripheral artery occlusive disease assessed with whole-body magnetic resonance angiography in the elderly. Acta Radiol. 2008; 49:143–49.
18. Maroules CD, Rosero E, Ayers C, Peshock RM, Khera A. Abdominal aortic atherosclerosis at MR imaging is associated with cardiovascular events: the Dallas heart study. Radiology. 2013; 269:84–91.

19. Laurent S, Katsahian S, Fassot C, Tropeano AI, Gautier I, Laloux B, Boutouyrie P. Aortic stiffness is an independent predictor of fatal stroke in essential hypertension. Stroke. 2003; 34:1203–06.
20. Blacher J, Guerin A, Pannier P, Marchais SJ, Safar ME, London GM. Impact of Aortic Stiffness on Survival in End-Stage Renal Disease. Circulation. 1999;99:2434–39.
21. Sutton-Tyrrell K, Najjar S, Boudreau R, Venkitachalam L, Kupelian V, Simonsick EM, Havlik R, Lakatta EG, Spurgeon H, Kritchevsky S, Pahor M, Bauer D, Newman A. Elevated Aortic Pulse Wave Velocity, a Marker of Arterial Stiffness, Predicts Cardiovascular Events in Well-Functioning Older Adults. Circulation. 2005; 111:3384–90.
22. Zureik M, Temmar M, Adamopoulos C, Bureau JM, Courbon D, Thomas F, Bean K, Touboul PJ, Ducimetière P, Benetos A. Carotid plaques, but not common carotid-media thickness, are independently associated with aortic stiffness. Hypertension. 2002; 20:85–93.
23. Turkbey EB, Redheuil A, Backlund JY, Small AC, Cleary PA, Lachin JM, Lima JA, Bluemke DA. Aortic Distensibility in Type 1 Diabetes. Diabetes Care. 2013;36:2380–87.
24. Brandts A, Westenberg J, Van Elderen S, Kroft LJ, Roes SD, Tamsma JT, van der Geest RJ, Lamb HJ, Doornbos J, Putter H, Stuber M, de Roos A. Site-specific coupling between vascular wall thickness and function. Invest Rad. 2013; 48:86–91.
25. Taniwaki H, Shoji T, Emoto M, Kawagishi T, Ishimura E, Inaba M, Okuno Y, Nishizawa Y. Femoral artery wall thickness and stiffness in evaluation of peripheral vascular disease in type 2 diabetes mellitus. Atherosclerosis. 2001; 158:207–14.
26. Westenberg JJ, Van Poelgeest EP, Steendijk P, Grotenhuis HB, Jukema JW, de Roos A. Bramwell-Hill modeling for local aortic pulse wave velocity estimation: a validation study with velocity-encoded cardiovascular magnetic resonance and invasive pressure assessment. J Cardiovasc Magn Reson Imaging. 2012; 14:2.
27. Suever JD, Oshinski J, Rojas-Campos E, Huneycutt D, Cardarelli F, Stillman AE, Raggi P. Reproducibility of pulse wave velocity measurements with phase contrast magnetic resonance and applanation tonometry. Int J Cardiovasc Imaging. 2012; 28:1141-1146.
28. Crowe LA, Ariff B, Keegan J, Mohiaddin RH, Yang GZ, Hughes AD, McG Thom SA, Firmin DN. Comparison between three-dimensional volumeselective turbo spin-echo imaging and two-dimensional ultrasound for assessing carotid artery structure and function. J Magn Reson Imaging. 2005; 21:282–89.

Chapter 8

Prognostic value of cardiovascular MR imaging biomarkers on outcome in peripheral arterial disease: a 6-year follow-up pilot study

Harrie CM van den Bosch
Jos JM Westenberg
Wikke Setz-Pels
Erik Kersten
Alexander Tielbeek
Lucien EM Duijm
Johannes C Post
Joep AW Teijink
Albert de Roos

Int J Cardiovasc Imaging 2016; 32(8):1281-1288

Abstract

The objective of this pilot study was to explore the prognostic value of outcome of cardiovascular magnetic resonance (MR) imaging biomarkers in patients with symptomatic peripheral arterial disease (PAD) in comparison with traditional risk factors. Forty-two consecutive patients (mean age 64 ± 11 years, 22 men) referred for contrast-enhanced MR angiography (CE-MRA) were included. At baseline a comprehensive cardiovascular MRI examination was performed: CE-MRA of the infra-renal aorta and run-off vessels, carotid vessel wall imaging, cardiac cine imaging and aortic pulse wave velocity (PWV) assessment. Patients were categorized for outcome at 72 ± 5 months follow-up. One patient was lost to follow-up. Over 6 years, six patients had died (mortality rate 14.6%), six patients (14.6%) had experienced a cardiac event and three patients (7.3%) a cerebral event. The mean MRA stenosis class (i.e., average stenosis severity visually scored over 27 standardized segments) was a significant independent predictor for all-cause mortality (beta 3.0 ± standard error 1.3, p=0.02). Descending aorta PWV, age and diabetes mellitus were interrelated with stenosis severity but none of these were significant independent predictors. For cardiac morbidity, left ventricular ejection fraction (LVEF) and mean MRA stenosis class were associated, but only LVEF was a significant independent predictor (beta −0.14 ± 0.05, p=0.005). Diabetes mellitus was a significant independent predictor for cerebral morbidity (beta 2.8 ± 1.3, p=0.03). Significant independent predictors for outcome in PAD are mean MRA stenosis class for all-cause mortality, LVEF for cardiac morbidity and diabetes mellitus for cerebral morbidity.

Introduction

Peripheral arterial disease (PAD) is an important clinical manifestation of vascular disease in atherosclerosis. Due to increased life expectancy the prevalence of PAD increased worldwide over the last decades by more than 20%.[1,2] The prevalence rates increase with age and are associated with increased mortality[3] and cardiac and cerebral events.[4,5] Identifying prognostic indicators for patients with PAD is important for risk factor reduction and for developing new therapies.[6,7] Assessment of traditional risk factors remains essential for risk stratification,[8] however, evidence on the utility of non-invasive imaging for risk assessment in cardiovascular disease (CVD) is growing.[9] Several previous studies observed high risk of mortality and cardiovascular events in patients with PAD, diagnosed with non-invasive testing techniques as segmental blood pressure, Doppler ultrasonography[3] and ankle-brachial index (ABI).[10,11] Moreover, progressive PAD with declining ABI values was shown to be significantly and independently associated with increased cardiovascular risk.[4] However, ABI has also been associated with high false negative rates in prediction of outcome[12] and underestimation of prevalence of PAD.[13]

In recent years contrast-enhanced magnetic resonance angiography (CE-MRA) has evolved into an important non-invasive imaging technique in patients suspected with symptomatic PAD.[14] In clinical routine, CE-MRA is now widely used for diagnosis, work-up and treatment planning. In our institute, a patient population with symptomatic PAD underwent a comprehensive MRI examination consisting of not only CE-MRA of the run-off vessels, but also carotid vessel wall imaging, cardiac cine imaging for assessing left ventricular volume, mass and function, and assessment of the aortic pulse wave velocity (PWV) from velocity-encoded MRI as a surrogate marker of aortic stiffness. This study was performed 6 years ago with the aim to evaluate the association of stenosis severity on CE-MRA with imaging biomarkers describing cardiovascular morphology and function. Our results showed a stronger association between PWV measured in the descending aorta and severity of PAD in the peripheral arteries than the PWV in the proximal aorta and the normalized wall index (NWI), measured with black-blood MRI in the common carotid artery.[15] The purpose of the current pilot study was to evaluate if these biomarkers obtained with cardiovascular MR imaging showed prognostic value of outcome after a follow-up period of 6 years in relation to traditional risk factors [i.e., age, gender, body mass index (BMI), hypertension, diabetes mellitus, levels of triglyceride (TG) and high-density lipoprotein (HDL) in blood plasma samples, ABI and Fontaine class]. Therefore, a follow-up evaluation of the patient population with symptomatic PAD was performed to examine which cardiovascular MR imaging biomarker or traditional risk factor is an independent predictor for all-cause mortality, cardiac or cerebral morbidity.

Materials and Methods

In our study, 42 consecutive patients (23 men; mean age 64±10 years) were included from July 2008 to October 2009. All patients were clinically referred for CE-MRA evaluation in the work-up for PAD. The following baseline patient characteristics were obtained: age, gender, weight, length, BMI, hypertension, diabetes mellitus, levels of TG and HDL in blood plasma samples, ABI and Fontaine class. A cut-off value of BMI>30 was used to classify obesity and levels of TG≥150 mg/dL and HDL≤50 mg/dL in women or ≤40 mg/dL in men as associated with metabolic syndrome.[16]
In all patients, a comprehensive cardiovascular MRI examination was performed consisting of CE-MRA of the run-off vessels, carotid vessel wall imaging, cardiac cine imaging and assessment of the aortic PWV from through-plane velocity-encoded MRI. In all patients, the glomerular filtration rate (GFR) was >60 mL/min/1.73 m^2. No adverse reactions or complications occurred during or after MRA. Institutional Review Board approval and written informed consent was obtained from all patients.
Of note, a study of this patient population has been published describing the site-specific association between descending aorta PWV and peripheral arterial stenosis severity.[15] Furthermore, data of 20 patients of the present study has been used previously in a study comparing different MRA techniques of the run-off vessels.[17] However, none of these publications reported outcome data, which is the purpose of the current study.

MRI protocol

MRI was performed using a 3T MRI system (Achieva X-series, release 2.1; Philips Healthcare, Best, The Netherlands). CE-MRA was performed in three consecutive stations and has been described before.[17] In short, standardized three-station single-injection CE-MRA was performed, including the abdominal aorta, iliac arteries and run-off vessels. The contrast protocol consisted of a biphasic contrast injection using an MRI-compatible injector (Spectris MR injector; Medrad, Indianola, PA). In total, 0.1 mmol/kg body weight gadoterate meglumine (Gd-DOTA, Guerbet, Paris, France) was administered. The first half of the contrast bolus was administered at 1.2 mL/s and the remaining half at 0.5 mL/s. Contrast injection was followed by 15 mL saline flush at 0.6 mL/s. Timing of the contrast arrival was determined by means of automatic bolus timing (BolusTrak; Philips Healthcare, Best, The Netherlands). For signal transmission and reception a quadrature body coil was used in all three stations. Preceding the CE-MRA procedure, the vessel wall of the left common carotid artery was imaged in all patients. A multi-slice two-dimensional (2D) black-blood imaging sequence was used.[18] Starting from the carotid flow divider, eight contiguous slices of 2 mm thick were acquired in caudal direction. To maximize contrast between the carotid vessel wall, the lumen blood pool and the surrounding tissue, a 2D dual-inversion-recovery

(black-blood) gradient-echo technique with spectral selective fat suppression was used. Vector-cardiogram (VCG)-triggering was used for gated data collection at end-diastole and data was acquired at each RR interval. A two-element Flex-M surface coil was positioned around the neck of the patient.
Furthermore, cardiac cine images were acquired in multi-slice short-axis orientation using a dedicated six-element cardiac coil for signal reception.[19] A balanced steady-state free-precession technique was used with retrospective VCG-gating. Each slice was acquired using breath-holding present one average heartbeat. Finally, the aortic PWV, defined as the flow wave propagation speed, was assessed regionally in the aorta, from two through-plane velocity-encoded MRI acquisitions: one transecting the ascending and descending thoracic aorta and one transecting the distal abdominal aorta.[20] The six-element cardiac coil was used for signal reception and both velocity-encoded MRI acquisitions were non-segmented gradient-echo sequences with a maximal velocity sensitivity of 150 cm/s at the proximal level and 100 cm/s at the distal level. Retrospective VCG-gating was used with a maximal number of phases reconstructed, resulting in a true temporal resolution of 9.8 ms.

Image analysis

MR angiographic images were reviewed at random and in consensus by two MR radiologists (HvdB and AT; 16 and 18 years of experience with CE-MRA, respectively). CE-MRA images were analyzed on a remote workstation. The arterial tree from infrarenal aorta down to the peripheral arteries was divided into 27 segments (Figure 8.1). The severity of each stenosis was visually graded according to a five point scale: class 1 (0%–stenosis), 2 (1–50%), 3 (51–75%), 4 (76–99%) and 5 (100%). The highest stenosis class per segment was determined, and next, the highest stenosis class over all available segments (maximal 27) was determined, resulting in one value per patient (max MRA stenosis class). Also, the mean MRA stenosis class, obtained from the highest stenosis class per segment and averaged over all available segments was calculated. Stenosis classification per patient was performed blinded from carotid vessel wall and aortic PWV analysis.
Cross-sectional carotid vessel wall area (VWA) and total vessel area were obtained using VesselMass software (Leiden University Medical Center, Leiden, The Netherlands). From the eight acquired slices over the common carotid artery, the center four slices were included for analysis. The NWI[21] was calculated as NWI = VWA/total vessel area.
Acquired cardiac short-axis images were analyzed on a remote workstation (View Forum, Philips Healthcare, Best, The Netherlands). Manual segmentation of the left ventricle was performed by a MR radiologist (HvdB, 16 years of experience with cardiac MR), resulting in endo- and epicardial contours for end systolic and end

diastolic phases. From planimetry, the end systolic and end diastolic volumes were calculated, as well as the left ventricular ejection fraction (LVEF) and LV mass.
The aortic PWV was obtained after velocity mapping at the ascending, thoracic descending and abdominal aorta. From systolic flow wave-time curves, aortic arch PWV and descending aorta PWV were obtained automatically using the transit-time method.[20]
In all patients mean MRA stenosis class, max MRA stenosis class, aortic arch PWV, descending aorta PWV, and carotid NWI were determined. In all patients but one the LVEF and LV mass were obtained. One patient could not tolerate multiple breath-holding and evaluation of short-axis LV images was not possible in this patient.
After a period of 6 years, mean baseline values of the cardiovascular MR imaging biomarkers were categorized for outcome. The primary outcome end point was all-cause mortality. The secondary end points were cardiac event (i.e. myocardial infarction, heart failure, coronary artery intervention) and cerebral event (i.e., stroke).

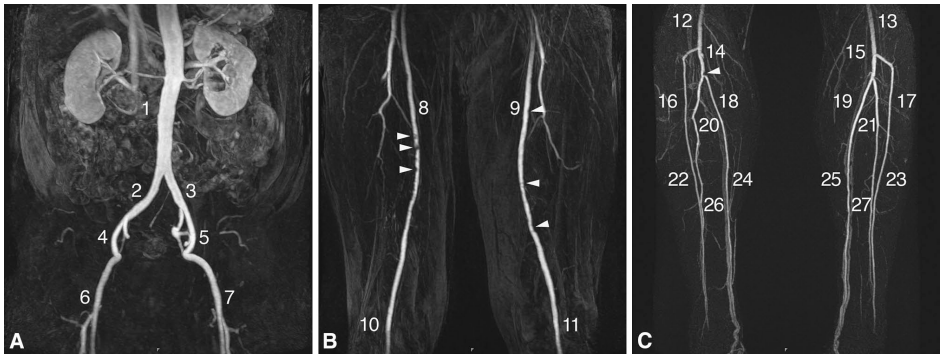

Figure 8.1 3T coronal CE-MRA maximum-intensity-projection images with 27 segments in a 68-year-old man presenting with claudication of the right leg. **A** Infra-renal aorta and iliac arteries with no stenosis. **B** Atherosclerotic changes in the right and left superficial femoral artery (*arrowheads*). **C** Stenosis in the right tibiofibular trunk (*arrowhead*). Minor venous enhancement on both sides. Segment numbering: *1* the infrarenal aorta; *2, 3* common iliac arteries; *4, 5* external iliac arteries; *6, 7* common femoral arteries; *8, 9* superficial femoral arteries; *10, 11* popliteal arteries in the thigh station; *12, 13* popliteal arteries in the calf station; *14, 15* tibiofibular trunk; *16–21* proximal and *22–27* distal halves of the anterior and posterior tibial arteries and peroneal arteries.

Statistical analysis

Shapiro–Wilk tests were performed to test normality of data distribution. Variables are expressed as mean ± standard deviation (SD) or median (interquartile range), where appropriate. Mann–Whitney *U* tests were performed to determine significance of differences between groups of patients. Binomial logistic regression analysis with backward likelihood ratio was performed to investigate which of the predictors was

an independent significant predictor for mortality, a cardiac or cerebral event. A p value of <0.05 is considered statistically significant. Statistical analysis was performed using IBM SPSS software version 23 (Armonk, NY, USA).

Results

For forty-one patients, 6 year follow-up data was available (one patient was lost to follow-up as no information of this patient was available since baseline examination). Baseline characteristics of these 41 patients are presented in Table 8.1. Only age of the patients, weight, length, BMI, ABI and LV mass were normally distributed. The mean follow-up period of the surviving patients was 72±5 months. Over the course of 6 years, six patients had died (mortality rate 14.6%). Six patients (14.6%) had experienced a cardiac event (i.e., three patients underwent bypass graft surgery from which one died after heart failure, one patient underwent percutaneous transluminal coronary angioplasty, one patient developed tachycardia and died, and one patient was diagnosed with heart failure and died). Three patients (7.3%) experienced a cerebral event (i.e., two cerebrovascular accident and one transient ischemic attack). One patient (2.4%) had undergone carotid endarterectomy.

Table 8.1 Baseline patient characteristics

Age (years)	64 ± 11
Gender (M/F)	22 / 19
Weight (kg)	76 ± 14
Length (cm)	170 ± 10
BMI	26.0 ± 3.7
BMI > 30 (yes/no)	8 / 33
Hypertension (yes/no)	27 / 14
Diabetes Mellitus (yes/no)	6 / 35
TG (mg/dL)	151 (115 – 213)
TG ≥ 150 mg/dL (yes/no)	13 / 28
HDL (mg/dL)	52 (43 – 62)
HDL ≤ 50 mg/dL in men, ≤ 40 mg/dL in women (yes/no)	13 / 28
Fontaine class (stages I/IIa/IIb/III/IV)	0 / 23 / 11 / 4 / 3
ABI in rest	0.75 ± 0.21
Mean MRA stenosis class	1.4 (1.2 – 1.8)
Max MRA stenosis class	5 (4 – 5)
Aortic arch PWV (m/s)	8.3 (7.0 – 10.5)
Descending aorta PWV (m/s)	8.6 (6.4 – 11.2)
LVEF (%)	60 (56 – 64)
LV mass (g)	90 ± 25
Carotid NWI	0.47 (0.43 – 0.52)

BMI: Body Mass Index; TG: Triglyceride; HDL: High-density lipoprotein; ABI: ankle-brachial index; MRA: magnetic resonance angiography; PWV: pulse wave velocity; LVEF: left ventricular ejection fraction; NWI: normalized wall index

Mean or median baseline values of the predictors, categorized for outcome (i.e., all-cause mortality, cardiac event, cerebral event), are presented in Table 8.2. Mann–Whitney *U* tests were performed to investigate the statistical significance between patient groups categorized for outcome. Age, diagnosis of diabetes mellitus, mean stenosis class and descending aorta PWV were significantly different among patients categorized for all-cause mortality. Mean stenosis class and LVEF were significantly different among patients categorized with or without cardiac event and diagnosis of diabetes mellitus was significantly different among patients categorized with or without cerebral event. Binomial logistic regression analysis was performed to investigate which of the predictors is an independent significant predictor for all-cause mortality, a cardiac or cerebral event. For all-cause mortality only the mean MRA stenosis class was a significant independent predictor (beta 3.0±standard error 1.3, p=0.02), for a cardiac event LVEF was a significant independent predictor (beta −0.14 ± standard error 0.05, p=0.005) and diagnosis of diabetes mellitus was a significant independent predictor for a cerebral event (beta 2.8 ± standard error 1.3, p=0.03).

Discussion

The present pilot study prospectively evaluated the prognostic value of cardiovascular MR imaging biomarkers (i.e., mean MRA stenosis class, max MRA stenosis class, aortic arch PWV, descending aorta PWV, LVEF, LV mass, and carotid NWI) obtained in a comprehensive MR imaging study in patients with PAD over an approximately 6 year period. The prognostic value of these imaging biomarkers was compared to traditional risk factors such as age, BMI, TG and HDL levels in blood plasma, diabetes mellitus and hypertension. We evaluated which biomarker is an independent predictor for all-cause mortality, or cardiac or cerebral morbidity. The main findings of our preliminary study are: (1) For all-cause mortality, age, diabetes mellitus, mean MRA stenosis class and descending aorta PWV were significant predictors. However only mean MRA stenosis class was independently significant. (2) For cardiac morbidity, mean MRA stenosis class and LVEF were significant predictors, however, only LVEF was a significant independent predictor. (3) For cerebral morbidity, only diagnosis of diabetes mellitus but none of the described cardiovascular MR imaging biomarkers was a significant independent predictor in this explorative study.

Table 8.2 Mean baseline value of predictors categorized for outcome at 6-year follow-up.

	All-cause mortality over 6-year follow-up			Cardiac event over 6-year follow-up			Cerebral event over 6-year follow-up		
	Yes (N=6)	No (N=35)	p	Yes (N=6)	No (N=35)	p	Yes (N=3)	No (N=38)	p
Age (years)	73 ± 9	63 ± 10	0.02*	71 ± 10	63 ± 10	0.11	62 ± 12	64 ± 11	0.66
Gender (M/F)	4/2	18/17	0.52	3/3	19/16	0.86	2/1	20/18	0.64
BMI	25.2 ± 3.4	26.1 ± 3.8	0.56	25.5 ± 3.6	26.1 ± 3.8	0.69	27.1 ± 4.0	25.9 ± 3.7	0.60
BMI>30 (yes/no)	1/5	7/28	0.85	1/5	7/28	0.85	1/2	7/31	0.54
Hypertension (yes/no)	5/1	22/13	0.34	4/2	23/12	0.97	2/1	25/13	0.98
Diabetes Mellitus (yes/no)	0/6	6/29	0.01*	1/5	5/30	0.88	2/1	4/34	0.007*
TG (mg/dL)	148 (75 – 281)	151 (115 – 213)	0.99	104 (75 – 190)	159 (115 – 213)	0.29	177 (124 – 283)	146 (113 – 213)	0.80
TG ≥150 mg/dL (yes/no)	3/3	10/25	0.31	1/5	12/23	0.40	1/2	12/26	0.95
HDL (mg/dL)	62 (43 – 73)	49 (43 – 60)	0.52	52 (38 – 73)	52 (43 – 61)	0.93	49 (48 – 62)	53 (42 – 63)	0.87
HDL ≤50 mg/dL in men, ≤40 mg/dL in women (yes/no)	0/6	13/22	0.07	3/3	10/25	0.31	1/2	12/26	0.95
ABI	0.68 ± 0.20	0.75 ± 0.16	0.31	0.64 ± 0.17	0.76 ± 0.16	0.10	0.78 ± 0.14	0.74 ± 0.17	0.69
Mean MRA stenosis class	2.1 (1.7 – 2.6)	1.4 (1.2 – 1.6)	<0.001*	1.8 (1.3 – 2.6)	1.4 (1.2 – 1.7)	0.02*	1.3 (1.3 – 1.3)	1.4 (1.2 – 1.9)	0.52
Max MRA stenosis class	5 (4 – 5)	5 (4 – 5)	0.52	5 (4 – 5)	5 (4 – 5)	0.52	4 (3 – 5)	5 (4 – 5)	0.60
Aortic arch PWV (m/s)	8.4 (6.7 – 14.3)	8.3 (6.8 – 10.3)	0.91	7.7 (6.7 – 11.5)	8.8 (6.8 – 10.7)	0.78	7.7 (4.6 – 7.7)	8.8 (7.1 – 10.7)	0.38
Descending aorta PWV (m/s)	11.3 (8.7 – 15.6)	7.9 (6.2 – 10.0)	0.01*	9.1 (5.3 – 14.5)	8.1 (6.6 – 11.2)	0.27	7.7 (5.3 – 7.6)	8.7 (6.5 – 11.3)	0.43
LV EF (%)	49 (38 – 66)	60 (56 – 65) (N=34)	0.10	39 (37 – 52)	61 (58 – 65) (N=34)	<0.001*	82 (63 – 82)	60 (54 – 64) (N=37)	0.34
LV mass (g)	100 ± 31	88 ± 24 (N=34)	0.33	106 ± 32	87 ± 23 (N=34)	0.09	88 ± 28	90 ± 26 (N=37)	0.86
Carotid NWI	0.45 (0.43 – 0.50)	0.47 (0.42 – 0.52)	0.85	0.49 (0.46 – 0.58)	0.46 (0.42 – 0.51)	0.14	0.47 (0.36 – 0.47)	0.47 (0.43 – 0.52)	0.96

BMI: Body Mass Index; TG: Triglyceride; HDL: High-density lipoprotein; ABI: ankle-brachial index; MRA: magnetic resonance angiography; PWV: pulse wave velocity; LVEF: left ventricular ejection fraction; NWI: normalized wall index. * statistically significant.

The Task Force of American College of Cardiology and American Heart Association emphasizes the value of traditional risk factors assessment for risk stratification in CVD,[8] but also acknowledged the added value of non-invasive imaging.[9] As atherosclerosis is a systemic process in CVD and each vascular bed shows differential patterns of plaque development, mediated by clinical, genetic and comorbid factors that are associated with the disease[22] the use of multisite imaging may improve risk discrimination for disease-specific outcomes.[15,23] To our knowledge this is the first prospective follow-up study to describe the prognostic value of cardiovascular MR imaging biomarkers obtained in a comprehensive MR imaging protocol in patients with symptomatic PAD and to compare to traditional risk factors. Large-scale studies in symptomatic PAD patients have found a three to six times higher risk for mortality from CVD and a 2.5 times higher overall mortality rate.[3,24] Moreover, long-term prognosis in patients with PAD after endovascular therapy is extremely poor for high-risk symptomatic patients.[25] Therefore, evaluation of new imaging biomarkers may be important in the work-up and risk stratification in patients with symptomatic PAD, or with CVD in general. Several studies have presented association of traditional biomarkers derived from conventional techniques with all-cause mortality, cardiac events, and cerebral events in patients with PAD. Kals et al. reported an independent relationship between arterial wall stiffness obtained with tonometry and all-cause and cardiovascular mortality. Increased small artery elasticity was directly related to mortality in patients with PAD whereas large artery stiffness was not significantly related.[26] In recent literature MRI with velocity-encoding has been reported and validated as an accurate non-invasive method to assess aortic PWV with high reproducibility.[20] In the present study aortic arch PWV and descending aorta PWV were evaluated for prognostic value in patients with symptomatic PAD. Aortic arch PWV showed no significant prognostic value when evaluated for all-cause mortality, or cardiac, or cerebral events. However, for all-cause mortality descending aorta PWV was a significant predictor, as well as age, diagnosis of diabetes mellitus and PAD stenosis severity visually scored on CE-MRA. This is in line with the reported result at baseline in these patients, where a strong site-specific association between descending aorta PWV and PAD stenosis severity was found, in contrast to the absent association with aortic arch PWV.[15] Also, it is well-known that aortic stiffness and aortic PWV are indeed age-dependent[27,28] and aortic PWV has been related to diabetes mellitus.[29] Therefore, interrelation between the biomarkers age, diabetes mellitus, descending aorta PWV and stenosis severity is expected. However, only stenosis severity remained a significant independent predictor for all-cause mortality whereas descending aorta PWV did not remain significant. Although our sample size maybe relatively small, this finding is in good agreement with the reported data in the study of Kals et al..[26]

Several studies using the ABI showed that a low ABI (low ABI defined as ABI <0.90) predicts all-cause mortality and cardiovascular events.[10,30] A strong trend for

increasing risk with decreasing ABI has been demonstrated.[31] Moreover, Resnick et al. showed a U-shaped association between low and high ABI (>1.40) and mortality risk, with significantly increased risk in patients with low ABI and high ABI.[11] In the clinical work-up of patients suspected of PAD, a low ABI is a strong indicator of the presence of arterial disease.[32] However, Doobay et al. showed that due to the false-negative rates a normal ABI does not rule out risk of PAD.[12] Furthermore, Wikström et al. reported that when compared with CE-MRA a low ABI may underestimate the prevalence of PAD.[13] These conflicting results indeed underline the need for evaluation of new imaging biomarkers as an alternative for ABI in the follow-up and risk stratification in patients with symptomatic PAD.

Nowadays, CE-MRA is an important tool in the diagnosis and clinical work-up in patients suspected for PAD. However, CE-MRA may not be possible in all patients, with respect to the association of nephrogenic systemic fibrosis and gadolinium.[33] Our results show that descending aorta PWV is interrelated with stenosis severity from CE-MRA and as such, may be useful as an alternative predictor for all-cause mortality when CE-MRA is not possible.

Assessment of LV systolic function is important in assessing prognosis of several cardiac diseases and risk evaluation for mortality[34] and is a recognized risk factor for postoperative morbidity after vascular surgery.[35] In our preliminary study LVEF was a significant independent predictor for cardiac morbidity in patients with symptomatic PAD. This finding underlines to assess LV function in patients with symptomatic PAD for work-up and risk stratification. Further evaluation of the underlying causes of reduced LVEF may add to the prognostic value for occurrence of future cardiac events. Reduced LVEF may have been associated with myocardial infarction in some of these patients, as this association has been shown in post infarction patients.[36] Specifically in such patients, delayed CE imaging may play an important role as an imaging biomarker additional to LVEF, as myocardial viability is related to ventricular pathology whereas LVEF does not contain such information.[37]

Araki et al. reported a markedly increased prevalence of cerebral infarction and carotid artery stenosis in patients with PAD.[38] In our patient population over 6 year follow-up period, however, in only one patient carotid endarterectomy was reported and the small number of cerebral events (N=3) did not show significant relation with the MR imaging biomarkers. Only diagnosis of diabetes mellitus showed to be a significant independent predictor for stroke. Although, the number of reported cerebral events did not account for asymptomatic cerebral events as no neuroimaging was performed.

We acknowledge important limitations of our study. First, this initial report is a pilot study and involves a relatively small size of prospectively included patients with symptomatic PAD. Second, in our study only 6 year follow-up data was available (mean follow-up period 72±5 months), which may be relatively short. Nevertheless, the findings described in this study are statistical significant and the MR imaging

biomarkers stenosis severity from CE-MRA and LVEF from cardiac cine MRI have shown prognostic value of outcome in PAD. In the present study, the novel MR imaging biomarkers PWV and carotid NWI did not show independent prognostic value on outcome in our patient population, however, their value in risk stratification has to be further elaborated in population-based long-term follow-up studies.

Conclusion

Mean MRA stenosis class was a significant independent predictor for all-cause mortality in patients with symptomatic PAD. Descending aorta PWV, age and diagnosis of diabetes mellitus were interrelated with PAD stenosis severity and as such associated with all-cause mortality, but did not show to be significant independent predictors. LVEF was a significant independent predictor for cardiac morbidity and diagnosis of diabetes mellitus a significant independent predictor for cerebral morbidity in this patient population. Further studies with larger patient groups have to confirm these results from preliminary data of the present study.

References

1. Fowkes F, Rudan R, Rudan I, et al. Comparison of global estimates of prevalence and risk factors for peripheral artery disease in 2000 and 2010: a systematic review and analysis. Lancet 2013;382: 1329-1340
2. Sampson UK, Fowkes FG, McDermott MM, et al. Global and regional burden of death and disability from peripheral artery disease: 21 world regions, 1990 to 2010. Glob Heart 2014;9:145–158
3. Criqui M, Langer R, Fronek A, et al. Mortality over a period of 10 years in patients with peripheral arterial disease. N Engl J Med 1992;326:381–386
4. Criqui M, Ninomiya J, Wingard D, Ji M, Fronek A. Progression of peripheral arterial disease predicts cardiovascular disease morbidity and mortality. J Am Coll Cardiol 2008;52:1736–1742
5. Araki Y, Kumakura H, Kanai H, et al. Prevalence and risk factors for cerebral infarction and carotid artery stenosis in peripheral arterial disease. Atherosclerosis 2012;223:473–477
6. Cooke J, Wilson A. Biomarkers of peripheral arterial disease. J Am Coll Cardiol 2010;55:2017–2023
7. Leeper N, Myers J, Zhou M, et al. Exercise capacity is the strongest predictor of mortality in patients with peripheral arterial disease. J Vasc Surg 2013;57:728–733
8. Goff DC Jr, Lloyd-Jones DM, Bennett G, et al. 2013 ACC/AHA guideline on the assessment of cardiovascular risk: a report of the American College of Cardiology/American Heart Association Task Force on Practice Guidelines. J Am Coll Cardiol 2013;63:2935–2959
9. Greenland P, Alpert JS, Beller GA, et al. ACCF/AHA guideline for assessment of cardiovascular risk in asymptomatic adults: a report of the American College of Cardiology Foundation/American Heart Association Task Force on Practice Guidelines. J Am Coll Cardiol 2010;56:e50–e103
10. Newman AB, Shemanski L, Manolio TA, et al. Ankle-arm index as a predictor of cardiovascular disease and mortality in the Cardiovascular Health Study: the Cardiovascular Health Study Group. Arterioscler Thromb Vasc Biol 1999;19:538–545
11. Resnick H, Lindsay R, McDermott M, et al. Relationship of high and low ankle brachial index to all-cause and cardiovascular disease mortality: the Strong Heart Study. Circulation 2004;109:733–739
12. Doobay AV, Anand SS. Sensitivity and specificity of the ankle-brachial index to predict future cardiovascular outcomes: a systematic review. Arterioscler Thromb Vasc Biol 2005;25:1463–1469
13. Wikström J, Hansen T, Johansson L, Lind L, Ahlström H. Ankle brachial index <0.9 underestimates the prevalence of peripheral artery occlusive disease assessed with whole-body magnetic resonance angiography in the elderly. Acta Radiol 2008;49:143–149
14. Leiner T, Kessels AG, Schurink GW, et al. Comparison of contrast-enhanced magnetic resonance angiography and digital subtraction angiography in patients with chronic critical ischemia and tissue loss. Invest Radiol 2004;39:435–444
15. Van den Bosch H, Westenberg J, Setz-Pels W, et al. Sitespecific association between distal aortic pulse wave velocity and peripheral arterial stenosis severity: a prospective cardiovascular magnetic resonance study. J Cardiovasc Magn Reson 2015;17:2
16. Alexander CM. The coming of age of the metabolic syndrome. Diabetes Care 2003;26:3180–3181
17. Van den Bosch H, Westenberg J, Caris R, et al. Peripheral arterial occlusive disease: 3.0-T versus 1.5-T MR angiography compared with digital subtraction angiography. Radiology 2013;266:337–346
18. Alizadeh D, Doornbos J, Tamsma J, et al. Assessment of the carotid artery by MRI at 3T: a study on reproducibility. J Magn Reson Imaging 2007;25:1035–1043
19. Kramer Ch, Barkhausen J, Flamm S, Kim R, Nagel E. Standardized cardiovascular magnetic resonance (CMR) protocols 2013 update. J Cardiovasc Magn Reson 2013;15:91
20. Grotenhuis H, Westenberg J, Steendijk P, et al. Validation and reproducibility of aortic pulse wave velocity as assessed with velocity-encoded MRI. J Magn Reson Imaging 2009;20:521–526
21. Saam T, Yuan C, Chu B, et al. Predictors of carotid atherosclerotic plaque progression as measured by noninvasive magnetic resonance imaging. Atherosclerosis 2007;194:34–42
22. Allison MA, Budoff MJ, Nasir K, et al. Ethnic-specific risks for atherosclerotic calcification of the thoracic and abdominal aorta (from the Multi-Ethnic Study of Atherosclerosis). Am J Cardiol 2009;104:812–817

23. Blaha MJ. The future of CV risk prediction: multisite imaging to predict multiple outcomes. J Am Coll Cardiol Cardiovasc Imaging 2014;7:1054–1056
24. Norgren L, Hiatt W, Dormandy J, Nehler M, Harris K, Fowkes F. Inter-Society Consensus for the Management of Peripheral Arterial Disease (TASC II). Eur J Vasc Endovasc Surg 2007;33:S1–S75
25. Miura T, Soga Y, Miyashita Y, et al. Five-year prognosis after endovascular therapy in claudicant patients with iliofemoral artery disease. J Endovasc Ther 2014;21:381–388
26. Kals J, Lieberg J, Kampus P, Zagura M, Eha J, Zilmer M. Prognostic impact of arterial stiffness in patients with symptomatic peripheral arterial disease. Eur J Vasc Endovasc Surg 2014;48:308–315
27. Rogers W, Hu Y, Coast D, et al. Age-associated changes in regional aortic pulse wave velocity. J Am Coll Cardiol 2001;38:1123–1129
28. Westenberg J, Scholte A, Vaskova Z, et al. Age-related and regional changes of aortic stiffness in the Marfan syndrome: assessment with velocity-encoded MRI. J Magn Reson Imaging 2011;34:526–531
29. van Elderen SG, Westenberg JJ, Brandts A, van der Meer RW, Romijn JA, Smit JW, de Roos A. Increased aortic stiffness measured by MRI in patients with type 1 diabetes mellitus and relationship to renal function. Am J Roentgenol 2011;196:697–701
30. McDermott M, Feinglass J, Slavensky R, Pearce W. The ankle-brachial index as a predictor of survival in patients with peripheral vascular disease. J Gen Intern Med 1994;9:445–449
31. McKenna M, Wolfson S, Kuller L. The ratio of ankle and arm arterial pressure as an independent predictor of mortality. Atherosclerosis 1991;87:119–128
32. Ouriel K, McDonnell AE, Metz CE, Zarins CK. Critical evaluation of stress testing in the diagnosis of peripheral vascular disease. Surgery 1982;91:686–693
33. Zou Z, Zhang H, Roditi G, Leiner T, Kucharczyk W, Prince M. Nephrogenic systemic fibrosis: review of 370 biopsy-confirmed cases. J Am Coll Cardiol Cardiovasc Imaging 2011;4:1206–1216
34. McMurray J, Adamopoulos S, Anker S, et al. ESC guidelines for the diagnosis and treatment of acute and chronic heart failure 2012. Eur Heart J 2012;33:1787–1847
35. Flu W, van Kuijk J, Hoeks S, et al. Prognostic implications of asymptomatic left ventricular dysfunction in patients undergoing vascular surgery. Anesthesiology 2010;112:1316–1324
36. Ingkanisorn WP, Rhoads KL, Aletras AH, Kellman P, Arai AE. Gadolinium delayed enhancement cardiovascular magnetic resonance correlates with clinical measures of myocardial infarction. J Am Coll Cardiol 2004;43:2253–2259
37. Otsuji Y, Handschumacher MD, Liel-Choen N, Tanabe H, Jiang L, Schwammenthal E, et al. Mechanism of ischemic mitral regurgitation with segmental left ventricular dysfunction: threedimensional echocardiographic studies in models of acute and chronic progressive regurgitation. J Am Coll Cardiol 2001;37:641–648
38. Arakia Y, Kumakura H, Kanai H, et al. Prevalence and risk factors for cerebral infarction and carotid artery stenosis in peripheral arterial disease. Atherosclerosis 2012;223:473–477

Chapter 9

Summary and conclusions

Samenvatting en conclusies

Summary and conclusions

The aim of this thesis was to evaluate new magnetic resonance imaging (MRI) techniques in cardiovascular radiology in clinical practice and to explore the prognostic value of new cardiovascular magnetic resonance (CMR) imaging biomarkers in patients with peripheral arterial occlusive disease.

The first part of the thesis focusses on cardiac MRI. **Chapter 1** provides a general background and introduction of the current role of MRI in cardiovascular disease in daily clinical practice.
In **chapter 2** the acquisition planning of the specific cardiac MR imaging planes is described and the normal cardiac anatomy assessed with CMR is addressed. Additionally, aspects and new developments of cardiac imaging on (ultra-) high-field MRI are discussed.
Chapter 3 describes the validation of a new free-breathing 2D delayed-enhancement imaging sequence, based on single-shot inversion-recovery steady-state free precession (SSFP), to be used for assessing myocardial infarction. This new technique was compared with a standardized and validated 3D gradient echo (FFE) technique which was used to image the entire left ventricle during end-expiratory breath-holding. In 33 patients with suspected chronic myocardial infarction, both sequences were performed. In the free-breathing 2D approach, respiratory motion was avoided using triggering from a respiratory belt. The intraclass correlation for infarct quantification between both delayed-enhancement techniques was excellent (ICC = 0.99 [$p<0.01$]). The agreement in assessing the transmural extent of infarction was good to excellent between the 2D free-breathing technique and the 3D breath-hold technique (kappa varied between 0.70 and 0.96 for all of the 16 standardized myocardial segments). Therefore, when used for quantification of left ventricular infarction, respiratory-triggered 2D single-shot inversion-recovery SSFP delayed-enhancement MRI is comparable to breath-hold 3D segmented gradient-echo inversion-recovery delayed-enhancement MRI. In conclusion, free-breathing 2D delayed-enhancement MRI sequence is a fast and reliable tool for detecting myocardial infarction and provides an alternative imaging technique when patients are not capable of performing (long) breath-holding.

The second part of the thesis addresses the application of CMR for the purpose of magnetic resonance angiography (MRA). First, the current state-of-art is described followed by the results of a study comparing MRA of the peripheral arteries on 1.5T and 3T MRI systems. Moreover, the results of a study comparing a conventional contrast-enhanced MRA (CE-MRA) scan protocol with a new and optimized, faster multiposition CE-MRA protocol are described. For the above mentioned studies, patients with suspected peripheral artery disease were included and follow-up studies

were performed. Another study describes which biomarkers may be required for full vascular risk assessment in the clinical workup of patients with peripheral arterial disease. Finally, the prognostic value of outcome of CMR imaging biomarkers in patients with symptomatic peripheral arterial occlusive disease are explored in a six year follow-up study.

In the first part of **chapter 4,** currently available techniques for MRA are described. CE-MRA, and black-blood and bright-blood non-CE-MRA techniques are discussed. Additionally, time-resolved 3D phase contrast (i.e., 4D flow MRI) is addressed. This relatively new technique may be used to visualize complex flow structures with the aid of newly developed visualization tools adding quantitative hemodynamic information as well. In the second part of this chapter, anatomical regions that are imaged by MRA and state-of-the-art applications are discussed. Special focus is on the carotid arteries, thoracic and abdominal aorta, renal arteries, mesenteric artery, and the peripheral arteries.
In **Chapter 5**, a new and optimized single-injection multiposition CE-MRA protocol is compared with a conventional scan protocol. The optimized single-injection multiposition CE-MRA protocol uses sensitivity encoding and random central k-space segmentation in a centric filling order. For this comparison, 15 patients with peripheral arterial occlusive disease were imaged with both protocols on 1.5T MRI. Midstream aortic Conventional digital subtraction angiography (DSA) was used as the standard of reference.
In the sensitivity-encoded CE-MRA protocol, imaging times in the pelvic and upper-leg positions were reduced and isotropic submillimeter voxel volumes were acquired in the lower-leg position. For analysis, the arterial tree in each patient was divided into 29 standardizes segments and in each segment, the most severe stenosis was chosen for classification.
In the trajectory from the aorta to the popliteal arteries, sensitivity-encoded CE-MRA showed a higher sensitivity for detection of stenoses with a severity of 50% and higher: 85% versus 79% for conventional CE-MRA. The specificity of both protocols was almost similar: 99% for sensitivity-encoded CE-MRA versus 97% for conventional CE-MRA. For the detection of stenoses of 75% and higher, the sensitivity of sensitivity-encoded CE-MRA was 100% versus 93% for conventional CE-MRA, while the detection of occlusion showed a sensitivity of 100% for sensitivity-encoded CE-MRA versus 92% for conventional CE-MRA. Specificities were equal (i.e., 100%). In the infragenual arteries, the sensitivity for the detection of a significant (i.e., 50% or higher) stenosis was 87% with both CE-MRA techniques, while the specificity showed a statistically significant increase from 84% with conventional CE-MRA to 93% with sensitivity-encoded CE- MRA. For the detection of diffuse stenoses in arterial segments, the specificity was significantly higher with sensitivity-encoded CE-MRA than that with conventional CE-MRA, 100% and 86% respectively. Sensitivities were similar (92% and

90% respectively). Furthermore, sensitivity-encoded CE-MRA significantly depicted more open infragenual arterial segments than midstream aortic DSA (p=0.001) and conventional CE-MRA (p<0.001). In conclusion, the application of a single-injection multiposition CE-MRA protocol at 1.5T MRI with sensitivity-encoding and random central k-space segmentation in a centric filling order with submillimeter isotropic voxel acquisition in the lower legs improves the diagnostic accuracy and depicts more open infragenual arterial segments compared with both midstream aortic DSA and conventional CE- MRA.

In **Chapter 6**, the diagnostic accuracy of CE-MRA at 3T is compared versus 1.5T. The diagnostic performance of a single-injection, three-station, moving-table protocol with high spatial resolution is evaluated in a prospective study performed at both field strengths in patients with peripheral arterial occlusive disease. Similar acquisition protocols and identical contrast agent dose were used on both 3T as well as 1.5T. DSA served as the standard of reference. In 19 patients suspected of peripheral arterial occlusive disease, who were referred for further work-up, peripheral CE-MRA at both field strengths as well as DSA was performed. Similar excellent agreement with DSA regarding stenosis classification was found for both 3T and 1.5T CE-MRA (kappa = 0.96 and 0.93, respectively). For classification of stenosis larger than 50%, the sensitivity of 3T CE-MRA was 99% and of 1.5T CE-MRA 92%. Specificity of 3T CE-MRA was 99.5%, and of 1.5T CE-MRA 99.6%. For classification of stenosis larger than 75%, sensitivity of 3T CE-MRA was 95% and of 1.5T CE-MRA 92%, while specificity was 100% for both techniques. At 3T CE-MRA a, on average, more than 3 times higher contrast-to-noise ratio (p<0.001) was achieved in the external iliac artery, superficial femoral artery and popliteal artery of the left and the right leg when compared to 1.5T CE-MRA, using the same contrast agent dose. Therefore, 3T and 1.5T single-injection CE-MRA with a three-station moving-table technique showed similar excellent agreement with DSA regarding agreement, sensitivity, and specificity of peripheral arterial occlusive disease stenosis severity classification. We concluded that both 1.5T and 3T CE-MRA with similar acquisition protocols and identical contrast agent dose can be used interchangeably in daily practice of peripheral arterial occlusive disease, because diagnostic performance proved to be similar.

Chapter 7 prospectively evaluates the association between aortic wall stiffness, expressed by pulse wave velocity (PWV), sampled in the distal aorta and the severity of peripheral arterial occlusive disease. This is compared to atherosclerotic markers sampled in remote vascular territories such as the PWV in the proximal aorta and vessel wall thickness of the left common carotid artery. Forty-two patients underwent CMR in the work-up for peripheral arterial occlusive disease using a 3T MRI system. PWV was assessed regionally in the aorta, between the ascending and descending thoracic aorta (i.e., the proximal aorta) and between the thoracic descending and distal abdominal aorta (i.e., the distal aorta). In all patients, whole-body CE-MRA and carotid vessel wall imaging were performed. Stenosis severity correlated well with

PWV in the distal aorta (r≥0.64) but to a lesser extent with PWV in the proximal aorta (r≤0.48). Carotid normalized wall index (NWI) was not associated with peripheral stenosis severity nor with PWV in the proximal or distal aorta. Correlation between stenosis severity and distal aortic PWV remained
statistically significant after correction for age and gender. In conclusion, in patients with PAOD, peripheral arterial stenosis severity is well correlated with aortic PWV sampled in the distal aorta but correlation with markers sampled in remote vascular territories, such as PWV in the proximal aorta or carotid arterial wall thickness, is only moderate at best. Only the correlation between stenosis severity and distal aortic PWV remains statistically significant after correction for age and gender. The association between aortic wall stiffening and stenosis severity in a vascular territory directly linked to this aortic segment suggests that site-specific evaluation of vascular disease may be required for full vascular risk assessment in the clinical workup of peripheral arterial occlusive disease.

Chapter 8 prospectively explores the prognostic value of outcome of CMR imaging biomarkers in patients with symptomatic peripheral arterial occlusive disease in comparison with traditional risk factors [i.e., age, gender, body mass index (BMI), hypertension, diabetes mellitus, levels of triglyceride (TG) and high-density lipoprotein (HDL) in blood plasma samples, ankle-brachial index (ABI) and Fontaine class]. In this study, 42 consecutive patients with symptomatic PAOD were included. At base-line, all patients underwent a comprehensive CMR examination consisting of CE-MRA of the run-off vessels and additionally, carotid vessel wall imaging, cardiac cine imaging for assessing left ventricular volume, mass and function, and assessment of the aortic PWV from velocity encoded MRI as a surrogate marker of aortic stiffness. Follow-up evaluation of the patient population over a 6 year period was performed to examine which CMR imaging biomarker or traditional risk factor is an independent predictor for all-cause mortality, cardiac or cerebral morbidity.

For all-cause mortality, age, diabetes mellitus, MRA stenosis severity and descending aorta PWV were significant predictors. However, only MRA stenosis severity was independently significant (beta 3.0 ± standard error 1.3, p=0.02). Descending aorta PWV, age and diabetes mellitus were interrelated with stenosis severity but none of these were significant independent predictors. For cardiac morbidity, left ventricular ejection fraction (LVEF) and MRA stenosis severity were associated, but only LVEF was a significant independent predictor (beta −0.14 ± 0.05, p=0.005). For cerebral morbidity, only diagnosis of diabetes mellitus (beta 2.8 ± 1.3, p=0.03), but none of the other described CMR imaging biomarkers was a significant independent predictor in this patient population. In conclusion, the CMR imaging biomarkers representing stenosis severity, aortic stiffness (i.e., descending aorta PWV) and left ventricular function (i.e., LVEF) play a role in prognosis of outcome in patients with symptomatic peripheral arterial occlusive disease.

Conclusions

Cardiovascular magnetic resonance imaging is an important noninvasive imaging modality for the diagnosis, clinical work-up and treatment planning in patients suspected for a wide range of cardiovascular pathology. CMR imaging is accurate and reliable, and provides invaluable information to evaluate the cardiovascular system without the need of ionizing radiation.

The studies described in this thesis evaluate new CMR imaging techniques in clinical practice and explore the prognostic value of new CMR imaging biomarkers in patients with symptomatic peripheral arterial occlusive disease.

New advances and innovations in MR imaging technology improve and further expand the clinical applications of cardiovascular imaging in daily clinical practice. In this thesis, a new, fast free-breathing 2D delayed-enhancement MRI sequence is validated and demonstrated to be a reliable tool for detecting myocardial infarction. Furthermore, new technical developments allow single-injection, three-station, moving-table MRA protocol at 3Tesla with similar diagnostic performance when compared to 1.5Tesla. Additionally, submillimeter isotropic voxel acquisition in the lower legs at 1.5Tesla improves the diagnostic accuracy and depicts more open infragenual arterial segments.

Additionally, it is demonstrated that new MRI biomarkers as distal aortic pulse wave velocity statistically significantly correlate with stenosis severity in symptomatic patients with peripheral arterial occlusive disease. Finally, we showed that CMR derived biomarkers relating to stenosis severity, aortic stiffness and left ventricular function play a role in prognosis of outcome in patients with symptomatic PAOD.

In the future, incorporation of the described new MRI biomarkers in the clinical workup of peripheral arterial occlusive disease may play an important role for full vascular risk assessment and ultimately, patients may benefit in clinical practice.

Dankwoord

Samenvatting en conclusies

Het doel van het onderzoek dat in dit proefschrift beschreven wordt, is om in de klinische praktijk nieuwe beeldvormende magnetische resonantietechnieken binnen de hart- en vaatradiologie te evalueren. Ook wordt de voorspellende waarde van nieuwe cardiovasculaire magnetische resonantie (CMR) technieken en nieuwe MRI (*magnetic resonance imaging*)-biomarkers bij patiënten met perifeer arterieel vaatlijden onderzocht.

In het eerste deel van het proefschrift ligt de nadruk op beeldvorming van het hart middels MRI.
Als algemene introductie wordt in **hoofdstuk 1** de huidige rol van MRI bij hart- en vaatziekten in de alledaagse klinische praktijk beschreven.
In **hoofdstuk 2** wordt de planning van specifieke beeldvlakken van het hart beschreven, die bij MRI-onderzoek worden gebruikt. De normale anatomie van het hart, zoals deze in beeld gebracht wordt met MRI, wordt beschreven. Daarnaast worden nieuwe ontwikkelingen van hartonderzoek, die worden uitgevoerd op (ultra)hoge magneetveldsterktes, behandeld.
Hoofdstuk 3 beschrijft de validatie van een nieuwe scansequentie, de zogenaamde *free-breathing* 2D *delayed-enhancement*, die gebaseerd is op een *single-shot inversion-recovery steady-state free precession* (SSFP) techniek. Deze sequentie wordt gebruikt voor het in beeld brengen en beoordelen van onder andere myocardinfarcering. Deze nieuwe *free-breathing*-techniek, waarbij de patiënt tijdens de acquisitie vrij kan doorademen, wordt vergeleken met een gestandaardiseerde en reeds gevalideerde 3D gradiënt-echo-techniek (*fast field echo*, FFE). Deze *breath-hold* 3D techniek beeldt de hele linkerventrikel af, terwijl de patiënt de adem inhoudt. Beide MRI-technieken werden uitgevoerd bij 33 patiënten met verdenking op een chronisch myocardinfarct. Bij de *free-breathing* 2D-techniek wordt de ademhalingsbeweging gecorrigeerd middels triggering met behulp van een ademhalingsband. De intraclasscorrelatie voor infarctkwantificatie tussen beide *delayed-enhancement*-technieken was uitstekend (ICC=0.99 [p<0.01]). De overeenkomst tussen de *free-breathing* 2D-techniek en de *breath-hold* 3D-techniek voor de beoordeling van de transmurale uitgebreidheid van het myocardinfarct was goed tot uitstekend (kappa varieerde tussen 0.70 en 0.96 voor alle 16 gestandaardiseerde myocardiale segmenten). De ademhalingsgetriggerde *free-breathing* 2D *single-shot inversion-recovery SSFP delayed-enhancement* MRI-techniek is daarom vergelijkbaar met de *breath-hold* 3D gradiënt-echo *inversion-recovery delayed-enhancement* MRI-techniek voor de kwantificatie van linkerventrikel infarcten. De conclusie van dit onderzoek is dat de *free-breathing 2D delayed-enhancement* MRI-techniek een snelle en betrouwbare methode is voor de beoordeling van myocardiale infarcering. Deze

techniek kan functioneren als alternatieve afbeeldingstechniek indien patiënten hun adem tijdens een MRI- onderzoek niet goed kunnen inhouden.

Het tweede deel van dit proefschrift behandelt de toepassing van MRI voor het afbeelden van bloedvaten (ook wel MR-angiografie, MRA, genoemd). Eerst wordt de huidige stand van zaken van de MRA-techniek beschreven. Vervolgens worden de resultaten behandeld van een klinische studie, waarin een conventionele MRA-techniek werd vergeleken met een nieuwe en snellere opnametechniek. Daarna wordt een vergelijkingsstudie tussen MRA van de perifere vaten verricht op 1.5T (Tesla) en 3T beschreven. Deze technieken werden getest bij patiënten met perifeer arterieel vaatlijden. In een andere studie wordt beschreven welke MRI-biomarkers het beste het vasculaire risicoprofiel van deze patiënten weergeven. Deze patiëntengroep wordt gevolgd in de tijd. Tot slot volgen de resultaten van een vervolgonderzoek na 6 jaar waarbij de voorspellende waarde van nieuwe MRI-biomarkers op *outcome* wordt beschreven.
In het eerste deel van **hoofdstuk 4** worden de MRA-technieken beschreven die op dit moment klinisch beschikbaar zijn. Achtereenvolgens worden contrastversterkte (*contrast-enhanced*, CE) MRA-technieken en niet-contrastversterkte MRA-technieken (non-CE; respectievelijk *black-blood*- en *bright-blood*-technieken) behandeld. Daarnaast wordt een nieuwe *time-resolved 3D phase-contrast*-techniek (ook wel 4D flow MRI genoemd) beschreven. Met deze techniek en nieuw ontwikkelde visualisatiemethodes kunnen complexe bloedstromen in beeld worden gebracht. Hierbij kan aan het MRI-beeld ook kwantitatieve informatie over de hemodynamica worden toegevoegd.
In het tweede deel van dit hoofdstuk worden de huidige klinische MRA-toepassingen van verschillende anatomische gebieden beschreven. Met name wordt het MRA-onderzoek van de halsslagaders, de thoracale en abdominale aorta, nierslagaders, mesenteriale slagaders en de perifere slagaders behandeld.
In **hoofdstuk 5** wordt een nieuw, geoptimaliseerd *single-injection multi-position* CE-MRA-protocol vergeleken met een conventioneel, standaard CE-MRA-protocol. Het geoptimaliseerde *single-injection multi-position* CE-MRA-protocol maakt gebruik van nieuwe acquisitietechnieken: *sensitivity encoding* en een *random* segmentatie van de centrale k-ruimte. Voor dit vergelijkend onderzoek werden 15 patiënten met perifeer arterieel vaatlijden geïncludeerd. Bij alle patiënten werden beide MRA-protocollen verricht. De onderzoeken werden op een 1.5T MRI-scanner uitgevoerd. Ook werd bij alle patiënten een digitale subtractieangiografie (DSA) verricht. Voor de gradering van de stenosegraad fungeerde DSA als gouden standaard. In het *sensitivity-encoded* CE-MRA-protocol was de scantijd van de bekken- en bovenbeensregio korter dan in het conventionele CE-MRA-protocol en werden van het onderbeen MRI-beelden met isotrope submillimetervoxels verkregen. Voor de analyse werd de arteriële vaatboom

verdeeld in 29 segmenten. In elk segment werd de ernstigste stenosegraad gebruikt voor classificatie.
In het traject van de aorta tot de arteria poplitea toonde het *sensitivity-encoded* CE-MRA-protocol een hogere sensitiviteit voor de detectie van stenosen van 50% of hoger: 85% versus 79% voor het conventionele CE-MRA-protocol. De specificiteit van beide protocollen was bijna gelijk: 99% voor *sensitivity-encoded* CE-MRA versus 97% voor de conventionele CE-MRA. Voor de detectie van stenosen van 75% en hoger was de sensitiviteit van het *sensitivity-encoded* CE-MRA-protocol 100% versus 93% voor het conventionele CE-MRA-protocol. De detectie van een occlusie toonde een sensitiviteit van 100% voor de *sensitivity-encoded* CE-MRA en 92% voor de conventionele CE-MRA. De specificiteit voor beide protocollen was gelijk (100%). Voor de detectie van een significante (>50%) stenose in de infragenuale arteriën was de sensitiviteit van beide CE-MRA-technieken 87%. De specificiteit was statistisch significant beter voor *sensitivity-encoded* CE-MRA wanneer deze met het conventionele CE-MRA werd vergeleken (93% versus 84%, $p<0.001$). De specificiteit voor de detectie van diffuse stenosen in de arteriële segmenten was significant hoger met het *sensitivity-encoded* CE-MRA-protocol dan met het conventionele CE-MRA-protocol (100% versus 86%). De sensitiviteit was vergelijkbaar (respectievelijk 92% en 90%). Met *sensitivity-encoded* CE-MRA werden significant meer open infragenuale arteriële segmenten afgebeeld dan met DSA ($p=0.001$) en conventionele CE-MRA ($p<0.001$). Concluderend kan in dit hoofdstuk worden vastgesteld dat de diagnostische accuraatheid van stenoseclassificatie met behulp van een *single-injection multi-position* CE-MRA-protocol op 1.5T MRI verbetert wanneer *sensitivity-encoding* en een *random* segmentatie van de centrale k-ruimte worden toegepast. De acquisitie van submillimeter isotrope voxels in het traject van de onderbenen heeft tot resultaat dat meer open infragenuale arteriële segmenten kunnen worden afgebeeld als *sensitivity-encoded* CE-MRA wordt vergeleken met DSA of conventionele CE-MRA.
In **hoofdstuk 6** wordt de diagnostische nauwkeurigheid van CE-MRA verricht op een MRI-scanner met een veldsterkte van 3T vergeleken met CE-MRA verricht met een veldsterkte van 1.5T. In een prospectieve studie bij patiënten met perifeer arterieel vaatlijden werd de diagnostische kwaliteit van een *single-injection, three-station, moving-table*-protocol met hoge spatiële resolutie op beide veldsterktes geëvalueerd. Vergelijkbare acquisitieprotocollen en overeenkomstige contrasthoeveelheden werden gebruikt op 3T en 1.5T. Conventionele DSA fungeerde als gouden standaard. Voor dit onderzoek werden 19 patiënten met de verdenking op perifeer arterieel vaatlijden geïncludeerd. Bij alle patiënten werden op beide MRI-veldsterktes een CE-MRA onderzoek van de perifere vaten en een DSA verricht. De classificatie van stenosen kwam op beide veldsterktes sterk overeen. De stenosegraad werd hierbij vergeleken met de verrichte DSA (kappa was respectievelijk 0.96 voor 3T MRA en 0.93 voor 1.5T MRA). Voor de classificatie van een stenose groter dan 50% was de

sensitiviteit van 3T CE-MRA 99% en die van 1.5T CE-MRA 92%. De specificiteit van 3T CE-MRA was 99.5% en die van 1.5T CE-MRA 99.6%. Voor de classificatie van een stenose groter dan 75% was de sensitiviteit van 3T CE-MRA 95% en die van 1.5T CE-MRA 92%. Voor beide veldsterktes was de specificiteit 100%. Bij een gelijke contrastdosis werd op 3T gemiddeld een 3 keer hogere contrast-ruisverhouding verkregen dan op 1.5T. Dit werd gemeten op MRA-beelden van de arteria iliaca externa, arteria femoralis superficialis en de arteria poplitea van het linker- en rechterbeen. De sensitiviteit en specificiteit voor stenoseclassificatie van 3T en 1.5T *single-injection* CE-MRA met een *three-station moving-table* techniek gaf een vergelijkbare, uitstekende overeenkomst met DSA bij patiënten met perifeer arterieel vaatlijden. De conclusie van dit onderzoek is dat 3T en 1.5T CE-MRA met vergelijkbare acquisitieprotocollen en dezelfde contrast-hoeveelheid in de dagelijkse, klinische praktijk onderling uitwisselbaar zijn, omdat de diagnostische kwaliteit van beide technieken vergelijkbaar is.

Hoofdstuk 7 evalueert prospectief de associatie tussen de stijfheid van de aortawand en de ernst van perifeer arterieel vaatlijden. In dit onderzoek werd de stijfheid van de aortawand gemeten met de *pulse wave velocity* (PWV, de golfsnelheid van de systolische golf) bepaald in de distale aorta. De associatie tussen de stijfheid van de aortawand en de ernst van perifeer arterieel vaatlijden werd vergeleken met andere markers van atherosclerose gemeten in - ten opzichte van de perifere vaten - verder afgelegen vasculaire gebieden, zoals de PWV in de proximale aorta en de vaatwanddikte van de linker arteria carotis communis. In de *work-up* van perifeer arterieel vaatlijden werd bij 42 patiënten een MRI-onderzoek verricht op een 3T-scanner. De PWV werd in twee trajecten gemeten: tussen de aorta ascendens en descendens (in dit hoofdstuk de ‘proximale aorta’ genoemd) en tussen de aorta descendens en de distale aorta abdominalis (‘distale aorta’). Ook werd bij alle patiënten een CE-MRA van het gehele lichaam gemaakt en tevens werd de carotisvaatwand met MRI afgebeeld. De ernst van stenosen in de perifere arteriën correleerde goed met de PWV in de distale aorta ($r \geq 0.64$), maar minder goed met de PWV in de proximale aorta ($r \leq 0.48$). De genormaliseerde carotisvaatwandindex (NWI) toonde geen associatie met de ernst van de stenosen in de perifere arteriën en ook niet met de PWV in de proximale of distale aorta. Na correctie voor leeftijd en geslacht bleef de correlatie tussen de ernst van de stenosen en de distale aorta PWV statistisch significant. De conclusie van dit hoofdstuk is dat bij patiënten met perifeer arterieel vaatlijden de ernst van stenosen in de perifere arteriën goed correleert met de PWV gemeten in de distale aorta. De correlatie is echter minder goed met andere markers, die gemeten zijn in verder afgelegen vasculaire gebieden, zoals de PWV in de proximale aorta en de carotisvaatwanddikte. Alleen de correlatie tussen de ernst van de arteriële stenosen en de distale aorta PWV blijft statistisch significant na correctie voor leeftijd en geslacht. Deze associatie tussen aortawandstijfheid en de ernst van de

stenosen in een vasculair gebied dat direct aansluit op dit aortasegment suggereert dat bij de klinische evaluatie van patiënten met perifeer arterieel vaatlijden er een specifieke lokale evaluatie van vasculaire afwijkingen vereist is om een volledig vasculair risicoprofiel te kunnen bepalen.

In **hoofdstuk 8** wordt prospectief de voorspellende waarde van verscheidene cardiovasculaire MRI-biomarkers onderzocht op *outcome* bij patiënten met symptomatisch perifeer arterieel vaatlijden. De voorspellende waarde van MRI-biomarkers wordt vergeleken met die van meer traditionele risicofactoren, zoals leeftijd, geslacht, BMI (body mass index), hoge bloeddruk, diabetes mellitus, de concentratie van triglyceriden en *high-density* lipoproteïnen in bloed, de enkel-armindex (ABI) en de Fontaine-classificatie. In deze studie werden 42 opeenvolgende patiënten met symptomatisch perifeer arterieel vaatlijden geïncludeerd. Aan het begin van de studie ondergingen alle patiënten een uitgebreid cardiovasculair MRI-onderzoek. Dit MRI-onderzoek bestond uit een CE-MRA van de perifere arteriële vaten, beeldvorming van de vaatwand van de halsslagader, *cardiac cine imaging* voor de kwantificatie van linkerventrikelvolume, -massa en -functie en de PWV van de aorta als maat voor de aortavaatwandstijfheid. Na 6 jaar werden de klinische gegevens van deze patiëntengroep geëvalueerd. Er werd onderzocht welke cardiovasculaire MRI-biomarkers of traditionele risicofactoren onafhankelijke voorspellers waren voor mortaliteit en cardiale of cerebrale morbiditeit.

Voor mortaliteit waren leeftijd, diabetes mellitus, MRA-stenoseclassificatie en PWV van de distale aorta significante voorspellers. Echter, alleen de MRA-stenoseclassificatie was een onafhankelijke significante voorspeller (beta 3.0 ± standard error 1.3, p=0.02). PWV van de distale aorta, leeftijd en diabetes mellitus waren gerelateerd aan de MRA-stenoseclassificatie, maar waren alle geen onafhankelijke significante voorspellers.

Linkerventrikelejectiefractie (LVEF) en MRA-stenoseclassificatie waren geassocieerd met cardiale morbiditeit, maar alleen LVEF bleek een onafhankelijke significante voorspeller (beta −0.14 ± 0.05, p=0.005). Voor cerebrale morbiditeit was alleen diabetes mellitus een onafhankelijke significante voorspeller (beta 2.8 ± 1.3, p=0.03).

De conclusie van dit hoofdstuk is dat cardiovasculaire MRI-biomarkers, die de ernst van stenosen, aortavaatwandstijfheid en linkerventrikelfunctie representeren, een rol spelen in de prognose van *outcome* bij symptomatisch perifeer arterieel vaatlijden.

Conclusies

Cardiovasculaire MRI is een belangrijke niet-invasieve beeldvormende techniek die wordt gebruikt voor het stellen van de diagnose, de klinische *work-up* en het maken van een behandelplan bij patiënten met verdenking op een cardiovasculair ziektebeeld. Het is een nauwkeurige en betrouwbare onderzoeksmethode, die belangrijke informatie verstrekt zonder gebruik te maken van ioniserende straling.

In de studies die in dit proefschrift worden beschreven, worden nieuwe cardiovasculaire MRI-technieken in de klinische praktijk geëvalueerd en wordt de voorspellende waarde van nieuwe MRI-biomarkers onderzocht bij patiënten met symptomatisch perifeer arterieel vaatlijden.

Nieuwe technische ontwikkelingen verbeteren en verruimen de klinische toepassingen van cardiovasculaire MRI in de dagelijkse praktijk. In dit proefschrift wordt een nieuwe, snelle *free-breathing 2D delayed-enhancement* MRI-sequentie beschreven. Deze nieuwe techniek werd gevalideerd en blijkt een betrouwbare methode voor het aantonen van myocardiale infarcering. Daarnaast maken nieuwe technische ontwikkelingen het mogelijk om een *single-injection, three-station, moving-table* MRA-protocol op 3T te verrichten, dat een vergelijkbare diagnostische betrouwbaarheid heeft als 1.5T MRA. Bovendien verbetert de acquisitie van submillimeter isotrope voxels van de onderbenen de diagnostische accuraatheid en beeldt meer open infragenuale arteriële segmenten af.

Ook wordt beschreven dat nieuwe MRI biomarkers, zoals de PWV in de distale aorta, statistisch significant correleren met de ernst van stenosen bij patiënten met symptomatisch perifeer arterieel vaatlijden. Ten slotte wordt beschreven dat MRI-biomarkers, zoals de aortavaatwandstijfheid en linkerventrikelfunctie, een rol spelen in de prognose van *outcome* bij symptomatisch perifeer arterieel vaatlijden. Incorporatie van de nieuwe – in dit proefschrift beschreven – MRI-biomarkers in de klinische *work-up* van patiënten met perifeer arterieel vaatlijden kan een belangrijke rol gaan spelen voor het verkrijgen van een volledig vasculair risicoprofiel en uiteindelijk een gunstige bijdrage leveren aan de zorg voor deze patiëntengroep.

Dankwoord

De meesten in mijn directe omgeving weten, dat het schrijven van dit proefschrift zich over enige tijd heeft uitgestrekt. Graag wil ik iedereen die telkens welgemeend geïnteresseerd informeerde naar de vorderingen van mijn wetenschappelijke werkzaamheden, dan wel aan de totstandkoming van dit proefschrift heeft meegewerkt, hartelijk danken. Veel dank ben ik in het bijzonder verschuldigd aan de volgende mensen.

Prof. dr. de Roos, mijn promotor, beste Albert, zeer erkentelijk ben ik je voor de vele goede adviezen over en heldere analyses van ons wetenschappelijk project. Ik bewaar ook goede herinneringen aan alle beschouwingen over andere (maatschappelijk) relevante vraagstukken tijdens onze afspraken op de afdeling radiologie in Leiden.

Dr. ir. Westenberg, mijn copromotor, beste Jos, mijn grote steun en toeverlaat bij dit wetenschappelijk project. Dat we beiden wel eens een marathon lopen, is waarschijnlijk ook een belangrijke reden dat dit boekje nu voor ons ligt. Dank voor alles, vooral ook voor de leuke en gezellige tijd. Gelukkig zijn we samen alweer aan een nieuwe wetenschappelijk uitdaging begonnen.

Graag wil ik mijn dank uitspreken aan alle medeauteurs van de artikelen in dit proefschrift. Dank voor jullie inbreng en tijd!

De leden van de leescommissie - prof. dr. Hildo Lamb, prof. dr. Birgitta Velthuis, prof. dr. Tim Leiner, prof. dr. Menno Huisman en dr. Xander Tielbeek - wil ik hartelijk danken voor de bereidheid het manuscript kritisch door te nemen en te beoordelen. Dank ook voor het zitting nemen in de promotiecommissie om met mij over de inhoud van gedachten te wisselen.

Een speciaal woord van dank aan mijn paranimfen, Marianne en Martin. Dank dat jullie aan mijn zijde staan bij de openbare verdediging van mijn proefschrift.

De volgende mensen ben ik zeer dankbaar voor hun collegialiteit en warme, inspirerende vriendschap: John Wondergem, Frits Jansen, Richenel Tjon A Tham, Astrid Donkers, Menno Krietemeijer, Alette Daniëls, Wikke Setz, Rianne Verhees, Lonneke Yo, Joost Nederend, Joris Hendriks, Philip Jürgens, Xander Tielbeek, Jan Korte, Lucien Duijm, alle (oud-) aios radiologie van het Catharina Ziekenhuis, alle MRI laboranten van het Catharina Ziekenhuis (in het bijzonder Cindy Maandag en Marleen Köhler), Hans Post, Patrick Houthuizen. Mijn Nijmeegse studievriendengroep: Ronald en Joke, Jan Joris en Marcelle, Martin en Elke, Wim en Jacqueline, Tom en Elvire, Michiel en Louise, Bea en Jos, Richard en Kathinka, Camille en Esther, en Marc, Pold en Boyd. Paul en Simone. Mijn lieve moeder (oma) Ria, Peer, Ben en Carmen, Marianne en Martin, Ties en Bram, Gerrit en Elly, Ada en Rutger, Joke en Frans. En natuurlijk Iris, Lotte, Tijmen en Freke.

Curriculum vitae

Curriculum vitae

Harrie van den Bosch werd geboren op 11 november 1965 in Eindhoven. In 1984 behaalde hij zijn Gymnasium-β diploma aan het Van Maerlantlyceum in Eindhoven. In datzelfde jaar begon hij met de studie Geneeskunde aan de Katholieke Universiteit in Nijmegen.

Op 5 juli 1991 behaalde hij zijn artsexamen. In 1992 startte hij met de opleiding Radiologie in het Catharina Ziekenhuis in Eindhoven bij opleider dr. G. Landman. Zijn opleiding tot radioloog rondde hij af op 1 december 1997, onder begeleiding van opleider dr. A.V. Tielbeek.
In 1998 was hij werkzaam als junior staflid Radiologie in het Academisch Ziekenhuis Utrecht onder begeleiding van Prof. dr. W. Mali, en volgde hij enkele maanden een fellowship Cardiovasculaire MRI op de afdeling Radiologie van het Leids Universitair Medisch Centrum onder leiding van Prof. dr. A. de Roos.

In 1999 trad hij toe tot de maatschap Radiologie van het Catharina Ziekenhuis in Eindhoven. Na in 2009 plaatsvervangend opleider te zijn geworden, volgde hij in 2013 dr. A.V. Tielbeek op als opleider Radiologie.

De afgelopen jaren is Harrie actief geweest in verschillende gremia en commissies, o.a. het Concilium Radiologicum, de plenaire visitatiecommissie en de accreditatiecommissie van de NVvR, commissie beeldvormende techniek en de subcommissie MRI, sectiebestuur cardiovasculaire radiologie, wetenschappelijke commissie radiologendagen en kennisagenda van de NVvR. Daarnaast is hij gastdocent aan de Fontys Hogeschool Eindhoven.

Harrie is getrouwd met Iris en ze zijn de trotse ouders van Lotte, Tijmen en Freke.

List of publications

List of publications

In this thesis

van den Bosch HCM, Westenberg JJM, de Roos A. CMR: imaging planes and anatomy. Chapter 7, p108-115 *in* MRI and CT of the cardiovascular system, 3rd Edition, 2013. *Ed.* Charles B Higgens and Albert de Roos.

van den Bosch HCM, Westenberg JJM, Post JP, Yo G, Verwoerd J, Kroft LJM, de Roos A. Free-Breathing MR imaging for the assessment of myocardial infarction: clinical validation. AJR Am J Roentgenol 2009;192(6):277-281.

van den Bosch HCM, Westenberg JJM, de Roos A. Cardiovascular magnetic resonance angiography: carotids, aorta, and peripheral vessels. Chapter 45 *in* Cardiovascular Magnetic Resonance: A Companion to Braunwald's Heart Disease, 3rd Edition, 2018. *Ed.* Warren J Manning and Dudley J Pennell.

van den Bosch HCM, Westenberg JJM, Caris R, Duijm LEM, Tielbeek AV, Cuypers PWM, de Roos A. Peripheral arterial occlusive disease: 3.0-T versus 1.5-T MR angiography compared with digital subtraction angiography. Radiology 2013; 266:337-346.

Bezooijen R, **van den Bosch HCM**, Tielbeek AV, Thelissen GRP, Visser K, Hunink MGM, Duijm LEM, Wondergem JHM, Buth J, Cuypers PWM. Peripheral arterial disease: Sensitivity-encoded multiposition MR angiography compared with intraarterial angiography and conventional multiposition MR angiography. Radiology 2004;231:263-271.

van den Bosch HCM, Westenberg JJM, Setz-Pels W, Wondergem JHM, Wolterbeek R, Duijm LEM, Teijink JAW, de Roos A. Site-specific association between distal aortic pulse wave velocity and peripheral arterial stenosis severity: a prospective cardiovascular magnetic resonance study. J Cardiovasc Magn Reson 2015;17:2.

van den Bosch HCM, Westenberg JJM, Setz-Pels W, Kersten EL, Tielbeek AV, Duijm LEM, Post JP, Teijink JAW, de Roos A. Prognostic value of cardiovascular MR imaging biomarkers on outcome in peripheral arterial disease: a 6-year follow-up pilot study. Int J Cardiovasc Imaging 2016;32:1281-1288.

Other publications

van Kints MJ, Tjon A Tham R, Klinkhamer PJ, **van den Bosch HCM**. Hemangiopericytoma of the breast: mammographic and sonographic findings. AJR Am J Roentgenol 1994;163:61-63.

van den Bosch HCM, Tjon A Tham RTO, Gooszen AW, Fauquenot-Nollen AMB, Lamers CBHW. Celiac disease: Small bowel enteroclysis findings in adult patients treated with a gluten-free diet. Radiology 1996;201:803-808.

Vos LD, Tielbeek AV, Vroegindeweij D, **van den Bosch HCM**, Buth J. Cystic adventitial disease of popliteal artery demonstrated by intravascular US. J Vasc Interv Radiol 1996;7:583-586.

Vroegindeweij D, Vos LD, Tielbeek AV, Buth J, **van den Bosch HCM**. Balloon angioplasty combined with primary stenting versus balloon angioplasty alone in femeropopliteal obstructions: a comparative randomized study. Cardiovasc Intervent Radiol 1997;20:420-425.

Vroegindeweij D, Tielbeek AV, Buth J, Vos LD, van den Bosch HCM. Patterns of recurrent disease after recanalization of femeropopliteal artery occlusions. Cardiovasc Intervent Radiol 1997;20:257-262.

van den Bosch HCM, Vos LD. Images in clinical medicine: achilles tendon xanthoma in familial hypercholesterolemia. N Engl J Med 1998;338:1591.

Han KM, Duijm LE, Thelissen GR, Cuypers PW, Douwes-Draaijer P, Tielbeek AV, Wondergem JH, **van den Bosch HCM**. Failing hemodialysis access grafts: Evaluation of complete vascular tree with 3D contrast-enhanced MR angiography with high spatial resolution: initial results in 10 patients. Radiology 2003;27:601-605.

Nieuwlaat WA, Huysmans DA, **van den Bosch HCM**, Sweep CG, Ross A, Corstens F, Hermus AR. Pretreatment with a single, low dose of recombinant human thyrotropin allows dose reduction therapy in patients with nodular goiter. JCEM 2003;88:3121-3129.

Stultiens GNM, Kortman J, **van den Bosch HCM**, van der Veen A. Fractuur van het os sesamoideus van de duim. Nederlands Tijdschrift voor traumatologie. 2004;4:106-108.

Froger CL, Duijm LEM, Liem YS, Tielbeek AV, Donkers–van Rossum AB, Douwes-Draaijer P, Cuypers PWM, Buth J, **van den Bosch HCM**. Stenosis detection with MR

angiography and digital subtraction angiography in dysfunctional hemodialysis access fistulas and grafts. Radiology 2005;234:284-291.

Heesakkers RAM, Futterer JJ, Hovels AM, **van den Bosch HCM**, Scheenen TWJ, Hoogeveen YL, Barentsz JO. Prostate cancer evaluated with Ferumoxtran-10-enhanced T2*-weighted MR imaging at 1.5 and 3.0T: early experience. Radiology 2006;239:481-487.

Duijm LEM, Liem YS, van der Rijt RHH, Nobrega FJ, **van den Bosch HCM**, Douwes-Draaijer P, Cuypers PWM, Tielbeek AV. Inflow stenoses in dysfuntional hemodialysis access fistulae and grafts. Am J Kidney Dis 2006:48:98-105.

Smoulders SA, **van den Bosch HCM**, Post JP, Vonk-Noordegraaf A, Postmus PE. Where is the heart after left-sided pneumectomy? JTO 2006;1:69-70.

van der Voort PH, **van den Bosch HCM**, Post JC, Meijer A. Determination of the spatial orientation and shape of pulmonary vein ostia by contrast-enhanced magnetic resonance angiography. Europace 2006;8:1-6.

Smulders SA, Holverda S, Vonk-Noordegraaf A, **van den Bosch HCM**, Post JC, Marcus JT, Smeenk FWJM, Postmus PE. Cardiac function and position more than 5 years after pneumonectomy. Ann Thorac Surg 2007;83:1986-1992.

Koch AD, **van den Bosch HCM**, Bravenboer B. Epstein–Barr Virus–Associated Cholecystitis. Ann Intern Med 2007;146:826-827.

Planken NR, Tordoir JH, Duijm LEM, **van den Bosch HCM**, van der Sande FM, Kooman JP, de Haan MW, Leiner T. Magnetic resonance angiographic assessment of upper extremity vessels prior to vascular access surgery: feasibility and accuracy. Eur Radiol 2008;18:158-169.

Mischi M, **van den Bosch HCM**, Jansen AM, Sieben M, Aarts RM, Korsten HHM. Quantification of regional left ventricular dyssynchrony by magnetic resonance imaging. IEEE Trans Biomed Eng 2008;55:985-995.

Jansen AH, Bracke F, van Dantzig JM, Peels KH, Post JC, **van den Bosch HCM**, van Gelder B, Meijer A, Korsten HHM, de Vries J, van Hemel NM. The influence of myocardial scar and dyssynchrony on reverse remodeling in cardiac resynchronization therapy. Eur J Echocardiogr 2008;9:483-488.

Heesakkers RAM, Hovels AM, Jager GJ, **van den Bosch HCM**, Witjes JA, Raat HPJ, Severens JL, Adang EMM, Hulsbergen-van der Kaa C, Futterer JJ, Barentsz JO. MRI with a lymph-node-specific contrast agent as an alternative to CT scan and lymph-node dissection in patients with prostate cancer: a prospective multicohort study. The Lancet Oncol 2008;9:850-856.

Breeuwer M, de Putter S, Kose U, Speelman L, Visser K, Gerritsen F, Hoogeveen R, Krams R, **van den Bosch HCM**, Buth J, Gunther T, Wolters B, van Dam E, van de Vosse F. Towards patient-specific risk assessment of abdominal aortic aneurysm. Med Biol Eng Comput 2008;46:1085-1095.

Van 't Veer M, Buth J, Merkx MAG, Tonino PAL, Pijls NHJ, **van den Bosch HCM**, van de Vosse FN.
Biomechanical properties of abdominal aortic aneurysms assessed by simultaneously measured pressure and volume changes in humans. J Vasc Surg 2008;48:1401-1407.

Mischi M, **van den Bosch HCM**, den Boer JA, Verwoerd J, Grouls, RJ, Peels CH, Korsten HHM. Intra-thoracic blood volume measurement by contrast magnetic resonance imaging. Magn Reson Med 2009;61:344-353.

Heesakkers RAM, Jager GJ, Hovels AM, de Hoop B, **van den Bosch HCM**, Raat F, Witjes JA, Mulders PFA, Hulsbergen-van der Kaa H, Barentsz JO. Prostate Cancer: Detection of lymph node metastases outside the routine surgical area with Ferumoxtran-10-enhanced MR imaging. Radiology 2009;251:408-414.

Stevenhagen J, van der Voort PH, Dekker LR, Bullens RW, **van den Bosch HCM**, Meijer A. Three-dimensional CT overlay in comparison to CartoMerge for pulmonary vein antrum isolation. J Cardiovasc Electrophysiol 2010:21:634-639.

Martincich L, Faivre-Pierret M, Zechmann CM, Corcione S, **van den Bosch HCM**, Peng W-J, Petrillo A, Siegmann KC, Heverhagen JT, Panizza P, Gehl H-B, Diekmann F, Pediconi F, Ma L, Gilbert FJ, Sardanelli F, Belli P, Salvatore M, Kreitner K-F, Weiss CM, Zuiani C. Multicenter, double-blind, randomized, intraindividual crossover comparison of gadobenate dimeglumine and gadopentetate dimeglumine for breast MR imaging (DETECT trial). Radiology 2010;58:396-408.

Moonen LA, **van den Bosch HCM**, Demeyere TB, Bravenboer B. Skin lesions depicting a systemic disease. Neth J Med 2011;69:41-42.

Mischi M, Kaklidou F, Houthuizen P, Aben JP, Prinzen FW, Bracke F, **van den Bosch HCM**, Korsten HHM. Three-dimensional quantification of regional left-ventricular

dyssynchrony by magnetic resonance imaging. Conf Proc IEEE Eng Med Biol Soc. 2011;2011:2646-2649.

Gilbert FJ, **van den Bosch HCM**, Petrillo A, Siegmann K, Heverhagen JT, Panizza P, Gehl HB, Pediconi F, Diekmann F, Peng WJ, Ma L, Sardanelli F, Belli P, Corcione S, Zechmann CM, Faivre-Pierret M, Martincich L. Comparison of gadobenate dimeglumine-enhanced breast MRI and gadopentetate dimeglumine-enhanced breast MRI with mammography and ultrasound for the detection of breast cancer. J Magn Reson Imaging 2014;39:1272-1286.

Saporito S, Herold IH, Houthuizen P, **van den Bosch HCM**, Korsten HHM, van Assen HC, Mischi M. Automatic indicator dilution curve extraction in dynamic-contrast enhanced imaging using spectral clustering. Phys Med Biol 2015;60:5225-5240.

Saporito S, Herold IH, Houthuizen P, **van den Bosch HCM**, den Boer JA, Korsten HH, van Assen HC, Mischi M. Model-based characterization of the transpulmonary circulation by dynamic contrast-enhanced magnetic resonance imaging in heart failure and healthy volunteers. Invest Radiol 2016;51:720-727.

Herold IH, Saporito S, Mischi M, van Assen HC, Bouwman RA, de Lepper AG, **van den Bosch HCM**, Korsten HH, Houthuizen P. Pulmonary transit time measurement by contrast-enhanced ultrasound in left ventricular dyssynchrony. Echo Res Pract 2016;3:35-43.

Saporito S, Dovancescu S, Herold IH, **van den Bosch HCM**, van Assen HC, Aarts RM, Korsten HHM, Mischi M. Comparison of cardiac magnetic resonance imaging and bio-impedance spectroscopy for the assessment of fluid displacement induced by external leg compression. Physiol Meas 2017;38:15-32.

Nerad E, Lambregts DM, Kersten EL, Maas M, Bakers FC, **van den Bosch HCM**, Grabsch HI, Beets-Tan RG, Lahaye MJ. MRI for local staging of colon cancer: Can MRI become the optimal staging modality for patients with colon cancer? Dis Colon Rectum 2017;60:385-392.

Saporito S, Houthuizen P, Aben JMM, Westenberg JJM, **van den Bosch HCM**, van Assen HC, Mischi M. Endocardial center motion for quantification of left ventricular discoördination in heart failure using cine MRI. Physiol Meas. 2018 Jan 25; *Epub ahead of print.*